THE PROCEEDINGS OF THE PHYSICAL SOCIETY

VOL. 59, PART 5 1 September 1947 No. 335

SOME PHYSICAL ASPECTS OF THE HEAT BALANCE OF THE HUMAN BODY

BY PROFESSOR D. BRUNT, SC.D., F.R.S.

Presidential Address, delivered 8 May 1947

§1. THE FACTORS IN THE HEAT ECONOMY OF THE HUMAN BODY

THERE is a continual generation of heat within the body, as a result of digestion and of the oxidation of body tissues associated with physical effort, the rate of generation being called the *metabolic rate*. The heat is conducted to the skin, partly by the normal conduction of the body tissues, partly by the blood stream, and from the skin is dissipated to the environment by the combined action of radiation, convection and the evaporation of sweat. The radiation exchange between the body and its environment will lead to a gain or loss of heat according as the radiating surfaces in the environment are warmer or colder than the skin, and the air will warm or cool the body by convection according as it is warmer or colder than the skin.

It is the temperature of the skin which determines the bodily gain or loss of heat by radiation and convection. While the internal temperature of the body remains nearly constant at about 98° F. in a wide variety of external conditions, the temperature of the skin will vary considerably with variations in these external conditions (temperature, humidity and rate of motion of the air), and will also vary over different parts of the body. Except at air temperatures above 90° F., the skin temperature of a man resting indoors is lowest over the feet, next lowest over the hands, and highest over the trunk and head ; when the air temperature is above 90° F., the skin temperature tends to be uniform or nearly so over the whole of the body (Hardy and DuBois, 1941).

The following notation is employed in accordance with the usual custom:—

M = metabolic rate of generation of heat in the body.

R = rate of radiative loss of heat to the environment, negative when the walls or other radiative surfaces are warmer than the skin.

C = rate of convective loss of heat to the environment, negative when the air is warmer than the skin.

E = rate of loss of heat by evaporation in the lungs and from the skin.

S = storage, or rate of net loss of heat due to lowering of body temperature, counted negative when the body gains heat.

H = rate of gain of heat by absorption of short-wave radiation from sun and sky.

T_a = temperature of the ambient air.
T'_a = wet-bulb temperature of the ambient air.
T_w = temperature of the radiating surfaces near the body.
T_B = temperature of the deep tissues of the body.
T_s = mean temperature of the skin.
T_o = operative temperature (defined below).
v = speed of air movement in m./sec.
P_s = saturation vapour pressure at temperature T_s.
p_a = actual vapour pressure in the ambient air.

The first six items above measured are in kg. cal. per m^2 of skin per hour.

§ 2. THE HEAT ECONOMY OF THE BODY INDOORS

In indoor conditions the heat exchange of the body is represented by the equation

$$M + S = R + C + E.$$

Out of doors the absorption of solar radiation, H, and the loss of part of the black-body radiation from solid bodies, are allowed for by adding to M a correction H, and subtracting a quantity which may be 25–30 units with a clear sky in the middle of the day in summer. Of the items in this equation M, S, and E are obtained by direct measurement. M is measured by the oxygen-carbon dioxide exchange in breathing. S is computed from the change in mean temperature of the body, the mean specific heat of the body being estimated to be 0·83. E is computed from the loss of weight of the body in an hour. When these items are known for a variety of conditions, it is possible to compute $R + C$ from the equation above. The experimental data quoted below were obtained at the John B. Pierce Laboratory of Hygiene, Newhaven, Conn., by the Director of the Laboratory (Dr. C.-E. A. Winslow), Dr. L. P. Herrington, and Dr. A. Gagge. The subjects of the experiments were placed in a specially designed booth, in which the temperature, humidity and movement of the air could be controlled, and the temperatures of walls could be controlled by reflecting or heating devices in the walls. The balance used for weighing the subjects was sensitive to 2 gm.

Experiments of this type have usually been limited to nude subjects, since clothing adds a complication to the interpretation of the experiments. The experiments summarized in figure 1 were, however, made with clothed subjects, the clothing consisting of a two-piece suit of cotton underwear, a cotton shirt without tie, socks, leather shoes, and a grey suit with three-quarter-lined coat and fully lined waistcoat. A summary of a considerable number of physiological experiments was given by Brunt (1943).

In figure 1 (Winslow, 1941) the unit is 1 kg. cal. per sq. m. of skin surface per hour, the scale on the right-hand side giving the appropriate total (per hour) for each item for a man of average size, having a skin area 1·8 sq. m., or 19·5 sq. ft. The operative temperature shown as ordinate in figure 1 is a weighted mean of the temperatures of the air and walls, estimated to give a joint representation of the radiation and convection when wall and air temperature are not identical. When these temperatures are identical, the operative temperature is equal to the air temperature.

Figure 1 summarizes observations on clothed subjects resting, with air movement of 17 ft./min. The metabolic rate M remains substantially steady in operative temperatures 21 to 30° C. (70 to 86° F.), but increases slowly and steadily as temperature departs above or below this range. The body cools (S positive) in operative temperatures below 25·5° C. (78° F.) and is slightly warmed at higher temperatures. The evaporative loss E is relatively low at temperatures below 29° C. (84° F.), but increases rapidly as the temperature increases above this limit. Below 84° F. the evaporative loss is entirely due to losses in the respiratory passages and lungs, and to the insensible perspiration which passes through the skin,

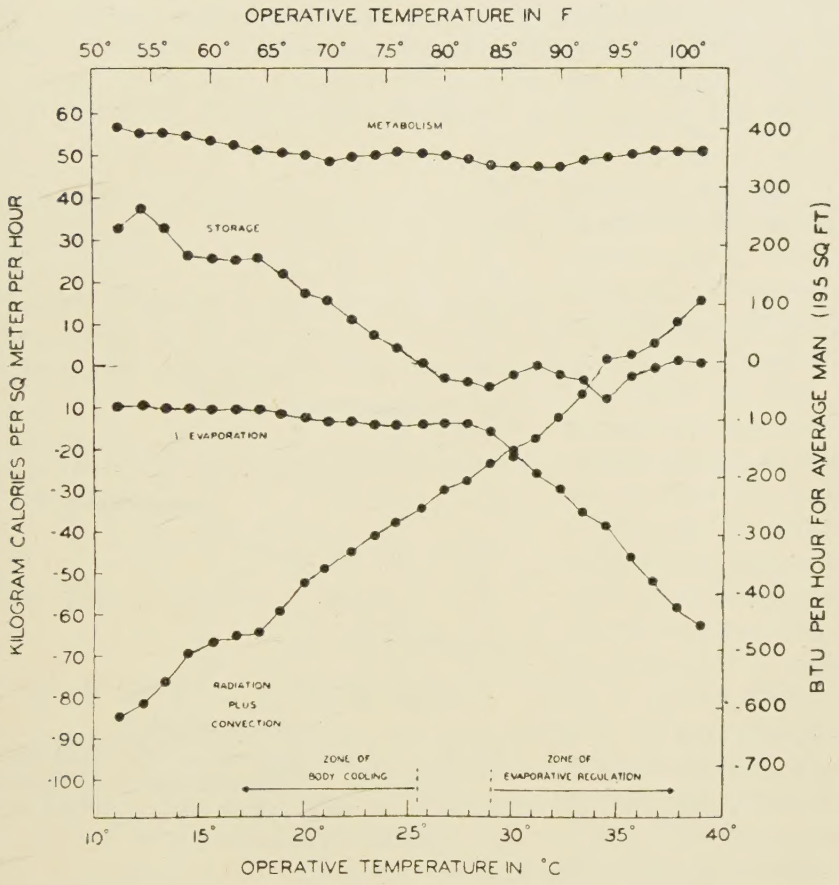
OPERATIVE TEMPERATURE IN F
50° 55° 60° 65° 70° 75° 80° 85° 90° 95° 100°
METABOLISM
STORAGE
EVAPORATION
RADIATION PLUS CONVECTION
ZONE OF BODY COOLING
ZONE OF EVAPORATIVE REGULATION
KILOGRAM CALORIES PER SQ METER PER HOUR
60 50 40 30 20 10 0 10 20 30 40 50 60 70 80 90 100
BTU PER HOUR FOR AVERAGE MAN (19.5 SQ FT)
400 300 200 100 0 100 200 300 400 500 600 700
10° 15° 20° 25° 30° 35° 40°
OPERATIVE TEMPERATURE IN °C

Figure 1. The relation of the different items in the heat exchange of the body to operative temperature. Clothed subjects. (Winslow, 1941.)

without wetting the surface. The joint radiative plus convective loss is very great at low temperatures, and is proportional to the difference of mean skin temperature and operative temperature. This item becomes an addition to bodily heat at operative temperatures above 35° C. (95° F.), the air being then warmer than the skin.

Figure 2, which refers entirely to observations on nude subjects (Winslow, 1941), shows, in the lowest curve, the variation of mean skin temperature with

changes of operative temperature. Active sweating through the sweat glands sets in at 31° c. for resting nude subjects indoors, instead of at 29° c. as with clothed subjects. The result of this sweating is to maintain the skin temperature at a steady value near 35° c. with operative temperatures above 31° c. With operative temperatures below 31° c. the mean skin temperature falls at a rate of about 1° c. for every 2° c. fall of operative temperature.

The rather irregular curve marked K in the upper part of figure 2 shows the variation of the "conductance" of the body, defined as $K=(M+S)/(T_B-T_s)$. K remains substantially constant at operative temperatures between 31 and 37° c., and increases slightly at temperatures above 37° c. It is also substantially constant at temperatures below 27° c., i.e. in the "zone of body cooling". In the intermediate zone from 27 to 31° c., K increases steadily. This is the "zone of vaso-motor control", in which body temperature is maintained steady by the control of the flow of heat to the skin by the dilation or contraction of the surface blood vessels or, in other words, by the control of the conductance.

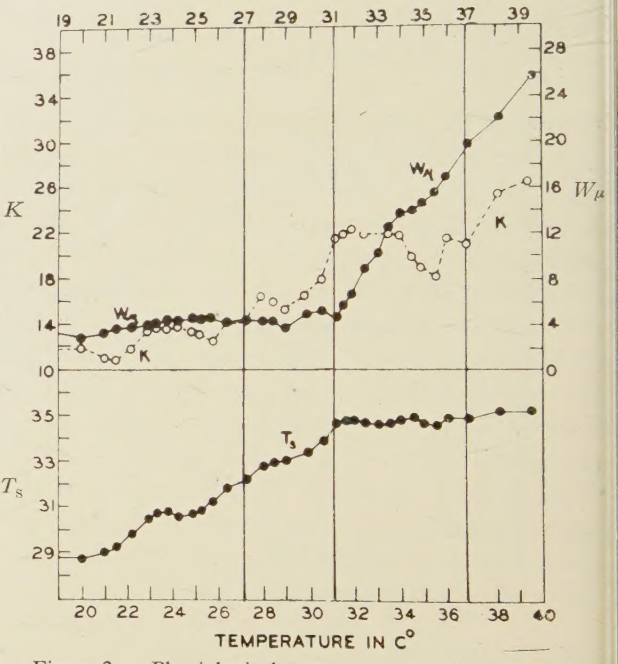

Figure 2. Physiological responses to varying operative temperature. W_μ=wetted area; K=conductance; T_s=mean skin temperature. Nude subjects. (Winslow, 1941.)

It will be noted that when the body is subjected to cold, the "conductance" of heat is decreased by the contraction of the surface blood vessels, while when the body is subjected to heat, above a certain limit the conductance is increased by the complete dilation of the surface blood vessels. It is only in the intermediate zone, known as the "zone of vaso-motor control", and in air temperatures exceeding 37° c., that the degree of dilation or contraction of the peripheral blood vessels is variable. The zone of vaso-motor control is from 25·5 to 29° c. for the clothed body, and from 27 to 31° c. for the nude body, both cases referring to persons resting indoors. An increase in physical activity shifts this zone towards lower temperatures.

Experiments have shown that the conductance is lower in fat than in lean subjects (Winslow, Herrington and Gagge, 1937) and in women than in men (Hardy, Milhorat and DuBois, 1941). Women generally have a more considerable layer of subcutaneous fat than men ; in addition, at low temperatures they have a readier tendency than men to increase their metabolic rate. For these

reasons women appear to bear with equanimity a degree of cold which men would find trying were they protected by the same amount of clothing.

The curve marked W in figure 2 gives, in arbitrary units, the area of the part of the skin from which evaporation of sweat is occurring. This area increases rapidly as temperature rises above 31° C. W. is defined as $E/(P_s - p_a)$.

We can now summarize some of the more important reactions of the body to its environment. In a cold environment the surface blood vessels contract, thereby checking the conduction of heat from the deeper tissues to the skin, while the skin temperature falls, thereby decreasing the rate of dissipation of heat from the skin. The metabolic rate is accelerated by the fluid discharged from the adrenal and other glands into the blood stream, when exposure to cold is prolonged. In a warm environment, or during strenuous physical exertion, the peripheral blood vessels dilate, and sweat is freely secreted, the evaporative loss of heat from the skin being the body's main safeguard against rise of temperature.

§ 3. THE RELATIONSHIP OF RADIATION, CONVECTION AND EVAPORATION TO THE ENVIRONMENTAL CONDITIONS, FOR NUDE SUBJECTS

The observational technique does not separate the quantities R and C. When the temperature of the radiating surfaces, such as walls etc., in the immediate environment, is equal to the air temperature, then for the nude subject

$$R + C = k(T_s - T_a).$$

A number of series of independent experiments showed that k is a linear function of $v^{1/2}$, and that

$$k = 3{\cdot}6 + 16v^{1/2}.$$

It follows that, in general,

$$R = 3{\cdot}6(T_s - T_w),$$
$$C = 16v^{1/2}(T_s - T_a).$$

It can readily be checked that the factor 3·6 for R is in agreement with the assumption that the body radiates as a black body. Various estimates based on experimental determinations agree in yielding for the radiative power of the skin a factor 0·99 of black-body radiation.

The measurements of evaporation (E) represented in figure 1 are those appropriate to a clothed subject reclining, and it is found that the maximum evaporation shown in this diagram is equal to the evaporation from rather less than 30% of the area of skin from which heat is lost by convection. This is not in general agreement with the experience of men in extremely hot conditions, when not reclining. When sawing wood, for example, one finds the whole body becoming wetted with sweat, as it does on exposure to very high temperature.

The curve for evaporation, in figure 1, shows that when the temperature of the ambient air rises above 29° C., the evaporative loss rises, and W in figure 2 shows that the area of skin wetted with sweat increases steadily with rise of temperature. Winslow, Herrington and Gagge (1937) have shown that when the evaporating

power of the air is increased by a decrease in humidity, the air temperature being kept constant, there is a decrease in the area of skin wetted by sweat, while the actual loss of heat by evaporation remains unchanged. This is readily seen by a comparison of figures 3 and 4. When the temperature and humidity of the air are kept unchanged, while the air speed is increased, so that the convective loss of heat is increased, the necessary evaporative loss of heat is decreased, and it is also found that the area of skin wetted by sweat is decreased. No instrument has yet been designed which is capable of simulating the human body's control over the area from which evaporation can occur, and it is not surprising that the interpretation of readings of such instruments as have been devised should be uncertain.

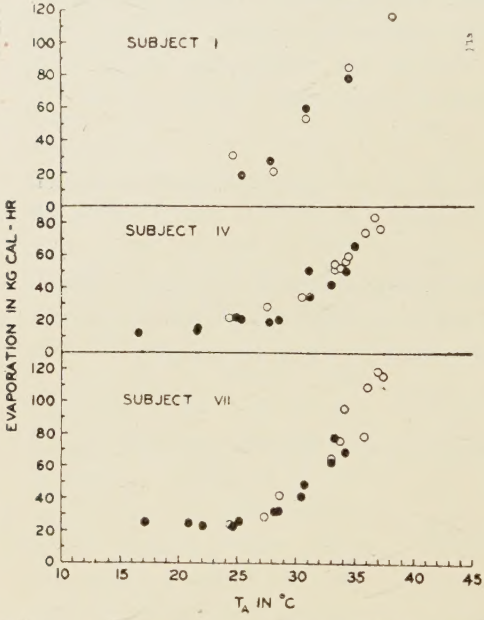

Figure 3. Evaporative heat loss in relation to air temperature for nude subjects. Solid circles, high humidity (40–80%). Open circles, low humidity (14–40%). (Winslow, Herrington and Gagge, 1937.)

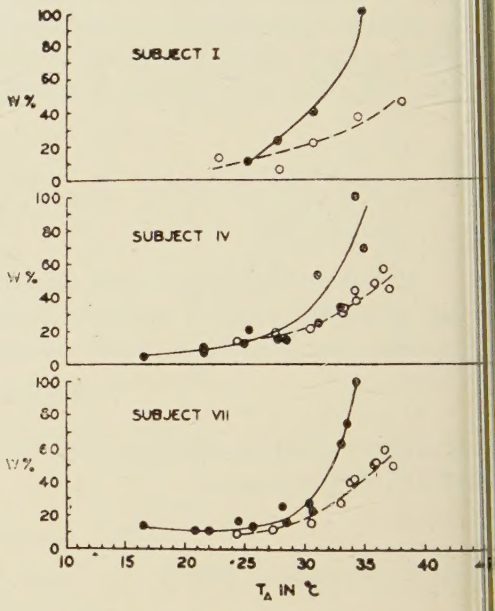

Figure 4. Percentage of maximum possible area of wetted skin surface at varying air temperatures. Nude subjects. Solid circles high humidity (40–80%). Open circles low humidity (14–40%). (Winslow Herrington and Gagge, 1937.)

If we may assume that in the limiting conditions of either great heat or great physical exertion the evaporation of sweat takes place from the same area of skin as the loss of heat by convection, the maximum evaporative loss of heat can be deduced from the convective loss. Convection and evaporation of sweat are then due to air from the environment being brought into contact with the skin, being there brought to saturation at the skin temperature and carried away by turbulent air motion. Thus the heat content and water-vapour content are diffused together, and the result is equivalent to the diffusion of the *total heat content* of air, the latter being the sum of the internal energy of the air and of the latent heat of the water vapour which it carries. If I_s is the total heat content of air saturated at the mean skin temperature, I_a is the total heat content of the ambient air, and I'_a is the total heat content of air saturated at the wet-bulb temperature, then

$$C + E = A(I_s - I_a) = A(I_s - I'_a),$$

for $I_a = I'_a$ is a statement of the ordinary hygrometric equation

$$(c_p + x_a c'_p)(T_a - T'_a) = L'(x'_a - x_a),$$

where x_a and x'_a are the humidity mixing ratios of the ambient air and of air saturated at the wet-bulb temperature. The humidity mixing ratio is defined as the mass of water vapour mixed with unit mass of dry air. The variation of latent heat with temperature can be neglected as of no importance in the practical problem.

In the equation

$$C + E = A(I_s - I_a),$$

the internal heat of the air, the diffusion of which is the convective loss of heat C, can be readily separated out, giving

$$C = Ac_p(T_s - T_a) = 16v^{1/2}(T_s - T_a).$$

Hence

$$A = 16v^{1/2}/c_p = \tfrac{200}{3}v^{1/2},$$

and

$$C + E = \tfrac{200}{3}v^{1/2}(I_s - I'_a).$$

The function I is only required for saturated air, and a table of its values is given in the Appendix.

§ 4. THE LIMITING CONDITIONS FOR HEAT-STROKE FOR NUDE SUBJECTS

In a very hot environment, particularly during great physical exertion, the rate of loss of heat by evaporation of sweat will fail to counteract the internal generation of heat plus the heating of the body by convection (when air temperature is above skin temperature). Before this stage is reached, the activity of the sweat glands will have attained its maximum, and the whole body will be wetted with sweat, much of which will drip from the body without evaporating. With continued failure of evaporative loss of heat to balance the internal generation plus convection gain or loss, the body temperature will rise, the pulse-rate will increase, strong palpitation will set in, followed by a condition of stupor; soon afterwards sweating suddenly decreases rapidly and, unless the subject is then immediately removed to a cooler environment, he dies of "heat-stroke".

The limiting conditions of temperature and humidity beyond which heat stroke will come as a result of continued exposure are given, for the *nude* man, by the equation

$$M = 3{\cdot}6(T_s - T_w) + \tfrac{200}{3}v^{1/2}(I_s - I'_a).$$

For given values of M and v the curve which fixes these limits is rapidly drawn. It is necessary to know T_s, the mean skin temperature, but sufficient observations are available to give a reasonably accurate value of T_s for given rates of physical effort. A series of such curves is given in figure 5, in which the ordinate is temperature of the radiating surfaces and the abscissa is the wet-bulb temperature of the air. With given values of M, v, and T_s, the equation is used to deduce I'_a and from this T'_a, corresponding to a series of values of T_w. Figure 5 shows the limiting curves corresponding to the following:—

(1) $M = 47$ (resting):

$T_s = 35{\cdot}6°$ C. $v = 0{\cdot}085$ m./s. Line AA

$v = 1{\cdot}0$,, ,, BB

(2) $M = 160$ (moderate work):

$T_s = 34{\cdot}3°$ C. $v = 0{\cdot}085$ m./s. Line CC
$v = 1{\cdot}0$,, ,, DD
$v = 2{\cdot}0$,, ,, EE
$v = 5{\cdot}0$,, ,, FF

Since 1 m./s. = 200 ft./min., the values of v are readily converted into ft./min.

Considering the line AA, we can state that continued exposure to conditions represented by a point above this line, for a man resting in air movement of 0·085 m./sec. (17 ft./min.),will eventually lead to death from heat-stroke. An increase of ventilation raises the tolerable limits, while an increase of physical effort, with its corresponding increase in the internal generation of heat, lowers them.

It would be of interest to obtain some direct check on the form of these curves. For men resting in nearly still saturated air, line AA shows that the maximum

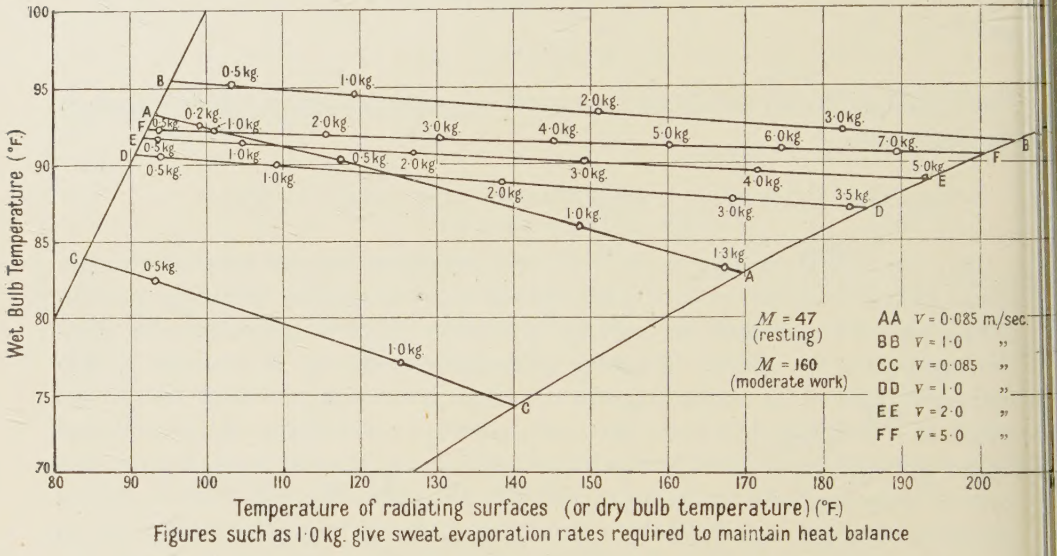

Figure 5. Heat-stroke limits for nude subjects in varying degrees of physical activity and ventilation.

tolerable temperature is 93·5° F. The temperature in the Black Hole of Calcutta has been stated to be 34° C. (93·2° F.), which is not in contradiction with this. An interesting comparison with line AA is given by an observation in a turkish bath at dry-bulb temperature 135° F., wet-bulb temperature 89° F., quoted from J. S. Haldane (1905). The point representing these temperatures is slightly above the limiting line, and it is possible to compute the initial rate of rise of body temperature, which should be 1·0° F. in the 93 minutes the subject of experiment spent in these conditions. The observed rise was 1·7° F., showing that the line AA in figure 5 is a very close representation of the true limits.

For men resting, with air movement 183 ft./min., a close approximation to 200 ft./min., Robinson, Turrell and Gerking (1945) found experimentally the following two limiting conditions:

Dry-bulb temp. 96·8° F. Wet-bulb 96·2° F.
,, ,, ,, 122° F. ,, ,, 94·0° F.

McConnell and Houghton (1932) gave 95° F. as the limit in saturated air. The three points thus obtained fit closely the line BB in figure 5.

It thus appears that the lines AA and BB of figure 5 give a reasonable representation of such experimental tests as are available. The factor multiplying $I_s - I_a'$ is rather uncertain for men doing physical work.

In the limiting conditions for any degree of activity and any degree of ventilation, the body is wetted with sweat, and the prevention of rise of body temperature is due to the evaporation. The amounts which must be evaporated from the whole body in the conditions represented by the lines in figure 5 are shown in kilogrammes, at various points along the lines, assuming $T_w = T_a$.

The rate of sweating from the whole body, assuming the skin area to be 1·8 m., is

$$\{M - (3{\cdot}6 + \tfrac{200}{3} v^{1/2})(T_s - T_a)\} \times 1{\cdot}8/L \text{ kg./hr.}$$

When T_w is not equal to T_a, the amount of sweating is increased by an amount

$$\frac{3{\cdot}6 \times 1{\cdot}8}{L}(T_w - T_a) \text{ kg./hr.}$$

In any given conditions it is therefore readily possible to evaluate the rate of sweating required to maintain temperature equilibrium of the body.

When a high rate of sweating is maintained for more than a short time, the loss of water from the body must be compensated, as also must the loss of salt in the sweat. When the rate of sweating exceeds 2 kg./hr., it is not possible to compensate completely for this loss by drinking, as 2 kg./hr. is about the maximum rate at which the body can absorb water. Drinking at a rate exceeding the rate of absorption by the body leads to nausea.

A general comparison of the curves of figure 5 with observation of body temperature of men working at known rates, in known atmospheric conditions, is not possible. It should be emphasized that the value of the conductance, K, in the limiting conditions when the body has become totally wetted with sweat, is not appreciably variable with degree of activity, i.e. with rate of internal generation of heat.

The rate of loss of heat from unit area of skin is given by

$$M + S = K(T_B - T_s).$$

Suppose a man is exposed to conditions in which, with a low value of M, this equation is satisfied with $S = 0$, and that he starts working at a rate which increases his total output of heat to a new value M'. Then

$$M' > K(T_B - T_s).$$

It will not be possible to attain thermal balance of the body until $K(T_B - T_s)$ is increased, either by an increase of T_B or a decrease of T_s, or an increase of K. Clearly the immediate reaction is an increase of K, if this is possible; but if M' is much greater than M, then $T_B - T$ must increase before thermal balance is attained, since K is not increased by even 100% in the range of environmental temperatures shown in figure 2.

In general, an increase of $T_B - T_s$ appears to be attained partly by a rise of T_B and partly by a fall of T_s. But the initial rise of T_B, which is the commonly observed physiological variable, does not indicate that the conditions make an eventual thermal equilibrium impossible.

§ 5. THE GENERAL EFFECTS OF TEMPERATURE AND HUMIDITY

Figure 6 gives in AA and BB a conversion of curves AA and BB of figure 5 into a diagram in which the coordinates are dry-bulb temperature and relative humidity, assuming the radiating surfaces to be at air temperatures. Both curves give the limiting conditions for a nude man at rest indoors, AA for air movement 17 ft./min. and BB for air movement 200 ft./min. CC gives the limiting conditions in which body equilibrium can be maintained by a clothed man resting in sunshine with only about one-third of his skin wetted by sweat, and DD the limiting conditions for a clothed man walking 3 miles per hour in bright sunshine, with the same area of skin wetted by sweat. Figures 5 and 6 are expressed in degrees Fahrenheit for convenience of comparison with observations made in industry and in meteorology.

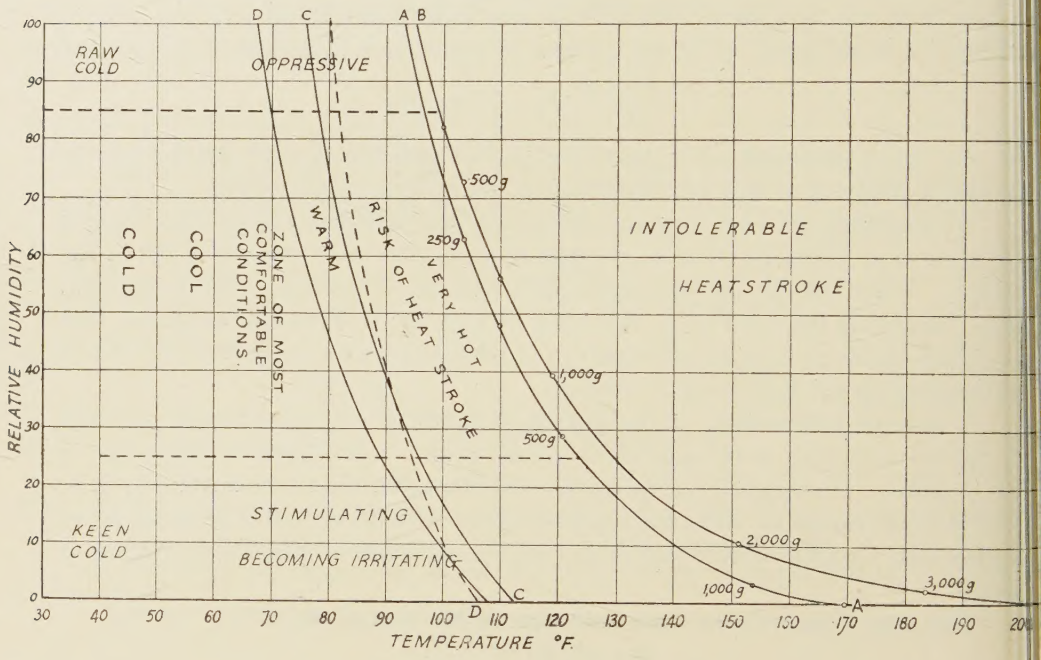

Figure 6. Tentative classification of climates.

AA. Heat-stroke limits for nude man resting in still air.

BB. Heat-stroke limits for nude man resting in air moving 200ft./min.

CC. Limiting conditions for clothed man resting in sunshine with about one-third of skin wetted with sweat.

DD. Limiting conditions for clothed man walking 3 m.p.h. with about one-third of skin wetted with sweat.

The broken line represents equivalent temperature 80° F. The figures 500 g., etc., indicate rate of evaporation of sweat in grammes per hour for men of average size in order to maintain heat balance of the body.

The character of the sensation experienced in conditions represented by different areas in the diagram is shown by the words printed in the diagram. The effect of high humidity is to give, in cold air, the feeling of cold usually called "raw", and in warm air a feeling of oppression. With low humidity, cold air gives that impression of cold which is usually called "keen", while warm, very dry air is at first stimulating, but ends by producing irritation and quarrelsomeness, as

exemplified by the Föhn wind, a warm dry wind which is frequently observed blowing down mountain slopes. Dwellers in hot desert regions manifest an unpleasant permanence of irritability.

The optimum conditions for human beings fall within the middle ranges of both temperature and humidity. With relative humidity of 50–60%, the optimum temperature is between 60 and 76° F., in reasonably good agreement with the recommendations of the heating and ventilating engineers. For air-conditioned rooms, the indoor temperature recommended in the U.S.A. is 76° F. in summer, and 72° F. in winter, and in Great Britain 66° F. in summer and 62–64° F. in winter.

Brunt (1943) has given a specification of the ideal outdoor climate on the assumption that this should permit a man, lightly clothed, (*a*) to walk at 3 miles per hour in sunshine without sweating, and (*b*) to rest in bright sunshine or to stand in the shade or indoors doing light work, with light air movement (17 ft./min.), without sweating or body cooling. The optimum for these prescribed conditions is 67° F., for a lightly clothed man, when the relative humidity is near 50%. For the *nude* man a slightly higher temperature, perhaps 70° F., is required.

§ 6. A COMPARISON WITH NATURAL CLIMATES

Figure 6 would exclude very cold and very hot climates, and also very damp and very dry climates, as undesirable for permanent residence. The most desirable climates are those having moderate temperature and humidity, and those are found in the middle latitudes of the globe. In the tropics the monotony of the weather from day to day is the most marked feature and is experienced even at tropical places so far above sea-level as to have temperatures which are not extreme.

Figures 5 and 6 are computed on the assumption that the heat balance of the body is determined by the rate of internal generation of heat, radiation, convection and evaporation of sweat, and figure 6 involves the further assumption that the radiating surfaces in the environment are at air temperature. The effect of very hot radiating surfaces can be great, and may be evaluated as shown earlier. In hot, sunny climates the walls and roofs of houses, and of any solid objects exposed to sunshine, all attain very high temperatures, and they not only radiate heat to the body at a higher rate than is allowed for in figures 5 and 6, but they are extremely uncomfortable to the touch. In these conditions an air temperature of 105° F. is about as high as a white man can tolerate.

There are two types of hot natural climates—the warm, damp, cloudy and oppressive type, and the hot, dry and sunny type. If air conditioning were possible, we should treat the first type by *drying* the indoor air, and the second by *cooling* it. Failing this, all that can be done in the warm damp climate is to increase ventilation, or to sit in the greatest draught, and in the hot, dry climate to close all doors and windows early in the morning, so as to exclude the entry of hot air from outside, while increasing ventilation by electric fan.

In warm, damp climates houses should be of an open type, permitting free air movement, and the clothing should be similar in character, being light and porous. In hot, sunny climates houses should have double walls and roof, with wide air spaces between, and should be capable of being closed tightly against the intrusion of hot air from outside during the day. Clothing should be such as to reflect as much as possible of the solar radiation falling upon it, and should be loose

and not very permeable. It should be added that white cotton of two thicknesses reflects 71% of incident radiation, while a khaki shirt reflects only 43%. A white skin reflects about 45%, a dark brunette skin 35%, and a negro's 16%.

Climatic conditions represented by points to the right of the line CC in figure 6 are considered unsuitable for permanent settlement by the white man. Allowing for the variation of temperature from day to day and from year to year in any given month, we arrive at the conclusion that, if the relatively frequent occurrence for 3–4 hours per day of conditions hotter than correspond to the line CC is to be avoided, the mean temperature of the hottest month should not exceed 75° F. in a dry climate, or 73° F. in a damp climate, if the wind is light at the hottest hours of the day. It is desirable that an analysis of, say, African climates should be made on this basis.

§7. ACCLIMATIZATION AND SETTLEMENT IN THE TROPICS

Within certain limits it is possible for a man to accustom himself to living and working in higher temperatures than can at first be tolerated by a newcomer. This acclimatization consists partly in "training" the sweat glands to function readily and economically, partly in a loss of weight, with a corresponding increase in conductance and of the ratio of skin area to total weight of the body, and partly in learning to avoid unnecessary physical exertion. After acclimatization the regulation of body temperature is more efficient, and the rise of body temperature following physical exertion is markedly less than it is initially. How precisely acclimatization is brought about is obscure, and it is found that during the later stages of acclimatization the usually observed physiological variables, such as rectal and skin temperatures, pulse-rate and rate of breathing, show a stable reaction from day to day. An interesting illustration of this will be found in Horvath and Shelley's (1946) description of their experiments in acclimatization of men to work in rather extreme conditions of heat and humidity. The work in question consisted in marching at about 3 miles per hour, carrying a 20-lb. pack. On the first day they marched for ½ hour only; on the next 13 days they marched for 1 hour. At the end of the march the rectal temperature, mean skin temperature pulse rate and sweat loss were measured. The rise of each of the first three factors all showed marked decrease from day to day during the first six days, and during the subsequent days maintained a stable level. The sweating rate increased during the whole 14 days. The men showed very marked improvement in gait, ease of working and general appearance during days 7–14, although no change was noted in the measured physiological variables. It is clear that in the later stages of acclimatization there occur physiological changes of an undetermined nature, which mark an improvement in bodily well-being but do not lend themselves to direct measurement.

Both laboratory experiments and experience in the tropics suggest that strenuous work or sport should form part of the daily life of any white man who desires to be healthy in the tropics. In Queensland, for example, it is found that the woman who does hard physical labour, such as scrubbing offices, remains healthy, while the sedentary worker, like the typist, deteriorates in health, and the woman who does nothing becomes sickly.

Professor D. H. K. Lee of the University of Queensland has written that a normal consequence of the acclimatization of the body to hot damp climates is a decline of the will to work in the absence of stimulus. If not corrected, this leads to reduced output of work or to carelessness, in either case reducing morale.

A summary of a very great volume of literature dealing with settlement in the tropics has been given by Grenfe'l Price (1939). A perusal of Price's book shows that there are wide divergences of opinion as to the possibilities of white men settling in the tropics. Many medical men appear to hold the view that, with the conquest of such diseases as malaria and hookworm,we shall have made it possible for men to reside in any part of the tropics. Experience has shown that while the white man can settle in the marginal tropics, i.e. the trade-wind coasts and islands and the tropical plateaux, the settlement of the inner tropical regions, where both temperature and humidity are high, cannot be made without loss of both physical and mental efficiency.

ACKNOWLEDGMENT

Thanks are due to the Royal Meteorological Society for the loan of blocks of figures 1, 2, 3 and 4.

REFERENCES

Brunt, D., 1943. *Quart. J. R. Met. Soc.*, **69**, 77.

Haldane, J. S., 1905. *J. Hygiene*, **5**, 494, Expt. XII.

Hardy, J. D. and DuBois, E. F., 1941. "Temperature, its Measurement and Control in Science and Industry" (Symposium, *American Inst. of Phys.* (New York: Reinhold Publ. Co.), p. 537.

Hardy, J. D., Milhorat, A. T. and DuBois, E. F., 1941. *Temperature, its Measurement, etc.*, p. 529.

Horvath, S. M. and Shelley, W. B., 1946. *Amer. J. Physiol.*, **146**, 336.

McConnell, W. J. and Houghten, F. C., 1923. *Jour. A.S.H.V.E.*, **29**, 131.

Price, A. Grenfell, 1939. "White Settlers in the Tropics." *Amer. Geog. Soc.*, Special Publ., No. 23.

Robinson, S., Turrell, E. S. and Gerking, S. D., 1945. *Amer. J. Physiol.*, **143**, 21.

Winslow, C.-E. A., 1941. *Temperature, its Measurement, etc.*, p. 509.

Winslow, C.-E. A., Herrington, L. P. and Gagge, A. P., 1937. *Amer. J. Physiol.*, **120**, 288.

APPENDIX I

Table of values of the total heat content of saturated air

T (° C.)	*I*	*T* (° C.)	*I*	*T* (° C.)	*I*	*T* (° C.)	*I*
0	2·3						
1	2·7	11	7·5	21	14·2	31	24·1
2	3·1	12	8·1	22	15·0	32	25·3
3	3·5	13	8·7	23	15·9	33	26·6
4	4·0	14	9·3	24	16·8	34	28·0
5	4·5	15	10·0	25	17·7	35	29·4
6	5·0	16	10·6	26	18·7	36	30·9
7	5·5	17	11·2	27	19·7	37	32·4
8	5·9	18	11·9	28	20·8	38	34·0
9	6·4	19	12·6	29	21·9	39	35·8
10	6·9	20	13·4	30	23·0	40	37·7

I is given in kilogramme-calories per kilogramme of dry air plus the water vapour it contains.

APPENDIX II

Value of M for man working

For a man working at the rate of 1000 W ft./lbs. per minute the rate of generation of heat which has to be dissipated from the skin, expressed in kg. cal per sq. m. of skin per hr. is given to a sufficient degree of approximation by

$$M = 64 + 35W.$$

This assumes that the efficiency of the human body regarded as a heat machine is about 24%.

SOME INVESTIGATIONS IN THE FIELD OF HEAT TRANSFER

By MAX JAKOB,
Illinois Institute of Technology, Armour Research Foundation, and Purdue University

Thirtieth Guthrie Lecture, delivered 3 October 1946

§1. INTRODUCTION

May I begin with thanks to the Council of the Physical Society for the high honour extended to me, first in 1937 and now again, by the invitation to give the lecture in commemoration of the founder of this Society, Professor Frederick Guthrie. In 1937, being just about to leave Europe, I was not able to accept this invitation. I can scarcely express how happy I am to have been given another opportunity to deliver the Guthrie Lecture. I understand that Mrs. Guthrie, until her death about two years ago, did not miss any of the lectures in honour of her late husband, and I am pleased that Professor Guthrie's daughter and other relatives of his are with us tonight in continuation of this tradition of their family.

Thinking of my former stays in London, I recall with particular gratitude the friendship extended to me by two prominent members of your Society; these were Sir Richard T. Glazebrook, whom I met first in 1929 when he was President of the First International Steam Tables Conference, and then when we had to deal with the international heat unit, and Professor H. L. Callendar, whose merits in flow calorimetry, resistance thermometry, and steam research I emphasized in a talk at the banquet of the Steam Tables Conference. I made friends with other members of your Society when giving a series of lectures on steam research at the University of London in 1931; for instance, Dr. Ezer Griffiths, your former Honorary Secretary, to mention only one of them. I also had the opportunity of attending the presentation of the Duddell Medal for

1930 to Sir Ambrose Fleming and was deeply impressed by that meeting at which the late Sir Arthur Eddington was in the chair.

Re-reading the list of Guthrie Lecturers, I feel that it was less because of my own small contributions to science that I was inserted in this brilliant list, but rather in appreciation of an engineer's work in some fields of science less cultivated by the physicists.

I often gave thought to the question why the science of heat transfer is so far in arrears compared to its sister sciences, optics, electricity, and fluid dynamics. Concerning heat radiation, the main difficulties may be found in the badly defined surfaces, complex geometrical configuration and temperature distribution, and in unexpected anomalies of the absorption by gas mixtures. The progress in experimental research on problems of heat conduction was so much slower than in corresponding work on electrical conduction because of the following facts :

1. The ubiquity of large temperature differences in nature, causing parasitic heat currents, whereas environmental electric potential differences will seldom influence electric conduction problems.

2. The difficulty of heat insulation, whereas electrical insulators for moderate voltage are usually almost perfect. This is particularly bad because of the existence of temperature differences, just mentioned.

3. The slowness of temperature propagation compared with the enormous velocity of electricity. This, of course, is due to the inclination of matter to store up heat energy instead of carrying all of it forward.

4. The complex configurations which have to be dealt with.

Considering finally heat convection, the situation becomes even worse. The Biot-Fourier equation of thermal conduction has to be combined with Stokes's equations of viscous flow; variable properties of the flowing medium, badly defined boundary conditions, and the phenomenon of unstable transition between laminar and turbulent flow have to be taken into consideration.

These facts made work in heat transfer difficult, inexact, cumbersome, and therefore unattractive. In fact, scientists were deterred from dealing with such unwieldy stuff, promising a scarce and belated crop only, not worth the labouring.

So it happened that other branches of science flourished and the branch of heat transfer developed only very slowly. Hence our knowledge of the processes in the interior of a molecule and even in the nucleus of an atom is better than our knowledge of the heat flow in a cup of tea, let alone in an industrial furnace.

I would have liked to draw a more detailed, but general picture of the field of heat transfer with its entangled roots of radiation, conduction, and convection and of special tools used in its cultivation, such as similarity and analogy methods. However, as your President, Professor D. Brunt, has so graciously mentioned, I had to prepare for this lecture at short notice and, therefore, I can show you only a few fruits from this field, just as I have them at hand from work done in recent years in cooperation with some younger colleagues. They may give you an idea of the variety of problems which pass the laboratory and desk of a specialist in heat transfer.

§ 2. HEAT RADIATION

(a) *A derivation of the basic law of gas radiation*

In work on the selective absorption of radiation by gases I started with a new derivation of the law of emission of radiation by a gas body of arbitrary shape. Koenigsberger's (1903) derivation for a rectangular parallelopiped is general but rather clumsy. Simpler derivations have been presented for a sphere, for instance, by Nusselt (1923); however, as Koenigsberger mentioned, they are not general because arbitrary bodies cannot be built up from elementary spheres. The following proof is simple and general. It follows a usual pattern but seems not to have been published previously.

Let * V be a volume of finite size and arbitrary shape (figure 1), containing an absorbing gas, and let S be the perfectly black inner surface of a spherical shell with centre C, inside V. The radius R of the sphere may be so large that the linear dimensions of the space V can be considered as differentials compared with R. The substance between S and V is to be non-absorbing, but have the same index of refraction as the gas in V. The whole system is to be kept in thermal equilibrium at the absolute temperature T.

All radiation from surface element dS that enters the volume V is contained in the solid angle ω_V. A differential part of it, in the solid angle $d\omega_V$, may cross the volume V in a cross-sectional area dA which, owing to our assumption concerning the size of V, can be considered as constant along the distance L. For the same reason the beam from dS to V is assumed to be perpendicular to dS.

Then the time rate of the radiation of wave-length λ which enters V in the solid angle $d\omega_V$ will be $d^2q = N_{b\lambda} \cdot d\omega_V \cdot dS$, where $N_{b\lambda}$ is the monochromatic areal radiant intensity for a black body.

The amount absorbed in V is

$$d^2q_\alpha = N_{b\lambda} \cdot d\omega_V \cdot dS(1 - e^{-m_\lambda L}), \qquad \ldots\ldots (1)$$

where m_λ is the logarithmic decrement of radiation for wave-length λ.

Since L is of differential magnitude compared to R, it can be taken so small that $m_\lambda L \ll 1$ and therefore $m_\lambda^2 L^2 \ll m_\lambda L$, so that $e^{-m_\lambda L} \to 1 - m_\lambda L$.

Further, by definition, $d\omega_V = dA/R^2$. Hence, from equation (1), $d^2q_\alpha = N_{b\lambda} \times (dA/R^2)\, dS \cdot m_\lambda L = N_{b\lambda}(dS/R^2) m_\lambda \cdot dV$.

By substitution of $dS/R^2 = d\omega_S$ and double integration (over S and V), $q = 4\pi m_\lambda N_{\gamma b} V$.

Since gases can be considered as non-reflecting, Kirchhoff's law requires the time rates of absorbed and emitted energy, q_α and q_ε, to be equal. Herewith the law of heat emission is obtained in the form used by Koenigsberger, $q_\varepsilon = 4 m_\lambda W_{b\lambda} V$ where $W_\lambda = \pi N_{b\lambda}$ is the monochromatic radiant flux density for a black body.

(b) *A photographic and photometric model method for the determination of surface and gas radiation*

Though the laws of emission and absorption of radiation by surfaces and absorbing gases are well known (see § 1 (a)) straight analytical determination

* In general the symbols recommended by the American Standards Association (1943) will be used in this lecture.

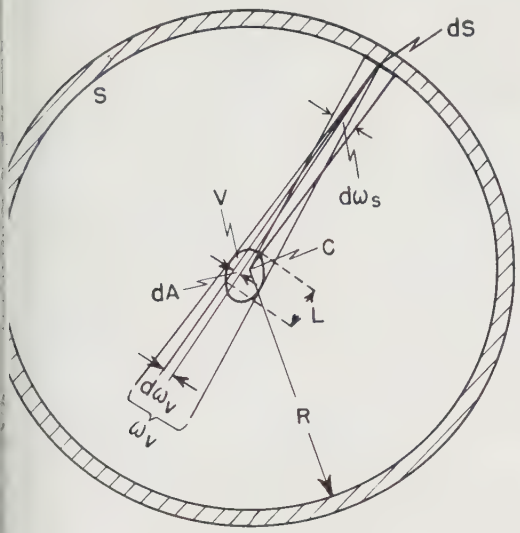

Figure 1. Radiation of a gas body.

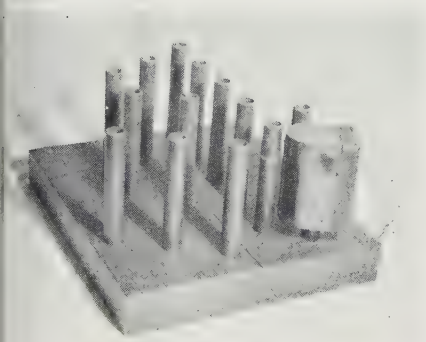

Figure 2. Model of a bank of tubes with lamp house.

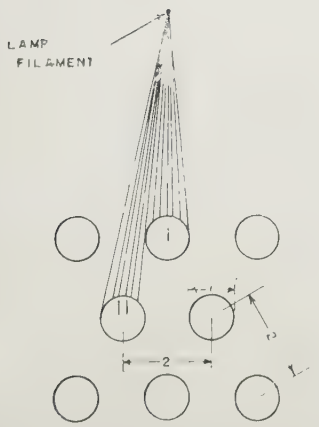

Figure 3. Configuration of tubes and rays

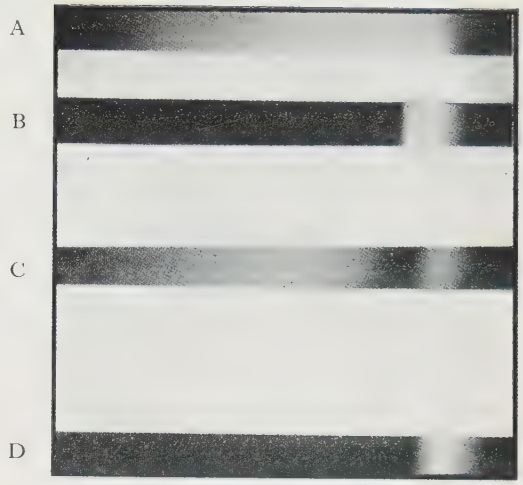

Figure 4. Spectrograms (A: lamp; B: lamp and filter; C: lamp and liquid; D: lamp, filter and liquid).

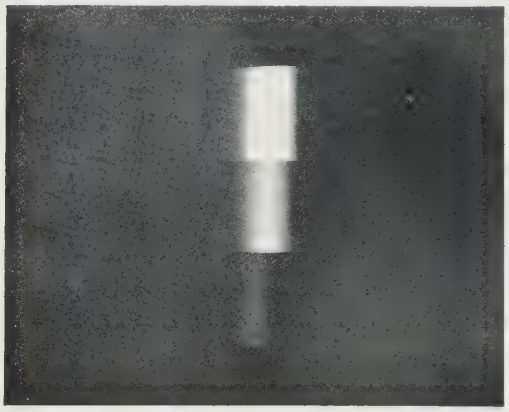

Figure 5. Spectrograms for three grades of the solution (top: weak; middle: medium; bottom: strong).

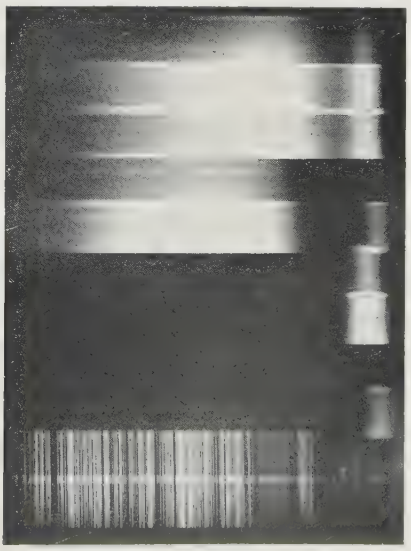

Figure 6. Spectrograms, as specified in

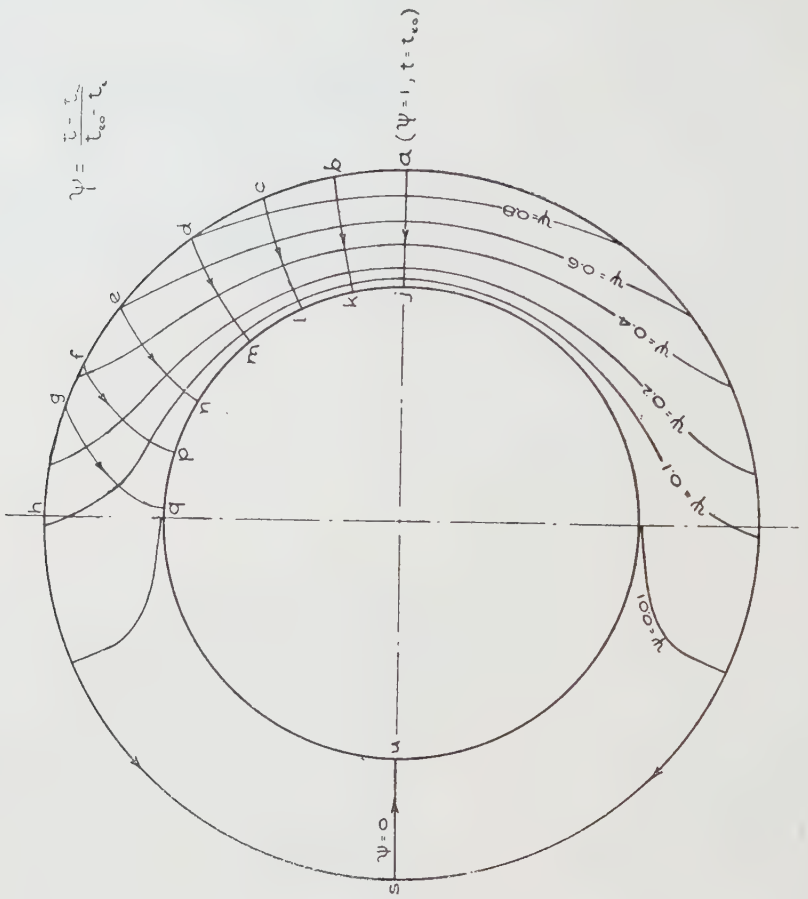

Figure 8. Isothermals and flow lines in boiler-tube wall.

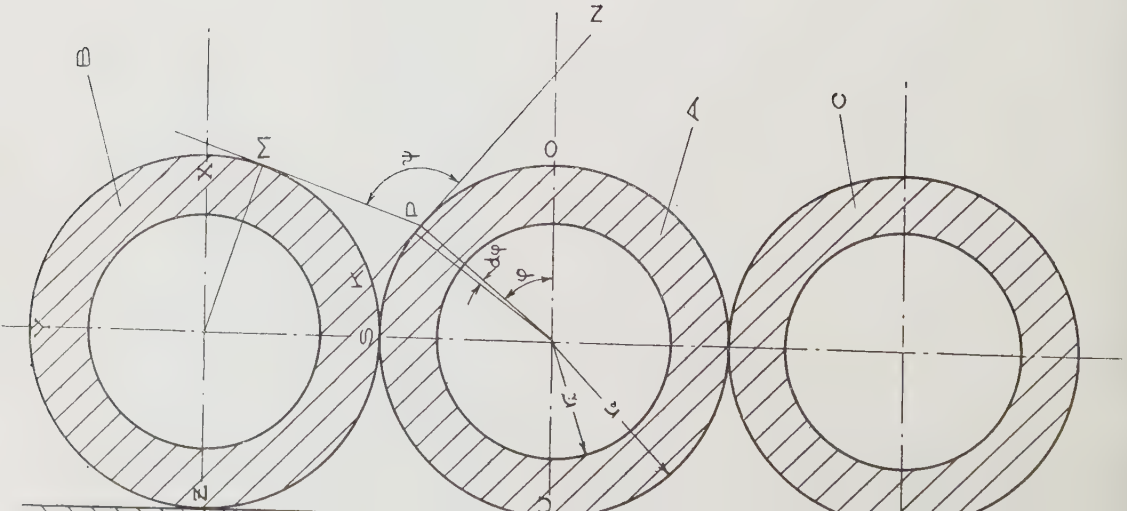

of the heat exchange by radiation in a device is possible only if the emitting and absorbing surfaces are very simple in shape and configuration. In most practical cases approximative calculations and graphical methods have been used in order to evade the mathematical difficulties. In this section, an experimental model method will be described which has been developed in cooperation with Professor Hawkins of Purdue University (Jakob and Hawkins, 1942). A small model, similar to the device under investigation, was constructed. Light was used instead of the long-wave heat radiation, and its absorption by photographic films which covered the surfaces of the model was measured by the methods of photometry. Liquids which absorb light in a narrow wave-length range were used instead of absorbing gases.

Figures 2 and 3 represent the model used. It consisted of a lamp-house and a number of pipes, 1 inch outer diameter, 10 inches long, mounted on a base plate. The light source was a single-filament galvanometer lamp which was located in the lamp-house or without that in an adjustable mounting. By horizontal slits in the housing, radiation could be restricted to a horizontal plane. When used without housing, the whole filament, about $4\frac{3}{4}$ inches long, acted as a source of radiation, parallel to the tube axes. With films wrapped around the pipes the device was ready for exposure.

Calibration consisted in exposing sections of the films for various lengths of time, developing the films and passing the resulting negatives through a recording photometer. The intensity of light transmitted through the clear film base was used as reference intensity in determination of the photographic density after different times of exposure.

The blackening of the films by exposure in the model was also measured with the recording photometer. It is apparent from figure 3 that the blackening was not uniform around the tubes. Tube I, for instance, causes a shading effect on tube II.

The complex case of absorption of radiation by gases was imitated by immersing the entire apparatus in water containing a dye. It was essential to use a combination of light source and filter which transmits light having a wave-length range in which the liquid transmits. This was not the only restriction, since it was also necessary to select a film which is sensitive to the wave-length range of light which is transmitted through the absorbing medium. The method would be useless if the film selected was "blind" to the radiation coming from the combination of light source, filter and absorbing medium.

After a great deal of experimentation, satisfactory results were eventually obtained using various concentrations of saffron dye in distilled water, Wratten light filters, and Wratten and Wainwright "hyperpanchromatic" cut films.

Figure 4 shows a series of spectrograms made with a Hilger spectroscope. The continuous spectrum of the lamp is shown in spectrogram A. Spectrogram B is taken with lamp and filter, C with lamp and liquid, showing that the liquid transmits light in almost the same range as does the filter. Spectrogram D is for light passing through filter and absorbing liquid.

In order to change the absorbing power of the medium, it was sufficient to change the concentration of the dye. Figure 5 shows the same as the spectrogram D for three grades of the absorbing solution.

Figure 6 contains eleven spectrograms which are explained by table 1.

Table 1. Explanation of figure 6

Spectrogram No. (from top to bottom)	Source of light and absorbing bodies	Time of exposure (seconds)
1	Lamp	10
2	Lamp	30
3	Lamp	90
4	Lamp and liquid	90
5	Lamp and liquid	300
6	Lamp and filter	90
7	Lamp and filter	300
8	Lamp, filter and liquid	180
9	Lamp, filter and liquid	600
10	Iron arc	3
11	Iron arc	3

Imitation of complex radiating surfaces may be obtained by suitable distribution of several filaments on the surface or, more simply, by bringing one filament to different places on the surface, exposing at each position, and superimposing the results. A variety of other possibilities, as well as of difficulties, has been indicated in the quoted publication.

§ 3. HEAT CONDUCTION

(a) *Temperature-distribution in the walls of boiler tubes*

In a boiler the outer surfaces of the steam tubes will be at a much lower temperature than other surfaces in the furnace. It is not easy to determine the temperature of these tube surfaces. Using optical pyrometers the reflexion of radiation which they receive must be carefully considered. Otherwise enormous errors may occur, as has been shown in previous papers (Reid and Corey, 1944; Jakob, 1944).

The present example (Jakob, 1943 a) deals with the determination of the outside temperature of boiler tubes by an indirect theoretical method, based on a close estimate of the distribution of the radiation outside and on calorimetric measurements of the increase of enthalpy of the fluid inside the tubes. These measurements were performed in a high-pressure boiler with forced circulation by Davidson, Hardie, Humphreys, Markson, Mumford, and Ravese (1943). The theoretical calculation further yielded information about the temperature distribution in the tube walls and about the thermal resistance between the tubes and the boiling water.

Figure 7 is a cross-section through three adjacent boiler tubes. The heat is assumed to arrive at a steady rate from the right (furnace side). The left side (wall side) is supposed to be virtually insulated by the boiler wall. It can be assumed that the main part of the heat energy arrives as radiation either from all directions of the furnace space with uniform intensity or in the direction OU. In the first case the time rate of heat radiation to a surface element at any point P of tube A is proportional to a solid angle ω which itself is proportional to the ordinary angle ψ; in the second case it is proportional to $\cos\phi$. A mathematical analysis showed that the two assumptions yield almost the same distribution

of absorbed energy. Neglecting, for the time being, the heat exchange by radiation between tubes A and B, it is as though heat sources existed at the surface which decrease in strength as $\cos\phi$ from $\phi=0$ to $\phi=\pi/2$.

The thermal conduction through the tube wall under the steady-state condition is governed by the partial differential equation

$$\frac{\partial^2 t}{\partial r^2}+\frac{1}{r}\frac{\partial t}{\partial r}+\frac{1}{r^2}\frac{\partial^2 t}{\partial \phi^2}=0$$

where t is the temperature at the radial distance r from the centre line and the angular distance ϕ from the direction UO.

For a complete circular ring (dashed area of tube A in figure 7), a solution of the differential equation was obtained by means of Fourier series. In putting up the boundary conditions the following physical assumptions were made :

$$t=t_i=\text{constant} \quad \text{for } r=r_e,$$

$$\left(\frac{\partial t}{\partial r}\right)_{r=r_e}=\frac{q_0''}{k}\cos\phi \quad \text{for } 0\leqq\phi\leqq\pi/2,$$

$$\left(\frac{\partial t}{\partial r}\right)_{r=r_e}=0 \quad \text{for } 0\leqq\pi/2\leqq\pi,$$

where

q_0'' = the heat energy * absorbed in unit time and area at $\phi=0$,

k = the thermal conductivity of the wall material, and

t_i = a temperature slightly above that of the saturated steam t_{sat} inside the tube.

Both k and t_i are considered to be constant.

Denoting by t_{e0} the temperature at the point 0 ($r=r_e$, $\phi=0$) a temperature ratio may be defined by $\Psi=\dfrac{t-t_i}{t_{e0}-t_i}$ having values between 0 (for $t=t_i$) and 1 (for $t=t_e$).

For the case of $r_e/r_i=1{\cdot}5$ the temperature distribution shown in figure 8 was obtained by numerical calculation. This figure contains isothermal lines for $\Psi=1$, 0·8, 0·6, 0·4, 0·2, 0·1, 0·01, and 0. Further, heat-flow lines are drawn from the points *a*, *b*, *c*, *d*, *e*, *f*, *g*, and *h* on the outside surface to *j*, *k*, *l*, *m*, *n*, *p*, *q*, and *u* on the inside surface, respectively. Each of the first four channels, beginning with the symmetry line *aj*, carries 1/5 of the total heat flow, the channel between *en* and *fp* carries 1/10, each of the two last channels carries only 1/20 of the heat flow. It is further seen that about 96% of the incoming heat is received in the range $\phi=0$ to $0{\cdot}4\pi$ at the outside and is given up inside in the first quadrant ($\phi=0$ to $0{\cdot}5\pi$) and only 4% in the rear quadrant. The temperature difference t_e-t_i at $\phi=\pi/2$ is about 12% of $t_{e0}-t_i$ (at $\phi=0$).

After some corrections for radiation exchange between tubes A and B and some other radiation due to the actual arrangement in the tests, a satisfactory agreement between theory and experiment was obtained regarding the values of t_{e0}. Other surface temperatures had not been measured because of the

* I use prime, double prime, and triple prime signs to designate unit length, area, and volume, respectively.

difficulties with thermocouples to be placed on tubes in a high-pressure steam boiler.

An additional qualitative result of this analysis was that inside the tube at $\phi = 0$ local coefficients of heat transfer of the order of 20000 or 30000 B.hr.$^{-1}$ ft.$^{-2}$F.$^{-1}$ occur, and in the range from $\phi = 0$ to $\pi/2$ mean coefficients of the order of 10000 or 20000 B.hr.$^{-1}$ft.$^{-2}$F.$^{-1}$. The high local heat transfer comes from the strong formation of steam bubbles at the front side which induces vehement radial and rotational movements of the mixture in the fluid cross-section, and from the wiping effect of fluid forced through the tubes. The rear half of the inner tube surface, on the other hand, is not engaged at all in the heat transfer; it acts solely as heat protection of the furnace wall. As an average, the investigation showed that the thermal resistance of the fluid film amounts only to about 10% of the total resistance, that is, the resistance against thermal conduction in the tube wall is the controlling factor.

(b) *Temperature distribution in electrical coils of simple form due to a linear increase of Joulean heat with temperature.*

Whereas § 3(a) dealt with a case of conduction of heat which was carried to the conducting body from outside by radiation and was carried away by convection, it will now be supposed that heat is developed in the conducting body.

An electrical coil is a rather inhomogeneous body because it is built up from conducting and insulating materials. However, considering equal volumes of such size that several layers of these materials are included, it can be assumed that in each volume the same Joulean heat is developed if the electric resistance of equal lengths of the conductor is the same all through the coil.

The heat developed in such a body is conducted to the surface as it would be in a homogeneous medium whose thermal conductivity is equivalent to that of the mixture of materials in the coil. In a steady state of heat development and heat flow, the temperature t decreases from a maximum value t_0 somewhere inside the coil to lowest values t_s at the surface. It will be assumed that t_s is uniform all over the coil surface. This holds approximately for a coil in an oil bath or in a fast gas stream and in numerous other cases.

Simple relations between maximum and mean temperature of a coil have been derived for the case of uniform generation of heat all over the volume. In particular, it was found that for coils, having the shape of an infinitely wide plane plate, an infinitely long cylinder, or a sphere, the temperature distribution may be expressed by

$$\theta = \theta_0(1 - \xi^2), \qquad \ldots\ldots (2)$$

where $\theta = t - t_s$ is the temperature excess over surface temperature for a point at the perpendicular or radial distance, $x = s$ or $r = s$ from the median plane, centre line, or centre of the plate, cylinder, or sphere, respectively; $\theta_0 = t_0 - t_s$ is the same for $x = 0$ or $r = 0$; s is the half thickness or the radius of the coil; and ξ is defined as the ratio x/s or r/s.

Owing to the increase of the electric resistance with temperature, the heat developed in a coil is not uniform, but increases from the surface to the point of maximum temperature. Having previously dealt with the case of uniform

development in a coil whose cross-section is a rectangle of finite side lengths (Jakob, 1919), I later studied the influence of non-uniform development of heat in coils of simple shape in ranges where the electric resistance can be assumed to increase linearly with temperature (Jakob, 1943 *b*). The general procedure and some surprising results of this study will be dealt with.

In addition to the above mentioned symbols, the following will also be used:

k = equivalent (apparent) thermal conductivity of the combination of electrically conducting and insulating material as used in the coil;

q''' = rate of heat energy developed in unit volume;

$$\frac{q'''}{k} = m + n\theta = m\left(1 + \frac{n}{m}\theta\right) = m(1 + \epsilon\theta), \qquad \ldots\ldots(3)$$

where $m = q_s'''/k_s$, $n = \epsilon q_s'''/k_s$, $\epsilon = n/m$ = temperature coefficient, $\sigma = s\sqrt{n}$. Subscripts s, 0, and m refer to the places of surface, maximum, and mean temperature, respectively.

For the infinitely wide plate, the differential equation of the temperature distribution is

$$\frac{d^2\theta}{dx^2} = -\frac{q'''}{k}.$$

For $q'''>0$ and $n>0$, its general solution is

$$0 = -\frac{m}{n} + M\cos(x\sqrt{n}) + N\sin(x\sqrt{n}),$$

where M and N are the constants of integration.

Boundary conditions are

$$d\theta/dx = 0 \quad \text{when} \quad x = 0, \quad \text{and} \quad \theta = 0 \quad \text{when} \quad x = s.$$

Using them if follows that

$$\theta = \frac{1}{\epsilon}\left[\frac{\cos(\xi\sigma)}{\cos\sigma} - 1\right], \qquad \ldots\ldots(4)$$

$$\theta_0 = \frac{1}{\epsilon}\left[\frac{1}{\cos\sigma} - 1\right], \qquad \ldots\ldots(5)$$

and

$$\frac{\theta}{\theta_0} = \frac{\cos(\xi\sigma) - \cos\sigma}{1 - \cos\sigma}. \qquad \ldots\ldots(6)$$

Thus, the temperature distribution across the plate is not parabolic, as in equation (2) which holds for $\sigma = 0$, but is more complicated. When σ approaches π 2, then θ approaches infinity for every value of x. Hence, if equation (3) were valid up to this limit, every point of the plate would be at infinitely high temperature. θ/θ_0, however, would keep the finite value

$$\frac{\theta}{\theta_0} = \cos\left(\xi \cdot \frac{\pi}{2}\right). \qquad \ldots\ldots(7)$$

The temperature distribution for $\sigma = 0$ and $\sigma = \pi/2$ is represented in figure 9; it changes surprisingly little in the whole range from $\sigma = 0$ to $\sigma = \pi/2$ (infinitely high temperature).

The mean temperature is obtained from the equation of definition

$$\theta_m = \frac{1}{s}\int_0^s \theta \,.\, dx.$$

Substituting from equation (4) and integrating,

$$\theta_m = \frac{1}{\epsilon}\left(\frac{\tan\sigma}{\sigma} - 1\right). \qquad \ldots\ldots(8)$$

From equations (5) and (8) one obtains the ratio

$$\phi = \frac{\theta_m}{\theta_0} = \frac{\sin\sigma - \sigma\,.\,\cos\sigma}{\sigma(1-\cos\sigma)}. \qquad \ldots\ldots(9)$$

This equation can be used to calculate the maximum temperature excess θ_0 from θ_m which is easily determined by measuring the increase of the coil resistance when carrying current.

For $\sigma = 0$, that is, uniform heat development, $\phi = 2/3$. For the other limit ($\sigma = \pi/2$) equation (9) yields $\phi = 2/\pi$, that is, only $4\frac{1}{2}\%$ less, independent of the thickness of the plate and the value of the temperature coefficient ϵ.

For cylindrical and spherical coils similar equations were derived to those for the plane plate.

The only difference in the solution for the cylinder is that the equations contain the Bessel function of zero order and first kind, J_0, wherever the cosine-function occurs in the equations above, and infinitely high temperature would take place where the Bessel function becomes zero, i.e. at the first zero point of J_0 which occurs for $\sigma = j_{0,1} = 2{\cdot}4048\ldots$

For the sphere the cosine-functions in equations (4), (5), and (6) have to be replaced by $[\sin(\xi\sigma)]/(\xi\sigma)$, including $(\sin\sigma)/\sigma$ and the temperature approaches infinity when $\sigma \to \pi$.

The temperature distributions (figures 10 and 11) cover a band which is only slightly wider than the one between $\sigma = 0$ and $\sigma = \pi/2$ in figure 9.

The upper limit ($\sigma = 0$) of this band is in all cases the parabolic distribution (equation (2)), the lower limit is given by equation (7) for the plate,

$$\theta/\theta_0 = J_0(\xi \,.\, j_{0,1}) \quad \text{for the cylinder,} \qquad \ldots\ldots(10)$$

and

$$\theta/\theta_0 = [\sin(\xi\pi)]/(\xi\pi) \quad \text{for the sphere.} \qquad \ldots\ldots(11)$$

The practically important ratio $\phi = \theta/\theta_0$ takes maximum values 0·667, 0·5, and 0·4 (for uniform heat development) and minimum values of 0·637, 0·432, and 0·304 (at infinite tempera-

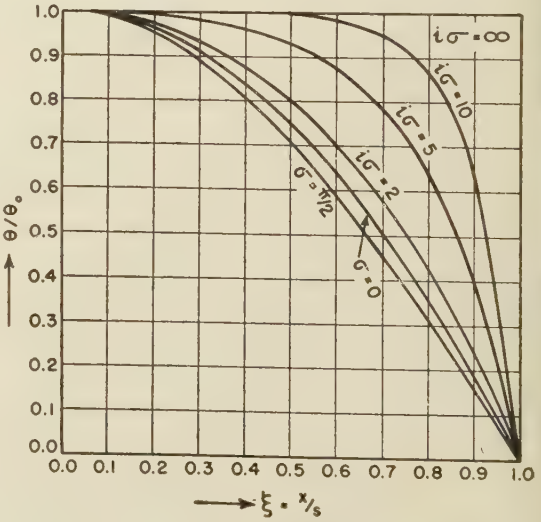

Figure 9. Temperature distribution in infinitely wide plates.

ture) for plane plate, cylinder and sphere, respectively.

Obviously, engineers neglecting in their calculations the influence of non-uniformity of heat generation in a coil, were just lucky; they could scarcely have foreseen that a relatively small increase in current would theoretically lead to infinitely high temperature and yet to such small influence upon the ratio ϕ.

(c) *Temperature distribution in bodies of simple form developing or absorbing heat at a linear function of temperature*

The relations for the temperature distribution in electrical coils given in §3 (b) are also valid for the case of chemical exothermic reactions in a range where a linear increase of the heat development with temperature can be assumed.

It is easily understood that they will hold also for endothermic reactions ($q''' < 0$; $m < 0$) in the range where equation (3) is valid and $n > 0$, that is, for heat absorption increasing with decreasing temperature. In particular, θ/θ_0 remains entirely unchanged; however, θ, θ_0, and θ_m assume negative values, as they must be in endothermic reactions.

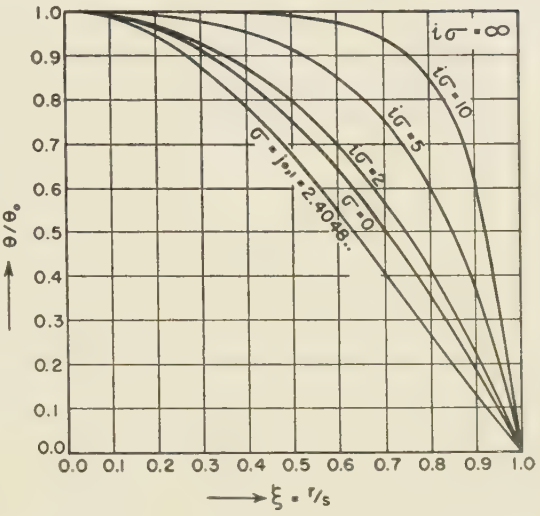

Figure 10. Temperature distribution in infinitely long cylinders.

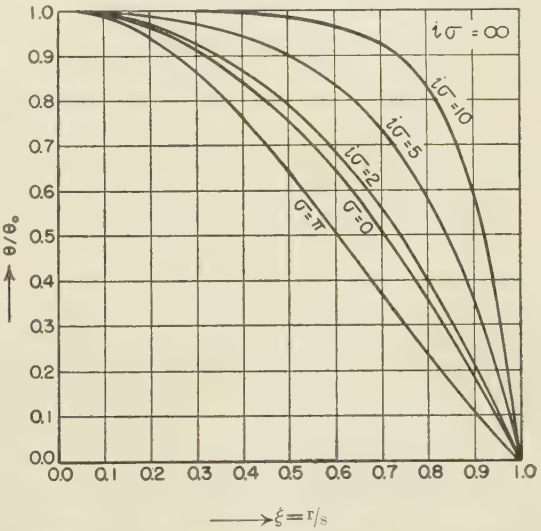

Figure 11. Temperature distribution in spheres.

Also the limit of an infinite temperature value, shown in figures 9, 10, and 11, would be theoretically the same. However, just as a coil would burn through, or equation (3) would cease to be valid long before an infinitely high temperature were obtained, any endothermic reaction would stop before the absolute zero point of temperature were attained.

Similar relations to those given in §3 (b) have recently been derived (Jakob, 1947) for electric heat sources with negative temperature coefficient of the Joulean heat, i.e. heat development decreasing linearly with increasing temperature, as may occur in the carbon of electric-arc lamps or graphite electrodes, or in electrolytes; these equations then are also valid for exothermic reactions with negative temperature coefficient, and for endothermic reactions

with $n<0$, that is, when the absorption of heat increases with temperature. In the latter case, again, θ assumes negative values.

The procedure of derivation is similar to that shown in §3(b). In general, the results, including those of §3(b), may be represented by two equations:

$$\frac{\theta}{\theta_0}=\frac{f(\xi\sigma)-f(\sigma)}{1-f(\sigma)}, \qquad \ldots\ldots(12)$$

and

$$\frac{\theta}{\theta_0}=\frac{g(i\xi\sigma)-g(i\sigma)}{1-g(i\sigma)}, \qquad \ldots\ldots(13)$$

where $i=\sqrt{-1}$ and f and g are function symbols. Considering, for instance, $f(\sigma)$ and $g(i\sigma)$, the first one means $\cos\sigma$, $J_0(\sigma)$, and $(\sin\sigma)/\sigma$, and the second one $\cosh(i\sigma)$, $I_0(i\sigma)$, and $[\sinh(i\sigma)]/(i\sigma)$ for the plate, cylinder and sphere, respectively. The function f belongs to exothermic and endothermic processes with positive n, the function g to the same with negative n; generation of Joulean heat is included in the exothermic processes. The argument $i\sigma$ is always real and positive. In figures 9, 10 and 11 the families of curves above the parabola which is common to plane, cylinder and sphere belong to equation (13). They approach an upper limit, $\theta/\theta_0=1$, when $\sigma\to\infty$.

§4. HEAT CONVECTION

(a) *Studies on free convection*

The Nusselt and Grashof numbers for the free convection on a vertical surface of height H and temperature t_s to a fluid of temperature t_m are usually defined by $(N_{\mathrm{Nu}})_{\mathrm{H}}=\frac{hH}{k}$ and $(N_{\mathrm{Gr}})_{\mathrm{H}}=\frac{\beta g}{\nu^2}H^3(t_s-t_m)$, where h is the film coefficient of heat transfer and k, β and ν are the thermal conductivity, coefficient of thermal expansion, and kinematic viscosity of the fluid, respectively.

Employing the principle of similarity, Nusselt (1915) showed that $(N_{\mathrm{Nu}})_{\mathrm{H}}$ is proportional to $H^{3/4}$, a result which previously had been obtained analytically by Lorenz (1881). This, however, is only a fair approximation to the actually much more complicated relation between h and H, as has later on been demonstrated by different workers. Moreover, Griffiths and Davis (1922) have shown by experiments that above a certain height (about 2 feet for air) h becomes independent of H and proportional to t_s-t_m. They correctly concluded that turbulence occurs above that height.

Considering the general form

$$N_{\mathrm{Nu}}=C(N_{\mathrm{Gr}}.N_{\mathrm{Pr}})^n, \qquad \ldots\ldots(14)$$

where N_{Pr} is the Prandtl number, a correlation of King (1932) proved that $n=\frac{1}{4}$ and $\frac{1}{3}$ occur for the laminar and turbulent range, respectively. This holds also for not too vehemently boiling water according to experiments of Jakob and Fritz (1931) and Jakob and Linke (1933, 1935).

The latter workers, in particular, showed that $n=\frac{1}{3}$ may be used for the convection on the upper side of a horizontal plate on which water is boiling, and they concluded that in the range of their experiments ($q''=7$ to 5200 B.hr.$^{-1}$ ft.$^{-2}$), the coefficient of convection on a horizontal plate is independent of the size

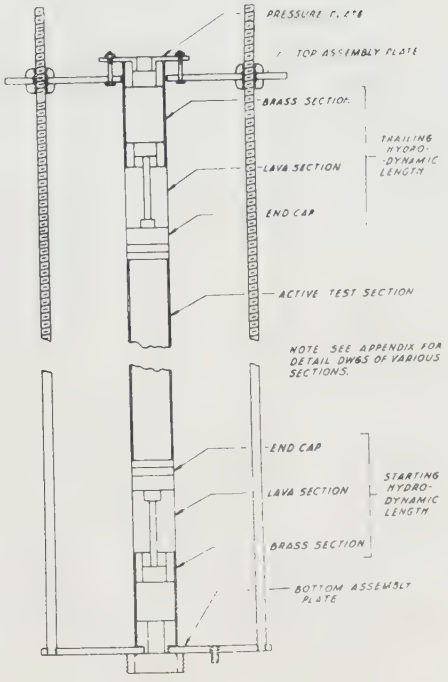

Figure 12. Vertical-cylinder arrangement for free-convection experiments.

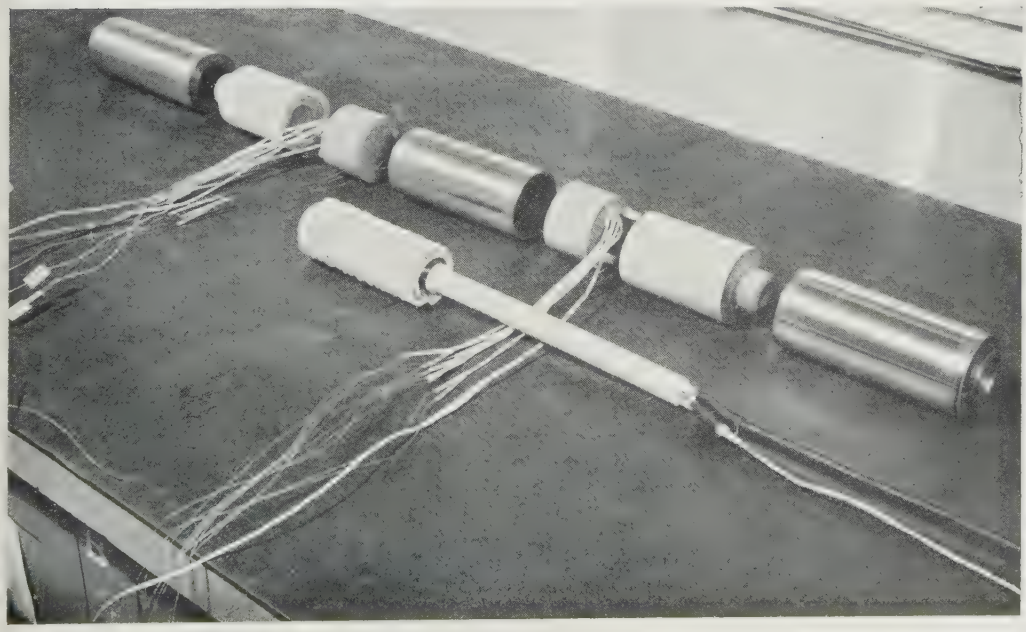

Figure 13 Parts of apparatus for free-convection experiments.

To face page 736

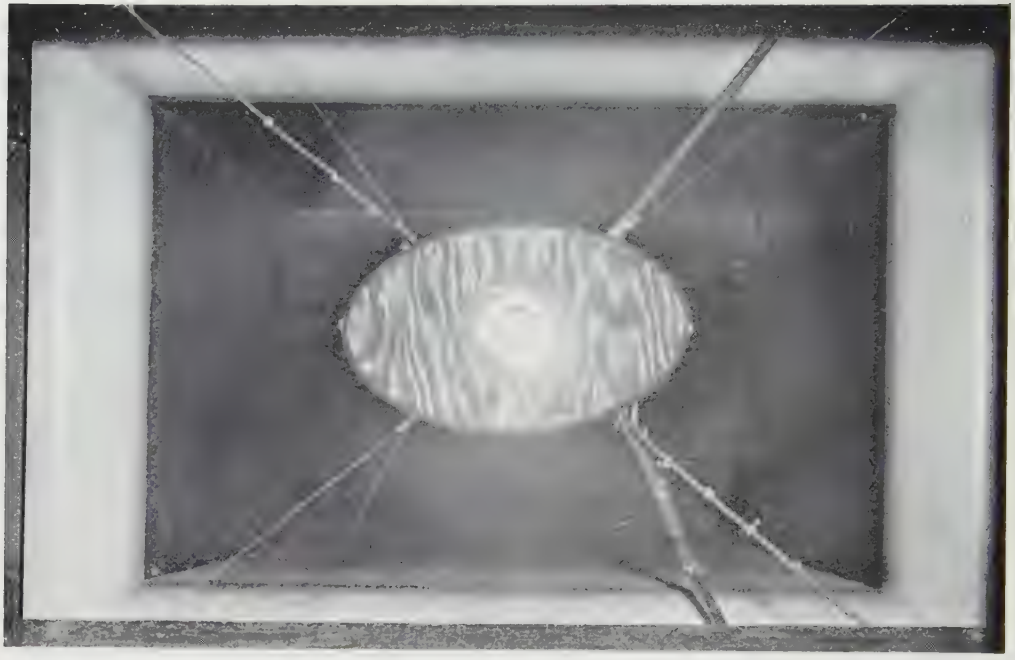

Figure 26. Arrangement of Calorimeter No. 2 in wind tunnel (front side).

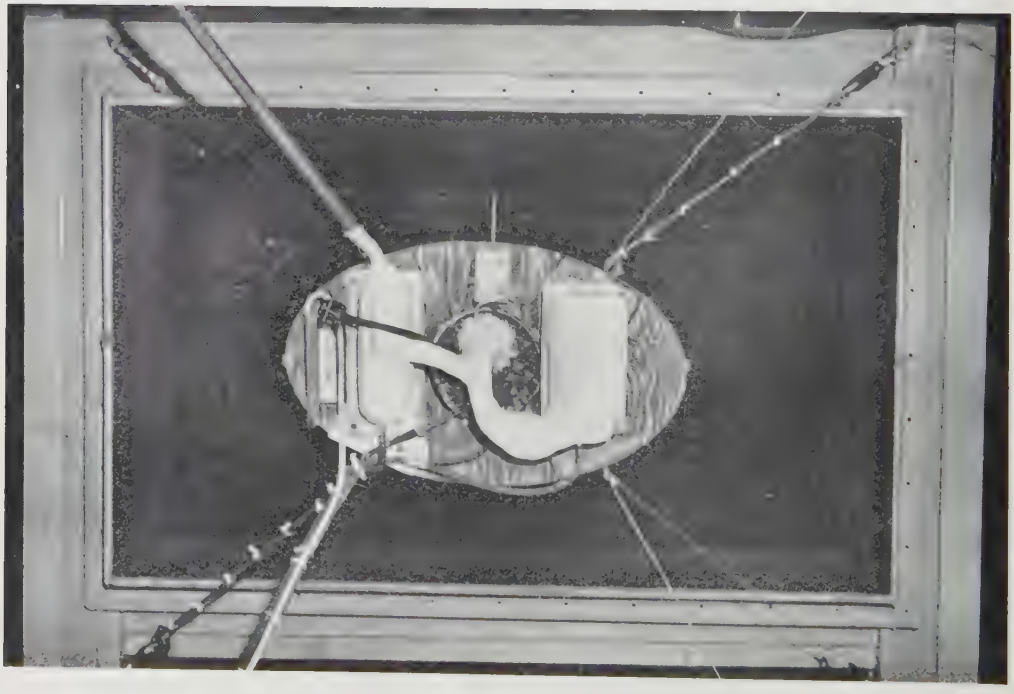

Figure 27. Arrangement of Calorimeter No. 2 in wind tunnel (rear side).

of the plate except for a possible effect of the edges. This was to be expected because there is no reason why the heat transfer on one place of a large horizontal plate should be different from that at any other place.

In other words, if equation (14) is valid, then $n = \frac{1}{3}$ must necessarily occur in all cases where no reason exists why h should depend on a characteristic length.

The heat transfer by free convection from vertical cylinders to non-boiling liquids (water and ethylene glycol) has recently been investigated by Touloukian, Hawkins, and Jakob (1947). Long cylinders, $2\frac{3}{4}$ inches in diameter, were composed from heating elements, starting and trailing pieces as is shown in figures 12 and 13. Three sizes of heating elements, 6, 12, and 36 inches long, but always the same starting piece (12 inches long) and trailing piece (13 inches long) were employed in the experiments. The cylinder assembly was placed in a cylindric shell of 12 inches inside diameter which contained the liquid.

The test sections consisted of brass tubes containing electrical heaters. Surface temperatures were measured on different places by means of thermocouples in slots which were cut into the surface and were afterwards closed by strips of lead. A number of thermocouples were distributed in the liquid bulk. Fifteen thermocouples inside each end-cap (see figure 12) served to determine the heat losses through the caps. These were made of Transite board, an insulating cement-asbestos compound.

The lava and brass sections (figure 12) served for mounting the test section and as hydrodynamic starting and trailing pieces.

In order to prevent the liquid from penetrating the joints of the cylindric test section and to make the porous Transite and lava sections impermeable to liquids, several thin coats of a special resin were applied to the surface with a spray gun and baked on with a battery of infra-red lamps.

The range of experiments is shown in table 2.

Table 2. Range of experiments about free convection in liquids on vertical surface

Item	Symbol	Minimum	Maximum	Units*
Height of heating section	H	0·5	3·0	ft.
Surface temperature	t_s	90·5	239·5	°F.
Temperature difference	$t_s - t_m$	3·5	83·5	F.
Coefficient of heat tranfer by convection	h	17·6	151·0	B.hr.$^{-1}$ ft.$^{-2}$ F.$^{-1}$
Nusselt number	N_{Nu}	89·0	903·0	—
Grashof number	N_{Gr}	2·2(10^6)	326(10^9)	—
Prandtl number	N_{Pr}	2·4	117·8	—
Product of Grashof and Prandtl numbers	$N_{Gr} \cdot N_{Pr}$	280(10^6)	904(10^9)	—

The tests in the laminar region led to an exponent $n = \frac{1}{4}$ in equation (14) as would be expected. In the turbulent region, however, equation (14) had to be replaced by

$$N_{Nu} = C(N_{Gr} N_{Pr}^{m})^{n}, \qquad \ldots\ldots(15)$$

* For several years the author has used the symbols C and F as units of temperature *differences* in the Centigrade and Fahrenheit scales, and the symbols °C. and °F. for temperatures in these two scales. This distinction seems to be useful and is recommended for general adoption.

with $m = 1{\cdot}29$ and $n = 1/3$ in order to correlate the results by a unique line. This indicates that the term of acceleration in Stokes' equations cannot be entirely neglected as is done when the same exponent is given to N_{Gr} and N_{Pr}.

The correlations are represented in figures 14 and 15.

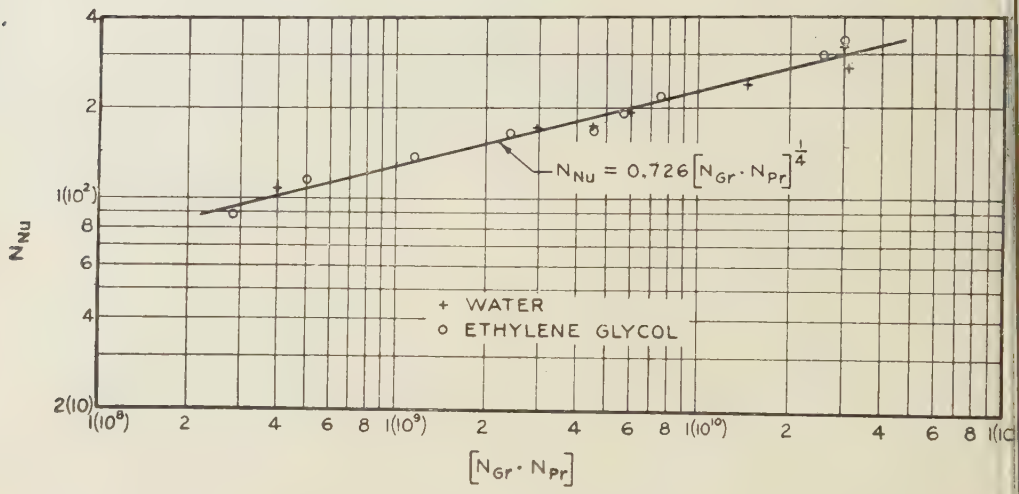

Figure 14. Heat transfer by free convection of liquids on vertical cylinders (laminar range).

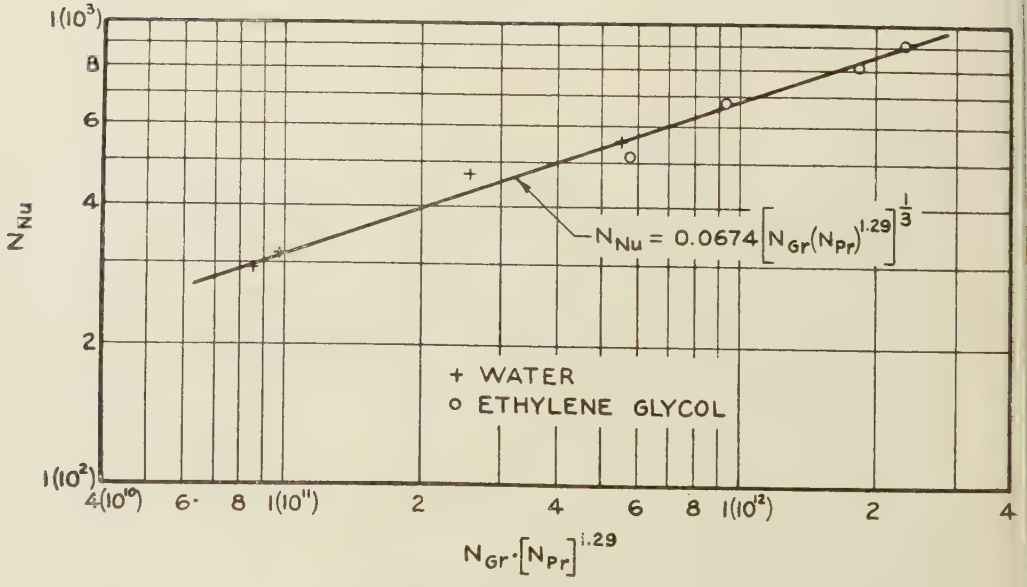

Figure 15. Heat transfer by free convection of liquids on vertical cylinders (turbulent range).

The characteristic exponents 1/4 and 1/3 were also applied in a new correlation of experiments on free convection through enclosed plane gas layers (Jakob, 1946). Mull and Reiher (1930), in a remarkable experimental investigation, had used two parallel plates, each 40 inches long and 24 inches wide, which were separated by air layers. These could be divided in different ways

so that it was possible to study enclosed air layers having areas of 30 to 960 square inches. Air layers of seven different thicknesses from $\frac{1}{2}$ to $7\frac{3}{4}$ inches were employed. One of the two plates was an electrical heating plate and the arrangement was made in a manner to ensure that exactly measured amounts of heat flowed across the air layers. The system of plates could be rotated in a horizontal bearing so that the air layers could be brought into horizontal, vertical, or oblique position. The authors introduced the concept of an equivalent conductivity, k_c, which includes the effect of conduction and convection through the air layer (after deduction of the effect of radiation) and studied the ratio k_c/k in which k is the true thermal conductivity of the air. This ratio, as is well known, is identical with a Nusselt number UL/k where

$$U = \frac{1}{1/h_1 + L/k + 1/h_2} = \text{overall coefficient of heat transfer.}*$$

h_1, h_2 = film coefficients of heat transfer on the two surfaces, and L = the thickness of the air layer.

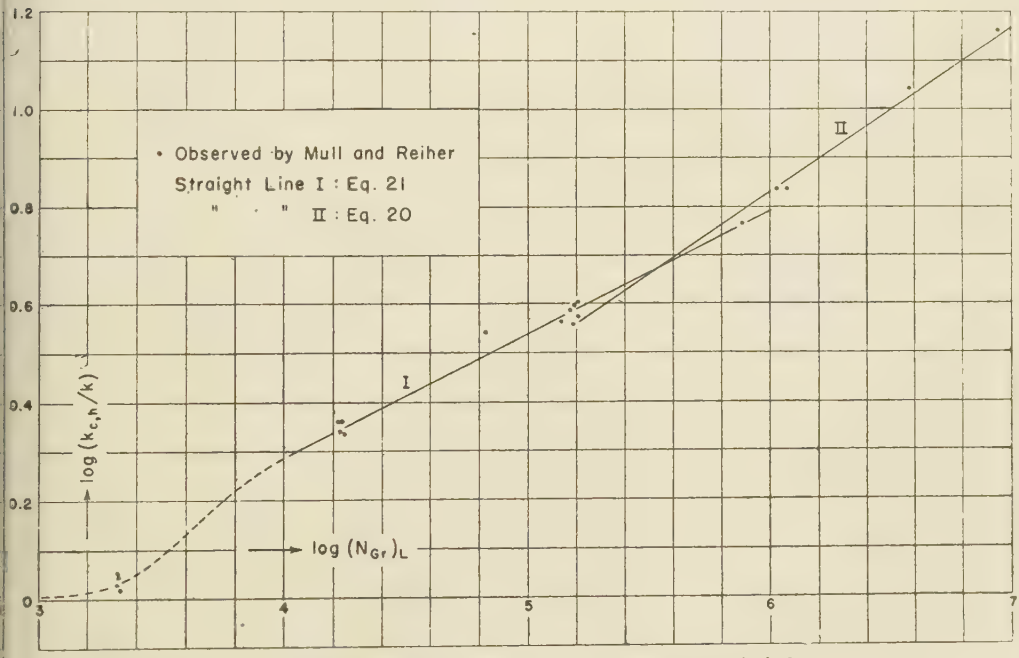

Figure 16. Heat transfer by free convection in horizontal air layers.

For horizontal layers (subscript h) with heat flow upward, Mull and Reiher represented their results by plotting $k_{c,h}/k$ versus $\log (N_{Gr})_L$, a Grashof number with the layer thickness L as characteristic length. In the experimental range of $(N_{Gr})_L = 2\,100$ to $8\,890\,000$ a smooth curve of increasing steepness was obtained which could not be represented by a simple formula. Representation in bilogarithmic coordinates, however (figure 16), reveals that in close relationship to other cases of free convection, two ranges must be distinguished and can be covered by two equations.

* After deduction of radiation.

In a lower range $(N_{Gr})_L \approx 10\,000$ to $(N_{Gr})_L \approx 400\,000$:

$$k_{c,h}\, k = 0{\cdot}195(N_{Gr})_L^{1/4}, \qquad \ldots\ldots(16)$$

In the turbulent range $(N_{Gr})_L > 400\,000$:

$$k_{c,h}/k = 0{\cdot}068(N_{Gr})_L^{1/3}. \qquad \ldots\ldots(17)$$

For $(N_{Gr})_L \to 0$, finally:

$$k_{c,h}/k \to 1, \qquad \ldots\ldots(18)$$

as indicated by a dotted line.

The meaning of equation (17), obviously, is that above a certain thickness L the coefficient of heat transfer does not change any more, but remains the same as for a single horizontal plate, facing upward. This was checked numerically and found to be in excellent agreement with an equation derived from the observations of Griffiths and Davis.

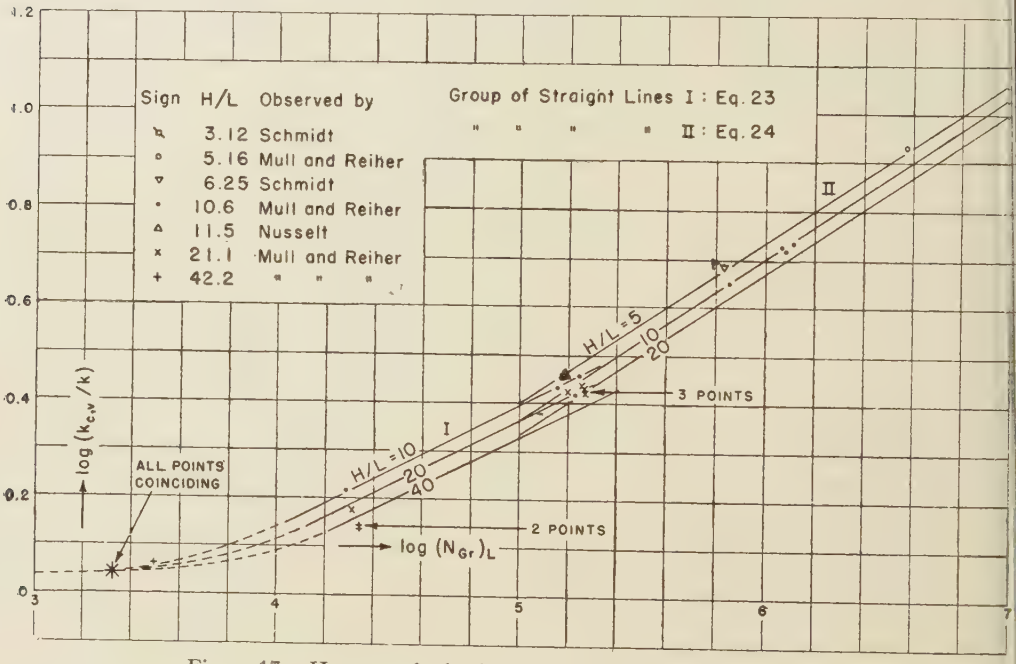

Figure 17. Heat transfer by free convection in vertical air layers.

For vertical layers (subscript v) of thickness L and height H, Mull and Reiher plotted $(k_{c,v}/k)(H/L)$, as measured, versus $\log (N_{Gr})_L$ and built up 27 curves with H/L as parameter, making ample use of interpolation and extrapolation since a total of only 21 points from their own and 3 from other experiments were available. Again, bilogarithmic plotting (figure 17) of the original points yields a much simpler and more reliable picture and two simple equations, namely for $(N_{Gr})_L = 20\,000$ to $200\,000$:

$$k_{c,v}/k = 0{\cdot}18(N_{Gr})_L^{1/4}(H/L)^{-1/9}, \qquad \ldots\ldots(19)$$

and for $(N_{Gr})_L = 200\,000$ to $10\,000\,000$:

$$k_{c,v}/k = 0{\cdot}065(N_{Gr})_L^{1/3}(H/L)^{-1/9}. \qquad \ldots\ldots(20)$$

Again, the exponents 1/4 and 1/3 of $(N_{Gr})_L$ are significant for laminar and

turbulent flow. The exponent $-1/9$ of H/L, however, was found empirically. At $H/L=0$, equations (19) and (20) would yield an infinitely large heat transfer, whereas the behaviour of single vertical plates should be approached; however, it seems that equation (20) is valid down to the ratio $H/L \approx 3$.

For oblique layers, linear interpolation between the results of equations (17) and (20) gives reasonable results.

Finally it must be mentioned that Mull and Reiher's tests, as well as the above equations, do not take account of any convection or conduction effect of the border strips which close the gas layers.*

(b) *Heat transfer to a fluid in laminar flow through an annular space*

The experimental part of this investigation (Jakob and Rees, 1941) was performed with an arrangement originally constructed and used for the determination of the true temperature and the heat exchange in a catalytic reaction (Jakob, 1938 and 1939). A sketch of the annulus with the thermocouples used is shown in figure 18, in which the distances in the length direction are represented in the right proportions; those in radial direction are magnified and not to scale. The annulus, 1500 mm. long, was formed by two vertical co-axial nickel tubes T_1 of 4·05 mm. o.d., and T_2 of 8·1 mm. i.d. A thin-walled steel tube containing a fine thermocouple could be shifted up and down inside T_1. On the outside of tube T_2 eleven fine iron-constantan thermocouples were fixed. Another thirteen couples were placed on the outer surface of a third nickel tube T_3 of 21 mm. o.d. A fourth tube T_4 of brass, 30·2 mm. o.d., was fitted with three heating coils, each covering a third of the tube length and provided with separate current control. Air, hydrogen, or ethylene were passed through the annulus and heated electrically so that the temperatures of the tubes T_1 and T_2 increased as linearly as possible over the length of Section II. Then a convection-heat coefficient h_{21} was found which was defined by the equation

$$V C_p \,.\, \Delta t = h_{21} .\, 2\pi r_2 \,.\, L \,.\, \delta t,$$

where $\dot{V}$ = the time rate of volume flow, C_p = the specific heat of unit volume of the gas at constant pressure, Δt = the temperature increase of the gas over a length L, r_2 = the inner radius of tube T_2, and δt = the average temperature difference between tubes T_2 and T_1.

Up to about 2% of the heating energy crossed the annulus in the form of radiation and was then supplied to the gas from the inner wall. Average gas temperatures were from 31 to 105° C. with temperature slopes from 0·15 to 0·80 C./cm. and differences δt from 0·4 to 12·9 C. The Reynolds number N_{Re} was varied from 50 to 1000; it was defined by

$$N_{Re} = \frac{\dot{V} D_e}{\nu A}. \quad D_e = 2(r_2 - r_1) = \text{equivalent diameter of annulus.}$$

r_1 = the outer radius of tube T_1. ν = the kinematic viscosity of the fluid.

$A = \pi(r_2^2 - r_1^2)$ = the cross-sectional area of the annulus.

* Only after delivery of this lecture was a thorough experimental and theoretical paper of Elenbaas (1942) brought to the author's attention, in which the heat transfer from *both* surfaces to air layers *open* at the perimeter is treated. This case is somewhat related to the one dealt with above. It was not possible to compare the results and include an analysis of the comparison in this lecture.

The experimental results were compared with the theory in which laminar flow and invariable physical properties of the fluid were assumed. The derivation was based on the known equation of the velocity distribution across an annular space and on the heat-flow balance for a volume differential of the annulus. This led to the differential equation

$$\frac{\partial}{\partial r}\left(r\frac{\partial t}{\partial r}\right)=Nr\left(r_1^2-r^2+B\ln\frac{r}{r_1}\right)\frac{\partial t}{\partial x}-r\frac{\partial^2 t}{\partial x^2}$$

where $N=\dfrac{2\dot{V}C_p}{\pi Mk}$, $M=(r_2^2-r_1^2)(r_2^2+r_1^2-B)$ and $B=\dfrac{r_2^2-r_1^2}{\ln(r_2/r_1)}$.

In the case of uniform heating or cooling of the fluid from either or both boundary surfaces of the annulus, it can be supposed that the heat energy is absorbed or given up by the fluid in such a manner that at any sufficiently large

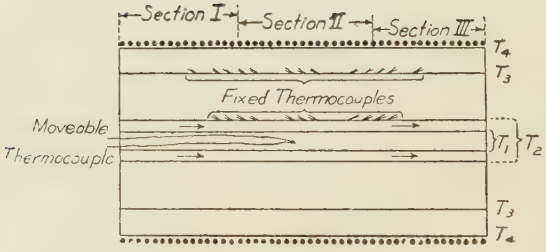

Figure 18. Sketch of annulus arrangement.

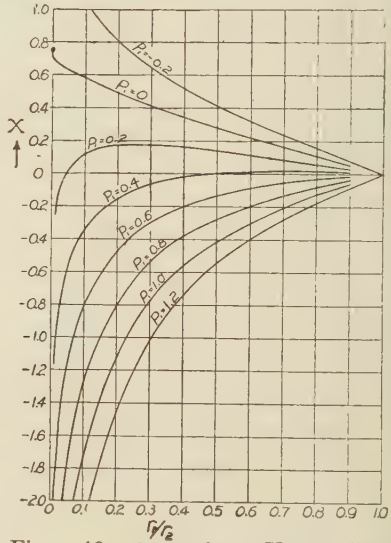

Figure 19. Shape factor X according to equation (21).

axial distance x from the entrance and at any radial distance r from the centre line the temperature increase per unit length is constant, so that

$$\frac{\partial t}{\partial x}=C=\text{constant, and }\frac{\partial^2 t}{\partial x^2}=0.$$

Let the time rates of heat entering the annulus from the inner and outer surface (subscripts 1 and 2) be q_1 and q_2, which can be different in numerical value and sign; further,

$$q=q_1+q_2 \quad\text{and}\quad P_1=q_1/q, \quad\text{whilst}\quad P_2=1-P_1=q_2/q.$$

Then for temperatures t_1 and t_2 and for any value x:

$$\frac{t_2-t}{CL}=\frac{\delta t}{\Delta t}=\frac{\dot{V}C_p}{2\pi kL}\frac{1}{(1-y^2)(1+y^2-z)}\{(1-y^2)[\tfrac{3}{4}(1+y^2)-z]$$
$$+y^2(y^2-z)\ln y+[1-z-y^2(y^2-z)]P_1\ln y\}$$
$$=\frac{\dot{V}C_p}{2\pi kL}X=\frac{1}{2\pi}N_{Gz}.X, \qquad \text{.....(21)}$$

where $y = r_1/r_2$ and $z = \frac{y^2-1}{\ln y}$, N_{Gz} = the Graetz number, and X is a function, both defined by equation (21).

By this equation it is possible to calculate the ratio of the temperature difference across the annulus, δt, to the temperature increase along the annulus, Δt, from the Graetz number and the term X which is also dimensionless.

Values of this term are represented in figure 19 and, according to equation (21), it is a linear function of fraction P_1 which is used as parameter in the chart. Since, by definition, $P_1 + P_2 = 1$, the inequality $P_1 > 1$ indicates that some of the heat which is supplied to the fluid from the inner tube is given up to the outer tube and from this to the environment as occurs in heat exchangers consisting of three co-axial tubes. In the inverse case, $P_1 < 0$, heat is given up to the inside. It is easily understood that for $r_1/r_2 \to 0$ the function X will approach $\pm\infty$ for every finite value of P_1, because the transfer of a finite amount of heat by an infinitely thin wire requires an infinitely great temperature drop. Only for $P_1 = 0$ a finite value X = 0·75 occurs (see figure 19). For $r_1/r_2 \to 1$, on the other hand, X → 0.

Making allowance for some experimental difficulties explained in the paper, the experimental results obtained with one annulus and three gases of very different thermal conductivities were in reasonable agreement with the theory.

(c) *Forced heat convection in laminar and turbulent flow parallel to a surface*

Heat transfer between a surface and air flowing parallel to it is a process of great practical importance which, for instance, occurs with all kinds of fins or on the skin of an airplane in flight. Previous knowledge of that process was based on a few sets of experiments which were performed with plane surfaces and led to a considerably higher heat transfer than a theory due to Latzko (1921). In particular, the influence of non-heated starting sections seemed to require a new investigation. This has been undertaken by Jakob and Dow (1946) who employed an electrically heated cylindrical specimen. Compared with the use of plane plates the cylindrical arrangement has the following advantages: A cylinder can be easily placed in the centre of an air jet and is free of the edge losses of a plate; for both reasons, air jets of moderate diameter can be used. Uniform heating is easier to provide, heat losses to the rear are easier to control, and noses of different shape and cylindrical starting sections can readily be used for studying the behaviour of the boundary layer of the fluid which is developing along the surface, first streamlined and then turbulent, and in which all resistance against heat transfer is concentrated. The experiments were performed with specimens of 1·3 inches diameter and 9 to 20 inches total length, the ratio of the heated length to the total length being varied from 0·4 to 0·9. Spherical, ellipsoidal, and conical nosepieces were used. The air velocity was varied from 10 to 150 ft./sec.

Figures 20, 21 and 22 show the general arrangement and details of the heating and supporting tubes. The heating coil consisted of nichrome wire wound on a stainless steel tube. Paper rings insulated the heating tube from the wooden starting piece or nosepiece and from the supporting steel tube; the junctions

were smoothed by means of paraffin. Eight fine copper-constantan thermocouples for the determination of the surface temperature, t_s, were placed in four axial slots machined in the copper tube. Another thermocouple served to measure the temperature t_a of the airstream. Different secondary thermocouples in the wooden nosepieces and in the rear part of the heating-coil tube were used

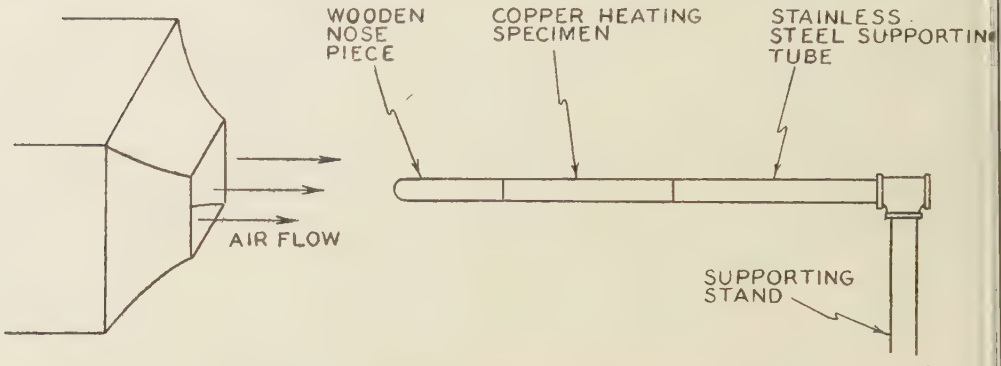

Figure 20. Arrangement for measurement of heat transfer in parallel flow.

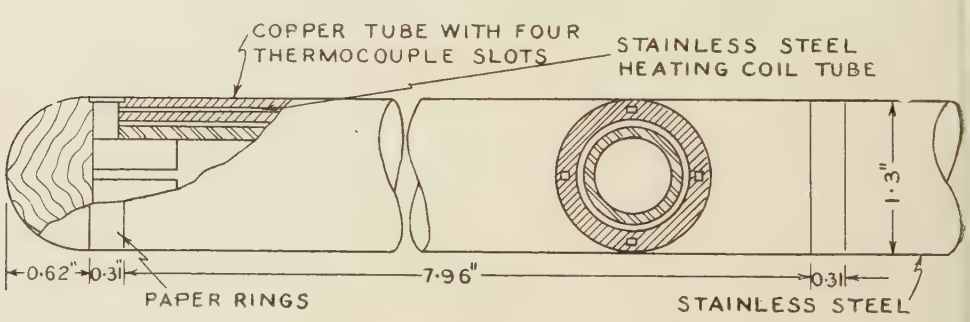

Figure 21. Heating specimen for parallel flow experiments.

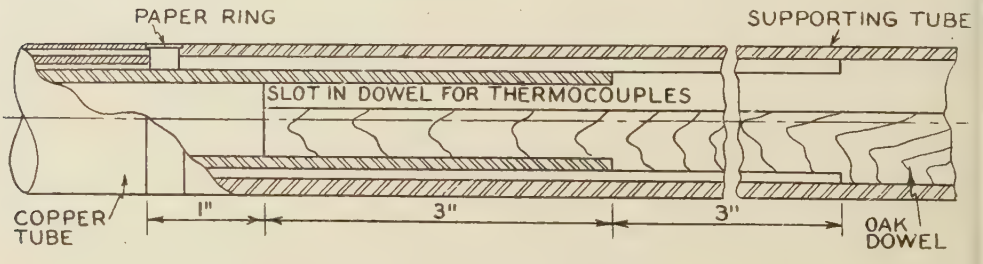

Figure 22. Supporting assembly for parallel flow experiments.

for heat-loss measurements. The air velocity, v_a, was measured by a Pitot tube.

A hemispherical nosepiece is shown in figure 21. The six different starting pieces used in the experiments are described in table 3. In this table L_{st} is the hydrodynamic starting length of the specimen, defined as the ratio of the surface area of the starting piece to the perimeter of the heating cylinder. The total

length, L_{tot}, is defined as the sum of L_{st} and the thermal or heating length, L_{th}, of 8 inches.

The experimentation consisted of velocity traverses, measurements of the input of the electrical heating coil, and thermoelectric measurements. The velocity traverses revealed that for a distance 2 feet downstream from the nozzle, the air velocity varied less than 1% within an 8-inch core. The rate of heat losses, q_j, including also radiation, was found to be 2·8 to 6·7% of the heat input, q_i. The mean coefficient of heat transfer by convection was found from the equation

$$h = \frac{q_i - q_j}{A(t_s - t_a)},$$

where A is the area of the heating surface.

Table 3. Starting pieces

Specification	L_{st} (ft.)	L_{tot} (ft.)	L_{st}/L_{tot}
Cylinder with hemispherical nose	1·026	1·693	0·606
Cylinder with hemispherical nose	0·689	1·356	0·508
Cylinder with hemispherical nose	0·354	1·021	0·347
Conical piece (4 in. long)	0·187	0·854	0·220
Ellipsoidal nose	0·092	0·759	0·122
Hemispherical nose	0·075	0·742	0·101

The experimental results were expressed in terms of Reynolds and Nusselt numbers, defined by $N_{Re} = v_a L_{tot}\, \nu$ and $N_{Nu} = hL_{tot}\, k$, where ν is the kinematic viscosity and k the thermal conductivity of the air. ν was taken at the temperature t_a, k at the temperature $(t_a + t_s)/2$.

By plotting N_{Nu} versus N_{Re} it was found that transition to turbulence started at $N_{Re} = 60\,000$ to 200 000 and was fully developed at $N_{Re} = 250\,000$ to 600 000.

For the range of laminar boundary layers the results could be represented by the equation

$$N_{Nu} = 0{\cdot}590(N_{Re})^{0{\cdot}5}; \qquad \ldots\ldots(22)$$

for the range of fully established turbulence by

$$N_{Nu} = 0{\cdot}0280(N_{Re})^{0{\cdot}80}[1 + 0{\cdot}40(L_{st}/L_{tot})^{2{\cdot}75}]. \qquad \ldots\ldots(23)$$

Figure 23 shows these relations and the transition from laminar to turbulent boundary layer.

Comparing these equations with those found theoretically for heat transfer in the flow parallel to plane plates, it is seen that equation (22) is in excellent agreement with the equation derived theoretically by Pohlhausen (1921) for heat transfer in the flow parallel to a plane plate, whereas the constant factor of equation (23) exceeds the one according to Latzko's (1921) derivation by 11%. In Jakob and Dow's paper it is shown that this is probably due to the surface curvature. It is further shown that Fage and Faulkner (1931) came to much higher values of the constant in equation (22), probably because starting conditions prevailed in their surfaces of only 0·333 to 1·27 cm. length. The only experiments in the turbulent range which can be compared with ours seem to be those of Juerges (1924) performed with a plane plate and yielding 15% higher values

than we obtained. A blunt leading edge may have caused this increase in hea transfer. Éliás' (1929, 1930) values, which lie between Juerges' and our results scatter considerably. A recent paper of Eckert and Drewitz (1940) shows tha Pohlhausen's theory is valid up to twice the velocity of sound if the fluid tem perature is replaced by a temperature impressed on the surface, due to adiabati stopping and friction of the stream. The same is claimed for the turbulen boundary layer. It may be concluded that, when the equilibrium fluid tempera ture is replaced by the "impressed temperature" of the surface, the result of Jakob and Dow can also be approximately employed to much higher than the experimental velocities. Considering that our results in the turbulen

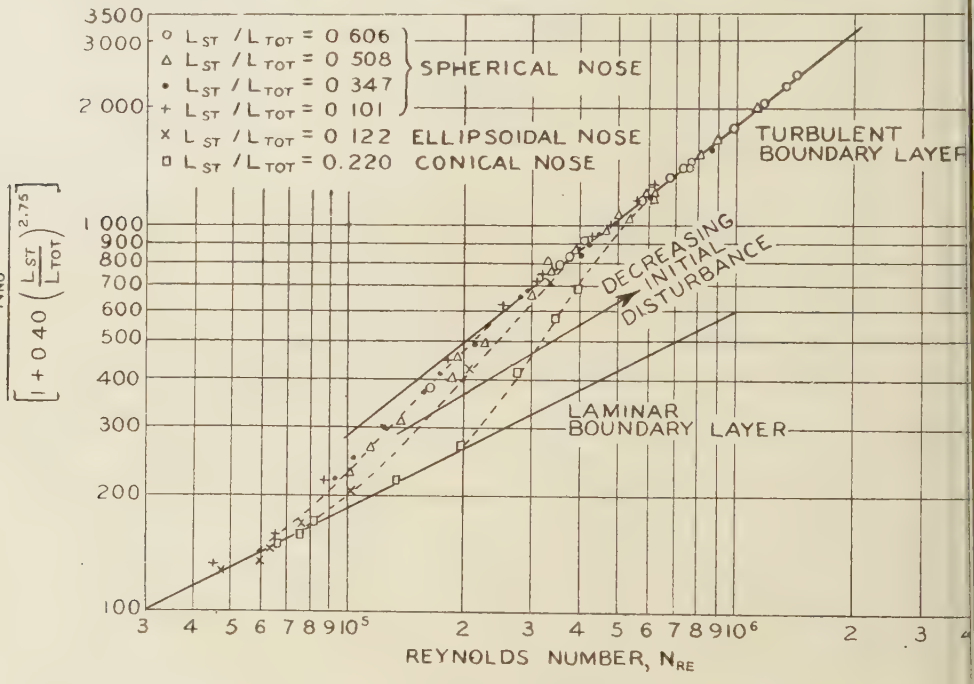

Figure 23. Heat transfer in parallel flow.

range are almost between the theoretical ones of Latzko and the experimental ones of Juerges, it seems to be safe to use equation (23) tentatively for any convex smooth surface with arbitrary starting section where the radius of curvature in a plane perpendicular to the main flow direction is more than $\frac{1}{2}$ inch.

(d) *Forced heat convection in turbulent flow against a surface.*

Surprisingly little has been published regarding the heat transfer in the flow of air perpendicular or oblique to a large surface. There is the following statement of Reiher (1929):

"In blowing air perpendicularly to a surface, coefficients of heat transfer have been measured which, depending on the air velocity, were seven to eight times those determined by Nusselt and Juerges in flow parallel to the plate surface."

However, no experimental data or theoretical deductions have been published to substantiate this statement according to which the heat transfer close to the

stagnation point would be unusually great. On the other hand, experiments by Rowley and Eckley (1931) at air velocities of less than 45ft./sec. indicated that the heat transfer of air impinging upon a surface perpendicularly is appreciably smaller than for parallel flow.

Since the heat transfer in the flow of air perpendicular or oblique to a surface plays an essential rôle in the formation, melting, and sublimation of ice on wind-shields and other parts of the outer surface of an airplane, experiments were sponsored by the U.S. Army Air Forces for the purpose of deciding between the above mentioned contradictory results, extending experience to higher velocities, furthering the understanding of the heat transfer in the flow of air against surfaces, and using the results for the calculations of ice formation and sublimation on wind-shields of airplanes. Two weeks before this lecture I presented a report on these experiments to the 6th International Congress for Applied Mechanics in Paris (Jakob and Kezios, 1946).

Owing to the practical purpose of the investigation one might have considered it as most promising to perform experiments under conditions of environment favourable to ice formation. However, quantitative experimentation imitating actual flight conditions would have been quite intricate. Fortunately, results obtained under conditions most convenient for laboratory tests can be converted to actual atmospheric conditions encountered in flight, by means of the theory of similarity. For this reason the experiments were performed with air approximately at standard atmospheric conditions and with surfaces at relatively high temperature (about 212° F.). The principle of similarity was then used to convert the results to conditions of flight at great altitude, i.e., low air pressure, low temperature, and considerably higher air velocities than were available in our laboratories. Finally, the theory of similarity between heat and mass transfer was used to calculate the amounts of ice that would be formed or sublimed on an exposed surface under conditions of flight.

The method of investigation was to expose the test plates to a homogeneous air-jet produced by a blower, or to bring them into the test section of a wind tunnel. The plates were heated from the rear by condensing steam and the heat transfer was determined by the rate of steam condensed (condensing-steam calorimeter). The temperature differences were measured by thermocouples. the flow velocities by Pitot tubes.

Figure 24 is a cross-section of our calorimeter No. 1. Its main parts are a heating plate A of 4 inches diameter and a guard-ring B, both of copper and chromium-plated, which are separated by air, except for the thin paper ring C; the main steam chamber D and the guard steam chamber E which prevents heat

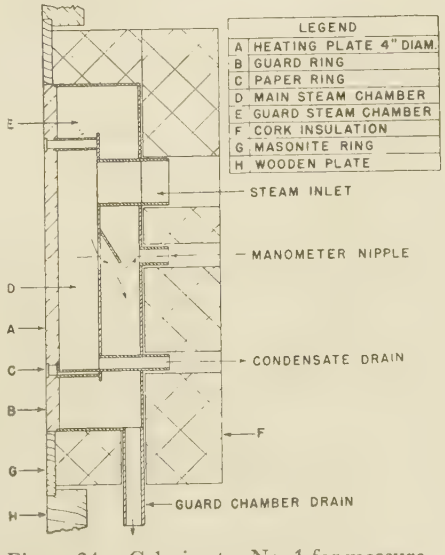

Figure 24. Calorimeter No. 1 for measurement of heat transfer in air flow against a plate.

loss from D; auxillary parts are the cork insulation F and the Masonite ring G which is inserted into the wooden plate H of rectangular shape, 34 inches (horizontal) × 37 inches (vertical).

Chamber D has its inlet at the top and its condensate outlet at the bottom. Chamber E is fed from the back of D. Four copper-constantin thermocouples were placed in holes drilled below the exposed surface of the calorimeters. Two more were attached to the back of the paper ring and served to determine the heat loss through this ring. A seventh thermocouple was used to measure the temperature of the incoming air.

Figure 25 is a schematic diagram of one of the experimental arrangements. The calorimeter was exposed to a free air stream delivered by a blower and could be turned around a horizontal axis to bring the surface into a position oblique to the air stream. Steam was formed in a small electrically heated boiler and dried by mechanical type steam separators.

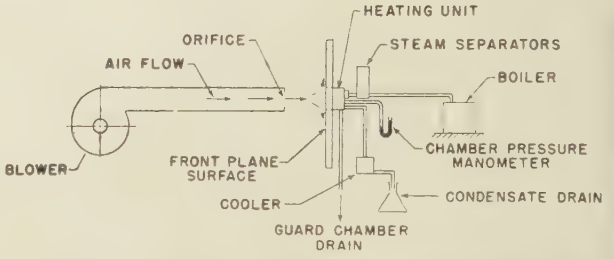

Figure 25. General arrangement for measurement of heat transfer in air flow against a plate.

Figures 26 and 27 are photos of the arrangement of our calorimeter No. 2, in the open section of the wind tunnel (throat dimensions 48 inches (horizontal) × 28 inches (vertical); distance between throat and diffusor 29½ inches). This calorimeter, whose main heating surface had a diameter of 2 inches, was inserted in a wooden plate of elliptical shape (axes 20·6 and 12 inches). Since the cross-sectional area of the free jet was 467 times that of the main heating surface, the conditions imposed approached those of the small stagnation area of a rather large surface in an infinitely wide air stream. Two steam separators which were connected in series and insulated by magnesia, and other apparatus, were placed in the wind shade on the rear of the wooden plate (see figure 27).

Experimentation consisted of measurements of air pressure and velocities, temperatures of air and calorimeter, steam pressure and condensate weight. The mean jet velocity as well as the velocity components parallel to the heat transferring surface were determined by traverses, the latter ones at $\frac{3}{16}$ inch distance from the plate surface.

Figure 28 is a sketch of the flow distribution over the exposed surface which is at an angle α from the vertical plane. For $\alpha = 0°$ the flow would have its stagnation point at the centre O of the plate for reasons of symmetry; at an angle $\alpha \lesssim 0$ the stagnation point will be shifted, for instance, to S. The velocities on the surface were determined as follows (see figure 29):

First the stagnation point was found as that point where impact and static pressure tubes showed identical values. The air flow over the heating plate is limited between the lines SL and SR. The radii, SL, SC, and SR and the arcs 1-1, 2-2, and 3-3 intersect in 9 points. At these points the radial velocity (with S as centre) of the air was determined.

The scope of five series of experiments with a total of 61 runs is given in table 4.

Table 4. Experiments with air flowing against a heating surface

Series	Run No.	Calori-meter No.	Air jet: Source	Air jet: Outlet	Air jet: Thickness (in.)	Distance between outlet and plate (in.)	Direction of impact	Diameter of heating plate (in.)
A	1–20	1	Blower	Orifice	7 (diam.)	20	Perpendicular	4
B	21–32	1	Blower	Orifice	7 (diam.)	10	Perpendicular	4
C	33–37	1	Blower	Orifice	10 (diam.)	10	Perpendicular	4
D	38–46	1	Blower	Orifice	10 (diam.)	10	Oblique ($\alpha=30°$)	4
E	47–61	2	Wind-tunnel	Throat	48×28	16	Perpendicular	2

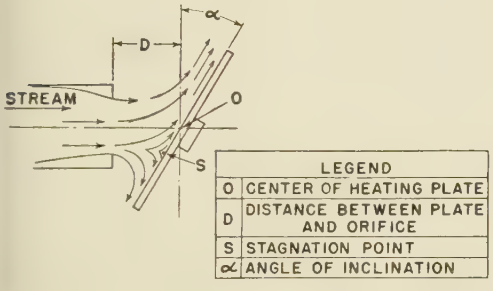

Figure 28. Sketch of air flow oblique to a plate.

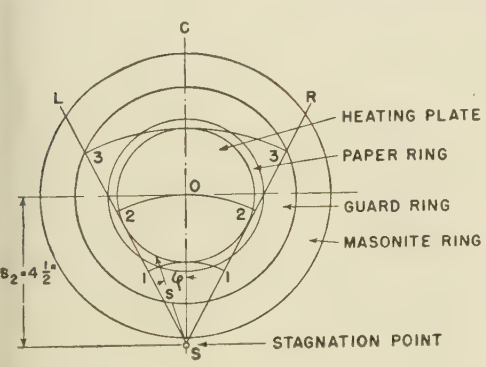

Figure 29. Range of air flow over inclined plate.

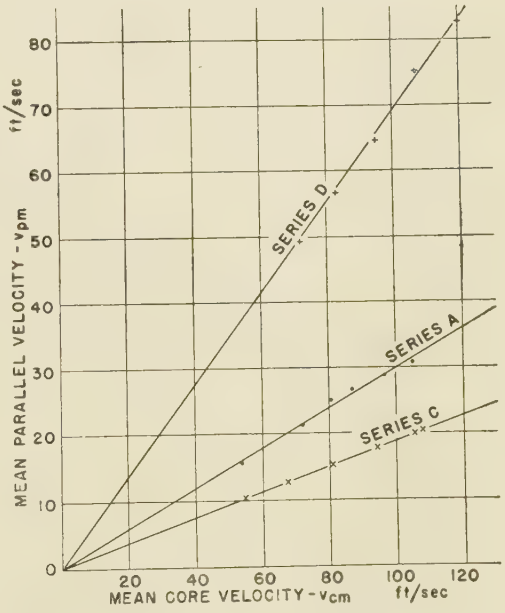

Figure 30. Parallel velocity versus core velocity in air flow against a plate.

The following definitions of velocities were used for representation and analysis of the experimental results:

The mean velocity of the core of the jet, v_{cm}, is the average velocity of that part of the jet which would hit the heating plate if the flow continued in the direction of the duct axis.

In Series A, B, C, and E the mean velocity parallel to the heating plate, v_{pm}, is identical with the mean radial velocity, v_{rm}, defined by the equation

$$v_{rm}=\frac{1}{\pi r_A{}^2}\int_{r=0}^{r=r_A} v_r \,.\, 2\pi r \,.\, dr,$$

where $r=r_A$ is the radius of the heating plate.

From figure 30 it is seen that, almost exactly,

$$v_{pm} = m \,.\, v_{cm}, \qquad \ldots\ldots(24)$$

where m is a constant for each series of tests ($m = 0{\cdot}300$ for Series A, $0{\cdot}191$ for C). This shows that the flow pattern in the experiments was not appreciably different from that of potential flow in which equation (24) should be strictly valid.

In Series D the stagnation point fell just outside of the Masonite ring (see figures 24 and 29), at $4\frac{1}{2}$ inches from the centre of the plate, independent of the velocity. It was found that v_p was almost constant over each of the circular arcs 1-1, 2-2, and 3-3. Graphical interpolation and integration then led to

$$v_{pm} = \frac{1}{A}\int_A v_p \,.\, dA,$$

where dA is an element of the surface $A = \pi r_A^2$.

As in Series A and C, the relationship between the measured mean core and mean parallel velocities could be represented by a straight line through the zero point of the coordinates in figure 30. Hence equation (24) was also valid for Series D, the constant being $m = 0{\cdot}694$.

The heat transfer by convection was determined from the latent heat of the steam and the weight of condensate formed in the main calorimeter chamber with due consideration of conduction and radiation losses. In the runs of Series D the stagnation point fell outside the guard-ring. Hence, the air in the boundary layer was pre-heated in flowing over the guard-ring plate, whereas the mean film coefficient of heat transfer was defined under the assumption that unheated air meets the main heating surface. An approximate analysis showed that for this particular arrangement the influence of preheating was almost negligible.

In figure 31 the observed values of h_m are plotted against v_{cm} in logarithmic coordinates. The lines A, B, C, and D belong to the series denoted by these letters. The points of Series A are considerably scattered, particularly at low velocities. Conceivably, the relative small ratio of jet width to distance between orifice and test plate caused some instability in the stagnation region. The points of the other series are much better in line.

For $v_{cm} > 50$ ft./sec. the film coefficient could be represented by

$$h_m = N c_{mc}^{\,n}, \qquad \ldots\ldots(25)$$

with the constants, N and n, as given in table 5.

Table 5. Constants of equation (25)

Line	N	n
A	1·037	0·567
B	0·991	0·571
C	0·856	0·571
D	0·889	0·567

However, Series B may be as well represented with $N = 0{\cdot}991$ and $n = 0{\cdot}475$ in the whole range of v_{cm} from 14 to 124 ft./sec. (dotted line B′). This exponent is close to the theoretical value 0·5 for the streamline region in parallel flow.

The component of $n \approx 0{\cdot}57$, according to table 5, on the other hand, seems to indicate that in general a turbulent state was prevalent at $v_{cm} > 50$ ft. sec. This is almost the same exponent as has been found in the flow across a cylinder.

Regarding the differences of N, only one detail may be discussed here. Line D is close to C, though in Series D the plate was tilted, the stagnation point was outside the heating plate, and the mean parallel velocities were much greater ($v_{pm} = 69{\cdot}4$ ft./sec. compared to 19·1 ft./sec., both at $v_{cm} = 100$ ft./sec.). Since case D is closer to the conditions of a true p rallel flow, a more pronounced impact effect in case C must have made good for the smaller parallel velocity.

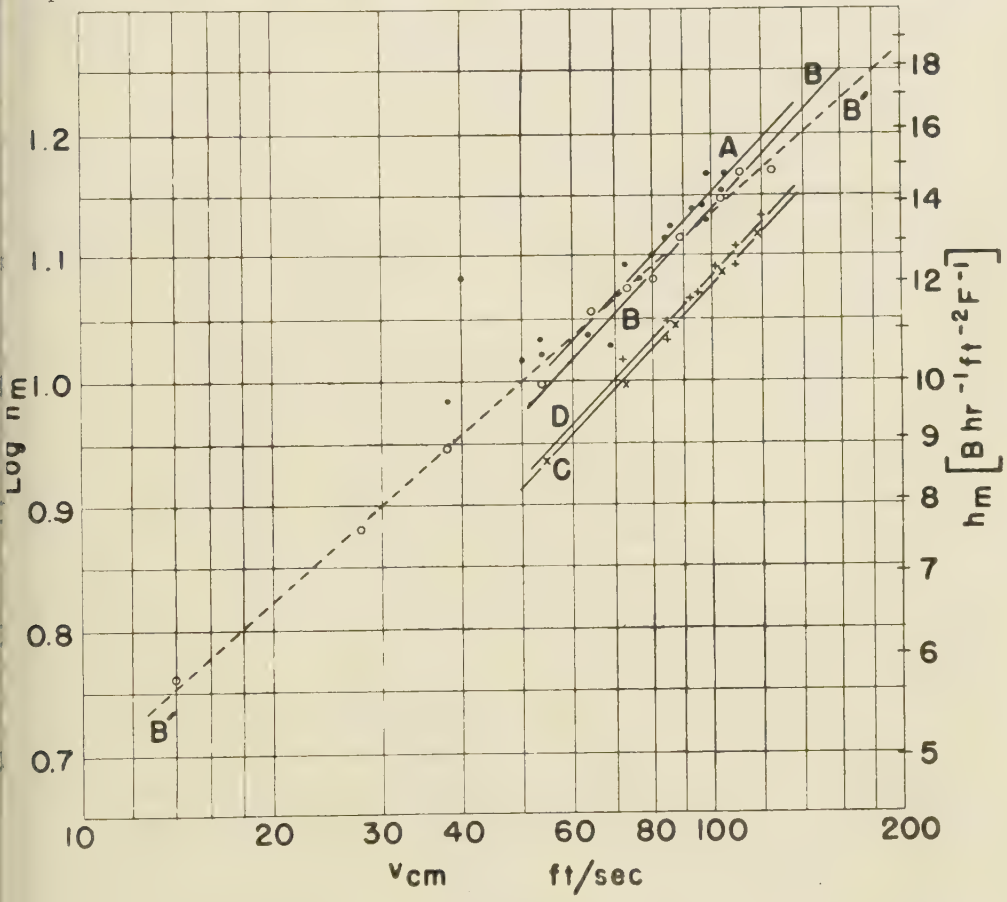

Figure 31. Heat transfer in air flow against a plate.

In the wind-tunnel tests with calorimeter No. 2, having a small heating surface, the heat transfer was so unstable that, notwithstanding all thinkable improvements of arrangement and frequent repetition of the tests, the points scattered by $\pm 30\%$. However, the average in these tests, $h_m = 11$ for $v_{cm} = 90$ ft./sec., is in good agreement with the corresponding point in line C, indicating that an increase of the jet thickness from 10 to about 40 inches and of the distance from 10 to 16 inches did not appreciably change the heat transfer.

It may further be concluded that the coefficient of heat transfer close to the stagnation point, as observed in a circular area of 1 inch radius, is not much

different from that observed in an area of 2 inches radius. No such singularit as mathematically might be expected seems to occur at the stagnation poin possibly just because the instability of flow masks any effect.

On the other hand, in strong contrast to Reiher's claim, the mean coefficien of heat transfer in the vicinity of the stagnation point remains much below tha for parallel flow at the same jet velocity, and the impact compensates only partl for the considerable reduction of heat transfer in the stagnation region. At bes the impact effect may be compared with a strong starting disturbance in the flo parallel to a surface.

Several applications of the results to flying conditions have been given i our report to the U.S. Air Corps. It may be sufficient to show the procedur on one of these examples.

An airplane, rising from relatively low altitude through an atmosphere i which some ice is formed on its wind-shields, continues travelling at 30000 fee altitude in dry air of $-50°$ F. with the speed of 300 miles per hour. Assuming that the surface temperature is kept slightly below 32° F., calculate the rate o sublimation of ice into the air per unit area close to the stagnation point and th rate of heat to be delivered to the wind-shield from inside the plane and given u to the atmosphere under these conditions.

The calculation may be based on equation (25) with $N=0{\cdot}87$ and $n=0{\cdot}57$ holding for standard atmospheric conditions ($p=760$ mm. Hg, $t_a=68$ F.).

The equation is a special case of the general form

$$N_{\mathrm{Nu}}=C(N_{\mathrm{Re}})^n, \qquad \ldots\ldots(26)$$

where $N_{\mathrm{Nu}}=h_m L$ $k=$the Nusselt number for a charateristic length L, $k=$the thermal conductivity of the air, $N_{\mathrm{Re}}=vL\rho$ $\mu=$the Reynolds number, $v=$the flight velocity, $\rho=$the density of the air, $\mu=$the dynamic viscosity of the air.

Assuming the same characteristic length for the considered spot of the wind-shield in flight as in the laboratory experiment, $L=1{,}6$ feet, N_{Re} is the same in both cases if

$$vL\rho/\mu=v_{cm0}L\rho_0/\mu_0 \quad \text{or} \quad N_{\mathrm{Re}}=(N_{\mathrm{Re}})_0, \qquad \ldots\ldots(27)$$

where subscript 0 refers to the laboratory test conditions. The air pressure at 30000 feet altitude is 226·1 mm. Hg, so that $\rho\ \rho_0=0{\cdot}383$. Further, from physical tables $\mu/\mu_0=0{\cdot}825$. By substitution in equation (27), $v_{cm0}=204$ ft./sec. Herewith, from equation (25), $h_{m0}=18{\cdot}0$ B.hr.$^{-1}$ft.$^{-2}$F.$^{-1}$.

Since $N_{\mathrm{Re}}=(N_{\mathrm{Re}})_0$, equation (26) leads to $N_{\mathrm{Nu}}=(N_{\mathrm{Nu}})_0$. From physical tables, $k/k_0=0{\cdot}804$. Hence $h_m=kh_{m0}/k_0=34{\cdot}5$. Herewith the time rate of convective heat flow per unit area becomes

$$q_c''=h_m(t_s-t_a)=14{\cdot}5\ (32+50)=1190\ \text{B.hr.}^{-1}\text{ft.}^{-2}.$$

According to the similarity of heat transfer and mass transfer, Nusselt (1930) has derived an equation for the case of small concentration of a diffusing vapour which, by combination with equation (26), becomes *

$$\frac{\dot{m}''}{q_c''}=\frac{\delta}{\bar{k}}\left(\frac{\alpha}{\bar{\delta}}\right)^n\frac{c_a-c_s}{t_a-t_s}, \qquad \ldots\ldots(28)$$

* Equation (28) was derived for diffusion and heat transfer not occurring in the same field. The more complicated formula for these processes taking place in the same field yields only a slightly different result.

where $\dot{m}''$ = the mass rate of sublimation for unit area in $lb._{mass} hr.^{-1} ft.^{-2}$.
δ = the mechanical diffiusivity of water vapour into air in $ft.^2/hr.$
$\alpha = k/(\rho c_p)$ = the thermal diffusivity of air in $ft.^2/hr.$
ρ = the density of the air in $lb._{mass}/ft.^3$
c_p = the specific heat of air at constant pressure in $B.lb._{mass}^{-1} F.^{-1}$.
c = the concentration of water vapour in the air, in $lb._{mass}$/cu. ft.
Subscripts a and s refer to bulk-air and surface conditions, respectively.

Assuming saturation of air with water vapour at the surface and entirely dry bulk air, from physical tables: $k = 0{\cdot}0119$; $\rho = 0{\cdot}0288$; $c_p = 0{\cdot}240$; $\alpha = 1{\cdot}72$; $c_a = 0$; $c_s = 303(10^{-6})$.

Further, from an equation of Mache (1874),

$$\delta = \frac{160}{p}\left(\frac{T_m}{492}\right)^{1.89} \text{ in cm}^2/\text{sec.}, \qquad \ldots\ldots(29)$$

where p is the air pressure in mm.Hg, and T_m is the absolute temperature of the air in degrees Rankine; $T_m = (T_a + T_s)/2$. This yields $\delta = 2{\cdot}325$ ft./^{2}hr. Hence, $\dot{m}''/q_e'' = 0{\cdot}000\,606$ $lb._{mass}/B$, $\dot{m}'' = 0{\cdot}785$ $lb._{mass} hr.^{-1} ft.^{-2}$.

The rate of heat flow due to sublimation per unit area is

$$q_{ig}'' = \dot{m}'' \lambda_{ig}, \qquad \ldots\ldots(30)$$

where λ_{ig} = the heat of sublimation.

With $\lambda_{ig} = 1219{\cdot}1$ $B/lb._{mass}$ (from steam tables) one obtains $q_{ig}'' = 970 B.hr.^{-1} ft.^{-2}$.

Though the temperature and concentration difference are large, only a small amount of ice, namely a layer of about 1/6 inch, will be sublimated in one hour of flight. The total rate of heat needed to keep the surface temperature at 32° F. and to sublimate this ice will be

$$q'' = q_c'' + q_{ig}'' = 1190 + 970 = 2160 \text{ B.hr.}^{-1}\text{ft.}^{-2}.$$

By moderately increasing the outer surface temperature, the ice could be melted. This would be preferable because only the relatively small melting heat (143 B./lb.) instead of the large heat of sublimation (1219 B./lb.) would have to be delivered from the inside of the plane and the water be wiped away by the air stream or mechanical devices.

It should be kept in mind that the above calculation is based on conditions close to the stagnation point. Since the heat transfer will be larger in the regions of parallel flow, a greater heat output will be needed in such regions in order to prevent freezing.

When I submitted this and similar calculations to the U.S. Air Corps I did not feel so confident, since the application of the equations of similarity between heat and mass flow to the present cases seemed not to be proved as yet by experiments. When, a few weeks ago, I was visiting the National Physical Laboratory, I learned, to my great satisfaction, that Drs. Griffiths and Powell had previously done and published appreciable work on evaporation and sublimation which during the war had not come to my attention. Concerning the method used by them, reference is made to their first paper (Powell and Griffiths, 1935). Powell (1940), in particular, has measured the evaporation of water from circular disks facing wind and expressed the measured values of the mass flow as a function of the 0·56 power of the Reynolds number, which is very close to the 0·57th power

determined in our experiments on heat flow. Moreover, he (Powell, 1939, 1940) also measured the sublimation of ice on a sphere and came to an exponent 0·62. Considering that he found 0·59 for the sphere in evaporation experiments, which is more than 5% higher than for a circular disk, it may be assumed that 0·62 found for sublimation on a sphere would correspond to a 5% smaller value, that is to 0·59, for sublimation on a disk, so that either his exponent 0·56 or 0·59 would have to be compared with our value 0·57 found in heat transfer experiments. I consider this very satisfactory agreement as a confirmation of Powell and Griffiths' experiments as well as of ours in the two different fields of observation.

§ 5. CONCLUSIONS

As mentioned in the introduction, I was not able to deal with general principles in this lecture, but only with some problems of heat transfer which occurred to me and had to be solved more or less exactly in one way or the other. Though many other methods of physics and mathematics have been employed in the field of heat transfer, the examples presented may have given you an idea of the kinds of procedure generally used in this branch of science. I also hope that you will have felt some satisfaction and stimulation due to the occupation with a variety of practical problems all of which can be reduced and are subordinated to a few general laws. In fact, recognizing possibilities of generalization in dealing with a special engineering problem not only raises the practical value of the work, but also causes a state of elation which is a sort of reward to those who take part in the scientists' mission to

> " Seek the familiar law in chance's frightening wonder,
> Seek the immovable pole in the phenomena's flight."

REFERENCES

American Standards Association, 1943. " American standard letter symbols for heat and thermodynamics, including heat flow " (published by *Amer. Soc. Mech. Engrs.*).

Davidson, W. F., Hardie, P. H., Humphreys, C. G. R., Markson, A. A., Mumford, A. R. and Ravese, T., 1943. *Trans. Amer. Soc. Mech. Engrs.*, **65,** 553.

Eckert, E. and Drewitz, O., 1940. *Forsch. Geb. Ingwes.*, **11,** 116 (translated 1943 in U.S., N.A.C.A. Techn. Memor. No. 1045, Washington, D.C.).

Elenbaas, W., 1942. *Physica*, **9,** 1.

Eliás, Fr., 1929 and 1930. *Z. angew. Math. Mech.*, **9,** 434 and **10,** 1, respectively. Also 1930. *Abhandlungen Aerodynam. Inst. Techn. Hochschule Aachen*, Nos. 9, 10 (translated 1931 in U.S., N.A.C.A. Techn. Memor. No. 614, Washington, D.C.).

Fage, A. and Falkner, V. M., 1931. *Great Britain Advisory Committee for Aeronautics, Rep. and Memor.* No. 1408.

Griffiths, E. and Davis, A. H., 1922. *Special Report* No. 9 (London: Dept. Scient. and Industr. Res.).

Jakob, M., 1919. *Arch. Elektrotechn.*, **8,** 117; 1938. *Trans. Amer. Inst. Chem. Engrs.*, **34,** 173; 1939. *Ibid.*, **35,** 563; 1943 a. *Trans. Amer. Soc. Mech. Engrs.*, **65,** 581; 1943 b. *Ibid.*, **65,** 593; 1944. *Combustion*, **16,** No. 2, 49; 1946. *Trans. Amer. Soc. Mech. Engrs.*, **68,** 189; 1947. *Ibid.* (in printing).

Jakob, M. and Dow, W. M., 1946. *Trans. Amer. Soc. Mech. Engrs.*, **68,** 123.

Jakob, M. and Fritz, W., 1931. *Forsch. Geb. Ingwes.*, **2,** 435.

Jakob, M., and Hawkins G. A., 1942. *J. Appl. Phys.*, **13,** 246.

Jakob, M. and Kezios, St. P., 1946. *Minutes* of 6th Internat. Congr. for Applied Mechanics (in printing).

Jakob, M. and Linke, W., 1933. *Forsch. Geb. Ingwes.*, **4,** 75 ; 1935. *Phys. Z.*, **36,** 267.

Jakob, M. and Rees, K. A., 1941. *Trans. Amer. Inst. Chem. Engrs.*, **37,** 619.

Juerges, W., 1924. *Beihefte zum Gesundheitsingenieur*, Reihe 1, Beiheft 19 (Germany: Muenchen and Berlin).
King, W. J., 1932. *Mech. Eng.*, **54**, 347.
Koenigsberger, J., 1903. *Ann. Phys., Lpz.*, **12**, 342.
Latzko, H., 1921. *Z. angew. Math. Mech.*, **1**, 268 (translated 1944 in U.S., N.A.C.A. Techn. Memor. No. 1068, Washington, D.C.).
Lorenz, L., 1881. *Ann. Phys. (Chem.)*, **13**, 582.
Mache, H., 1874. *Sitsungsber. k. Akad. Wiss. Wien (Math.-Naturwiss. Kl.)*, **1**, 385.
Mull, W. and Reiher, H., 1930. *Beihefte zum Gesundheits-Ingenieur*, Reihe 1, Heft 28 (Germany: Muenchen and Berlin).
Nusselt, W., 1923. *Forsch.-Arb. Geb. Ingwes.*, Heft. 264 (Germany: Berlin); 1930. *Z. angew. Math. Mech.*, **10**, 105.
Pohlhausen, E., 1921. *Z. angew. Math. Mech.*, **1**, 115.
Powell, R. W., 1939. *Proc. Brit. Assoc. Refrig.*, **36**, 1; 1940. *Trans. Inst. Chem. Engrs.*, **18**, 36.
Powell, R. W. and Griffiths, E., 1935. *Trans. Inst. Chem. Engrs.*, **13**, 175.
Reid, W. T. and Corey, R. C., 1944. *Combustion*, **15, No. 8**, 30.
Reiher, W., 1929. In W. Wien and F. Harms, *Handb. Experimentalphysik*, **9**, part 1, 313 (Leipzig).
Rowley, F. B. and Eckley, W. A., 1931. *Amer. Soc. Heating and Ventilating Engrs.*, **3**, 870.
Touloukian, Y. S., Hawkins, G. A. and Jakob, M., 1947. *Trans. Amer. Soc. Mech. Engrs.* (in printing).

ION CONCENTRATIONS IN SPARK CHANNELS IN HYDROGEN

By J. D. CRAGGS and W. HOPWOOD,
Metropolitan-Vickers Electrical Co. Ltd.

MS. received 18 *October* 1946

ABSTRACT. Ion concentrations in hydrogen spark channels may, it is shown, be found by observing the Stark broadening of the Balmer lines. The line breadths are measured in two ways: by the normal techniques of photography or by plotting the line breadths with a photoelectric electron multiplier, amplifier and cathode-ray oscillograph. The advantages of the latter method is that the light emission/time relation can be studied. Representative oscillograms are shown in the paper.

Full account must be taken of the fine structure of the lines in assessing their true breadths, and Holtsmark's theoretical analysis of the Stark effect for inhomogeneous fields is used for that purpose.

§ 1. INTRODUCTION

The physical properties of spark channels have not, in general, been accurately determined, largely because of the experimental difficulties involved and the uncertain and often erratic nature of the discharge. For the present purpose a spark channel is defined as the path of a spark discharge between two electrodes after complete bridging of the gap by a streamer and, more particularly, after conduction across the gap has persisted for $<0{\cdot}25$ microsec. A gap 5 mm. in length would be bridged by a streamer in $\sim 3 \times 10^{-8}$ sec. or less (Loeb and Meek, 1940). The consecutive stages of avalanche, streamer and established channel are shown, for example, by Raether (1949) using Wilson-chamber techniques. Other

papers dealing with spark channels in the present sense are, for example, I Flowers (1943) and Fucks and Bongartz (1943).

Modern techniques enable controllable spark sources to be used, especial with rapidly recurrent (50–1000/sec.) sparks at low currents ($\gtrsim 500$ amp.). T present experiments are a continuation of earlier work (Craggs and Meek, 194 carried out with such techniques but are still to be considered as preliminary the investigation of higher current discharges. The properties of short lo current sparks are of interest because of their importance in many aspects of t performance of electrical apparatus, and more particularly in spark-ignitic problems and in spectroscopic analysis, etc., and also because their behaviour probably in many ways reproduced in a slightly modified form in longer sparks in those in which much higher currents are used. The latter are also of gre technical interest.

The main objective in the present work was to investigate the Stark broadenin of the Balmer lines for hydrogen sparks and so to deduce the ion concentrations the channels. Early work was carried out by Lawrence and Dunnington (193 and by Finkelnburg (1931). Qualitative observations using spark sources who characteristics were largely unknown were made, e.g. by Merton and Hulburt.

The most recent work is that of Finkelnburg, whose conclusions are ill defin and whose methods of analysis (different from that described in the present pape of line broadening are very inaccurate. The results of this work are discusse in § 6.

§ 2. DETAILS OF APPARATUS

The sparks were passed between pointed tungsten electrodes about 5 mm apart in hydrogen at pressures 10 cm. Hg above the atmospheric value. Th tungsten electrodes were mounted in collars attached in turn to electrodes seale into the two halves of a demountable Pyrex bulb some 150 c.c. in volume. Sin some photographs were required of the u.v. emission from the spark, all measur ments were made through a quartz window waxed on to a tubulation in the side the experimental tube.

The circuit used for supplying square-voltage pulses was that devised originall in this laboratory by Mr. M. E. Haine and Professor J. M. Meek for use in radi location modulators, and is described in some detail by Craggs, Haine and Mee (1946). The circuit is shown here in figure 1. L is the choke through which th artificial line M is charged from a high-voltage D.C. supply, provided by a half-wave rectifier set. It is shown (Craggs, Haine and Meek, *loc. cit.*) that it is advantageous to use a choke whose inductance is large compared with the value necessary to give resonance with the line capacity at half the required resonant frequency. The frequency can then be adjusted by alteration of the frequency of the incoming trip-pulse applied at T to the trigger electrode of the special three-electrode ga (Trigatron) shown in figure 1, developed and described by Craggs, Haine an Meek. In steady-state conditions the voltage on the line always builds up t nearly twice the D.C. charging voltage. The spark-gap current and voltage, o

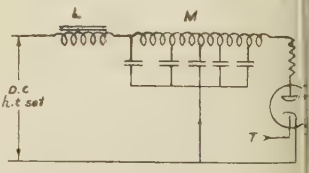

Figure 1.
H.T. source for spark excitation

light output (figure 14), can be monitored by an oscillograph tripped synchronously from the circuit used to fire the Trigatron.

If it is required to study sparks in a two-electrode gap, such a gap may be included in the circuit of figure 1 between the artificial line and the Trigatron. The use of the resistive matching load R, necessary to give non-oscillatory square voltage pulses with the line, is not affected by the inclusion of the test gap, except possibly during the first 0·5 microsec. when the spark-gap impedance falls from infinity to ~2 ohms (hydrogen). The pulse time, for a constant peak current, was varied from 1 to 4 microsec. by inclusion of several artificial lines, all of constant impedance (about 80 ohms) in cascade. For the 10- and 20-microsec. pulses it was more convenient to use special lines of higher impedance and smaller bulk. The arrangement of two gaps was used in the earlier work of Craggs and Meek (1946), although the circuit was not there described in detail.

The D.C. supply voltage (figure 1) was measured with a calibrated high-resistance voltmeter and the test-gap voltage may be derived from that value by calibration of the charging circuit or by direct measurement with a sphere gap or calibrated oscillograph and potential divider.

The controlled sparks produced with the above circuit were observed with a spectrometer and also with a system comprising a photoelectric electron-multiplier, amplifier and cathode-ray oscillograph.

The spectrometer (small Hilger constant-deviation model) gave a spectrum, from 4000 to about 6700 A., some 4·5 cm. in length. In order to ensure uniform illumination of the spectrometer slit, and thus of the neutral step wedge (placed immediately before it) necessary to provide plate calibrations, a two-lens collimating system was used (figure 2). This arrangement also minimizes undesirable reflections in the collimator tube of the spectrometer. Figure 2 shows that an image of the spark was formed by L_1 on L_2 and an image of L_1 was projected by L_2 in the plane of the slit. The adoption of such a system is essential in work of this kind where the path of the spark varies slightly in position for successive discharges.

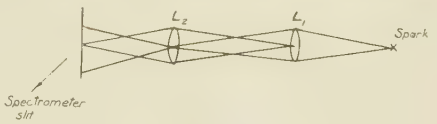

Figure 2.
Optical system for slit illumination.

A photograph of the slit, with step-wedge removed, was taken on each plate in order to ensure uniform illumination of the slit in all the analysed records.

The line profiles and step-wedge marks on the plates were measured with a Hilger microphotometer in the University of Manchester. One of us (W. H.) in collaboration with W. K. Donaldson modified the instrument to a self-recorder, and this work will be described in a separate publication. The microphotometer sensitivity was such that a net deflection of 15 cm. was obtained for a change from zero to infinite plate density. The magnification could be made either 140, 70 or 35 to 1 by choice of suitable gears in the automatic drive, and vertical lines were flashed on to the records at intervals of 0·05 mm. along the photographic plate.

After many preliminary experiments, Ilford S.G. Panchromatic plates were adopted since they were found to have the most suitable spectral response for the particular Balmer series decrements obtained with the sparks. Each plate was carefully rubbed with cotton-wool during development to avoid spurious local

variations in plate density, and the results showed clearly that the treatment wa adequate.

The electron multiplier system in its earlier form was similar to that describe by Craggs and Meek (1946). In order to improve linearity, a lower load resistanc and a smaller multiplier output current were used for the present work, in conjunction with a VT60A amplifier valve to feed the oscillograph. The amplifier valve had its frequency response improved by the use of the circuit of figure 3 (see Brainerd *et al.*, 1942).

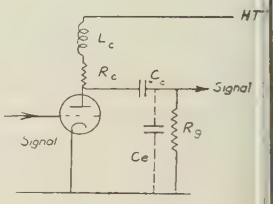

Figure 3.
Correcter circuit for H.F. amplifier.

A characteristic frequency f_e is defined by $2\pi f_e = 1/R_cC_e$ (C_e = effective capacitance shunting the coupling circuit). For $C_e = 20$ pf. and $R_c = 2200\,\omega$, $f_e = 3{\cdot}7 \times 10^6$ c./s.

A quantity D is defined by

$$D = \frac{L_c}{C_eR_c^2}.$$

The relative stage gain is plotted as a function of frequency f (Brainerd *et al. loc. cit.*) and with D as a parameter. The following data are relevant:

Frequency f	D	Relative stage gain
f_e	0	0·7
	0·4	0·92
	0·5	1·0
	0·6	1·08
$1{\cdot}4f_e$	0	0·58
	0·4	0·8
	0·5	0·88
	0·6	0·94

A value of $D \sim 0{\cdot}5$ is therefore desirable. In practice the value of L_c is best found by trial, using a square pulse generator to excite the amplifier. The results showed that only with the 1-microsec. pulses would an error arise, and even in that case the error would be negligible. The frequency response at 1 Mc./sec. was finally about 90%.

The usual load resistance for the VT60A was 15,000 ohms (which gives a time constant of 0·3 microsec. with the oscillograph input capacitance of 20 pfs.). Experiments were performed with the load varied from 15,000 to 3000 ohms and the effect on the spark light/time oscillograms was barely detectable. This system was used in preliminary work with new multipler tubes to confirm with greater accuracy some of the earlier experiments of Craggs and Meek (1946).

For the new experiments on plotting Stark profiles of the separate hydrogen lines it was necessary to use higher amplification. A three-stage h.f. amplifier, using SP41 valves with 2000 ω anode resistances and choke correction for improvement of frequency response, was then used in conjunction with the multiplier, and the VT60A valve was retained to provide a sufficiently great voltage swing for the oscillograph deflector plates. The frequency response was of the order of that for the VT60A alone, and careful tests were again carried out to check the frequency response. The linearity of response of the multiplier and amplifier system was checked with the spark in operation by interposition in turn of a number of calibrated gauzes between the light source (spark) and the multiplier.

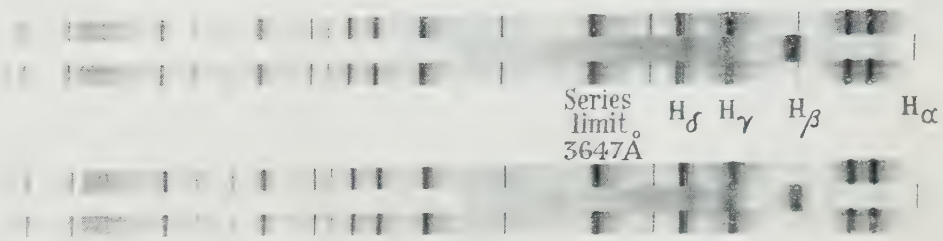

Figure 4. Spectra of hydrogen sparks (centre) with copper electrodes, and mercury vapour for comparison.

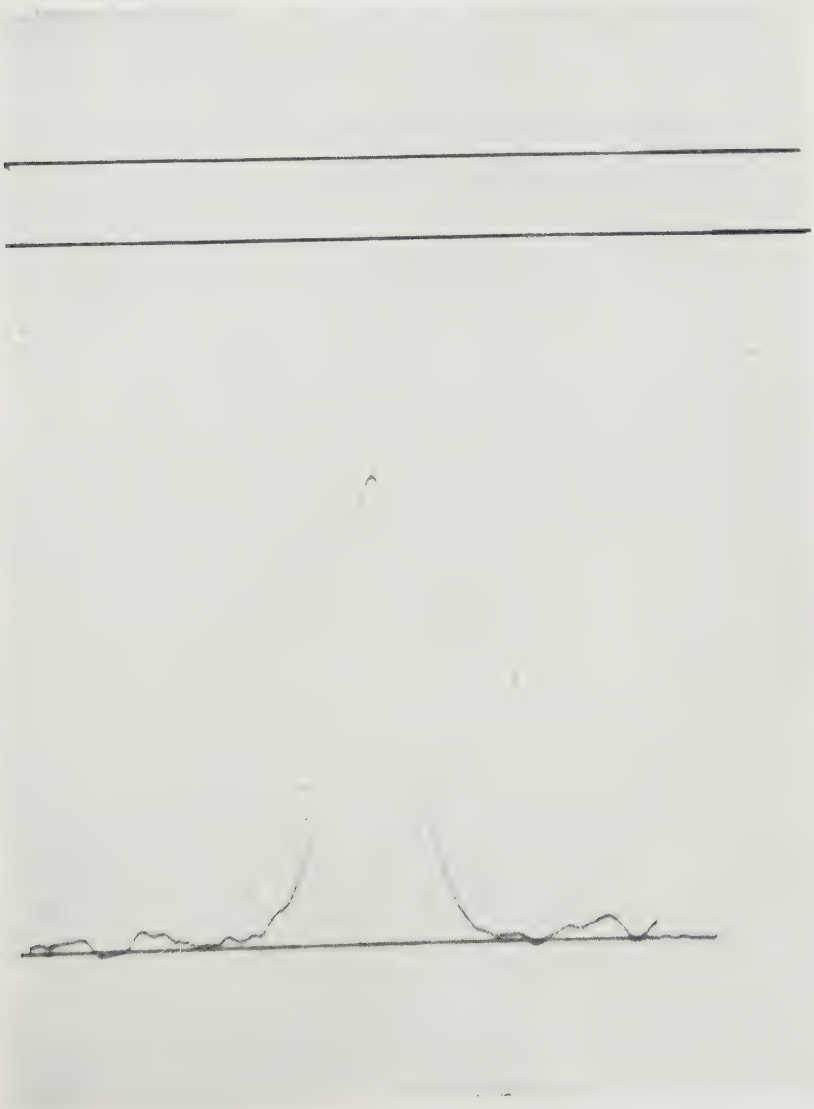

Microphotometer tracing of H_α for 1-microsec. current pulse.

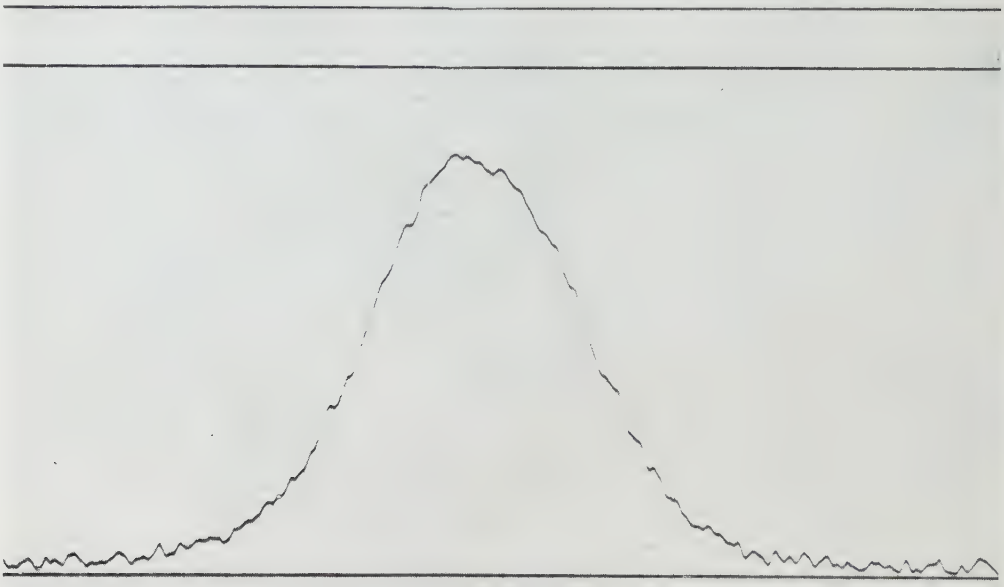

Figure 6. Microphotometer tracing of H_β for 1-microsec. current pulse.

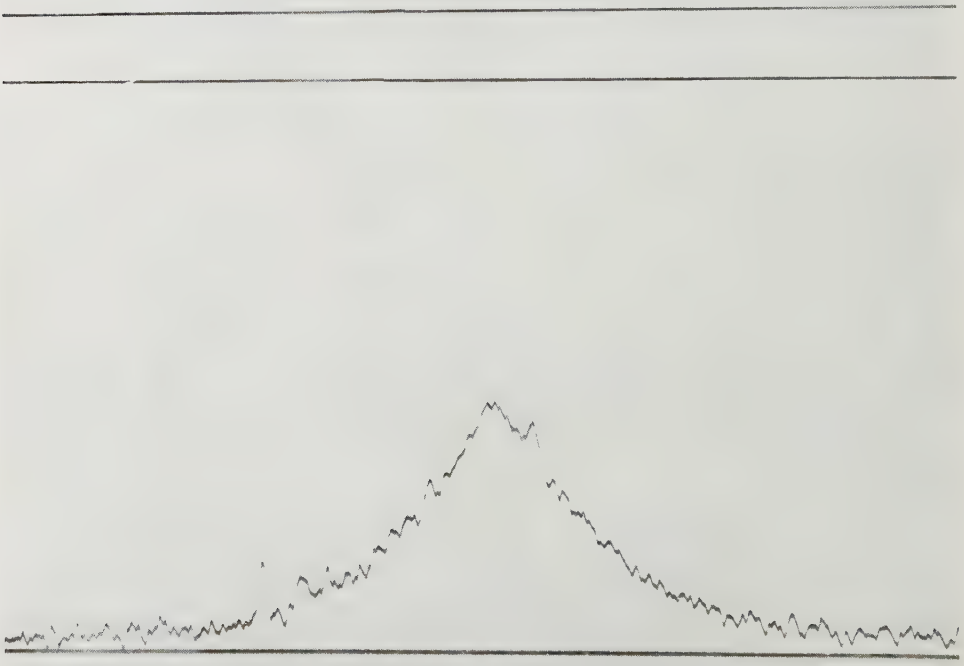

It is of interest to note that the complete system gave an amplification of 10^9–10^{10} times, i.e. $\times 1{\cdot}7 \times 10^6$ with the multiplier, about $\times 300$ with the three-stage amplifier and about $\times 10$ with the VT60A. Considerable trouble with pick-up from the spark supply circuits was experienced, and even the final records (e.g. figure 14) show a small dip at the beginning of the oscillograms, where its presence is not important. If the multiplier was irradiated with feeble steady light, the random fluctuations in the photo-current were noticeable on the oscillograph screen, but with the stronger light from the sparks such effects were negligible. It was, however, extremely important to use a light-tight box for the multiplier.

§ 3. EXPERIMENTAL RESULTS WITH THE PHOTOGRAPHIC TECHNIQUE

Every plate was calibrated with the Hilger step-wedge, using microphotometer measurements taken at the peak of each broadened line. The general appearance of the H_α, H_β and H_γ lines is shown in the spectrogram of figure 4, taken with a quartz prism spectrograph.

Experiments were made with pulse lengths of nominally 1, 4 and 10 microsec. with respective peak currents of 120, 120 and 30 amp. Figure 14(9) shows a typical 10-microsec. pulse. The 1- and 4-microsec. pulses were used in order to determine, if possible, the changes in ion concentration during the afterglow period which, being the same for both pulses and the same peak current, constitutes a greater fraction of the total time of light emission with the shorter, i.e. 1 microsec., discharge. Further reference to afterglows are made in § 6.

Representative microphotometer tracings, using 1-microsec. pulses of peak current 120 amp., are given in figures 5, 6 and 7 for H_α, H_β and H_γ respectively. The fact that the shape of H_α was not distorted by the time lag of the galvanometer system in the microphotometer was confirmed by taking a slow manual plot of H_α.

The microphotometer tracings were corrected, by the use of plate response curves, and typical examples of such corrected tracings are given in figures 8 to 13. A complete set of profiles for H_α, H_β and H_γ for the pulse lengths 1 and 10 microsec. (pulses of figure 14) is reproduced here in order that, if desired, methods other than that described below for the estimation of ion concentration may be tested. The curves for the 4-microsec. pulses are the same as for the 1-microsec. pulses. One unit on the wave number scale for H_α, H_β and H_γ corresponds respectively to 31·2, 40 and 65 $cm.^{-1}$.

The analysis of these results is given in detail below (§ 5).

§ 4. EXPERIMENTAL RESULTS WITH THE ELECTRON-MULTIPLIER TECHNIQUE

In order to take plots of the broadened lines with the electron multiplier, the constant deviation Hilger spectrometer was fitted with a telescope adaptor using a standard slit taken from another spectrometer of the same type. The telescope-slit assembly was made to project into the metal box containing the multiplier, and stray light was thus eliminated (see § 2). It was essential, in order to avoid obtaining distorted line profiles, to focus the collimator slit on to the exit slit.

The colour response of the multiplier was measured in a subsidiary series of experiments, using the above spectrometer as a monochromator with a tungsten

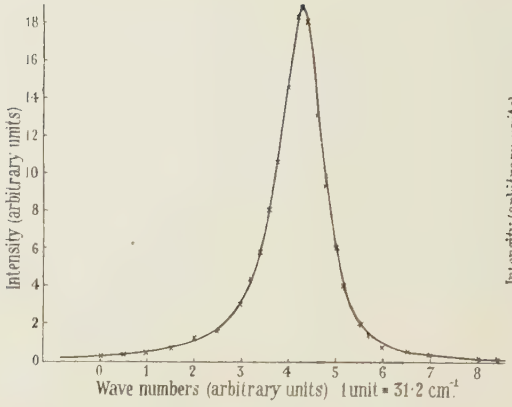

Figure 8. Profile of H_α with 1-microsec. pulse.

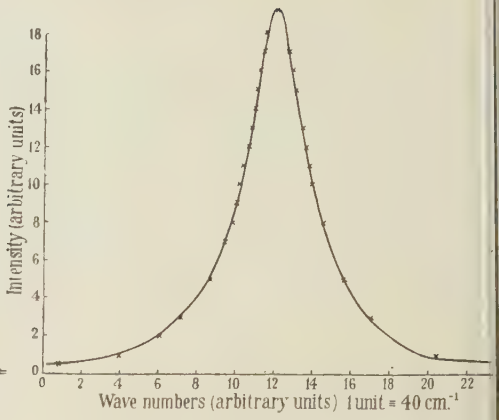

Figure 9. Profile of $H\beta$ with 1-microsec pulse. Full line shows photographic results, crosses show multiplier results. The curves are scaled to the same size at the peaks and at one other point.

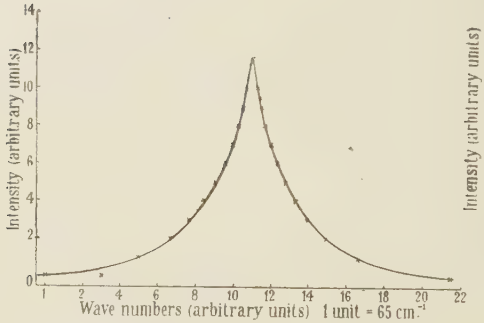

Figure 10. Profile of $H\gamma$ with 1-microsec. pulse. Full line shows photographic results; crosses show electron multiplier results when the curves are scaled to the same size at the peak and at one other point.

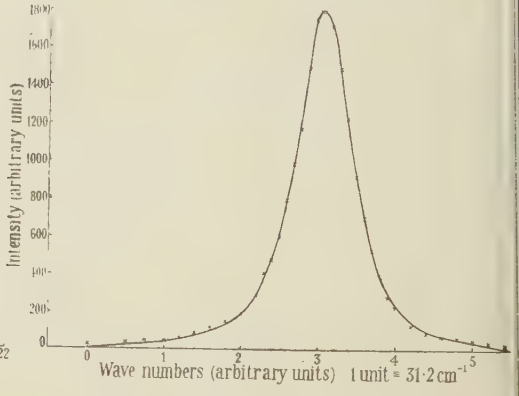

Figure 11. Profile of $H\alpha$ with 10-microsec. pulse.

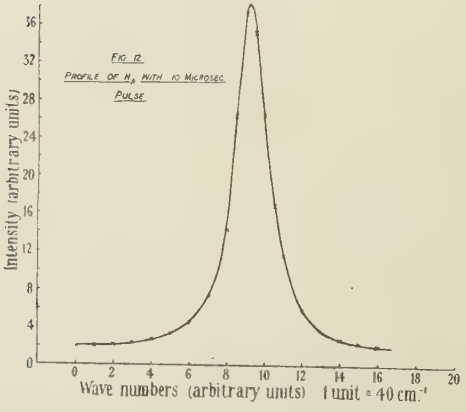

Figure 12. Profile of $H\beta$ with 10-microsec. pulse.

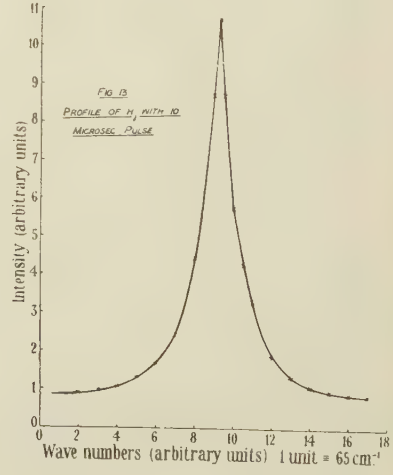

Figure 13. Profile of $H\gamma$ with 10-microsec. pulse.

filament lamp, running at known temperature, as source. The emission characteristics of such lamps are known and comprehensive data have been published by Forsythe and Adams (1945). The probably negligible but unknown differential absorption in the glass system of the spectrometer and external illumination system (figure 2) were the same since identical optical systems were used for the sparks and for the standard lamp and so did not introduce errors. The colour response of the multiplier, corrected for spectrometer dispersion, was used to check that the very wide line profiles of H_β and H_γ were not spuriously distorted by such colour response. The red response of the multiplier is extremely poor, and reliable profiles for H_α could not be obtained since it was not possible to reduce the telescope slit (normally about 50 microns wide) for the narrow H_α profiles. This difficulty did not arise with H_β and H_γ since the colour response was good and the line-breadths were such that a 50-micron slit was sufficiently narrow.

The fully corrected profiles for H_β and H_γ with 1-microsec. pulses and a peak current of 120 amp. are shown respectively in figures 9 and 10, and analysis of the data is given in § 5. The multiplier profiles in figures 9 and 10 are fitted to the photographic profiles at the peaks and at one other point, although (see tables 3 and 4) the multiplier profiles are slightly wider and thus give higher ion concentrations. The importance of figures 9 and 10 is that, after scaling, the photographic and multiplier curves should be found to be identical. This fact is discussed in § 6. The line profiles taken with the electron multiplier for 1- and 4-microsec. pulses were found to be identical.

Before proceeding to a discussion of the above results it is of interest to show spark-light emission as a function of time for the different Balmer lines. The records are similar to those shown for total (polychromatic) spark radiation by Craggs and Meek (1946), but are taken with the greatly improved techniques described above in §§ 2 and 3. The selected oscillograms are conveniently described in tabular form (table 1).

Table 1

Light/time diagrams. Figure No.	Spectral line	Current wave		
		Nominal deviation (microsec.)	Figure No.	Peak current (amp.)
14·1	H_β	1	14·7	120
14·2	H_β	2	14·8	120
14·3	H_β	10	14·9	30
14·4	H_α	2	14·8	120
14·5	H_β	2	14·8	120
14·6	H_γ	2	14·8	120

It is noticeable that the shapes of the light/time diagrams for H_α, H_β and H_γ are the same within the close limits of observational error. It is noticeable that the smaller diagrams (e.g. figure 14(2)) are sharper than the larger ones (e.g. figure 14(5)), due to the slight non-linearity of the multiplier and amplifier system (see § 2). Hence the Balmer decrements, i.e. the intensity ratio of H_α to H_β and H_β to H_γ, do

not change during the time of discharge, and this means in turn that the mode of excitation responsible for light emission is also constant for that period. The investigation of Balmer decrements will be discussed, it is hoped, in another paper. The afterglow discussed by Craggs and Meek (1946) is again apparent on comparing, for example, the duration of current and light in figures 14(1) and 14(7), and it is hoped in later experiments to determine Stark profiles for the broadened Balmer lines as a function of time and so including measurements taken during and after the flow of current. In § 5 the interpretation of results taken with different pulse lengths is given. It is clear that for afterglows of equal duration and for the same peak currents, the effect of such an afterglow would be more noticeable for shorter pulses when time averages of light-output were determined. The afterglow shown in e.g. figures 14(1) and 14(2) is artificially long because of the slight mismatching of the artificial line as shown by the current pulses of figures 14(7) and 14(8). For that reason, the record of figures 14(3) and 14(9) and those given by Craggs and Meek (1946) are more satisfactory for measurements of afterglow, with which the present paper is not primarily concerned. It is further proposed that this work, now being continued for higher current discharges, where detectable afterglows are longer, will be extended, in collaboration with Professor J. M. Meek to include experiments made also with different techniques.

§ 5. ANALYSIS OF EXPERIMENTAL RESULTS

It is well known that the Balmer lines are split into several discrete components if the radiating atoms are subjected to a uniform and uni-directional electric field. The Stark patterns are different according to the direction of observation, i.e. whether the latter is parallel or perpendicular to the field. In the case of inhomogeneous spherically symmetrical fields, the two sets of discrete components are merged into a continuous pattern, and it is this form of the Stark effect that obtains in spark and other discharges where the operative field is that due to the mutual actions of ions. Observations of the Stark effect in such conditions may thus be used to determine ion concentrations, which is the object of the present work. As mentioned in the Introduction, § 1, Merton (1915) noticed the peculiar form of the Balmer lines in such inhomogeneous fields but made no quantitative measurements. Holtsmark (1919) formulated a detailed theory of the Stark effect for such conditions, and even gave an approximate calculation of the ion concentration for an arc discharge in a gas containing lithium vapour voltatilized from the arc electrodes, using only the total width of the Stark pattern, ignoring fine structure, and comparing it with the separation of the outermost components of the lithium Stark pattern for uniform fields of known value. Holtsmark's analysis has been quoted by many other writers (e.g. de Groot, 1931; Weisskopff, 1933; and Margenau and Watson, 1936), none of whom applied the theory in detail to any particular practical case, although de Groot made approximate calculations, again ignoring the effects of fine structure, for a hydrogen arc. Hulbert (1923, 1924 a and b, and 1926) made an instructive independent attempt (1923) to work out inhomogeneous field Stark profiles but admitted its approximate nature (1923, 1924 a) and applied it to certain ill-defined practical cases (1924 a and 1926). Holtsmark's fuller analysis seems preferable and is used in the present case, as very recent and exact work by Spitzer (1939 a and b) accepts the validity

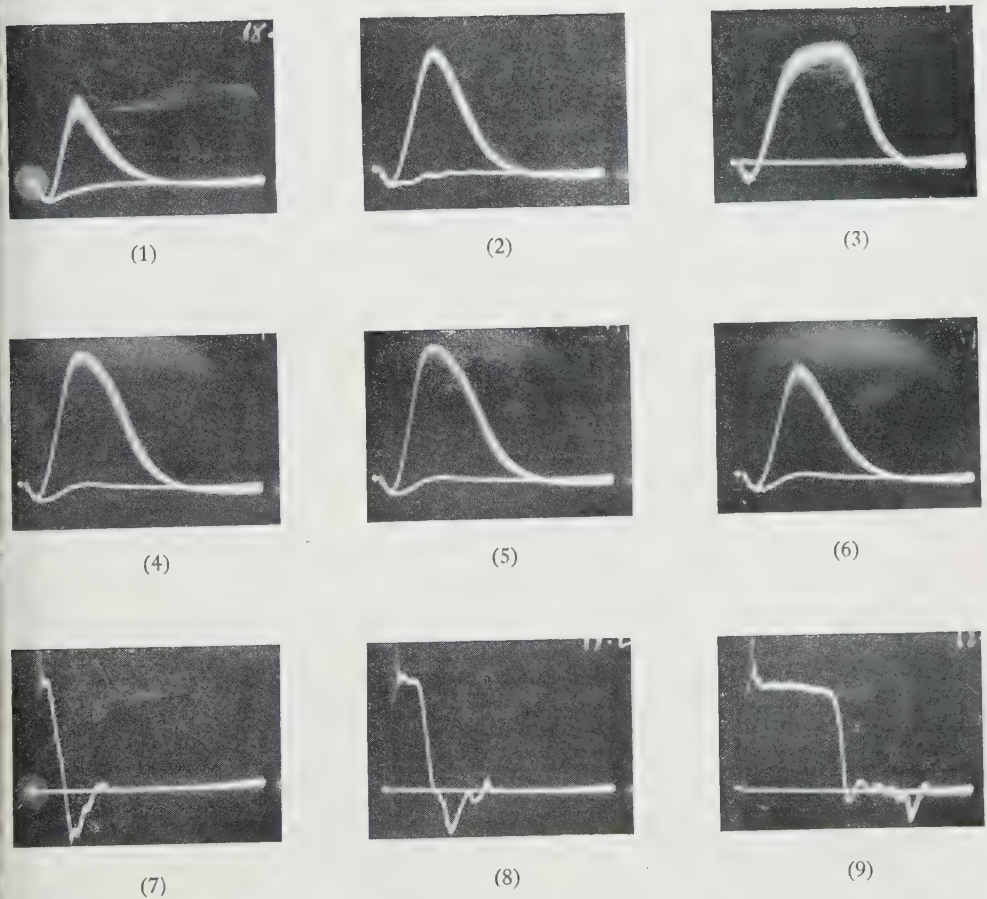

Figure 14. Oscillographic records of light-output time and current time for hydrogen sparks.

To face page 762

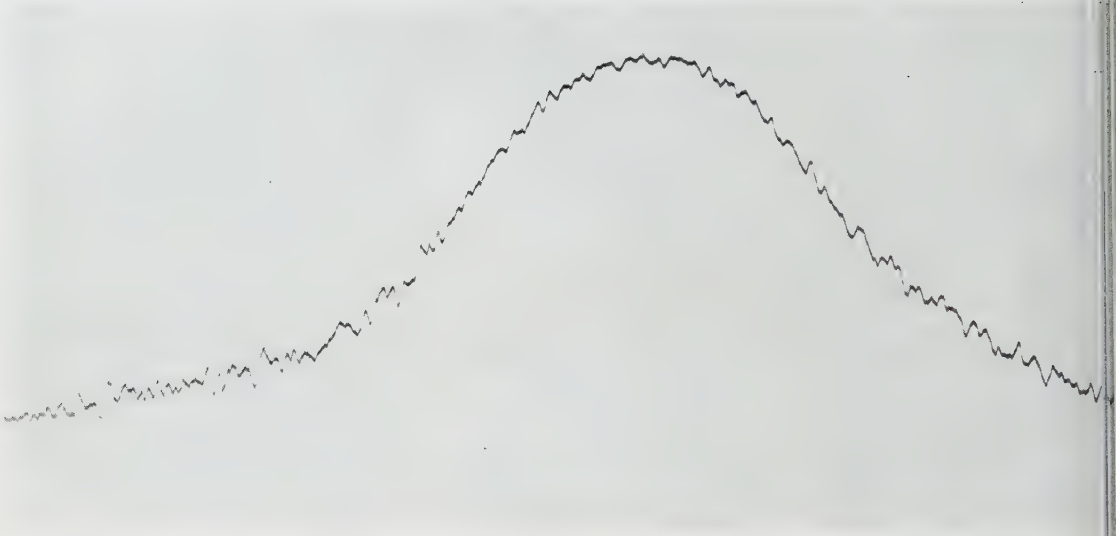

Figure 21. Microphotometer plot of spark channel for 1-microsec. current pulse.

Figure 22. Microphotometer plot of spark channel for 4-microsec. current pulse.

of his treatment. As mentioned above, the profiles of H_α, H_β and H_γ are given in full (figures 8–13) in order that further formulae may be applied. Verweij (1936) had computed Holtsmark's probability function $W(F)$, which is explained below, and thus built up the Stark profiles for inhomogeneous fields in a manner similar to that described here. Verweij's results apply to stellar conditions and to absorption lines.

Holt mark's theory (1919) of the Stark effect in an inhomogeneous field leads to the equations

$$W(F)dF = \frac{4}{3\pi} - \beta^2 d\beta[1 - 0{\cdot}4628\beta^2 + 0{\cdot}1227\beta^4 - 0{\cdot}02325\beta^6 \ldots .] \quad \ldots\ldots(1)$$

and

$$W(F)dF = \frac{d\beta}{\pi\beta^{5/2}} 2{\cdot}350\left[1 + \frac{5{\cdot}106}{\beta^{3/2}} - \frac{7{\cdot}4375}{\beta^3} + \ldots .\right], \quad \ldots\ldots(2)$$

where $W(F)dF$ is the probability of an atom being subjected to an electric field lying between F, $(F+dF)$ and

$$\beta = F/F_n, \quad \ldots\ldots(3)$$

where F_n is an effective mean or normal field strength given by

$$F_n = C_1 \boldsymbol{e} N^{2/3} \quad \ldots\ldots(4)$$

for ionic fields, where C_1 is a constant calculated by Holtsmark (see also Weisskopff, 1933; Verweij, 1936) as 2·10, giving $C = 2{\cdot}61$, $\boldsymbol{e}$ is the electronic charge, and N the ion concentration (ions/c.c.). Other expressions similar to equation (4) hold for dipole and quadrupole fields, both of which may be ignored in the case of hydrogen (Margenau and Watson, 1936). The above equations evaluate the field acting on a particular radiating atom by virtue of the surrounding atoms, located at varying distances according to a classical distribution formula and so contributing individually in different amounts to the total field at the radiator. The complete Holtsmark profile for a line showing fine structure in a homogeneous field consists of a summation of intensity/wave-length patterns with one pattern for each component of the line. The maximum width of the line, for the case of inhomogeneous fields giving a normal field strength F_n, is the separation of the outermost components for a homogeneous field equal in magnitude to F, where $F = F_n$ for the first-order Stark effect. The second-order effect, in which the separation of a given component varies as (field)^2, is negligible for the fields considered here, as can be shown by a consideration of data for the second-order effect (Gebauer and von Traubenberg, 1930, and White, 1934). The second-order effect is only $\sim 10\%$ of the first-order effect, in wave number separations, for $F = 10^{11}$ volts/cm.

Equations (1) and (2) apply respectively for $0 < \beta < 1{\cdot}7$ and $1{\cdot}7 < \beta < \infty$ respectively, and are plotted separately and added together in figure 15. For the computation of the resultant shape of a complex line, such as H_α, H_β or H_γ, the curve of figure 15 is applied to each component of the line and the different curves are then superimposed.

It is assumed that only the first-order Stark effect is operative, i.e. for any component

$$\delta\nu = CF, \quad \ldots\ldots(5)$$

where $\delta\nu$ is the separation (cm.$^{-1}$) of the component from the undisturbed line in a homogeneous field F. C is a constant. The highest components disappear first

as the field is increased, owing to level perturbations (Finkelnburg, 1931, and references there cited), and Finkelnburg used this fact and the available data to estimate inter-ionic fields in hydrogen sparks. The method is very inaccurate and uncertain, and Finkelnburg apparently made no attempt to carry out the full Holtsmark analysis (given here,) which uses Stark-effect data in a different manner. The level smearing is negligible for $F_n \sim 100$ kv./cm., which is the value obtained in the

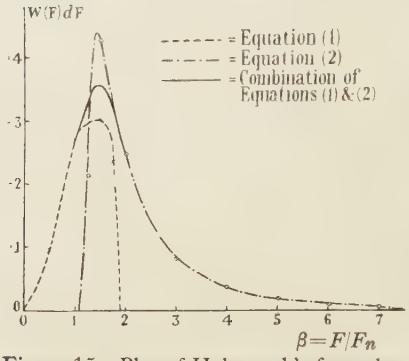

Figure 15. Plot of Holtsmark's formulae.

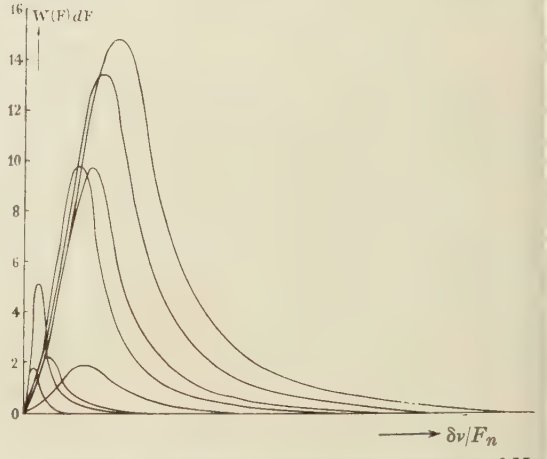

Figure 16. Holtsmark plots for components of H_γ.

present work. The values of C were then found for all important components (table 2) of the different lines, using data given by Minkowski (1929) for $F = 104$ kv./cm. The weakest components were ignored.

Table 2

Line	$n's' - ns$ (quantum number term)	$\Delta\nu$ (cm.$^{-1}$)	C (cm.$^{-1}$/kv./cm.)	Relative intensity
H_α p components	2	14·4	0·138	729
	3	20·4	0·196	2,304
	4	26·6	0·256	1,681
H_α s components	0	0	0	5,290
	1	6·0	0·058	1,936
H_β p components	6	42·3	0·407	81
	8	55·7	0·536	384
	10	69·3	0·666	361
H_β s components	2	14·4	0·1385	72
	4	27·9	0·268	456
	6	41·0	0·394	294
H_γ p components	2	14·3	0·137	15,625
	5	35·0	0·336	19,200
	12	84·3	0·810	16,641
	15	105·0	1·01	115,200
	18	127·0	1·22	131,769
H_γ s components	0	0	0	141,650
	3	20·3	0·195	46,128
	10	70·7	0·680	88,050
	13	91·0	0·875	83,232

From equations (3) and (5)

$$\beta \times \text{constant} = \delta\nu/F_n, \qquad \ldots\ldots(6)$$

and the plot of $W(F)dF$ against β may be converted to a plot of $W(F)dF$ against $\delta\nu/F_n$, so that each fine-structure component is represented by a separate curve, the area under which is given by

$$A = \int_0^\infty W(F)dF \,.\, d\left(\frac{\delta\nu}{F_n}\right). \qquad \ldots\ldots(7)$$

If the areas obtained for the curves drawn for the different components are arranged by scaling to be proportional to their respective relative intensities (table 2), the curves may then be compounded to give the final curve $\left(\text{intensity} \Big/ \frac{\delta\nu}{F_n}\right)$ for the complete line. Scaled plots for H_γ components are shown in figure 16.

In order to determine ion concentrations from equation (4), the curve of observed broadening (intensity/wave number) is fitted on both axes to the calculated curves derived by the calculations described above. Figures 17–20 show typical results using data derived from the photographic work. From a knowledge of the scaling factor on the wave-number axis, it is then easy to find a value of F_n in order that the $\delta\nu/F_n$ axis of the calculated curve should fit the $\delta\nu$ axis of the experimental curve, since F_n is that scaling factor. N is then calculated from equation (4).

For figures 17, 18, 19 and 20 respectively, one unit on wave-number axis corresponds to 12·4, 26·5, 65 and 26·5 $cm.^{-1}$.

The sensitivity of the method may be judged from figure 20, which shows the fitting obtained for $F_n = 120$ kv./cm. in a case where the best fit is obtained for 130 kv./cm. It thus appears possible by this method to measure F_n to $\pm 10\%$. The close agreement between experimental and calculated profiles indicates that absorption effects in the channel are negligible. This was confirmed indirectly by measurements on Zn and Cd vapour, in similar sparks, using the triplet terms in the spectra, whose relative intensities are independent of the mode of excitation. It is hoped to publish these results in a later paper.

Neither the Holtsmark theory, nor that of Hulbert cited above, applies to the undisturbed radiation at the centre of the profile, where the experimental and calculated intensities are widely different, due to the central undisplaced Stark components and the fact that $F \to 0$ for some of the radiating atoms. The form of the line near the centre of the pattern is probably governed partly by other effects, e.g. a Doppler broadening.

§ 6. ION CONCENTRATIONS IN THE HYDROGEN SPARK CHANNELS EXAMINED

Some results of the photographic technique are summarized in table 3. The peak currents for the 1, 4 and 10 microsec. pulses were respectively 120, 120 and 30 amp.

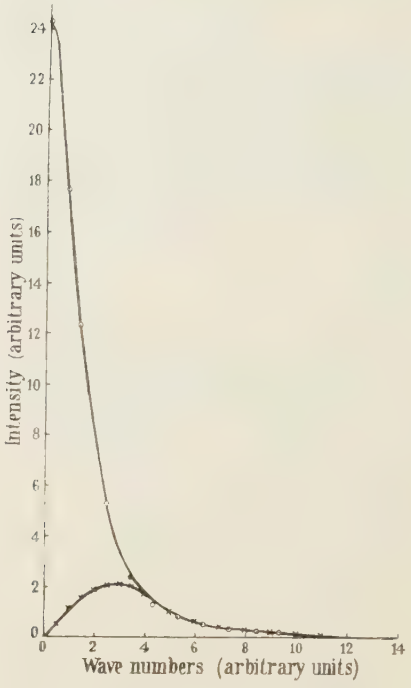

Figure 17. Observed (⊙) and calculated (×) profiles for $H\alpha$, 1-microsec. pulse, photographic technique. $F_n = 124$ kv./cm.

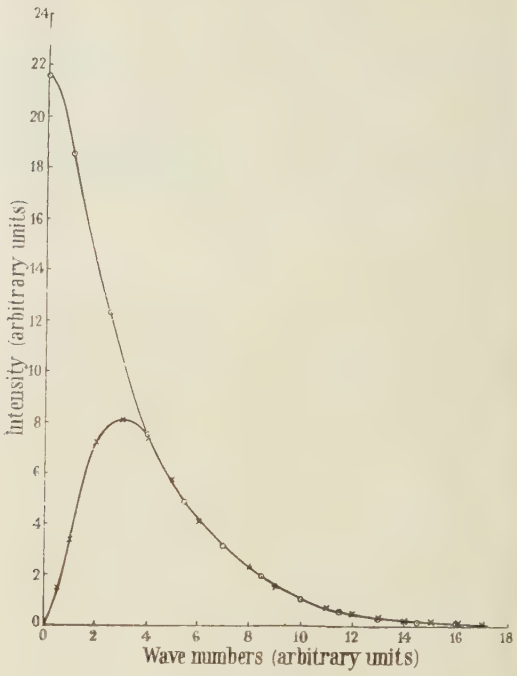

Figure 18. Observed (⊙) and calculated (×) profiles for $H\beta$, 1-microsec. pulse, photographic technique. $F_n = 133$ kv./cm.

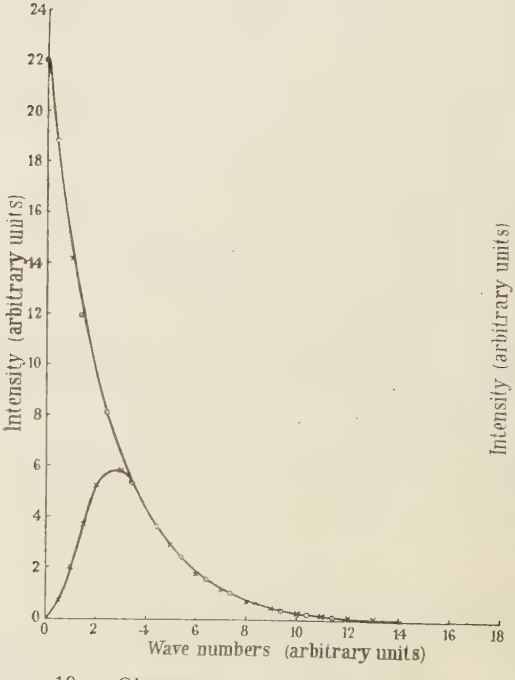

Figure 19. Observed (⊙) and calculated (×) profiles for $H\gamma$ 1-microsec. pulse, photographic technique. $F_n = 130$ kv./cm.

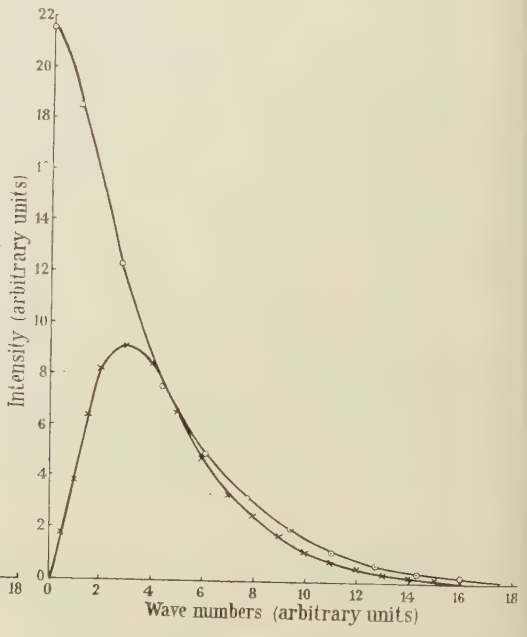

Figure 20. Observed (⊙) and calculated (×) profiles for $H\beta$, 1-microsec. pulse, photographic technique. $F_n = 120$ kv./cm. Observed results correspond to $F_n = 130$ kv./cm.

Table 3

Plate No.	Pulse length (microsec.)	F_n (kv./cm.)			Mean F_n	N (ions/c.c.)
		H_α	H_β	H_γ		
1.5.4	1	124	133	130	130	$2{\cdot}1\times10^{17}$
30.4.3	4	as with 1-microsec. pulse to within about $\pm5\%$			130	$2{\cdot}1\times10^{17}$
1.0.3	10	85	79	76	80	$1{\cdot}0\times10^{17}$

Other plates agreed with that given above to within the approximate limits of observation of $\pm5\%$over a period of about 9 months, after the technique had been developed and tested, during which time the apparatus was dismantled and reassembled several times for other experiments. Some 40 microphotometer tracings were taken and examined.

The electron multiplier results are exemplified by the data of table 4. 10-microsec. pulses were not used in this part of the work since the spark light was relatively feeble and the narrower lines rendered necessary the use of excessively fine slits.

Table 4

Pulse length (microsec.)	F_n (kv./cm.)		Mean F_n	N (ions/c.c.)
	H_β	H_γ		
1	165	163	164	$2{\cdot}9\times10^{17}$
4	as with 1-microsec. pulse to within about $\pm5\%$		164	$2{\cdot}9\times10^{17}$

After the technique had been developed, the results were extremely consistent, and records taken over a period of about 4 months agreed within about $\pm10\%$.

Since the Holtsmark analysis applies only to the skirts of the line profiles, the photographic measurements in which the total light from the discharges is examined still tend to show the maximum ion concentrations which will be found in the early stages of the passage of current. The electron multiplier results could be taken for any part of the light/time diagram (see figure 22) although the results analysed in detail here refer to the instant of maximum light emission, since the usual method of observation was to measure the peak height on the light/time diagram on the oscillograph screen as the spectrometer wave-length drum was rotated. It was checked, however, that the shape of the light/time diagrams did not change as the line under examination was traversed across the multiplier slit; hence, for example, the extreme skirts of the Stark profile (corresponding to the highest fields encountered during the whole "visible" discharge) did not occur especially at the beginning of light emission.

Since, also, the photograph and multiplier plots for 1 and 4 microseconds agree extremely closely in shape, it seems likely that the field, or ion concentration, changed very little during the observed part of the discharge. This subject will be discussed below in detail. The conclusions from the above argument appear

to be that (*a*) the ion concentration varies little during the time of discharge in which observations are made, and therefore (*b*) the ion concentrations measured by the two methods should agree. Hence from (*b*), the difference in values of N for the same discharges, see tables 3 and 4, is due to some unexplained consistent error in one of the measurements, since both methods give accurately repeatable results ($\sim \pm 10\%$ error) after all precautions have been taken. The error in N which is $2{\cdot}5 \pm 0{\cdot}4 \times 10^{17}$ ions c c., is, however, small for this kind of work, and the results appear to be the most accurate so far published. Since the electron multiplier gave the same results for 1- and 4-microsec. pulses of the same peak current, as would be expected, it seems unlikely that its frequency response was inadequate. The circuits were carefully tested for response (§ 2). It is considered more likely that the photographic results are in error since other work (to be published separately) indicated that the spectral response of the plates, particularly as regards intermittency effects (see, for example, Mees, 1944), might not be as consistent and predictable as existing theory indicates. There appear to be little published data on the response of plates to light pulses lasting 1–5 microsec. The discussion in §§ 2 and 3 shows that all the usual precautions were taken in the photographic work (Sawyer, 1944).

The implications of conclusion (*a*) are of interest. It is immediately clear (Lawrence and Dunnington, 1930, and others) that the ion concentration probably varies greatly during the early parts ($\sim 10^{-7}$ sec.) of spark discharges. Lawrence and Dunnington obtained $\sim 30\%$ ionization of Zn vapour in $\sim 10^{-\frac{1}{2}}$ sec. from the commencement of discharge, corresponding to a temperature of $\sim 13{,}000°$. It seems probable that Saha's equation will not apply to 1–10 microsec. sparks, in which case spark temperatures deduced in that way from measured ion concentrations will be inaccurate. In the present case ($T \sim 12{,}000°$ from $N = 2{\cdot}5 \times 10^{17}$ ions/c.c.), Craggs and Meek (1946), figure 14(1), for example, shows that the light emission from the hydrogen sparks is negligible for perhaps the first 0·25 microsec. of discharge. The current reaches its maximum value in $\sim 0{\cdot}1$ microsec., so that the discharge is passing the full current before visible light emission is appreciable. The present experiments are not intended to refer to this early period of the discharge, which will be treated in later work. It is known, however, that the voltage gradient in the present type of spark changes greatly only during the first 0·5 microsec. of conduction (Flowers, 1943; Craggs, Haine and Meek, 1946; and others) and that the ratio of the numbers of ionizing and exciting collisions will vary greatly, for that reason, during the early part of the spark. Thus Penning (1938), using infinitely small currents, showed that between X/p 20 v./cm./mm. and $X/p \to 0$ (which are the approximate values for a hydrogen spark at the beginning and end of the high field period) the ratio of electron energy spent in exciting and ionizing was rapidly increasing, i.e. more light was being emitted at low X/p.

It is perhaps fortunate that the early part of the discharge is not recorded with visible light, since that fact enables some information to be deduced for the afterglow period, i.e. the time, after the current has fallen to zero, within which light is still emitted. Craggs and Meek (1946) discussed mechanisms of afterglows in hydrogen and argon, and it was suggested (*loc. cit.*) that the light could only be due to recombination if $\alpha \sim 10^{-11}$ (α is the recombination coefficient

for electron ion collisions). Whilst recombination certainly takes place in the hydrogen sparks, as shown by the series limit continuum of figure 4, it appears from the present experiments, which show that the ion concentration varies little during the whole discharge (since the multiplier and photographic Stark profiles are identical in shape, see figures 9 and 10), that electron/ion recombination must indeed be slight, and hence that $\alpha < 10^{-11}$ for the spark channels. It is likely that the ion concentration during the afterglow has dropped by $<20\%$, i.e. $\alpha \sim 2 \times 10^{-12}$ (see table 5 and discussion, both in Craggs and Meek (1946)).

Massey (1938) and Bates *et al.* (1939) quote values of the total cross-section for radiative electron/ion recombination,

$$Q_e = \Sigma_n Q_e^n, \qquad \ldots\ldots(8)$$

where Q_e^n is the coefficient for recombination into the nth state; $\sum_1^\infty Q^n = 23 \times 10^{-21}$ cm^2 for an electronic energy V of 0·28 volt. The cross-section varies approximately as $1/2$. Assuming an electron temperature in the spark channel of 15,000°, then $V \sim 2$ volts, so $v \sim 8 \times 10^7$ cm./sec. Since

$$\alpha = vQ_e, \qquad \ldots\ldots(9)$$

then $\alpha \sim 8 \times 10^7 \times 3 \times 10^{-21} \sim 2 \times 10^{-13}$. To this must be added $Q_r^0, \sim 6 \times 10^{-22}$ cm^2 for 2-volt electrons (Massey 1938, p. 35) and the total value of α is $\sim 10^{-13}$ for the spark channel. Radiationless three-body collisions (Smith, 1936) can be shown to have a cross-section about equal to that for radiative capture if the electron concentration is $\sim 10^{18}$/c.c. Smith suggests that such concentrations are unlikely to be encountered in electrical discharge experiments, but an exception could apparently be made for spark channels of higher current than those described here. It is hoped to re-examine recombination problems in spark channels, particularly for the highest attainable ion concentrations.

In the earlier paper (Craggs and Meek, 1946), the ion concentration for the present sparks (120-amp. 1–4-microsec. pulses) in hydrogen was deduced by several methods as being approximately 10^{17} ions/c.c., in excellent agreement with the present results. In particular, attention is here directed to the method of equations (2) and (3) of the early paper, in which the ion concentrations is found from a knowledge of channel radius (taken as 0·75 mm.) and voltage drop. The latter, about 90 v./cm., corresponded to $N \simeq 6 \times 10^{17}$ ions/c.c.

In order to obtain preliminary information on channel structure, some photographs of single 1-, 2- and 4-microsec. sparks were taken and the channel images traced on the micro-photometer. Results for 1- and 4-microsec. sparks are shown in figures 21 and 22. The full diameters are about 1·3 mm. for both cases, which would give $N \simeq 4 \times 10^{17}$ ions/c.c. from the other data published (Craggs and Meek, 1946). The fact that the ion concentration is much less for the lower current 10-microsec. discharges (table 3) is of interest. Since the 1- and 4-microsec. sparks give the same values of N, it seems unlikely that the length of the 10-microsec. current pulse, which might allow expansion of the spark channel, is the controlling factor. It is suggested that the spark channel expands less rapidly than would be necessary to give constant-current density (or ion concentration), so that the higher current discharges are relatively more constricted (C. J. Flowers, 1943). However, figures 21 and 22 show that the channels

are non-uniform in luminosity and are brighter at the centre. Although th relation between intensity of light emission and ion concentration is not ye accurately known, it is reasonable to suggest a correspondingly high radial ion concentration, in which case N, as determined from voltage drop, would nee further correction. Figures 21 and 22, which were taken in order to sho that the spark channels expanded inappreciably between 1 and 4 microsec after their time of origin, could owe their shapes to the mechanism of growt of a channel from a streamer, in the sense that the photographic record integrate an infinite number of succeeding stages of the spark from its beginning as streamer thin compared with the spark channel which succeeds it (we ar particularly indebted to Professor J. M. Meek for discussions on this topic) in which case the postulation of radial charges in ion concentration would require verification. It is considered, since the growth of spark luminosity is so slow (see figure 22) with visible light, that this alternative explanation is not likely and that figures 21 and 22 indicate strong radial changes in N at the times 1-4 microsecs. It is intended that the technique illustrated by figures 21 and 22 shall be developed for other spark discharges.

§ 7. CONCLUSIONS

The ion concentration in certain hydrogen spark channels has been measured and found to be about $2{\cdot}5 \times 10^{17}$ ions/c.c. by observations of the Stark broadening of the Balmer lines H_α, H_β and H_γ. The analysis takes full account of the fine structure of the above lines. It is deduced from observations of the Stark profiles with an electron multiplier technique that the electron ion recombination coefficient in the experimental conditions is $\sim 2 \times 10^{-12}$. The spark temperature, as deduced from Saha's equation, is about 12,000°.

§ 8. ACKNOWLEDGMENTS

The authors wish to express their thanks to Mr. F. R. Perry, in whose laboratory the work was carried out, for his continuous interest and support. The authors are also indebted to Professor J. M. Meek (University of Liverpool) for many stimulating discussions, to Dr. S. Tolansky (University of Manchester) for the use of a microphotometer, and to their colleagues Mr. G. J. Scoles and Mr. C. J. Braudo for advice and help with circuit problems. Thanks are due to Sir Arthur P. M. Fleming, C.B.E., D.Eng., Director of Research and Education, and Mr. B. G. Churcher, M.Sc., M.I.E.E., Manager of Research Dept., Metropolitan-Vickers Electrical Co. Ltd., for permission to publish this paper.

REFERENCES

Bates, D. R., Buckingham, R. A., Massey, H. S. W. and Unwin, J. J., 1939. *Proc. Roy. Soc.*, A, **170,** 322.

Brainerd, J. G., Koehler, G., Reich, H. J. and Woodruff, L. F., 1942. *Ultra High Frequency Techniques* (London: Chapman and Hall).

Craggs, J. D., Haine, M. E. and Meek, J. M., 1946. *J. Inst. Elect. Engrs.*, **93,** IIIA, 936.

Craggs, J. D. and Meek, J. M., 1946. *Proc. Roy. Soc.*, A, **186,** 241.

Finkelnburg, W., 1931. *Z. Phys.*, **70,** 375.

Flowers, J. W., 1943. *Phys. Rev.*, **64,** 225.

Forsythe, W. E. and Adams, E. Q., 1945. *J. Opt. Soc. Amer.*, **35,** 108.

Fucks, W. and Bongartz, H., 1943. *Z. Phys.*, **120,** 468.

GEBAUER, R. and VON TRAUBENBERG, H. R., 1930. *Z. Phys.*, **62**, 289.
DE GROOT, W., 1931. *Physica*, **11**, 307.
HOLTSMARK, J., 1919. *Ann. Phys., Lpz.*, **58**, 577.
HULBURT, E. O., 1923. *Phys. Rev.*, **22**, 24.
HULBURT, E. O., 1924 a. *Phys. Rev.*, **23**, 106.
HULBURT, E. O., 1924 b. *Astrophys. J.*, **59**, 177.
HULBURT, E. O., 1926. *J. Franklin Inst.*, **201**, 777.
LAWRENCE, E. O. and DUNNINGTON, P. G., 1930. *Phys. Rev.*, **35**, 396.
LOEB, L. B. and MEEK, J. M., 1940. *J. Appl. Phys.*, **11**, 438.
MARGENAU, H. and WATSON, W. W. 1936. *Rev. Mod. Phys.*, **8**, 22.
MASSEY, H. S. W., 1938. *Negative Ions* (Cambridge University Press).
MEES, C. E. K., 1944. *The Theory of the Photographic Process* (New York : Macmillan).
MERTON, T. R., 1915. *Proc. Roy. Soc.*, A, **92**, 322.
MINKOWSKI, R., 1929. *Handbuch der Experimental Physik*, **21**, p. 389 *et seq.* (Leipzig : Springer).
PANNEKOEK, A., 1937. *Mon. Not. R. Astr. Soc.*, **93**, 694.
PENNING, F. M., 1938. *Physica*, **5**, 286.
RAETHER, H., 1939. *Z. Phys.*, **112**, 464.
SAWYER, R. A., 1944. *Experimental Spectroscopy* (New York : Prentice-Hall).
SMITH, R. A., 1936. *Proc. Camb. Phil. Soc.*, **32**, 482.
VERWEIJ, S., 1936. *Publ. Astr. Inst. Univ., Amsterdam*, No. 5,
WEISSKOPF, V., 1933. *Phys. Z.*, **34**, 1.
WHITE, H. E., 1934. *Introduction to Atomic Spectra* (New York : McGraw-Hill), p. 402.

ELECTRON/ION RECOMBINATION IN HYDROGEN SPARK DISCHARGES

BY J. D. CRAGGS AND W. HOPWOOD,
Metropolitan-Vickers Electrical Co. Ltd., Manchester

MS. received 10 *January* 1947

ABSTRACT. The afterglows following short sparks in hydrogen at a pressure of one atmosphere have been described in earlier publications. The present communication presents later results and a detailed analysis of the afterglows. It is shown that an electron/ion recombination process is apparently the cause of the light emitted in the afterglow. On this basis the appropriate coefficient of recombination has been calculated. The implications of the results, and relevant literature, are discussed.

§1. INTRODUCTION

EXPERIMENTAL data relating to electron/ion recombination are very scarce, and some interest is attached to them. Further efforts to obtain recombination cross-sections are also to be encouraged, since the results would be of considerable fundamental and technical interest. For example, the de-ionization of gases following electrical discharges in them depends partly on the recombination processes and in certain cases (for example, in high-temperature discharges in hydrogen) the interacting particles are electrons and positive ions, since negative ions and molecules can often be shown to be relatively insignificant.

Recombination data are used also in studies of the upper atmosphere, and their importance in that field is stressed in the Gassiot Committee's report (1942/43).

Attention has recently been directed to the existence of afterglows followi spark discharges, in high pressure gases (Meek and Craggs, 1943; Rayleigh, 194 Craggs and Meek, 1945 and 1946) and the possibility of determining electron/i recombination coefficients from such observations has been stressed by Crag and Meek (1946). The results thus obtained refer to the special conditic obtaining in such discharges, and their relevance to other problems can only decided after a study of such conditions.

§ 2. DISCUSSION OF PREVIOUS WORK

Many excellent investigations of recombination between positive and negati ions have been made (Sayers, 1938, and references there cited), but experimen data on electron/positive ion recombination are scarce, as has been pointed o in § 1.

Mohler (1937) found that the recombination coefficient α, defined (where t time and N is the number of ions or electrons, assumed equal, per cc. of gas) the equation

$$dN/dt = -\alpha N^2, \qquad \ldots\ldots(1)$$

could be determined for an interrupted Cs vapour glow-discharge as $3{\cdot}4 \times 10^{-}$ The discharge pressure was $10 - 33 \times 10^{-3}$ mm. Hg, and the electron temperatu about 1200°. This paper followed earlier reports by Mohler (1928 etc.) similar work; attention is particularly directed to the experiments of Mohler ar Boeckner (1929) on the recombination spectra of ions and electrons in Cs and H The great increase in the recombination coefficient with decreasing electr energy is there emphasized. The above data, and those of Kenty (1928) for t afterglow of an argon arc, may be summarized by stating that $\alpha \sim 10^{-10}$ for t conditions studied.

There seem to be no published results for hydrogen, but Mohler (1937) h discussed the case using the theory of Stueckelberg and Morse (1930). It appea that when the kinetic energy of the electrons is small relative to that of the level in which the electron falls, the recombination coefficient α_n for that level n is given b

$$\alpha_n = 5{\cdot}94 \times 10^{-13} A_n V^{-1/2}, \qquad \ldots\ldots(2)$$

where A_n is a simple function of n for $n \geqslant 3$. V is the electron energy in electron volts. When the electron's kinetic energy is much greater than that of the level Oppenheimer (1928) gives

$$\alpha_n = 6{\cdot}3 \times 10^{-11}/V^2 n^3. \qquad \ldots\ldots(3)$$

Equation (2) is used for $n < n_0$, where

$$n_0 = (13{\cdot}54/V)^{1/2},$$

and equation (3) is valid for $n \gg n_0$ although it may be used when $n = n_0$ to giv approximate results.

Take as an example $V = 0{\cdot}1$ ev. Then $11 < n_0 < 12$, and total α (i.e. $\Sigma\alpha_n$) i $2{\cdot}3 \times 10^{-11}$, but the errors involved are probably large and are not assessed i detail by Mohler (*loc. cit.*). The values of A_n published by Stueckelberg an Morse (1930) were used for these calculations.

More recently, the observations by Lord Rayleigh on long duration Balme series emission in hydrogen (1944) led Zanstra (1946) to calculate the electron/ion

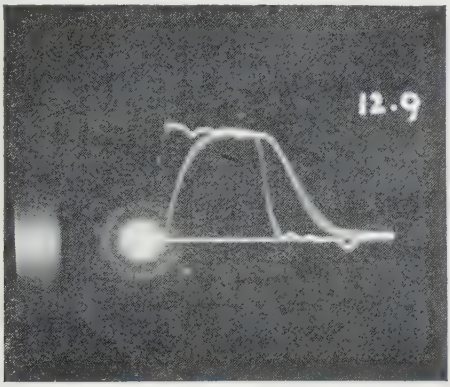

(*a*)

4-microsec. 120-amp. pulse. (Light/time and current oscillograms.)

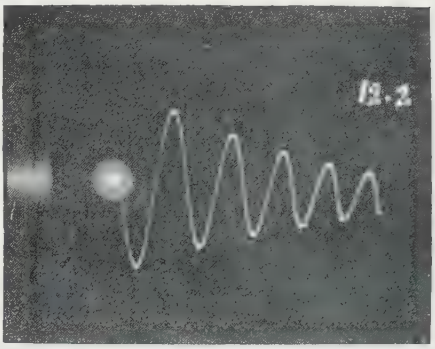

(*b*)

Time base for (*a*).

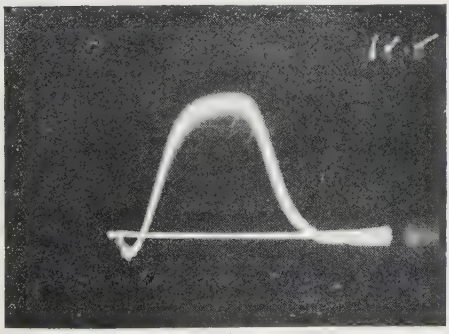

(*c*)

Light/time oscillogram for (*d*).

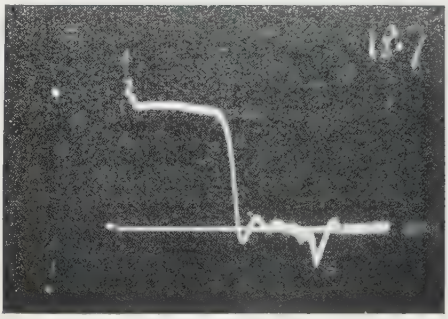

(*d*)

10-microsec. 30-amp. pulse-current oscillogram.

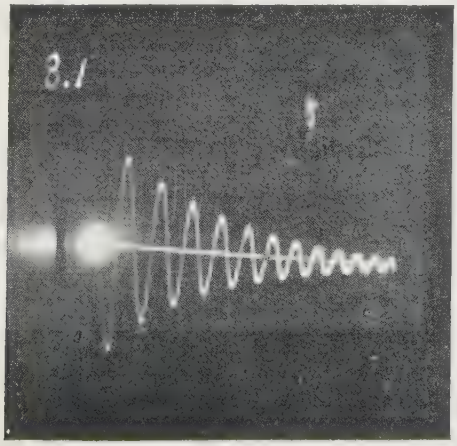

(*e*)

Time base for (*c*) and (*d*).

Figure 1. Oscillograms of current, light emission and time-base speeds. The timing oscillation has a period of 2·8 microsec.

To face page 772

ecombination cross-sections for Rayleigh's experiments, making certain reasonble assumptions in the process. The results will be discussed more fully in § 4, ut an electron temperature of 1000°, corresponding to an average electron energy Maxwell distribution) of about 0·13 ev., gives $\alpha = 1{\cdot}2 \times 10^{-12}$.

§ 3. EXPERIMENTAL TECHNIQUES

Mohler and Kenty (references given in § 1) were able to use mechanical means or stopping the flow of current in their discharges which were arcs or glows of long luration, i.e. by the use of commutators short circuiting the terminals of the lischarge tube. The decay of ionization was then studied in the absence of current y various means such as probes.

This technique is clearly impracticable for spark discharges lasting only a few nicroseconds, but the utilization of square current pulses (~100 amp. peak), ollowing normal radiolocation practice, leads to the possibility of observing the

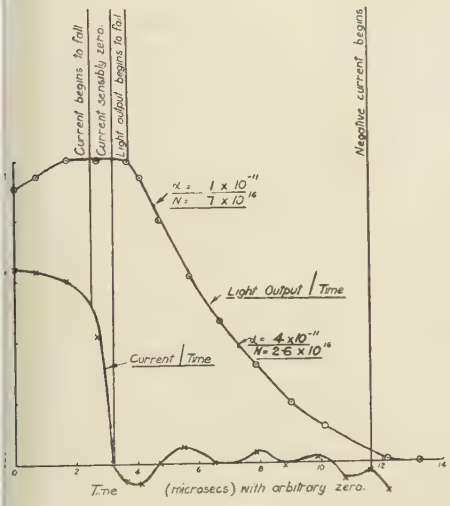

ure 2. Analysis of hydrogen afterglow (*a*) 10 microsec. 30 amp. pulse.

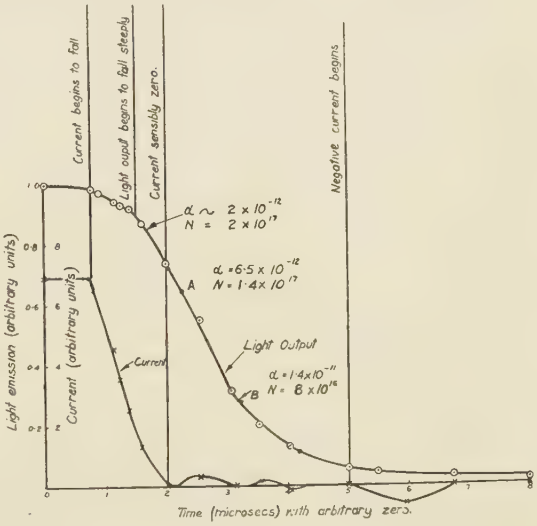

Figure 3. Analysis of hydrogen afterglow (*b*) 4 microsec. 120 amp. pulse.

short hydrogen afterglows and deriving approximate values for recombination oefficients from them. The circuits have been briefly mentioned by Craggs and Meek (1946) and will be described in more detail in a forthcoming publication by Craggs, Haine and Meek (1946). A typical current pulse (10 microsec., 30 amp.) is shown in figure 1 (*d*) and a typical light emission/time record, figure 1 (*c*), indicates that a short afterglow is observable. Figure 1 (*c*) was taken with a photoelectric electron multiplier tube and cathode ray oscillograph.

The current pulse of figure 1 (*d*) (reproduced in figure 2 after a correction by calibrations of the photo-tube and oscillograph), which is produced with an artificial transmission line arranged in a suitable discharging circuit, shows a fall-off of current taking a finite time, i.e. about 0·5 microsec. This current therefore vitiates measurements of the afterglows, but only for perhaps the first 20% or less of its life (figure 3) if a suitably matched transmission line is used for pulse generation.

It will be noticed from figure 1 (*a*), (*c*) and (*d*) that the peak light-output (visi radiation) is reached some time after the current has begun to fall. This is fou by careful fitting of the current and light output oscillograms at the beginning the current pulse, and hence appears to be a real effect. A possible explanatio that, during current flow, the electrical energy is stored in the discharge in form of positive ions, fast electrons and possibly highly excited atoms, and that t distribution needs a finite time ($\sim$1 microsec.) to establish some form of transi equilibrium at a lower electron temperature. Some support for this argument n be derived qualitatively from, e.g., figure 1 (*a*), which shows that, even when t current is established, the maximum light-emission is not reached for so further 3 microsec. or more.

Penning (1938) and others have studied similar effects for low-pressure gl discharges for vanishingly small currents, where the problem is much simplifi by the time stability of the discharge. However, it is hoped to obtain informati from further experiments on short-time sparks bearing on this interesting proble of the variation of electron temperature with time.

It is important to consider the frequency response of the amplifier/photo-tu arrangement. The high-frequency amplifier has been briefly described Craggs and Hopwood (1946). The circuit time-constant was about 0·3 microse i.e. was low compared with an afterglow time of 3–4 microsecs. (15,000-Ω outp load, and 20 mmF. oscillograph input capacitance) and the light/time diagra were not sensibly altered in shape when the load was decreased to 3000 Ω, but t latter load gave inconveniently low output voltages. The frequency response the amplifiers was checked with pulse generators and figures 4 (*a*) and (*b*) sho typical results.

The response of the multiplier tube to light pulses of known shape is mu more difficult to determine, and would be limited by transit-time effects, or a lag the photo-emission mechanism. Zworykin *et al.* (1936) show these to be negligib for ordinary photocells at, e.g., 1 mc./sec., which may be considered as an effecti frequency for the present work. R. A. Houstoun (1936) showed that with standard commercial vacuum photocell the difference in response for exposures $1{\cdot}59 \times 10^{-6}$ and $7{\cdot}4 \times 10^{-8}$ sec. was only about 0·1%. Further experiments cite by Houstoun showed that the response from $4{\cdot}4 \times 10^{-3}$ sec. and $1{\cdot}47 \times 10^{-7}$ se exposures were the same within the limits of experimental error. Recent wor by Geist (1941) proved that even for 10 cm. diameter photocells at only 150 v., th transit time effect was negligible for operating frequencies of 1 mc./sec.

The authors performed some experiments with a rotating mirror and sl system arranged to give short light pulses, but a more satisfactory and simple way exists of showing that the multiplier tubes are capable of responding to ligh changes occurring more rapidly than those in hydrogen afterglows, viz. the rat of increase of light output from argon sparks, during the initial stages of the spark is seen to be considerably greater than that for hydrogen sparks when examine with electron multipliers (Craggs and Meek, 1946).

§ 4. EXPERIMENTAL RESULTS

Many new data have been collected since the earlier work was reporte (Craggs and Meek, 1946). Typical records are shown in figures 1 and 2, an

afterglow curves taken with two different sets of apparatus more than two years apart are shown superimposed in figure 5. Figure 5 (*a*) shows a record from the previous research (Craggs and Meek, *loc. cit.* in which no amplification between multiplier and oscillograph was used) compared with one of the new oscillograms taken with a different type of electron multiplier and with the introduction of an amplifier (figure 5 (*b*)).

Now, Craggs and Hopwood (1946) have shown that the ion concentration for the hydrogen spark channels used in these experiments is $2{\cdot}5 \times 10^{17}$ ions/cc. (N_{i_0}), i.e. at the commencement of the fall of light emission. The fact that such high ion

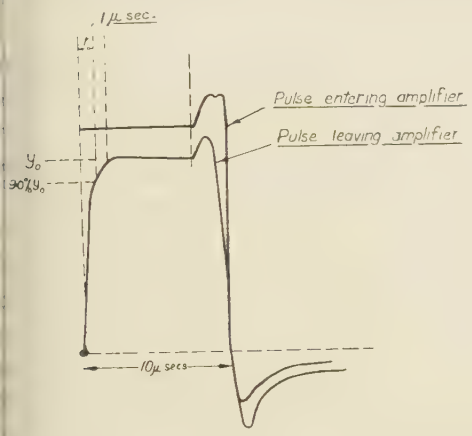

Figure 4. Frequency response of one of the amplifiers used with the photo-tube and oscillograph system. The amplifier gives ~90% in microsec.

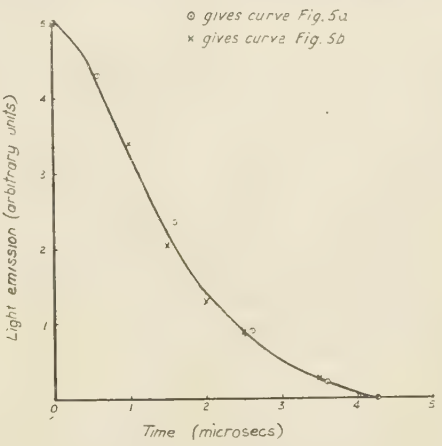

Figure 5. Afterglows as measured with two sets of recording equipment.

concentrations (giving a pronounced Stark effect) are found suggests at once that calculations of recombination coefficients will apply only approximately to spark channels, i.e. to an extent depending on the importance of the "level smearing". It is hoped to discuss this matter in more detail elsewhere. Since the recombination coefficient α is given by

$$dN_i = -\alpha N_i^2 dt, \qquad \ldots\ldots(4)$$

which is equation (1) re-written, and if it is assumed that recombination is responsible for the afterglow, then the light output L_t at time t is given by (k is a constant)

$$L_t = k \cdot \frac{dN_i}{dt} = k \cdot \alpha N_i^2. \qquad \ldots\ldots(5)$$

The positive ion and electron concentrations are supposed equal, since diffusion of electrons must be negligible (see below). Thus

$$\frac{1}{N_{i_1}} - \frac{1}{N_{i_0}} = \alpha \cdot \Delta t,$$

where Δt is the time interval during which N_{i_0} (the ion concentration with current flowing) falls to N_{i_1}. Assuming α constant during Δt, which is taken as 0·5 microsec., then since $L_t = KN_i^2$, N_{i_1} is found from N_{i_0} and α is determined. A more accurate method of determining α at various points on the afterglow curve is by graphical integration, using the following procedure. When the light has

fallen sensibly to zero, as it does for example at $t = 13$ microsec. in figure 2, th the ion concentration at that time may be taken as zero. The area of the cur included from an earlier time, when the ion concentration is say N_{i_1}, to the tir when the ion concentration is zero, is (see equation (5))

$$k\int_{t_{N_i=0}}^{t_{N_i}} \frac{dN_i}{dt} = kN_i.$$

This integral taken from the beginning to the end of the afterglow is kN_{i_0}, whe N_{i_0}, is known, and so k may be found. Thus N_i can be found at any point in t afterglow. Finally, since the ordinate at any point is $k\alpha N_i^2$ with the values of and N_i obtaining at that point, α may be found since it is then the only unknow It was in this way that the values of α shown in figures 2 and 3 were determined.

Figures 2 and 3 show afterglow curves in which α has been calculated for th marked points, and α is shown to rise (figure 3) from about 2×10^{-12} to 1×10^{-11} about 2 microsec. As mentioned above, the persistence of a small current for th first period (perhaps one-third) of the afterglow would vitiate the results ther The records of figures 1, 2 and 3 are, however, not affected in this way. Thes values of α are total recombination cross-sections if the fraction of recombinatio giving Balmer quanta is approximately independent of temperature over the rang say, 1000–5000° C. This assumption seems reasonable (Zanstra, 1946; Cillie 1932, 1946).

§5. DISCUSSION OF THE EXPERIMENTAL RESULTS

It is next necessary to justify the assumption that electron/ion recombinatio is the controlling process for the hydrogen afterglows. Molecular hydrogen i apparently absent from the discharge (100% dissociation) because no molecula spectrum is observed; the electrical and thermal properties of the spark channel are such (Craggs and Meek, 1946) that this result, in accordance with Lord Rayleigh's experiments (1944), is to be expected. It is not certain that negativ ions are absent in the hydrogen sparks but this difficulty is eliminated by showing that the afterglow curves of figures 1 etc. are those which are, in fact, given by the continuous radiation on the short wave-length side of the Balmer serie limit at 3647 A., as well as by the visible radiation in the Balmer series, since the series limit continuum is due to electron/ion recombination.

Loeb (1939, pp. 144, 145 and elsewhere) has discussed the other forms of recombination, i.e. preferential, columnar and initial recombination. It is unlikely that these processes are relevant to the case of spark channels in hydrogen, and so volume electronic recombination is the only mechanism of importance.

A Wratten filter No. 1 passes radiation for $\lambda > 3600$ A. (95% transmission at $\lambda = 3800$ A. and 0·1% transmission at $\lambda = 3650$ A.) and the spark radiation for $\lambda < 3650$ A. can thus be found by measuring the total radiation and that passing through the filter and performing a subtraction. Some results are shown in figures 6 and 7, and it is clear from the latter that the recombination radiation decays at the same rate as the visible radiation in the Balmer series. The subtractive process is rarely used since it is more convenient to observe the visible radiation. Later records taken with a spectrometer and sensitive amplifier show that H_α, H_β and H_γ all decay at sensibly the same rate, which is that of the Balmer continuum in figure 7.

In order to calculate the recombination coefficient it is not necessary to show that all the afterglow radiation is due to recombination, but it would clearly be of interest to do so, since the relative importance of other processes (e.g. thermal excitation) could then be assessed.

It is fortunate that astrophysicists have studied the hydrogen recombination spectrum in great detail, and it is interesting to apply the results of their calculations to the present case. Pioneer work in this field is due to Zanstra (1927). Menzel and Cillié (1937) show that E_c, the energy emitted (frequency ν) per second per c.c. of gas for a unit wave number range in the continuum, is given by

$$E_c \propto e \frac{\chi_2 - h\nu}{kT_e}. \qquad \ldots\ldots(6)$$

χ_2 is the ionization potential from the second quantum state, i.e. approximately 3·38 v., k is Boltzmann's constant and T_e is the absolute electron temperature.

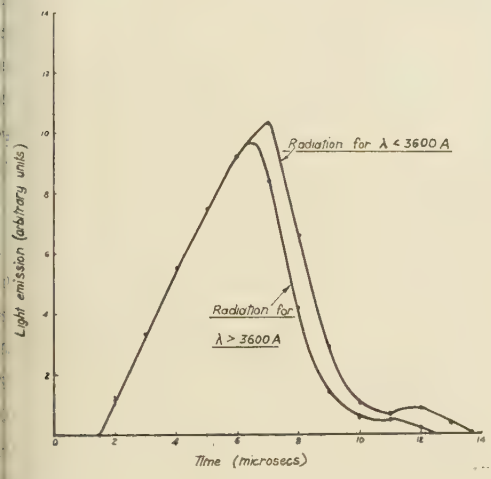

Figure 6 (*a*). Radiations emitted from a hydrogen spark, above and below the Balmer series limit. The curves have scaled together at the 6 microsec. point.

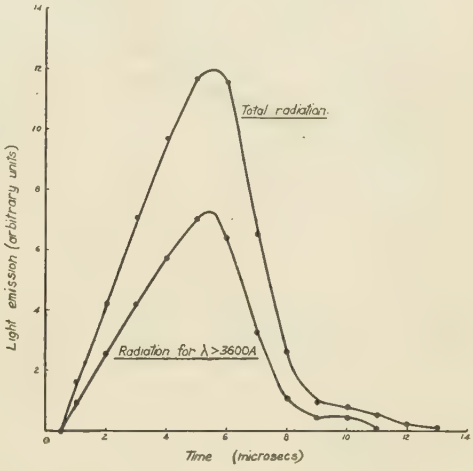

Figure 6 (*b*). The light emission from a hydrogen spark, taken with and without a Wratten No. 1 filter between source and photo-tube.

For $T = 20000°$, equation (3) gives the results plotted in figure 8, where it is seen that E_c varies only by about 10% from the mean at about 3500 A., over the range from the series limit at 3647 A. down to 3300 A. which is about the cut-off limit of the glass optical system used in the present experiments. This range covers some $2{\cdot}5 \times 10^3$ cm^{-1}. Cillié (1936) calculated the strength of H_β (and the other Balmer lines for a recombination spectrum) in terms of the energy emitted per unit wave number at the series limit and found this ratio to be about 10^3 at $T_e = 20000°$. The intensities of 8 Balmer lines (excluding H_α, which is much attenuated by the extremely low multiplier response for red light) are plotted in figure 9. It is easily shown that the total continuous radiation is probably ~50% of the total Balmer radiation, making allowance for the colour response of the multiplier. The latter is discussed in a forthcoming paper by the present authors.

Figures 7 and 8 show that the continuous radiation is of this order when allowance for the multiplier's colour-response is made. This approximate

experiment which is to be extended in a separate investigation, strongly suggest that the hydrogen afterglows are due almost entirely to recombination radiation.

Zanstra (1946) has proposed, as Craggs and Meek (1945 and 1946) had done, that Rayleigh's observations of long duration Balmer spectra should be explained by recombination, and worked out the electron/ion recombination coefficient from the theoretical results of Cillié (1932) and others, giving the data of table 1.

Table 1

T (° c.)	1000	5000	10 000	20 000	50 000
$10^{14}\,C$	218	74	46·0	27·0	13·5
$10^{14}\,C'$	122	33	17·7	9·4	3·6

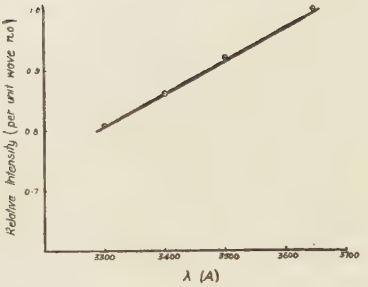

Figure 7. The intensity distribution in the Balmer series limit continuum for $T_e = 20\,000°$.

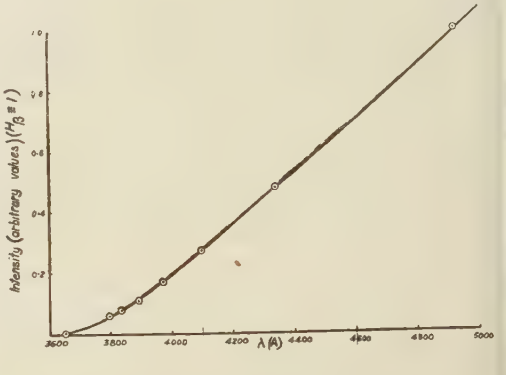

Figure 8. Intensity distribution in Balmer series (recombination) from Cillié's data. $T_e = 2000°$.

C is given by

$$dN/dt = -N^2C, \qquad \ldots\ldots(7)$$

where

$$C = \sum_{n=1}^{n=\infty} C_n, \qquad \ldots\ldots(8)$$

and n refers to a particular energy level,

$$C' = \sum_{n=3}^{n=\infty} C_n, \qquad \ldots\ldots(9)$$

and gives (with equation (7)) the number of recombinations/c.c./sec. giving quanta emitted as Balmer radiation.

Comparison of our results (figure 3) with Zanstra's computations show that the electron temperature probably falls from its value of 10 000° in the spark to $<1000°$ in less than a microsecond. The rough estimate of spark temperature just given is based on various experiments (Craggs and Meek, 1946, and references there cited). For example, experiments in this laboratory (Craggs, Haine and Meek, 1946) have shown that for 120 amp., 4 microsec. argon sparks at about 1 atmos. pressure X/p falls to about 0·1 v./cm./mm. Hg at the end of the period of current flow.* If the data of Allen (1937) can be considered relevant, which is probably only approximately true, T_e is then 10 000°, with higher values up to

* X is the electric field.

$>100\,000°$ in the preceding parts of the discharge. The fall may take place during current flow, since (Craggs, Haine and Meek, 1946) $X\,p$ falls from an initial value of ~40 v./cm./mm. to <1v./cm./mm. whilst current is still flowing in a spark in which a 4 microsec. square current pulse is used, or it may have taken place after the current has fallen to a very low value.

It is of great interest to note that from figures 2 and 3 the recombination coefficients for comparable periods* in the afterglow are nearly the same despite the great difference in the initial values of ion concentration (the latter quantities were measured in a separate research and details will shortly be published). The conclusion from this finding is that the electron temperature is largely dependent on ion concentration for sparks of the type described here. Further experiments on this and other aspects of spark channels are in progress. It is interesting also to note (figure 2) the slower afterglow decay for the lower value of initial ion concentrations, in accordance with expectations. The diffusion of electrons out of the spark channel in the times involved here can be shown by approximate methods to be negligible (Margenau *et al.*, 1946, and Loeb, 1939, p. 175). Because of the large number of positive ions present, diffusion will be at a slower rate than that for free electrons and the movement should certainly be <0·1 mm. in 4 microsec.

Zanstra points out that since the cross-section for electron excitation is $\sim 10^{-16}$ cm^2 and that for capture is $\sim 10^{-21}$ cm^2 the former process will predominate in the earlier part of the de-ionization process. By virtue of this, however, the electronic kinetic energy is soon spent and the recombination process then assumes control.

An illustration is provided by elementary consideration of energy loss at electronic collisions, for which the tables of Healey and Reed (1941) have provided the numerical data. It must be emphasized that conditions in spark channels are so transitory and ill-defined that the following treatment is necessarily approximate. At $X/p = 0{\cdot}25$ v./cm./mm. the mean electronic velocity is 2×10^7 cm./sec. in hydrogen, with a mean free path of

$$\frac{3{\cdot}6 \times 10^{-2}}{760} \text{ cm.}$$

at $p = 760$ mm. Hg. The spark channel temperature is much higher than room temperature but in the times involved (few microsec.) gas movement is negligible and so the gas density remains constant. In 1 microsec. the number of electronic collisions is therefore

$$\frac{2 \times 10^7 \times 10^{-6} \times 760}{3{\cdot}6 \times 10^{-2}} \sim 4 \times 10^5.$$

The fraction of the energy lost per collision is (Townsend and Bailey, *loc. cit.*) 26×10^{-4}, so the total energy loss in 1 microsec. is thus $\geqslant 100\%$ or, at least, is very great. It is therefore clear that a rapid fall in electron temperature, such as that indicated by the results shown in figure 2 etc. is reasonable. Experiments intended to determine the electron temperatures in these sparks are in progress.

Since this paper was first written, Margenau *et al.* (1946) have studied the dissipation of energy of an electron swarm in T.R. switches (radar practice). They show by similar arguments to the above that, in argon at 10 mm. Hg pressure,

* i.e. when the ion concentrations are equal.

free electrons will lose most of their energy in ~4 microsec. At 760 mm. Hg pressure, the relaxation time would then be <0·1 microsec.

The importance of recombination processes in determining electrical conditions in the earth's upper atmosphere is well known. Appleton (1937) has summarized the situation and has pointed out that from the data of Morse and Stueckelberg (1930) $\alpha = 1{\cdot}1 \times 10^{-11}$ for $T = 400°$ K. (0·05 ev. energy of electrons) and for capture to the ground state; α varies as T^{-1}. The contribution to α due to recombination into excited states does not appreciably increase α. Appleton showed that α deduced from Milne's work cited by Chapman (1931) is in agreement with that already given, and thus that there certainly appears to be a discrepancy between theoretical and experimental values of α. Sayers (1943) pointed out that α (F_2 region) is apparently $\sim 10^{-10}$ cm^3/sec., in agreement with the existing low-pressure data (Mohler *et al.*), but emphasized that conditions in the two sets of circumstances may not be comparable. Massey and Bates (1943) discuss the electron/ion recombination of oxygen also with reference to conditions in the ionosphere and show that, for example, at 1000° K. the total calculated coefficient is only $\sim 1{\cdot}5 \times 10^{-12}$ cm^3/sec., which is much lower than the experimental values of Mohler and Kenty and those determined for the F_2 layer. Massey and Bates stress the need for further investigations.

Bates *et al.* (1939) have worked out some useful expressions for recombination processes used by Craggs and Hopwood (1946), where it is shown that α (hydrogen) is about 2×10^{-13} cm^3/sec. for an electronic energy of 2 ev. ($T_e \sim 15\,000°$). Using the same expressions, the values of α at 5000° and 1000° respectively are about 5×10^{-13} and 10^{-12}, thus agreeing satisfactorily with Zanstra's data given above.

§ 6. CONCLUSIONS

It would appear that the present experiments on electron /ion recombination in hydrogen spark channels confirm the theoretical values. Uncertainties still exist, however, in that the electron temperatures have not yet been determined for these conditions, and the general physical properties of spark channels need further investigation. The effect of radiationless 3-body collisions, leading to recombination, has been discussed by Craggs and Hopwood (1946).

§ 7. ACKNOWLEDGMENTS

The authors wish to thank Professor S. Tolansky for the use of his microphotometer, which was modified by one of us (W. H.) to a self-recorder.

The authors are also indebted to Mr. F. R. Perry for his support of the programme on spark channel investigations now being carried out in the High-Voltage Laboratory. The authors also wish to thank Sir Arthur P. M. Fleming, Director, and Mr. B. G. Churcher, Manager, of the Metropolitan-Vickers Research Department, for permission to publish this paper.

REFERENCES

Allen, H. W., 1937. *Phys. Rev.*, **52**, 1707.
Appleton, E. V., 1937. *Proc. Roy. Soc.*, A, **162**, 451.
Bates, D. R., Buckingham, R. A., Massey, H. S. W. and Unwin, J. J., 1939. *Proc. Roy. Soc.*, A, **170**, 322.
Chapman, S., 1931. *Proc. Roy. Soc.*, A, **132**, 352.
Cillié, G. C., 1932. *Mon. Not. R. Astr. Soc.*, **92**, 820.

Cillié, G. C., 1936. *Mon. Not. R. Astr. Soc.*, **96,** 771.
Craggs, J. D., Haine, M. E. and Meek, J. M., 1946. *J. Instn. Elect. Engrs.* (in the press) : an abstract has appeared (*J. Instn. Elect. Engrs.*, **93,** IIIA, No. 1, 191 (1946)).
Craggs, J. D. and Hopwood, W., 1946. Submitted for publication.
Craggs, J. D. and Meek, J. M., 1945. *Nature, Lond.*, **156,** 21.
Craggs, J. D. and Meek, J. M., 1946. *Proc. Roy. Soc.*, A., **186,** 241.
Gassiot Committee, 1942–43. *Rep. Progr. Phys.* (*Phys. Soc.*).
Geist, H., 1941. *Hochfreq. u. Elektroakust*, **57,** 75.
Healey, R. H. and Reed, J. W., 1941. *The Behaviour of Slow Electrons in Gases* (Amalgamated Wireless (Australasia) Ltd.).
Houstoun, R. A., 1936. *Proc. Roy. Soc., Edin.*, **57,** 163.
Kenty, C., 1928. *Phys. Rev.*, 32, 624.
Loeb, L. B., 1939. *Fundamental Processes of Electrical Discharge in Gases* (London : John Wiley).
Margenau, H., McMillan, F. L., Dearnley, I. H., Pearsall, C. S. and Montgomery, C. G., 1946. *Phys. Rev.*, **70,** 349.
Massey, H. S. W., 1938. *Negative Ions* (Cambridge : The University Press).
Massey, H. S. W. and Bates, D. R., 1943. *Rep. Prog. Phys.* (*Phys. Soc.*), **9,** 62.
Meek, J. M. and Craggs, J. D., 1943. *Nature, Lond.*, **152,** 538.
Menzel, D. H. and Cillié, G. C., 1937. *Astrophys. J.*, **85,** 88.
Mohler, F. L., 1928. *Phys. Rev.*, **31,** 87.
Mohler, F. L., 1937. *J. Res. Nat. Bur. Stds., Wash.*, **19,** 559.
Mohler, F. L. and Boeckner, C., 1929. *J. Res. Nat. Bur. Stds., Wash.*, **2,** 489.
Penning, F. M., 1938. *Physica*, **5,** 286.
Rayleigh, Lord, 1944. *Proc. Roy. Soc.*, A, **183,** 26.
Sayers, J., 1938. *Proc. Roy. Soc.*, A, **169,** 83.
Sayers, J., 1943. *Rep. Prog. Phys.* (*Phys. Soc.*), **9,** 52.
Stueckelberg, E. C. G. and Morse, P. M., 1930. *Phys. Rev.*, **36,** 16.
Zanstra, H., 1927. *Astrophys. J.*, **65,** 50.
Zanstra, H., 1946. *Proc. Roy. Soc.*, A, **186,** 236.
Zworykin, V. K., Morton, G. A. and Malter, L., 1936. *Proc. Inst. Radio Engrs.*, **24,** 351.

THE VARIATION OF THE REFLECTIVITY OF NICKEL WITH TEMPERATURE

By ROBERT WEIL,
South-West Essex Technical College

MS. received 16 *December* 1946 ; *in revised form* 18 *February* 1947

ABSTRACT. A new method for the measurement of the reflectivity of metals in the visible part of the spectrum is described : the multiple-reflection arrangement is applied to an investigation of the reflectivity of nickel at different temperatures. A novel way of polishing mirrors is given, and the construction of a vacuum furnace described. This is followed by an account of the experimental technique. Results are presented and it is suggested that the observed positive temperature coefficient of reflectivity is a relaxation phenomenon.

§ 1. METHOD

The objects of reflectivity measurements on metals are twofold: by means of Kirchhoff's law,

$$E+R=1, \qquad \ldots\ldots(1)$$

where E stands for emissivity and R for reflectivity, we obtain a value for the former by determining the latter. If the temperature variation is known for one of these

quantities this knowledge is of use in pyrometry. Also any irregularities which appear when R is plotted against the wave-length give an indication of absorption bands and thus of the natural frequencies of vibration of the bound electrons in the metal of which the mirror under investigation is made.

The use of a multiple-reflection method reduces the error of the values to small proportions and is to be preferred to the direct measurement of emissivity. Let the measured ratio of the intensity of a beam of light after n reflections to the original be S; let the error of the measurement be x, which may be positive or negative; let R be the true reflectivity of the metal; then

$$S+x=R^n, \quad S^{1/n}(1+x/S)^{1/n}=R,$$

or

$$R=S^{1/n}\left(1+\frac{x}{nS}\right). \qquad \ldots\ldots(2)$$

For a given error x the corresponding error in R will be proportional to the nth part of x. To measure small effects like the temperature coefficient of reflectivity in the visible, a multiple-reflection method thus seems indicated. Hagen and Rubens (1910) used a multiple-reflection arrangement for such a purpose, but it cannot give absolute values. The method described below has been devised in

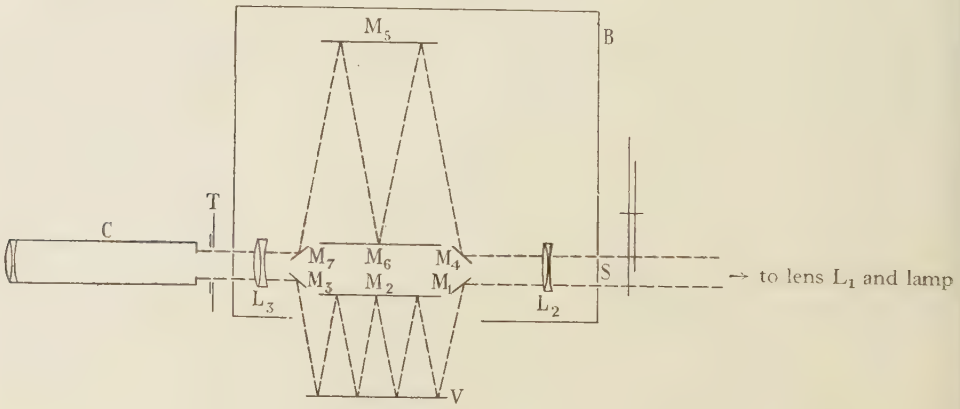

Figure 1. Elevation.

order to gather information about the temperature coefficient of reflectivity of both solid and liquid metals.

The set-up is such that four reflections take place on the surface under test, but this number can be increased. A null method is used to determine the loss in intensity due to these reflections: a beam from the same source of light as the one reflected at the mirror is compared directly with the latter, and a rotating sector is adjusted till a match is obtained between the two beams.

The source of light used was a 100-watt Mazda filament lamp run off a 36-volt battery. It was placed at the focus of a convex lens L_1 ($f=15$ cm.), and the beam uniformly illuminated a metal screen S in an aperture of the box B (figure 1). Two circular holes of equal diameter (<1 cm.) were drilled above each other in the screen S. The latter was at a distance of 5 yards from the source: this ensured that the images of the source on the mirrors mentioned below were small. The

two holes were the effective source of light. A rotating sector was placed between them and the lamp. Light from the lower hole passed through an achromatic lens L_2 and was reflected from an aluminized mirror M_1 on to the specimen V. This reflected it to the mirror M_2, etc. until, after four reflections, the beam struck the mirror M_3 which reflected it through another lens L_3 and a shutter T on to the slit of the collimator C.

Clearly, the beam reflected at the specimen was also reflected at M_1 and M_3, and three times at M_2. To balance the loss in intensity due to these reflections, the other beam—the standard—must be reflected as many times under similiar conditions. This was achieved by $M_{4,5,6,7}$ as shown in figure 1. These mirrors were prepared under identical conditions: the identity of the reflecting powers of $M_{1,3,4,7}$ on the one hand, and $M_{2,5,6}$ on the other, is essential for the success of the experiments. M_7, then, reflected the standard beam through the same lens L_3 on to the slit of C just above the image of the lower hole in S. The images of the two holes touched each other for reasons which will be given below.

The mirrors M_2, M_5, M_6 and V were all sufficiently parallel: symmetry for both beams was also obtained in connection with $M_{1,3,4,7}$. The mirrors could be adjusted in several ways. Inside the box B there were six vertical iron rods, three pairs being aligned as in figure 2. Iron bosses were used to attach to them

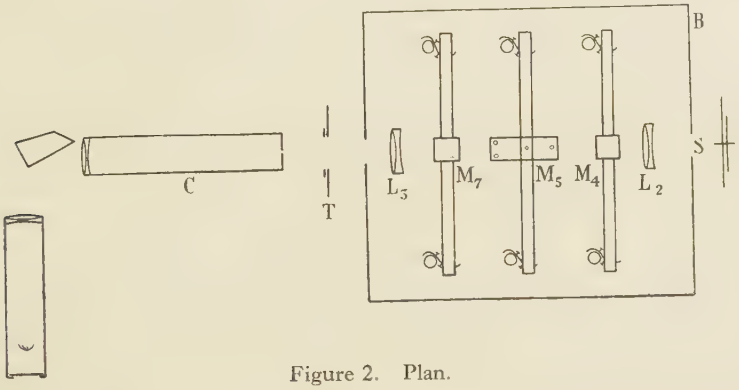

Figure 2. Plan.

horizontal bars, and these held the frames which, in turn, gripped the mirrors (figure 3). Two screws in the small, and three in the large, frames allowed a fine adjustment to be made in the inclination of the mirrors. This was not very critical from the optical point of view, since it has been found that at an angle of incidence of 45° the reflectivity differed from that at normal incidence only by 1%, but was vital for the geometry of the arrangement. The path-lengths of the two beams focused on C had to be equal. This was achieved by fixing the length of the lower beam and adjusting the mirrors until measurement by means of a ruler indicated approximately equal paths. The final fine adjustment was carried out by fixing a thin wire across the two holes in S and adjusting the mirrors of the upper beam until the images of both holes were in focus on the slit. Then the wire was removed.

On passing through the collimator, the beams were deflected by a constant deviation prism. They were then transmitted as two separate spectra through a lens which focused them on a ground-glass screen or a photographic plate.

Some further adjustment of the inclinations of the mirrors proved necessary to place corresponding wave-length ranges vertically above each other. This was ensured by replacing the filament lamp with a 250-watt Mazda mercury-vapour lamp. Both lamps were fixed to one stand, and by a simple rotation either the one or the other was made to illuminate S. Two well defined line spectra appeared on the ground-glass screen and were soon aligned. Their combined width was about 1 cm., and they were made to appear near the top of the screen: they could illuminate any part of the latter, since it could be moved vertically upward. This condition was important when photographic detection was used.

The following procedure was adopted in determining the spectral reflectivity of any specimen. The rotating double sector, devised by the author (Weil, 1947), was situated so that the standard beam was interrupted by the variable angle α_1, and the reflected beam by the fixed angle α_2. The former was varied until a

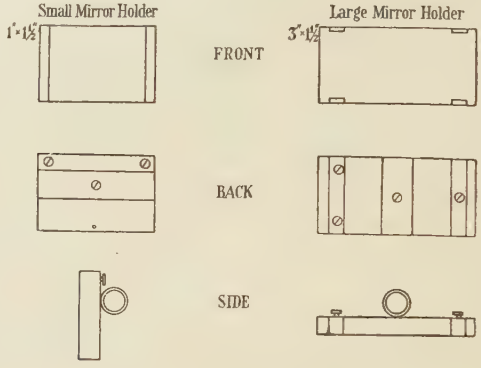

Figure 3. (Drawn to scale.)

match was obtained between corresponding spectral regions. If α_1 and α_2 are the two sector apertures, then

$$R^4 = \alpha_1/\alpha_2. \qquad \ldots\ldots(3)$$

In visual photometry it is important to bear in mind the Stiles-Crawford (1933) effect. To ensure that the matching of the intensities of the two visual fields was correct, the observer was placed in such a position as to keep his head vertical and his eyes in a plane perpendicular to the ground-glass screen. This position was made comfortable. Further, the field of observation was restricted by means of a slit in a movable opaque screen to a comparatively small area on either side of the dividing line between the two spectra. The slit also limited the wave-length range under observation. When a match was obtained, the line separating the two spectra from each other could not be discerned as they were touching. The calibration of the spectra was carried out with the mercury-vapour lamp.

Several assumptions have been made in the above, and they require some scrutiny. First, it was taken for granted, as explained above, that the illumination of the screen S was uniform. Secondly, the auxiliary mirrors are supposed to have identical reflecting powers. Prepared by evaporation under identical conditions, they were opaque to visible light, and, while there is no doubt that they aged, there is no reason to expect that the rates of ageing for the various mirrors differed.

Treating $M_{1,3}$ and $M_{4,7}$ as two items, it will be seen that 120 separate experiments would have to be performed to eliminate the effect of these mirrors. Even then it is assumed that the same part of each mirror is used every time. Preliminary experiments on mercury showed that interchanging the mirrors did not affect the results.

When the specimen is enclosed in a furnace, as in the case of nickel, and the lower beam passes eight times through a silica window, the symmetry of the arrangement is destroyed unless the standard beam is reduced in intensity to a corresponding degree. This was achieved by fitting two pieces of plane transparent silica underneath M_5.

The advantages of the above method can be summed up as follows:—

1. Multiple reflection gives rise to an increased accuracy in the value obtained for the reflectivity and facilitates the detection of small effects.

2. The direct and the reflected beams are observed simultaneously: thus a change in the intensity of the source of light has no influence on the measurements.

If photographic detection is used—

3. The limit to the number of wave-lengths examined is given only by the width of the plate and the nature of the emulsion, and the record of the experiment is permanent.

4. Only one specimen mirror is required (cf. Hagen and Rubens (1910) and Burger and van Milaan (1939), in whose arrangements two are used).

5. Assuming that differences in intensity equal to 1% can be detected visually (Helmholtz puts the limit at 1/167), the accuracy is about 1% for very low reflectivities, but improves rapidly with an increase of the latter. The above figures are conservative estimates.

The method described in the previous paragraphs was tested by measuring the reflectivity of aluminium. One of the mirrors used in the present work was prepared by Messrs. A. Hilger and another by Messrs. Bellingham & Stanley. The same mirrors were investigated by an arrangement due to Bor (1937). With this apparatus another observer obtained results which agree with the author's to within the experimental error. This represents an agreement between two entirely different methods as applied to one specimen which has so far not been obtained elsewhere. Tate (1912) determined the reflectivity of steel by a catoptric and a direct method and found that the agreement between the two was poor. Evidently better agreement can be achieved by using a more accurate direct method.

§ 2. THE EXPERIMENTS ON NICKEL

The work performed by Hurst (1937), Reid (1941) and others on the infra-red emissivity and reflectivity of nickel at different temperatures led to the belief that the temperature coefficient of reflectivity would be positive in the visible parts of the spectrum. This coefficient is determined by that of the electrical conductivity when R is measured at wave-lengths $\lambda > 10\mu$, since the Hagen-Rubens formula is then valid:

$$R = 1 - 2\sqrt{\frac{c}{\lambda\sigma}}, \qquad \ldots\ldots(4)$$

where λ is the wave-length of the radiation and σ is the conductivity of the metal of

which the mirror is made: c is the velocity of light. From this it is seen that, in the infra-red, the temperature coefficient of reflectivity is negative. Hence, if its positive sign can be confirmed for the visible, there must be a wave-length in the near infra-red for which the temperature coefficient is zero. The only determination of the temperature coefficient in the visible in the case of nickel has been carried out by Bidwell (1914), who measured the emissivity at a high temperature. He used the results of Hagen and Rubens (1902) for room temperature to deduce the temperature coefficient of emissivity for $\lambda = \cdot 66\,\mu$: it was $-1{\cdot}25 \times 10^{-4}$ per °C., or by (1) the corresponding reflectivity coefficient was positive. It is doubtful whether results obtained by entirely different methods can be combined in such a manner. As no measurements of the reflectivity of nickel in the visible have been carried out at different temperatures, it seemed worth while performing the work, especially as one and the same method was going to be used over a temperature range of over 400° C.

(1) *The mirrors*

Since preliminary experiments had made it desirable that the four reflections at the mirror under test should be in one line, the dimensions of the specimen were chosen as $4'' \times 0{\cdot}75'' \times 0{\cdot}2''$. Cold-rolled blocks of nickel of this size were obtained from Messrs. H. Wiggins, Birmingham. As the mirror was to be subjected to considerable temperature changes, there was no question of sputtering or evaporating nickel on glass or another substrate: the different coefficients of expansion would have ruined the surface. The only possibility, therefore, was polishing solid nickel.

Hothersall and Hammond (1940) state that, in the course of polishing nickel anodically, it has not yet been possible to eliminate the appearance of furrows: these are due to the explosive liberation of bubbles of gas on the mirror. Neither stirring nor changing the position of the anode removed this obnoxious effect in the present work. Thus a mechanical method of polishing had to be employed. Owing to the large surface of the mirror, and the occasional necessity of carrying out local polishing, it was not feasible to use a polishing machine. The whole preparation of the mirrors, with the exception of the surface-grinding, was therefore carried out manually.

To begin with, the specimen was surface-ground. The stone left marks parallel to the longest edge. After this, Oakey's emery paper was used in the usual manner. It was observed that, when the finer grades were moistened with water, the process was considerably accelerated. However, the paper dried fairly quickly and, while paraffin-oil also dried rapidly, it modified the surface of the paper in such a way as to render unnecessary its repeated application. Polishing the surface immediately afterwards with a paste of levigated magnesia powder in distilled water on Selvyt cloth gave rise to polishing pits. According to Ferguson (1943), these can be reduced by using No. 100 carborundum in a 1 : 1 liquid soap solution on a paraffin disc as an intermediate stage. The writer found it possible to eliminate them altogether by using a pitch surface in the following manner. Commercial pitch was heated until liquid, when it was poured on to a flat surface. A piece of plane glass, on which moist soap had been rubbed to prevent the pitch from sticking to it, was pressed on the latter when it was about to solidify. This surface was not perfectly continuous, but the small crevices and hollows in it were

useful as reservoirs of the thin suspension of alumina in distilled water, then poured on it. After a few minutes' polishing, striking results were obtained: the 4 0 scratches had more or less disappeared. The pitch surface was washed and dried, as was the specimen, and distilled water poured on the former. The polishing process was continued, the direction of the movement being changed, as the alumina was found to have a slight abrasive action. Finally, a piece of Selvyt cloth was wrapped round a small wooden block, a paste of magnesia applied, and the mirror touched up. It was possible to obtain very good mirrors consistently. As comparison with other work showed, their room-temperature reflectivity was amongst the highest measured. This is of interest, since Coblentz and Stair (1929) also used a solid nickel mirror made of a rolled rod of the refined metal, but their results are rather low.

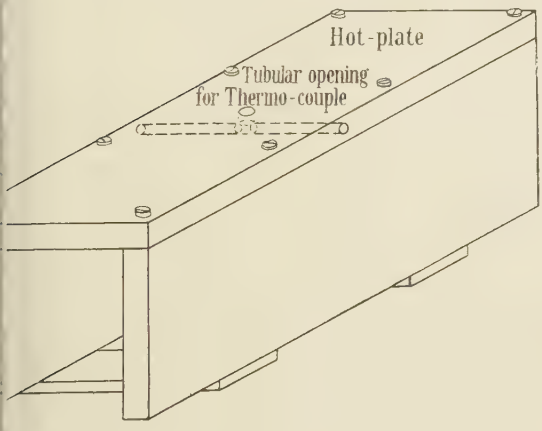

Figure 4.

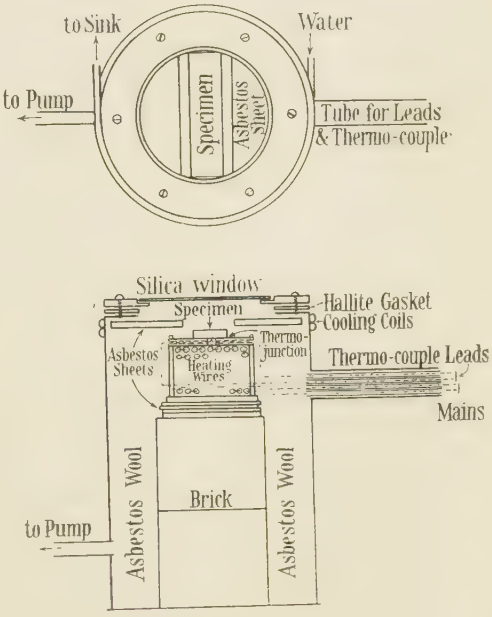

Figure 5.

(2) *The furnace*

After some preliminary work it was decided to use resistance heating. The specimen was placed on a hot-plate which formed part of the heating element. The latter consisted of a box (figure 4). Two steel plates, ($5{\cdot}75'' \times 1{\cdot}5'' \times \frac{3}{8}''$) were connected by two strips of steel along one of their longitudinal edges, and by the hot-plate ($5{\cdot}75'' \times 1{\cdot}5'' \times 0{\cdot}25''$) along the other. A tubular opening, $0{\cdot}1''$ in diameter, was drilled into the hot-plate parallel to its large planes and at right angles to its longitudinal edge, and a hole, $\frac{3}{16}''$ in diameter, at its centre. One small silica tube was placed into the opening on either side of the hole, and a platinum platinum-rhodium thermocouple threaded through them. The spot-welded junction protruded through the hole. Enough spring was provided for the specimen to depress the junction when lying on the plate: thus contact was ensured between the thermocouple and the specimen.

Sixty silica tubes, whose length was 6″, external diameter 3 mm. and bore 1 mm. were threaded on more than ten yards of Brightray wire (S.G.30). This chain was folded up, care being taken to avoid potential short circuits between the joints, and placed in the framework described above.

The furnace proper consisted of a cylinder (figure 5). A thin sheet of steel was bent into a cylindrical shape, the two straight edges being silver-soldered together. To one end of this cylinder, whose height was 10″ and whose diameter 7″, there was silver-soldered a circular plate made of mild steel, and to the other a circular flange. The external diameter of the latter was 7″, its internal 5·5″. The frame carrying the quartz window was screwed to it. It was made of another piece of mild steel, diameter 7″, thickness $\frac{3}{8}$″. An aperture of 4·5″ was cut into it, and a recess of 5·25″ was cut out of the plate: the quartz-window, whose diameter was 5″, fitted into it, an allowance being made for the vacuum wax. The window was fixed to the frame by pouring liquid Apiezon W (melting point 80–90° c.) into the recess, placing the silica plate there, and playing the flame of a Mekker burner around the frame until all the air holes in the wax had disappeared.

A steel tube of 3″ length and about 0·5″ diameter was fitted near the top of the furnace. The heater and thermocouple wires, adequately insulated by means of silica beads, were threaded through it, and connected to two pairs of terminals on two ebonite blocks. The latter were fixed rigidly to the tube. Some insulating tape was wound round the open end of the tube, and provided a suitable base on which to deposit vacuum wax. Diametrically opposite to this tube, another opening was made near the bottom of the furnace, and the connection fitted to a vacuum pump.

Water running through two turns of copper tubing cooled the joint between the furnace and the window-frame to such an extent that the vacuum wax applied there stayed solid even when the temperature in the furnace was 500° c. or more.

Two half-bricks were placed on top of each other inside the furnace. Several layers of asbestos board were put on top of them, and the heating element rested on the latter. Its direction was perpendicular to the line joining the two tubes mentioned above. No radiation therefore reached them directly, and thus they stayed cool. The whole of the furnace was lagged with asbestos wool. Two semi-circular discs of asbestos were placed just below the silica window, leaving an adequate gap for the beam reflected to and fro between the specimen and M_2.

(3) *Experimental technique*

Since it was not desirable to confine the measurements to one mirror only, several were prepared, or, alternatively, when one had been examined its surface was ground down with aluminium oxide and a fresh one prepared. The technique involved in carrying out these measurements will be described in the following.

The freshly polished mirror was placed on the hot-plate. Copper-foil was put around it to act as a getter. The pressure in the furnace could be reduced with a Cenco-Hyvac pump to 1 or 2 mm. of mercury and did not exceed 4 mm. at the highest temperatures used. The presence of the getter ensured, however, that the residual oxygen did not tarnish the specimen. This was easily ascertained by measuring the reflectivity also when the mirror cooled: since these results tallied

for identical temperatures with those obtained when the mirror was being heated, it was concluded that no noticeable tarnishing took place. Then a Hallite gasket was placed on the flange, and the window-frame screwed to the furnace by means of six screws. Apiezon W wax was next applied to the joint and a Mekker flame played over it. The six screw-heads were similarly covered: this operation lasted about five to seven minutes. Next the pump was started to test the pressure and to detect any leaks. Then the furnace was placed on a wooden box below M_3. The mains were connected to the heater, and a potentiometer, made by Messrs. Tinsley & Co., Type 3387 B, to the thermocouple. The water-mains and sink were fitted to the cooling coil. When the pressure in the furnace was a minimum, the mirrors $N_{2,3}$ were adjusted so that the reflected beam fell on the slit of the spectroscope as previously described. When this was done, and the equality of the path-lengths of the two beams ensured, the reflectivity of nickel was determined for different wave-lengths at room temperature. Then the heater, controlled by a transformer and a rheostat, was switched on. The reflectivity was measured at intervals of 80 or 100° c. and checked again as the furnace cooled.

(4) *Results*

The experimental results are presented in the table below. The temperature coefficient is defined by

$$\alpha = \frac{1}{R} \cdot \frac{dR}{dT}. \qquad \ldots\ldots(5)$$

A priori it is possible for dR/dT to be less affected by the condition of the surface of the specimen than α. This surmise was confirmed: initially, when not much experience had been gained in polishing mirrors, R was low, but dR/dT did not differ appreciably from later values. This is the reason why the results for the gradient are quoted in addition to those for R and α. The data represent mean values obtained from a number of measurements. Plotting R against the temperature gives straight lines for the whole range in which measurements were taken.

Table

Wave-length (μ)	0·47	0·53	0·59	0·64
Reflectivity (%) at room temperature: .	58·0	62·8	65·5	66·8
Reflectivity gradient, $\frac{dR}{dT}$ ($\times 10^3$) ..	9·28	7·53	6·55	5·68
Reflectivity coefficient, α ($\times 10^4$) ..	1·61	1·2	1·01	0·85

It is to be noted that, owing to a slight temperature gradient across the specimen, the temperature of the mirror was somewhat less than that given by the thermocouple. This is of no consequence as far as the results are concerned. The accuracy of the values varied from 0·9% in the blue to 0·5% in the red regions of the spectrum, improving with the reflectivity, as mentioned before. There was no discontinuity at the Curie point. This was to be expected since Löwe (1936) has shown in some experiments on the emissivity of nickel in the infra-red that such a discontinuity does not occur for wave-lengths $\lambda < 4{\cdot}5\ \mu$. Ornstein and Kofoed (1938), however, find a decrease in R amounting to 0·5% for a wave-length of $0{\cdot}65\ \mu$. Nor is there a discontinuity at what Schubert (1937) calls the temperature

of recrystallization, approximately 320° C. This refers only to the recrystallizatio of the amorphous surface layer of the mirror, for it is well known that the whole o the metal crystallizes at temperatures much nearer to the melting point. Th values of α are plotted against the wave-length in figure 6. This makes it possibl to compare them with those obtained by Hurst (1933) (emissivity) and Reid (1941 (reflectivity). The latter quotes in his results only three values, one of them at 5 μ and consequently a broken line represents his work.

It is seen that the temperature coefficient of the reflectivity of nickel in the visible parts of the spectrum is positive. Its numerical value increases as the

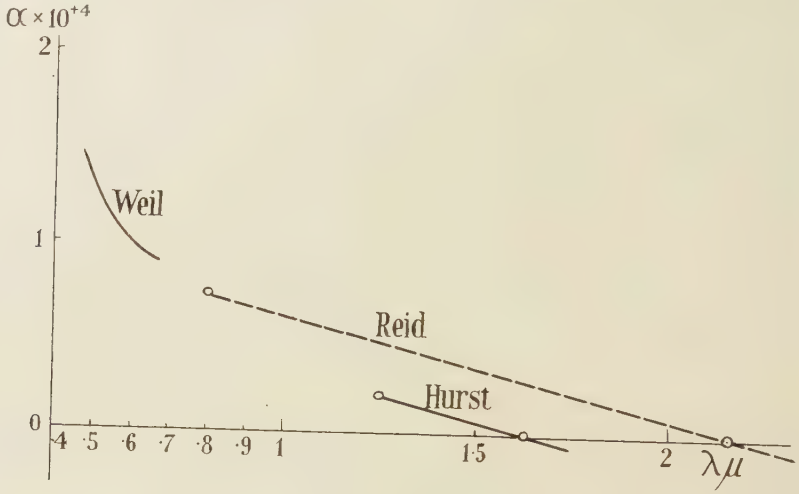

Figure 6.

violet end of the spectrum is approached, but this is largely due to the fact that the reflectivity is reduced. The writer (Weil, 1946) suggested a possible explanation of the positive sign of this coefficient. In the far infra-red the coefficient is negative since, as is seen from (4), it depends only on the temperature coefficient of the conductivity. As the visible parts of the spectrum are approached, the dielectric portion of the metal plays a greater rôle and it can be shown that its temperature coefficient tends to diminish the absolute value of dR/dT. If the term for the dielectric is greater than the one representing the free electrons, a positive value is obtained for α. The fact that the time of relaxation of the free electrons should be considered in the short-wave region is also relevant. It can be shown that under such conditions the temperature coefficient of $\sigma(\nu)$ (the conductivity for a frequency ν) is positive. An analysis of the whole problem will be presented in the near future.

ACKNOWLEDGMENTS

The above work has been carried out under the auspices of the Pyrometry Sub-Committee, British Iron and Steel Research Association. The writer would like to thank Dr. H. Lowery, for his interest in the work, and Mr. J. Bor, M.Sc. (Tech.), for many valuable discussions. The help given by Mr. R. J. Donato, B.Sc., and Mr. W. Bennett is also greatly appreciated.

REFERENCES

BIDWELL, 1914. *Phys. Rev.*, **3**, 439.
BOR, 1937. *Nature, Lond.*, **139**, 716.
BURGER and VAN MILAAN, 1939. *Physica*, **6**, 435.
COBLENTZ and STAIR, 1929. *Bur. Stand. J. Res., Wash.*, **2**, 343.
FERGUSON, 1943. *Metal Progress*, **43**, 743.
HAGEN and RUBENS, 1902. *Ann. Phys., Lpz.*, **8**, 1 ; 1910. *S.B. Preuss. Akad. Wiss.*, **23**, 467.
HOTHERSALL and HAMMOND, 1940. *J. Electrodepositors' Technical Soc.*, **16**, 83.
HURST, 1933. *Proc. Roy. Soc.*, A, **144**, 466.
LÖWE, 1936. *Ann. Phys., Lpz.*, **25**, 212.
ORNSTEIN and KOFOED, 1938. *Physica*, **5**, 175.
REID, 1941. *Phys. Rev.*, **60**, 161.
SCHUBERT, 1937. *Ann. Phys., Lpz.*, **29**, 473.
STILES and CRAWFORD, 1933. *Proc. Roy. Soc.*, B, **112**, 428.
TATE, 1912. *Phys. Rev.*, **34**, 321.
WEIL, 1946. *Nature, Lond.*, **158**, 672 ; 1947. *Proc. Phys. Soc.*, **59**, 161.

MAGNETIC FOCUSING BETWEEN INCLINED PLANE POLE-FACES*

BY H. O. W. RICHARDSON,

George Holt Physics Laboratory, University of Liverpool

(Now at Department of Natural Philosophy, University of Edinburgh)

MS. received 20 *November* 1946

ABSTRACT. Electron orbits have been computed in the magnetic field between inclined equipotential plane pole-faces. The field, if applied to β-ray spectroscopy, should give high dispersion and resolving power combined with a fair solid angle of collection Ω. In a particular case, Ω is estimated to be 16·5 times that of a conventional semi-circular spectrograph of similar dimensions.

If the inclined planes are bevelled so as to become parallel at their closest parts, both lateral and longitudinal focusing should occur. This case is treated approximately, and it seems probable that, although aberrations may reduce the resolution below that given by the first method, high values of Ω (of the order of 1 per cent of 4π) may be obtainable.

§ 1. INTRODUCTION

METHODS have recently been described for increasing the resolving power of the type of β-ray spectrograph which uses semi-circular focusing (Voges and Ruthemann, 1939; Korsunsky, Kelman and Petrov, 1945). The increase has been obtained by making small departures from uniformity in the magnetic field, for example—by altering the profile of the pole-faces of the magnet. In order to get good reproducibility and ease of construction, the simplest possible profile is evidently desirable.

It is thus of interest to calculate the orbits of electrons in the non-uniform field between two inclined plane pole-faces which are treated as infinite equipotential planes.

* Apart from minor corrections, these calculations were given in a report circulated in January 1944, but publication was delayed by the war.

The field is the same as that due to a straight current flowing along the lin of intersection of the two planes, and the lines of force are arcs of circles.

The orbits lose their circular shape and become periodic loops which ar a special case of the "enroulements trochoïdaux" used by Thibaud and other (Thibaud, 1938). Some features of the orbits, such as their turning point have been given by J. J. Thomson (1903).

It seems possible that a marked improvement in the resolving power an the solid angle of collection could be obtained in a spectrograph in which th orbits traversed a region in which the field strength varied by a factor of about 1C The gain in solid angle is partly due to the rate of sideways spreading of the beam being less than it is in the uniform field.

The sideways spreading can be further reduced by a modification of th profile of the pole-faces. In the modified profile, shown in figure 5, the inclined planes are bevelled so as to become parallel at their closest parts. The orbits in the case of bevelled poles are treated only approximately, but it seems tha this field should give some degree of both lateral and longitudinal focusing and should avoid the attenuation of the beams due to sideways spreading, which lowers the solid angle of collection of the semi-circular spectrograph.

As the pole-faces are treated as equipotentials, we assume infinite permeability and ignore the field of the magnetizing current.

§ 2. MATHEMATICAL THEORY

(a) *The magnetic vector potential*

Let r, z, and ϕ be cylindrical coordinates representing radial, longitudinal and azimuthal displacements with respect to the axis $r=0$ defined by the line of intersection of the two planes which contain the inclined pole-faces. The equipotential planes $\phi=$ constant all intersect along this axis, on which lie the centres of the circular lines of force. The field $\vec{H}$ satisfies

$$H=H_1/r, \qquad \ldots\ldots(1)$$

where H_1 is the intensity at $r=1$. The vector potential $\vec{A}$ obeys $\vec{H}=\text{curl } \vec{A}$ and, by Stokes' theorem,

$$\int(\vec{H}.\vec{d\sigma}) = \oint(\vec{A}.\vec{ds}), \qquad \ldots\ldots(2)$$

where $\vec{ds}$ is a vector forming an element of a closed path and $\vec{d\sigma}$ is a vector normal to an element of area $d\sigma$ of the surface bounded by the path over which the integral is taken. In our case $\vec{A}$ reduces to a single component parallel to the axis $r=0$, varying only with r, and of magnitude $A(r)$. Apply (2) to a rectangular path 1234 lying in an equipotential plane, then

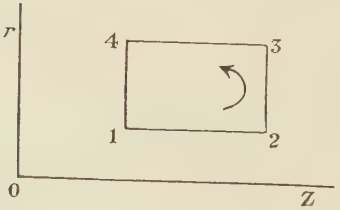

Figure 1.

$$\iint H_1/r\,.\,dr\,dz = A(r_1)(z_2-z_1)+A(r_2)(z_4-z_3). \qquad \ldots\ldots(3)$$

Thus $$A(r_1)-A(r_2)=H_1\log r_1/r_2. \qquad \ldots\ldots(4)$$

Let $A=0$ when $r=0$. Then

$$A(r)=H_1(1-\log r). \qquad \ldots\ldots(5)$$

(b) *Three-dimensional equations of the orbits*

The relativistic Lagrangian for a particle of rest-mass m and charge e_0, in e.m.u., moving with velocity $\vec{v}$ in a magnetic field, is

$$L = mc^2(1-\sqrt{1-v^2/c^2}) + e_0(\vec{v}.\vec{A}). \qquad \ldots\ldots(6)$$

$v^2 = \dot{r}^2 + \dot{z}^2 + r^2\dot{\phi}^2$ is a constant of the motion because the energy does not change. From (5)

$$L = mc^2(1-\sqrt{1-v^2/c^2}) + H_1 e_0 \dot{z}(1-\log r). \qquad \ldots\ldots(7)$$

The angular momentum p_ϕ about the z-axis is

$$p = \frac{\partial L}{\partial \dot{\phi}} = \frac{mr^2\dot{\phi}}{\sqrt{1-v^2/c^2}} = m_t . r^2\dot{\phi},$$

where m_t is the constant transverse mass. The first of Lagrange's equations gives $\dfrac{d}{dt}\left(\dfrac{\partial L}{\partial \dot{\phi}}\right) = \dfrac{\partial L}{\partial \phi} = 0$. Thus p_ϕ is constant. This is because the Lorentz force $\vec{F}$ always lies in an equipotential plane, so that it has no turning moment about the common axis of intersection of all these planes.

$$\frac{d}{dt}\left(\frac{\partial L}{\partial \dot{r}}\right) = \frac{d}{dt}(m_t . \dot{r}) = \frac{\partial L}{\partial r} = m_t . r\dot{\phi}^2 - \frac{H_1 e_0 \dot{z}}{r}. \qquad \ldots\ldots(8)$$

Thus
$$\ddot{r} = -\frac{H_1 e_0 \dot{z}}{r m_t} + \frac{p_\phi^2}{r^3 m_t}, \qquad \ldots\ldots(9)$$

$$\frac{d}{dt}\left(\frac{\partial L}{\partial \dot{z}}\right) = \frac{d}{dt}(m_t . \dot{z} + H_1 e_0(1-\log r)) = \frac{\partial L}{\partial z} = 0. \qquad \ldots\ldots(10)$$

Thus
$$\ddot{z} = \frac{H_1 e_0 \dot{r}}{m_t . r} \quad \text{and} \quad \dot{z} = \frac{H_1 e_0 \log r}{m_t} + C. \qquad \ldots\ldots(11)$$

At the longitudinal turning points of the orbits, $\dot{z} = 0$. Let the turning points be at $r = A$. Then

$$\dot{z} = \frac{H_1 e_0}{m_t} . \log\frac{r}{A}. \qquad \ldots\ldots(12)$$

Putting this in (9) and using $\int \ddot{r}\, dr = \int \dot{r}\, d\dot{r} = \dfrac{\dot{r}^2}{2} + \text{constant}$,

$$\dot{r}^2 = -\left(\frac{H_1 e_0}{m_t} . \log\frac{r}{A}\right)^2 - \frac{p_\phi^2}{r^2 m_t^2} + c'. \qquad \ldots\ldots(13)$$

From (12) and (13), $c' = \dot{r}^2 + \dot{z}^2 + r^2\dot{\phi}^2 = v^2$. Let

$$K = \frac{m_t . v}{H_1 e_0} \quad \text{and} \quad a_0 = \frac{p_\phi}{m_t . v}. \qquad \ldots\ldots(14)$$

K is proportional to the momentum $m_t . v$ if H_1 is constant.
From (13)

$$\dot{r} = \pm v\sqrt{1 - \frac{a_0^2}{r^2} - \frac{1}{K^2}\left(\log\frac{r}{A}\right)^2}. \qquad \ldots\ldots(15)$$

For computing the orbits it is convenient to express r, z, and ϕ in terms of a parameter ψ which satisfies $v\cos\psi = \dot{z}$. We see that ψ is the angle between

the velocity vector $\bar{v}$ at a point P on the orbit and a vector through P parallel to the axis $r=0$, pointing in the direction of increasing z. Equation (12) becomes

$$r = A\exp.\frac{m_t.\dot{z}}{H_1 e_0} = Ae^{K\cos\psi}, \qquad \ldots\ldots(16)$$

$$z = \int \frac{\dot{z}}{\dot{r}}\,dr = \frac{1}{K}\int \frac{\log\frac{r}{A}\cdot dr}{\sqrt{1-\frac{a_0^2}{r^2}-\frac{1}{K^2}\left(\log\frac{r}{A}\right)^2}}$$

$$= -AK\int \frac{e^{K\cos\psi}.\cos\psi.\,d\psi}{\sqrt{1-\frac{a_0^2.e^{-2K\cos\psi}}{A^2\sin^2\psi}}}, \qquad \ldots\ldots(17)$$

$$\phi = \int \dot{\phi}\,dt = a_0 v\int \frac{dt}{r^2}$$

$$= a_0 v\int \frac{dr}{\dot{r}r^2} = -\frac{a_0 K}{A}\int \frac{e^{-K\cos\psi}.\,d\psi}{\sqrt{1-\frac{a_0^2 e^{-2K\cos\psi}}{A^2\sin^2\psi}}}. \qquad \ldots\ldots(18)$$

Equations (12) and (15) were given by Thomson (1903), who used them to find the value of r at the turning points at which either $\dot{z}$ or $\dot{r}$ is zero.

(c) *Orbits from a point source*

Let a point source S lie in the mid-plane $\phi=0$ at $r=r_s$. At S let $\psi=\psi_s$ and let the velocity vector be inclined at an angle ξ_s to the mid-plane. ξ_s is a measure of the angular width of the emitted beam and is related to the constant a_0 by

$$a_0 = \frac{p_\phi}{m_t.v} = r\sin\xi = r_s\sin\xi_s. \qquad \ldots\ldots(19)$$

ξ is the inclination of the orbit at any point P to the meridional plane $\phi=$ constant, passing through P.

Consider a family of orbits of equal momentum coming from S with different angles of emission ψ_s. Each orbit has $r=r_s$ when $\psi=\psi_s$ so that, from (16),

$$A = r_s.e^{-K\cos\psi_s}. \qquad \ldots\ldots(20)$$

The equations of the family are

$$r = r_s.e^{K(\cos\psi-\cos\psi_s)}, \qquad \ldots\ldots(21)$$

$$z = -Kr_s.e^{-K\cos\psi_s}\int \frac{\cos\psi.e^{K\cos\psi}.\,d\psi}{\sqrt{1-\frac{\sin^2\xi_s}{\sin^2\psi}.e^{-2K(\cos\psi-\cos\psi_s)}}}, \qquad \ldots\ldots(22)$$

$$\phi = -K\sin\xi_s.e^{K\cos\psi_s}\int \frac{e^{-K\cos\psi}.\,d\psi}{\sqrt{1-\frac{\sin^2\xi_s}{\sin^2\psi}.e^{-2K(\cos\psi-\cos\psi_s)}}}. \qquad \ldots\ldots(23)$$

The integrands in (22) and (23) become infinite when $\psi(=\psi_m)$ is one of the solutions of

$$\sin^2\psi.e^{2K\cos\psi} = \sin^2\xi_s.e^{2K\cos\psi_s}. \qquad \ldots\ldots(24)$$

The infinities occur at the maxima and minima of r, where $\dot{r}=0$. The parameter ψ is excluded from the ranges of values in which the integrand is imaginary.

These ranges are centred on $\psi = n\pi$, where n is an integer, and are small if ξ_s is small.

(d) *Orbits lying in the mid-plane*

In β-ray spectroscopy the image will be formed by orbits which lie in or near the mid-plane $\phi = 0$, and for which the inclination ξ is small or zero. For $\xi_s = 0$, the equations of the family of coplanar orbits are

$$r = r_s \cdot e^{K(\cos\psi - \cos\psi_s)}, \qquad \ldots\ldots(25)$$

$$z = -Kr_s \cdot e^{-K\cos\psi_s} \int \cos\psi \cdot e^{K\cos\psi} \cdot d\psi. \qquad \ldots\ldots(26)$$

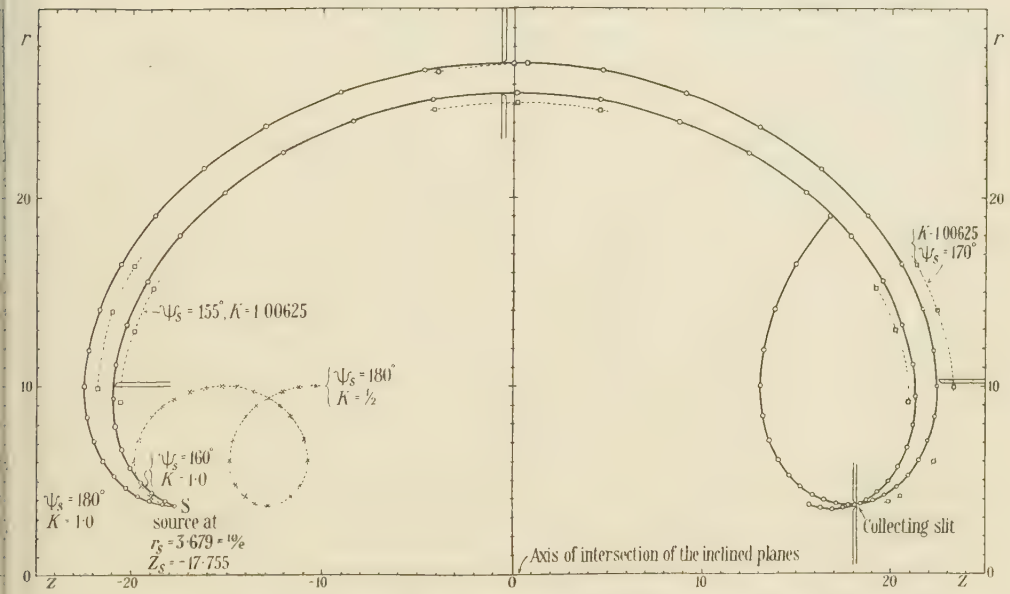

Figure 2. Orbits in the mid-plane $\phi = 0$ between inclined plane pole-faces. The baffles are adjusted for high resolution. They completely exclude the two ranges of rays with 0·625% higher momentum which would otherwise enter the slit. One narrow range is near $\psi_S = 155°$. The other, a wider one, is from 170° to about 190°.

If we put the source S at $z = 0$, the lower limit of the integral is at $\psi = \psi_s$. The integrand is always real, so ψ can now have any value. r varies periodically between Ae^K and Ae^{-K}, with maxima at $\psi = 2n\pi$ and minima at $(2n+1)\pi$, where n is an integer. The orbits, which are shown in figure 2, are a series of loops in which the radius of curvature ρ is equal to Kr. The z-displacement in a complete loop increases rapidly with K, as can be seen from the orbits with $K = \frac{1}{2}$ and $K = 1$. The loops contract to coincident circles as K, which is proportional to the momentum, approaches zero. Orbits with the same value of K have the same shape but different sizes, because both r and z are proportional to $e^{-K\cos\psi_s}$, which varies with the angle of emission ψ_s.

Let z_0 be the integral of (26) from $\psi = 0$ to $\psi = \psi$.

$$z_0 = -Kr_s \cdot e^{-K\cos\psi_s}\left[\frac{K\psi}{2} - \frac{K}{4}\cdot\sin 2\psi + \sin\psi \cdot e^{K\cos\psi}\right.$$
$$+ \frac{K^2}{3}\cdot\sin^3\psi\cdot\left(1+\frac{K^2}{3.5}+\frac{K^4}{3.5^2.7}+\frac{K^6}{3.5^2.7^2.9}+\ldots\right)$$
$$+ \frac{K^3}{16}\cdot\left(\psi-\frac{\sin 4\psi}{4}\right)\left(1+\frac{K^2}{4.6}+\ldots\right)+\frac{K^4}{3!5}\sin^3\psi\cdot\cos^2\psi\left(1+\frac{K^2}{5.7}+\ldots\right)$$
$$\left.+\frac{K^5}{4!6}\cdot\sin^3\cdot\cos\psi\cdot\left(1+\frac{K^2}{6.8}+\frac{K^4}{6.8^2.10}+\ldots\right)+\text{etc.}\right]. \qquad \ldots\ldots(27)$$

It is usually easier to find z by numerical integration than by summing the terms in (27). Because the loops are symmetrical about the maxima and minima it is convenient to use the central difference formula (Whittaker and Robinson, p. 146), starting at $\psi=0$. Values of $\int_0^{\psi} e^{K\cos\psi}\cdot\cos\psi\, d\psi$ are given in table 1 for $K=\frac{1}{2}$, 1·0, and 1·00625. The close pair of values can be used to estimate the resolving power.

Table 1. Values of $\int_0^{\psi} e^{K\cos\psi}\cdot\cos\psi\cdot d\psi$, in radians. (For $K=\frac{1}{2}$ and 1·00625, 5-figure, and for $K=1$, 7-figure, trigonometrical functions were used.)

ψ	K			ψ	K		
(°)	0·5	1·0	1·00625	(°)	0·5	1·0	1·00625
10	0·2856	0·46965	0·4726	100	1·4755	2·23040	2·2421
20	0·5583	0·91157	0·9173	110	1·4360	2·19582	2·2076
30	0·8068	1·30243	1·3103	120	1·3765	2·14771	2·1596
40	1·0219	1·62648	1·6360	130	1·3015	2·09147	2·1035
50	1·1975	1·87685	1·8875	140	1·2150	2·03071	2·0430
60	1·3309	2·05483	2·0660	150	1·1202	1·96774	1·9804
70	1·4221	2·16785	2·1793	160	1·0197	1·90386	1·9169
80	1·4737	2·22688	2·2385	170	0·9158	1·83976	1·8531
90	1·4898	2·24395	2·2556	180	0·8102	1·77550	1·7893

The equation $r=A\cdot e^{K\cos\psi}$ was given by Larmor (1884) for the catenary curve assumed by a flexible conductor carrying a current and lying in a plane in a magnetic field produced by a stronger current flowing along the axis $r=0$, in the same plane.

§ 3. APPLICATION OF THEORY

(a) *Focusing of orbits lying in the mid-plane*

Because the orbits are symmetrical about the maximum at $\psi=0$, a ray emitted from S with $\psi=\psi_s$ will return to the initial radius r_s when $\psi=-\psi_s$. On plotting the orbits, it seems that the greatest concentration of returning rays is near $r=r_s$, so we expect to find an image I of the source S at some point on this radius. Let z_i be the distance from S to the point at which the ray returns to $r=r_s$. Then from (26)

$$z_i = -2Kr_s\cdot e^{-K\cos\psi_s}\int_{\psi_s}^{0}\cos\psi\cdot e^{K\cos\psi}\cdot d\psi. \qquad \ldots\ldots(29)$$

The displacement z_i is plotted against ψ_s in figure 3. It can be seen, for $K=1$,

to have a maximum at $\psi_s = 169°$, where the envelope of the family of orbits crosses $r = r_s$, giving an image with a sharp outer edge just as in semicircular focusing.

At $\psi_s = 180°$, a second stationary value of z_i can be seen. This arises because the loop near the image is cut by the line $r = r_s$ in two points which become coincident when $\psi_s = \pi$. The line is then a tangent to the loop. For certain positions of the slit this second kind of image can make a small addition to the solid angle of collection.

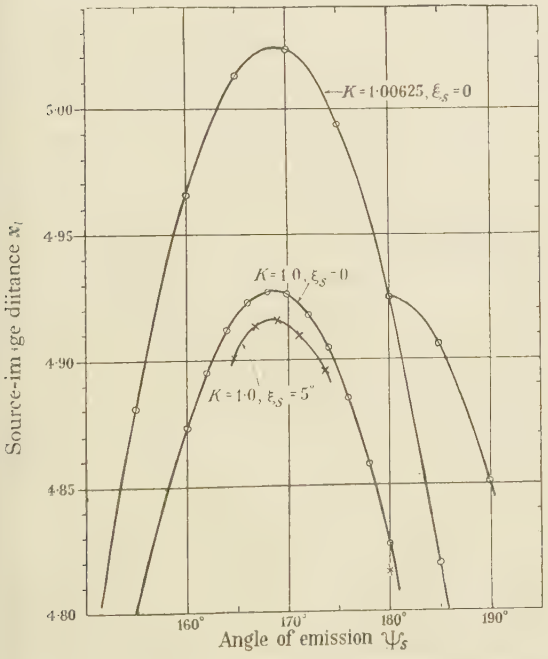

Figure 3. Focusing of orbits of differing inclinations ξ_s and momenta KH_1e_0.

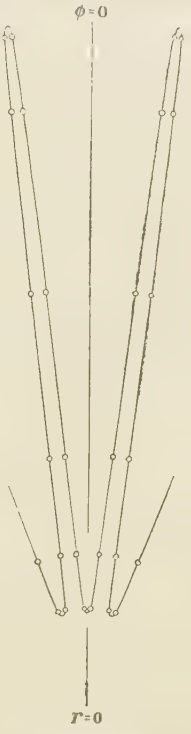

Figure 4. The projection of an orbit on the (r, ϕ) plane. Initial inclination $\xi_s = 5°$, with $\psi_s = \pi$, and $K = 1$.

(b) *Focusing of inclined orbits*

For inclined rays, (29) becomes

$$z_i = -2Kr_s \cdot e^{-K\cos\psi_s} \int_{\psi_s}^{\psi_m} \frac{\cos\psi \cdot e^{K\cos\psi} \cdot d\psi}{\sqrt{1 - \frac{b^2}{\sin^2\psi} \cdot e^{-2K\cos\psi}}}, \qquad \ldots\ldots(30)$$

where

$$b = \sin\xi_s \cdot e^{K\cos\psi_s}. \qquad \ldots\ldots(31)$$

The upper limit ψ_m is a value of ψ satisfying (24), at which the integrand is infinite. In the particular case in which $\psi_s = \pi - \xi_s$, the lower limit ψ_s also satisfies (24). The three lines forming the angles ψ_s and ξ_s are then coplanar, so that the projection on the mid-plane at S of $\vec{v}$ is parallel to $r = 0$. Thus S is at a minimum of r and an integration with the limits $\pi - \xi_s$ and ψ_m covers a complete half-cycle of ψ.

Expressions (23) for ϕ and (30) for z_i have been integrated numerically over this range of ψ with $\xi_s = 5°$. The projection of the orbit in the (r, ϕ) plane is plotted in figure 4. It consists of periodic peaks and troughs radiating from $r = 0$.

The angle ϕ_0 between adjacent troughs is 14°·60. For other values of ξ_s it is nearly proportional to $\sin \xi_s \cdot e^{-K \cos \xi_s}$ because the integral in (23) over a complete cycle of ψ only varies slowly with ξ_s for small values of ξ_s. It increases from 7·6647 to 7·9204 radians between $\xi_s = 0$ and 5°.

The integrations are made difficult by the infinities at the termini of ψ, which make successive differences Δ decrease slowly. ψ was broken up into the five ranges $175° - 170° - 160° - 10° - 2° - \psi_m = 40{\cdot}298$ minutes. The three inner ranges were integrated by the Gregory formula using intervals h of 2°, 10° and 1° respectively. For the outer ranges the formula of Jeffreys (1939) was used:

$$\int_0^{3h} (\alpha x^{-\frac{1}{2}} + \beta x^{\frac{1}{2}} + \gamma x^{\frac{3}{2}}) dx = h\left(\frac{14}{5}\sqrt{3} \cdot y_1 - \frac{8}{5}\sqrt{6} \cdot y_2 + \frac{12}{5} y_3\right). \quad \ldots\ldots (32)$$

y_1, y_2, and y_3 are the values of the integrand at $x = h$, $2h$, and $3h$ respectively.

In order to locate the image formed by rays with the same inclination ξ_s, it is necessary to find z_i with different angles of emission ψ_s. This introduces a difficulty because b in (30) then varies with ψ_s and a new set of integrands must be computed for each value of ψ_s. We can avoid this labour by allowing ξ_s to vary with ψ_s by the small amount needed to keep b constant. Then the same set of integrands can be used for all values of ψ_s, with the same upper limit at $\psi = \psi_m$.

Let $\sin \xi_s = b \cdot e^{-K \cos \psi_s}$, where $b = \sin 5° \cdot e^{-\cos 5°}$. Using $K = 1$ and $r_s = 1$, we get the values of z_i in table 2, which also contains some values for comparison found for rays in the mid-plane, with $\xi_s = 0$. In figure 3, z_i is plotted against ψ_s' where ψ_s' is the angle between the axis $r = 0$ and the projection on the mid-plane of the velocity vector $\vec{v}$ at S. It satisfies the relation

$$\cos \psi_s = \cos \psi_s' \cdot \cos \xi_s. \quad \ldots\ldots (33)$$

The use of the projected angle ψ' for inclined rays is convenient because, unlike ψ, it is excluded from no ranges of values.

Table 2

ψ_s	ψ_s'	ξ_s	z_i	ψ_s	ξ_s	z_i
175°	180°	5°	4·8156	180°	0	4·8263
172°	173° 45′	4° 58′	4·8953	172°	0	4·9178
170°	171° 6′	4° 57′	4·9096	170°	0	4·9261
168°	169° 2′	4° 55′	4·9153	168°	0	4·9269
166°	166° 52′	4° 52′	4·9135	166°	0	4·9222
164°	164° 42′	4° 50′	4·9049	164°	0	4·9115

The focusing of the inclined rays closely resembles that of the rays in the mid-plane, but the maximum displacement z_i is less by a factor of 0·9976. This shortening can be seen from the curve for $K = 1{\cdot}00625$ to be equivalent to that due to a decrease in momentum of 0·08%. It is less than with semi-circular focusing, where the shortening factor is $\cos \xi_s = 0{\cdot}99620$.

The length l of the image will be approximately $2r_s \cdot \phi_0$ because most of the rays which form the image will have ψ_s' just less than π, so that they will return to the initial radius after an azimuthal displacement ϕ just less than that between two troughs, ϕ_0. With the semi-circular spectrograph the image length l' is

$2\pi\rho \sin \xi_s$. With inclined poles with the same ξ_s, and $z_i = 2\rho$, the image length $2r_s\phi_0$ is only 0·3785 l'. This shortening of the image is due to the lower sideways spreading of the beam caused by the presence over the long outer parts of the inclined orbits of an inward component of the Lorentz force directed back towards the mid-plane. In the uniform field, in contrast, the rays spiral away from the mid-plane with the constant outward velocity $v \sin \xi_s$.

The curvature of the image is a little greater than with semi-circular focusing, because the smaller shortening of z_i is outweighed by the larger shortening of the image length l. The values of z_i in table 2 are calculated for intersections of rays with the cylinder $r = r_s$, so that the curved image is presumed to lie on this cylinder. The intersection of the envelope of the family of rays with a tangent plane to $r = r_s$, normal to the mid-plane, would have less curvature.

§ 4. THE SOLID ANGLE OF COLLECTION

Let Ω be the maximum solid angle formed at the point source S by the beam of rays of given momentum which enters the collecting slit when the field H is correctly adjusted. A fraction $\Omega/4\pi$ of all electrons emitted with this momentum will then be collected.

We consider an idealized case in which the slit, of constant width W, is curved to fit the curvature of the image, so that the entry of rays emitted with inclination ξ_s to the mid-plane is not reduced until their sideways displacement exceeds half the length of the slit. Ω is then approximately the product of two constant angular ranges $\Delta\psi_s$ and $\Delta\xi_s$, where $\Delta\psi_s$ is the range of ψ_s, measured in the mid-plane, which enters the slit, and $\Delta\xi_s$ is the range in lateral inclination.

The relation between W and $\Delta\psi_s$ has been found graphically by drawing orbits with different ψ_s, putting $\xi_s = 0$. For each range $\Delta\psi_s$, the slit was placed across the beam in the position which made the width W a minimum. The optimum source-to-slit distance z_i varies slightly with $\Delta\psi_s$. The results for $K = 1$ and $K = \frac{1}{2}$ are given in table 3, which also gives the slit width W' of a semi-circular comparison spectrograph of the same length which collects the same range $\Delta\psi_s$.

It can be seen that, with $K = 1$, a slit of given width collects about six times the range $\Delta\psi_s$ that is collected by the comparison spectrograph with a slit of equal width.

Table 3

$K = m_t \cdot v/H_1 e_0$	1·0				0·5	
Extreme angles of emission ψ_s (degrees)	200 150	190 150	190 160	180 160	160 110	140 120
Range collected $\Delta\psi_s$ (degrees)	50	40	30	20	50	20
Slit width W	0·064	0·038	0·0205	0·009	0·125	0·02
Source-to-slit distance z_i	3·41	3·46	3·52	3·60	2·55	2·55
Ratio $W : z_i$	0·019	0·011	0·0058	0·0025	0·049	0·0079
$W' : z_i$ for semi-circular spectrograph	0·097	0·06	0·0341	0·0152		
Ratio $W : W$	5·0	5·5	5·8	6·1	1·91	1·93

The largest value of the inclination ξ_s which allows the ray to enter the collecting slit is set by the azimuthal angle $2\phi_0$ between the two meridional planes $\phi = \pm\phi_0$ which contain the ends of the slit. This angle, in turn, is limited by the angle of inclination of the pole-faces.

For $\xi_s = 5°$, equating ϕ_0 to the angle between the minima in the (r, ϕ) plane, we have $\phi_0 = 14°{\cdot}60$. It is clear that a higher value of ξ_s, for example $7°{\cdot}5$, could be used with steeply inclined pole-faces.

For comparison we can calculate ξ_s'. for a semi-circular spectrograph of radius ρ and slit-length l. Then $\sin\xi_s' = l/2\pi\rho$.

Let $l = 1$ cm. and $\rho = 5$ cm. The range $\Delta\xi_s'$ is then $3°{\cdot}64$ compared with $\Delta\xi_s = 10°$.

If $\Omega = \Delta\xi_s \,.\, \Delta\psi_s$, we find that for $K = 1$ the inclined pole spectrograph has a solid angle of collection Ω about 16·5 times that of a parallel pole spectrograph with a slit of equal width and of length $\rho/5$, with the same source-image distance.

§ 5. MOMENTUM DISPERSION AND RESOLVING POWER

A knowledge of Ω makes it possible to estimate the counting rate at the peak of a β-ray line, but it does not give the shape of the line, or transmission factor, which would be a measure of the resolving power.

This shape would be difficult to compute in the present case, but we can get some interesting information from what may be called the momentum dispersion. This can be defined as the longitudinal displacement Δz_i in the position of the image I due to a fractional increase in momentum $\Delta p/p$, the field H being unchanged.

In the semi-circular spectrograph

$$z_i = 2\rho = \frac{2p}{He_0},$$

Thus

$$p\frac{dz_i}{dp} = \frac{2p}{He_0} = z_i.$$

The dispersion is proportional to the length of the spectrograph. With inclined poles, for K near to or greater than unity, ψ_s is near to π, so that

$$z_i = 2Kr_s \,.\, e^K \int_0^{\pi} e^{K\cos\psi} \,.\, \cos\psi \,.\, d\psi, \quad \text{approximately,}$$

$$= K^2 r_s \,.\, e^K \,.\, \pi\left\{1 + \frac{K^2}{2.4} + \frac{K^4}{2.4^2.6} + \cdots\right\}, \qquad \ldots\ldots(34)$$

from (27). We have $p = KH_1e_0$, giving

$$p\frac{dz_i}{dp} = \frac{Kdz_i}{dK} = K^2 r_s \,.\, e^K \,.\, \pi\left\{(K+2) + \frac{K^2}{2.4}(K+4) + \frac{K^4}{2.4^2.6}(K+6) + \text{ etc.}\ldots\right\}$$

$\ldots\ldots(35)$

For $K = 1$ this gives $p\frac{dz_i}{dp} = 4{\cdot}24z_i$, which represents 4·24 times the dispersion of a semi-circular spectrograph of the same length. Because $p\frac{dz_i}{dp}$ increases very rapidly with K, a spectrograph of high resolving power is possible.

A possible arrangement of defining baffles is shown in figure 2.

§6. LATERAL FOCUSING WITH BEVELLED POLES

Let the inclined plane pole-faces be modified, as in figure 5, so that the planes become parallel at a radius $r = r_p = \mathrm{OP}$ from the axis of intersection $r = 0$. The field near O is uniform and equal to H_0, whereas above P it will, after passing through a region of transition, become equal, as before, to H_1/r.

Possible advantages of such an arrangement of what may be called bevelled poles are (1) that more space is made available near the source and slit, and (2) that with a given source-to-slit length z_i, about half the flux density near the source is needed to focus a given momentum. A third advantage is that lateral focusing allows the use of a wider range $\Delta\xi_s$, so that the solid angle of collection Ω can be increased.

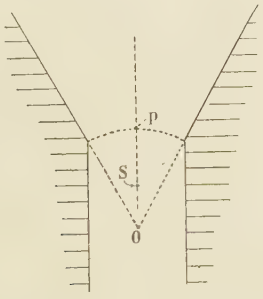

Figure 5. Profile view of the bevelled poles.

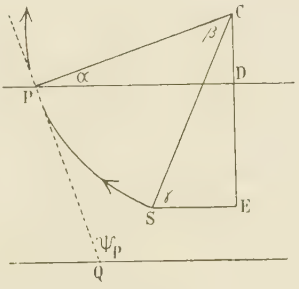

Figure 6.

Let ψ' be the angle between the axis $r = 0$ and the projection on the mid-plane of the velocity vector $\vec{v}$ at a point on the orbit. Lateral focusing is possible because, apart from small aberrations, we can find a position of the source S which allows all the members of a fan of rays with the same ψ'_s, but different inclinations ξ_s, to enter tangentially the equipotential planes $\phi = \text{constant}$ of the upper part of the field in figure 5. The tangential entry is made where the planes bend over in the transition zone near the cylinder $r = \mathrm{OP} = r_p$. The rays will remain in their respective planes until they return to $r = r_p$, when they will converge again to an image I lying in the mid-plane at $r = r_s$. Owing to small aberrations, the image will be a short line in the mid-plane rather than a point. It would be difficult to compute the orbits in the transition zone, but the uncertainty arising there should be small provided that the beam traverses the zone nearly at right angles to the axis $r = 0$.

The Lorentz force $\vec{F}$ will then be nearly parallel to that axis and will have no component in the (r, ϕ) plane, so the projections of the rays in that plane will be nearly straight when crossing the transition zone. Small variations of F with the azimuth ϕ may thus cause more disturbance of longitudinal than of lateral focusing.

§7. THE CONDITION FOR LATERAL FOCUSING

Let H_0 be the strength of the uniform field near the source S and let $2\phi_0$ be the angle between the inclined planes. The field at large r, $H = H_1/r$, is related

to H_0 by the requirement that the pole-faces must be equipotential surface This gives

$$H_1 = \frac{H_0 r_p \sin\phi_0}{\phi_0}. \qquad \ldots\ldots(36)$$

Let us make the paraxial approximation in which $\phi = \sin\phi$ and let the uniform field $H = H_0$ change abruptly at the cylinder $r = r_p$ to the decreasing field

$$H = \frac{H_1}{r} = \frac{H_0 r_p}{r}.$$

In figure 6 an orbit from S emitted in the mid-plane $\phi = 0$ crosses the boundary cylinder $r = r_p$ at P where $\psi = \psi_p$. Consider a fan of rays, emitted with different inclinations ξ_s, such that the projections on the mid-plane all have the same angle of emission ψ_s'. The projections will have radii of curvature $\rho_1' = Kr_p \cos\xi$ in the uniform field below r_p. Thus to the approximation that $\cos\xi_s = 1$, all the rays below P are spiral screws on a cylinder of radius $\rho_1 = Kr_p$.

Let the cylinder be straightened out so that the arc SP coincides with the straight line QP drawn along the tangent at P. Then the spiral screws coming from S become straight lines radiating from Q. If Q lies on the axis $r = 0$, the straight lines are all tangential to equipotential planes in the decreasing field above P. Thus the condition for lateral focusing is

$$\mathrm{PQ} = r_p/\sin\psi_p = \text{arc PS} = \rho_1\beta = Kr_p\beta. \qquad \ldots\ldots(37)$$

The condition cannot be exactly satisfied for large ξ_s because of the more complicated nature of the transition field and the variation of $\cos\xi_s$. Further, it is only valid for one value of ψ_s', other values giving fans of rays which, after straightening out, will radiate from points a little above or below the axis $r = 0$. This latter aberration gives rise to orbits which have small inclinations to the equipotential planes. For practical ranges of ψ_s the inclinations ξ are so small that the shortening of z_i will be negligible, and longitudinal focusing will be very little disturbed.

In order to satisfy (37) for the rays at the centre of the focused beam we must place the source S at the optimum distance above the axis $r = 0$. Let $\mathrm{DE} = C.r_p = \mathrm{CE} - \mathrm{CD} = Kr_p(\sin\gamma - \sin\alpha)$. Then

$$C = K(\sin\gamma - \sin\alpha). \qquad \ldots\ldots(38)$$

From (37)

$$\beta = \frac{\mathrm{PQ}}{Kr_p} = \frac{1}{K\sin\psi_p}.$$

We have $\alpha = \psi_p - \pi/2$, so that β can be eliminated and we can find the value of DE which gives lateral focusing for a given angle of emission $\psi_s = \gamma + \pi/2$.

This value of ψ_s should also satisfy the condition for longitudinal focusing. It seems that for $K = 1$, the fraction C should be about 0·7.

§ 8. LONGITUDINAL FOCUSING

As before, we seek for a stationary value of z_i, the distance from S at $r = r_s = r_p(1 - C)$ to the point at which the returning ray again crosses $r = r_s$. z_i will be the sum of a displacement z_p in the uniform field below $r = r_p$ and a displacement z in the decreasing field above.

$$z_p = -2(\mathrm{PD} - \mathrm{SE}) = -2\rho_0(\cos\alpha - \cos\gamma)$$
$$= -2\rho_0\left\{\cos\alpha \mp \sqrt{1-\left(\frac{C}{K}+\sin\alpha\right)^2}\right\}. \qquad \ldots\ldots(39)$$

The minus sign applies when $\gamma < \frac{\pi}{2}$.

$$z = 2Kr_p \,.\, e^{-K\cos\psi_p}\int_0^{\psi_p} e^{pK\cos\psi}\,.\cos\psi\,.\,d\psi. \qquad \ldots\ldots(40)$$

$z_i = z + z_p$ is plotted against ψ_s in figure 7. For $K = 1{\cdot}00$, $\psi_s = 160^\circ$ gives a maximum value of z_i. Families of orbits with $K = 1{\cdot}0$ and $1{\cdot}00625$ are plotted in figure 8.

Owing to small variations of H with the azimuth ϕ in the transition zone, orbits emitted with differing inclinations ξ_s will have slightly different values of z_i. This will give rise to a lower resolving power with bevelled poles because the presence of lateral focusing will make the image length so small that it would be impossible to separate the rays with differing z_i by the use of a curved slit. It therefore seems probable that inclined plane poles have advantages where high resolving power is important, but that bevelled poles may be useful for the study of continuous spectra where they would give a higher counting rate, or for

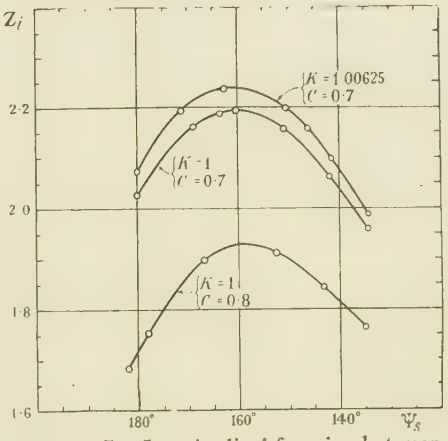

Figure 7. Longitudinal focusing between bevelled pole-faces. Source-image distance z_i against angle of emission ψ_s.

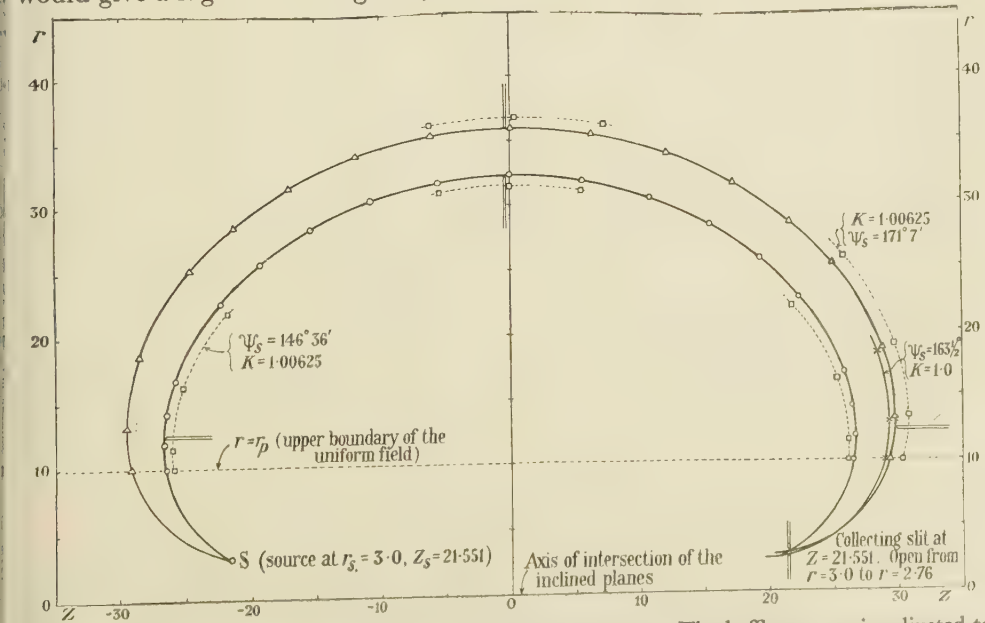

Figure 8. Orbits in the mid-plane between bevelled pole-faces. The baffles are again adjusted to exclude the two ranges of rays with 0·625% higher momentum which would otherwise enter the slit. The two orbits at S have $K = 1{\cdot}0$ and $\psi_s = 150^\circ\ 53'$ and $168^\circ\ 40{\cdot}5'$.

high energies where the approach to saturation of the iron is a factor. The sol angle Ω could be made large enough to collect 1% of the rays emitted with given momentum.

ACKNOWLEDGEMENT

I wish to express my thanks to Dr. J. C. P. Miller for his most valuab guidance in integration and computation.

REFERENCES

Jeffreys, H., 1939. *Mon. Not. R. Astr. Soc.* (Geophys. Supp.), **4**, 594–615.
Korsunsky, M., Kelman, V. and Petrov, B., 1945. *J. Phys. Acad. Sci. U.S.S.R.*, No. 1, 7–13.
Larmor, J., 1884. *Proc. Lond. Math. Soc.*, **15**, 158–184.
Thibaud, J., 1938. *Nuovo Cimento*, **15**, 313–342.
Thomson, J. J., 1903. *Recent Advances in Electricity and Magnetism* (3rd Editio Cambridge).
Voges, H. and Ruthemann, G., 1939. *Z. Phys.*, **114**, 709–718.
Whittaker and Robinson, 1924. *The Calculus of Observations* (Blackie), p. 146.

THE PRODUCTION OF A UNIFORM MAGNETIC FIELD OVER A SPECIFIC VOLUME BY MEANS OF TWIN CONDUCTING CIRCULAR COILS

By H. CRAIG,
Birkbeck College, London

MS. received 5 *March* 1947

ABSTRACT. An investigation is made into the uniformity of axial magnetic field attainable on the central plane between twin parallel co-axial circular coils arranged in conjunction. Information is derived and set out graphically which permits of the optimum coil separation for a given circular area with given coil diameter, as well as the highest degree of uniformity attainable over that area, being read off directly. The modification for, and consequent improved uniformity possible over, an annulus is indicated.

The investigation is then extended to volumes of cylindrical shape and some useful field characteristics, including regions of remarkably constant axial field, are considered. Two special cases are taken and axial field contours are plotted to show the deviation from uniformity of the field at any point in them. The radial field between coils with the particular separation of the two special cases is then examined.

Some important practical details are supplied. The best ratio of radial depth to axial length for the coils is determined and a method is given by which the equivalent separation of parallel coils of finite cross-section can be found very exactly by means of a search coil of particular shape.

§ 1. INTRODUCTION

Peculiarities associated with the magnetic field between a pair of coaxial twin coils have been noted and made use of by Rosa (1909), Llewellyn (1934), Nettleton and Balls (1935 and 1942) and Nettleton and Sugden (1939), and the Helmholtz position has not always proved the best for the requirements of these experimenters. Von Ziepel (1944) has considered the

use of parallel coils for the production of a uniform field over a Wilson cloud chamber and has derived theoretically a means of establishing such a field. Two general cases are cited. Of these, the first, utilizing twin parallel coils, converges in uniformity attainable and in position upon those of the ideal Helmholtz pair as the axial length of the coil decreases. The second case, employing four axially extensive coils, is capable of producing a very homogeneous field. The calculations involved in the final solution are indirect, and it is not always convenient to have the region subjected to the field difficult of access via the interstices of an interrupted solenoid. Tables are being published shortly by Comrie giving the values of the axial field at points off a conducting circular wire.

The object of the present communication is to show by means of these tables that a coil separation less than the Helmholtz is advantageous when the problem is that of securing optimum uniformity of field over a definite volume of specific shape, a matter of special importance in work with compound β-ray spectrometers and mass spectrographs, and to draw up data in a graphical form which will enable the appropriate separation to be read off, the deviation from uniformity to be estimated and other characteristics of the field to be appreciated.

For the production of uniform transverse or longitudinal fields in one dimension, a common requirement, as, for example, in the neutralizing of the earth's field over a single lens β-ray spectrometer, where particle paths are considerable only in one dimension, there are well-known standard methods. In the lens-magnet-lens system of compound β-ray spectroscope or in some types of mass spectrograph the particle paths are long and of appreciable extent in two dimensions. In cases such as these the effect of the earth's field can be a serious one and its neutralization over an area becomes a matter of importance. It is found convenient to compensate this effect by means of twin parallel circular co-axial coils arranged in conjunction and with an appropriate number of ampère-turns associated with them.

§ 2. NOMENCLATURE AND TABLES

Because the fields produced by all circular coils have the same shape, in the following outline all distances are given in arbitrary units of which the coil or the twin coils considered have radii of ten. Because of the axial symmetry of the field, cylindrical coordinates are used, Oz being the common axis of the coils and the origin being taken for convenience at the centre of one coil.

The values of the axial fields supplied in the tables to which reference has already been made were computed using elliptic integrals in place of the more usual zonal harmonic series and so permitting of their being established over a much wider range of r than would otherwise be possible. The field may be considered as due to a current in a circular conductor such that the ratio of ampère-turns to radius is as ten is to one, and the values of H_z are supplied in gauss to the fourth decimal place over a lattice of z and r at integral values of r and in planes of z separated by one half unit. Fields at intermediate points were calculated from these by interpolation. From the lattice of axial fields and their interpolations, other requirements can be procured as necessary. Thus, H_z at $r = r_1$ in the plane midway between two parallel circular coils in conjunction with separation Z units is twice H_z due to a single coil at $r = r_1$ when $z = Z/2$. In this plane there is no radial

component of magnetic field. The H_z at any point off this plane is found b summation of the H_z due to each coil at that point.

§ 3. OPTIMUM COIL SEPARATION FOR A CIRCULAR AREA

Taking the axial field due to a single coil in a plane with constant z, and plottin as a percentage of H_z at $r=0$ the field difference at any particular value of r from it magnitude at $r=0$, against r, gives a smooth curve. If this is done successively fo

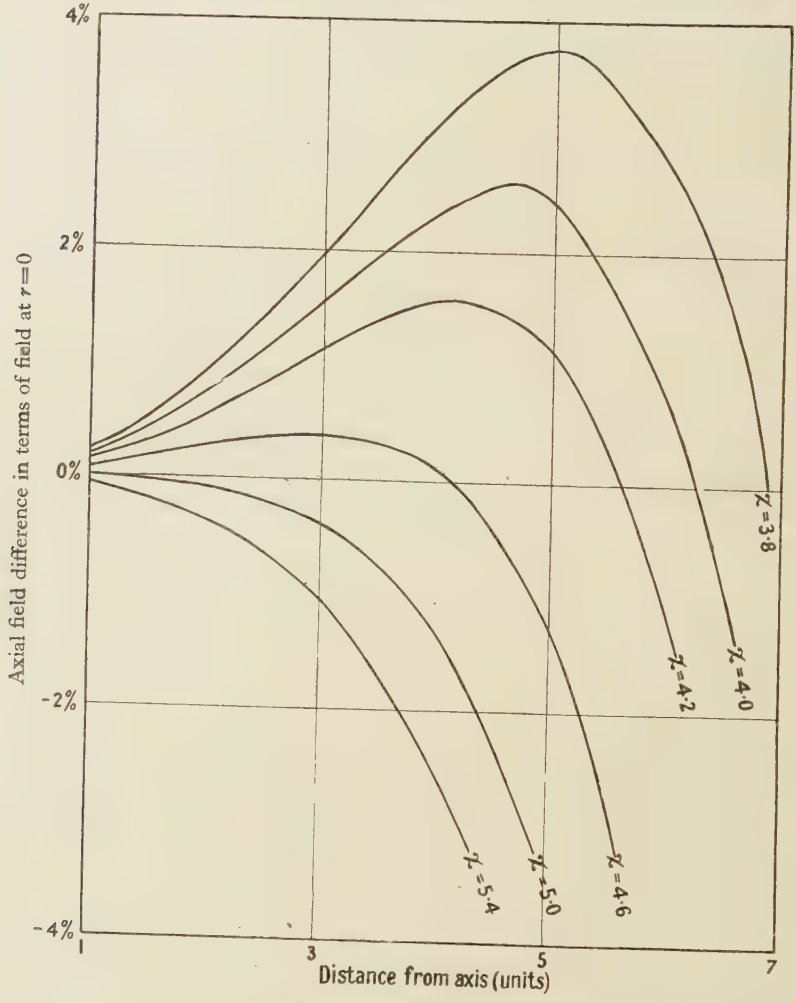

Figure 1. Variation of axial field with distance from the axis for a number of planes parallel to the coil.

values of z from 3·8 to 5·4 a series of graphs, some of which are shown in figure 1, results. Each of the curves must, of course, intersect the ordinate at 0% when $r=0$. Curves for z planes outside the extreme ones shown are not included because they diverge very rapidly from the origin at small values of r and so are not important. From this family of curves it can be seen approximately how the uniformity of field over an area around $r=0$ varies with the z plane in which the area lies, and it becomes obvious that the best z plane for any particular area

depends upon the maximum value of r in that area. It is noteworthy that the curves over the range shown fall very steeply as r increases beyond certain limits, that the Helmholtz separation is only of use for small areas and that a coil separation greater than the Helmholtz is comparatively inferior.

If now the variation of H_z over the area from $r=0$ to $r=3$ be found as a percentage of the mean field over that area, and this be plotted against z for different values of z, a curve results. If this be repeated for $r_{\max}=4$, $r_{\max}=5$, $r_{\max}=6$ and

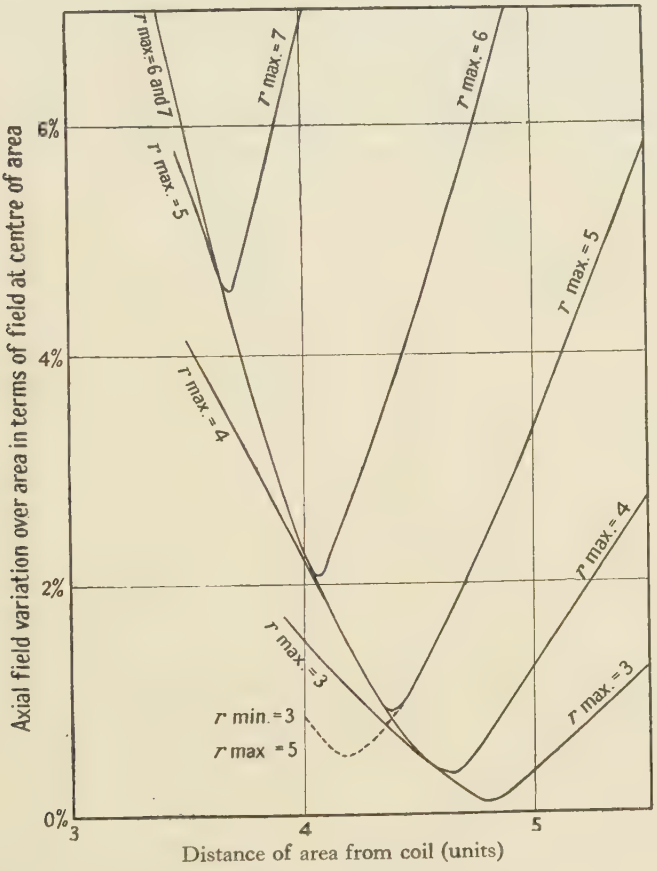

Figure 2. Variation of axial field uniformity over an area parallel to a coil against distance from coil.

$r_{\max}=7$ the family of partly coincident curves shown in figure 2 is produced and the values of z for greatest uniformity over any of the areas are then seen as minima. The twin coil separation required for any area is twice the z for the area at its minimum variation. Curves for r greater than 7 are not shown, as the field variation even at the optimum coil separation becomes too great to be of practical use. Most important features which are emphasized by these curves are that the smaller the area as compared with the coils the more critical is the distance of separation of the coils at the best position, and that the larger the area as compared with the coils the greater is the deterioration of the field on departing from the best position. Thus, an axial displacement of 0·2 units from the optimum position (brought

about by an error of coil separation of 0·4 units) causes an increase in coarseness o the overall field of 33% for the area containing $r_{max} = 7$ and 400% for the are containing $r_{max} = 3$, whereas the actual increase in the coarseness in the forme case is 1·5% as against 0·27% in the latter. Furthermore, it can be seen fro figure 2 that as each curve is approximately symmetrical about its minimum, to small and too great separations of the coils are equally harmful to the fiel uniformity.

The z value of each minimum plotted against the r value associated with th curve provides a useful graph seen in figure 3, from which the best coil separatio for any area including a known r_{max} may be procured by doubling the ordinate o the point on the graph with the known r_{max} as abscissa. Here it is seen that th Helmholtz position is approached for small areas and that the larger the area th closer must the coils be brought together. For larger areas the overall variatio

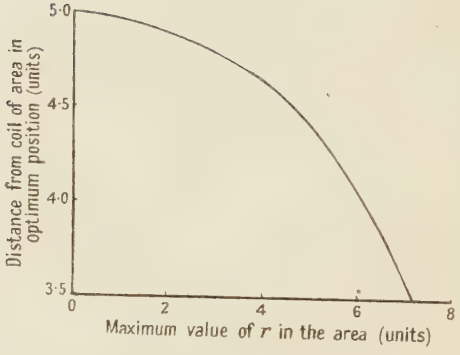

Figure 3. Optimum position for a given area.

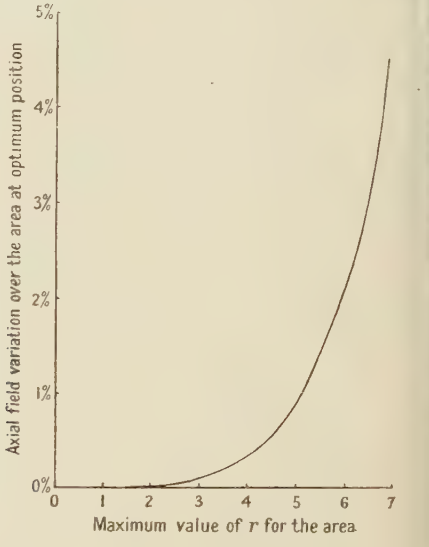

Figure 4. Field uniformity attainable over a given area.

increases even at the best setting, as would be expected, and figure 4 shows the relation between the percentage variation of H_z over the area in the optimum z plane against r_{max} for that area. This curve shows clearly how the field uniformity attainable deteriorates as the area increases, but shows also that even between the limits $r = 0$ and $r = 7$, by suitable coil placing (seen to be 7·35 units apart) the field can be kept uniform to within 4·5%.

§ 4. OPTIMUM COIL SEPARATION FOR AN ANNULUS

In the event of a region, say from $r = 0$ to $r = 3$, being unoccupied or of relatively little importance, as can occur for example in the particular case of a pair of long magnetic lenses at right angles in the compound β-ray spectrometer cited above, the degree of uniformity over the remainder of the region, say from $r = 3$ to $r = 5$, can be improved further by disregarding the variation between $r = 0$ and $r = 3$. In this way a more uniform field over the instruments can be obtained by suitable

placing of the components over such an annulus, than by any other disposition of them. Taking this as an example and plotting the variation of axial field over the new area (i.e. between $r=3$ and $r=5$) as a percentage of the mean field over that same area, against z, and adding the resulting curve as a broken line to figure 2 gives a new minimum extending below the minimum of the $r_{\max}=5$ graph and with one arm of the former curve, if continued, almost coincident at first with the corresponding arm of the latter. It is seen that the optimum separation for the coils

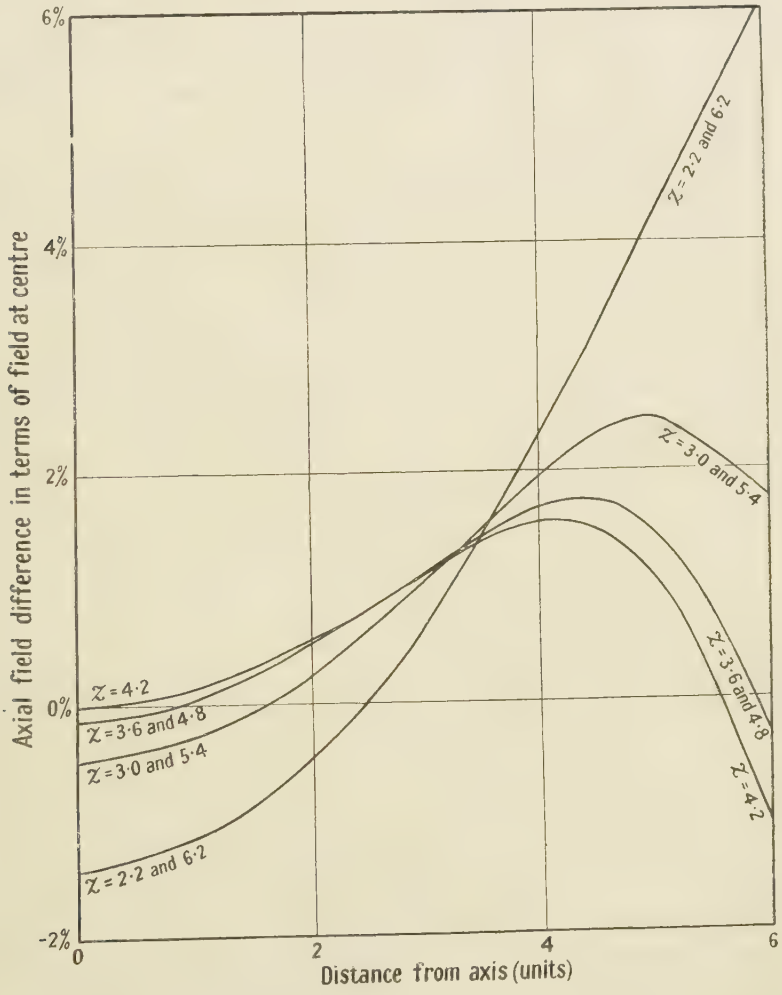

Figure 5. Variation of axial field over a number of planes between the coils.

becomes 8·38 units instead of 8·8 as would have been required for the area $r=0$ to $r=5$ and that the overall variation is now as low as 0·5%. Repeating for the areas $r=2$ to $r=5$ and $r=1$ to $r=5$ gives intermediate values both of optimum coil separation and of overall uniformity.

§ 5. FIELD IN A VOLUME

Taking H_z for positions off the central plane between the coils, it is found that the field variation from its magnitude at the same r on the central plane is small for

small differences of z, but as the difference approaches two units the variation may become pronounced. Each coil separation has, of course, its own particular field form. Because of the variation of H_z with r on the central plane it is more convenient and more useful to take the H_z difference at any point in terms of the H_z on the central plane at $r = 0$. A series of curves for different z planes between coils separated by 8·4 units is shown in figure 5. Other separations give families of curves of the same general character. It is observed that the curves shown within the z limits indicated, i.e. up to 2 units on either side of $z = 4{\cdot}2$, intersect near $r = 3{\cdot}5$ although they are not exactly concurrent. In the region of this waist the variation of H_z with z, r being constant, is a minimum and in this particular instance is of the order of 0·1 % for a range of 4 units, which is nearly one half of the distance between the coils.

The r value at the waist of the family of curves changes with the coil separation in the manner shown in figure 6. It is apparent at once that the axis of Helmholtz coils is not the best line for H_z uniformity over a range as great as two units on either side of the plane of symmetry, the best position being located near $r = 1{\cdot}3$, where the uniformity is twice as good as it is along $r = 0$. The axis of Helmholtz coils has a variation of 0·18 % of the centre field over the central four units of its length and an overall variation between the coils of 5·5 % of the same field. It has, of course, the advantage of being free of all radial component of magnetic field and has in addition a surrounding region extending radially as far as $r = 1{\cdot}5$, in which the H_z uniformity is very good. If the region examined were reduced from that used in establishing figure 6 the curve is slightly changed. Thus for half the range, i.e. up to 1 unit from the central plane, it would intersect the ordinate at 10 units. When a z range not so close to the central plane is considered for any specific coil separation, the value of r at which the waist appears increases from its value for a z range near the central plane. Furthermore, for higher r values at the waist, i.e. for closer coils, the position is more critical and consequently the region of uniform H_z is less extensive.

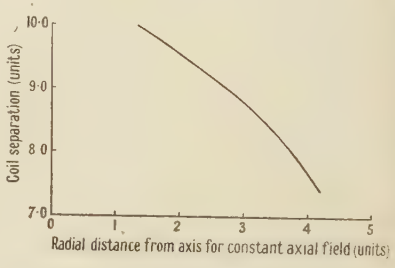

Figure 6. Variation of constant axial field position with coil separation.

For any predetermined coil separation, the way in which the axial field between them varies with z and r can best be seen by taking z and r as axes and drawing contours through points which have the same magnitude of H_z. This has been done in figure 7 (*a*) for a separation of 8·4 units over the range $r = 0$ to $r = 7$ and for $z = 4{\cdot}2$ to $z = 6{\cdot}2$. The field is symmetrical about $z = 4{\cdot}2$. From the curve in figure 3 it is seen that 8·4 units is the optimum separation for the area with $r_{max} = 5{\cdot}6$ units and from the broken line addition to figure 2 for the area $r = 3$ to $r = 5$. For convenience the contours are drawn through the coordinates of points whose axial fields differ from that at the point $z = 4{\cdot}2$, $r = 0$, by the same positive or negative percentage. From such a figure as this it can be seen immediately over which region between the coils the axial field variation lies within any particular limits. It is observed that the field is very uniform on the central plane from $r = 0$

to $r=5{\cdot}6$ and that the region between $r=3$ and $r=5$ on $z=4{\cdot}2$ has H_z entirely within successive contours. In the event of this latter region being the one of importance, the field would be adjusted for the mean one required over that area; contours in terms of this mean field are shown in figure 7 (*b*). They closely resemble the others in general character but have, of course, different positions, and because they are percentages of a somewhat greater field have slightly increased spacing. The particular contours for $+\frac{1}{2}\%$ and $-\frac{1}{2}\%$ have been included in this case (as broken lines) in order to indicate the trend of the field over the rather large space which otherwise would have been left ungraphed.

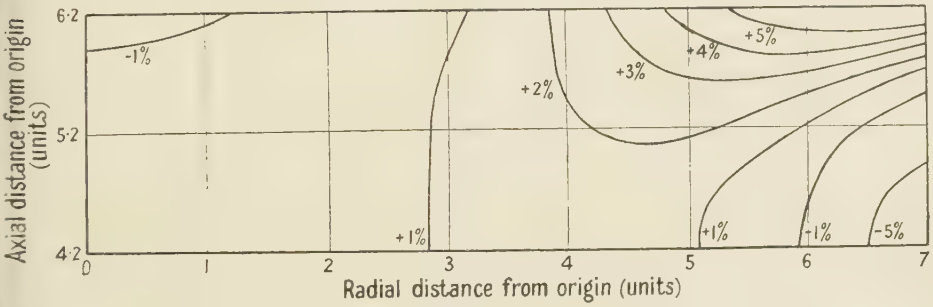

Figure 7 (*a*). Field contours in terms of field at centre between coils.

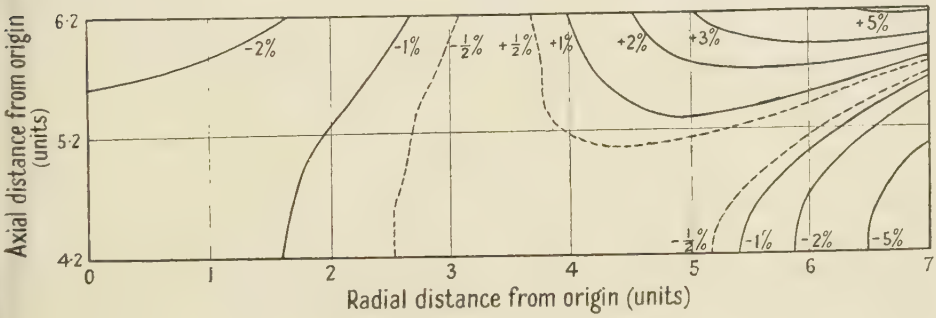

Figure 7 (*b*). Field contours in terms of mean field over annulus $r=3$ to $r=5$ on $z=4{\cdot}2$.

§6. THE RADIAL FIELD

This brief survey of the field pertaining to the central region between parallel coils in conjunction cannot be left without some reference to the radial component of field which obviously must be present over most of the region and of which at least an approximate knowledge is advisable. Once more each coil spacing requires separate attention, as the radial field at any point is the algebraic sum of those due to each of the two coils at that point. In general, on the central plane and along the $r=0$ axis, H_r is zero, and for small z displacements from the central plane, r being constant, the H_r at the point will be proportional to the amount of the displacement. As an individual case, the particular coil separation of 8·4 units has again been taken, and the H_r calculated for points removed from the central plane at $z=4{\cdot}2$ by one and two units respectively, and from $r=0$ to $r=7$ inclusive. The calculations were made using Laplace's equation and approximate integration methods. The values of the first differential coefficients of H_z with respect to z were supplied by Comrie's tables over the same lattice of points as were the H_z

supplied. Intermediate values were obtained, as before, by interpolation. The results were calculated as percentages of H_z at $z=4{\cdot}2$, $r=0$ and are shown graphically in figure 8. The sign is arbitary as it changes everywhere in crossing the

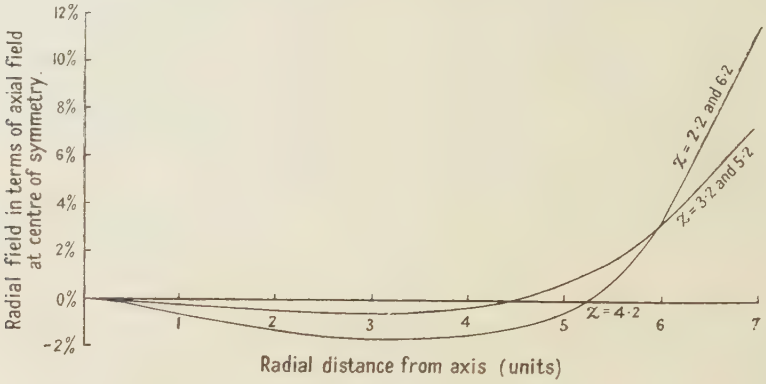

Figure 8. Variation of radial field over a number of planes between the coils.

plane of symmetry. Disregarding sign, the quantities are symmetrical about $z=4{\cdot}2$. The magnitude of H_r, like the variation of H_z, is seen to be comparatively small over the important region in which H_z uniformity is being effected, and to increase rapidly as r becomes large off the central plane. Throughout the volume $r=0$ to $r=5{\cdot}6$ and $z=2{\cdot}2$ to $z=6{\cdot}2$ it is seen that H_r is never greater than the satisfactorily low proportion of 2% of the H_z at the centre.

§ 7. PRACTICAL CONSIDERATIONS

(a) *Coil dimensions*

All quantities from which the preceding results are derived are based on the assumption that the current is concentrated in a line, and this in practice cannot be attained perfectly. However, it can be approached very closely. The author has constructed a pair of coils 10 feet in diameter, capable on a 400-volt supply of compensating with ease the earth's field at centre between them, and they have each a cross-sectional area of less than 0·375 square inches, which is very small in comparison with the area of the section taken between the coils in a plane containing the central axis.

In such coils of mean separation $2z_1$ and mean radius a, let the radial depth and axial length be d and l respectively (see figure 9). Then considering one coil only, it follows that the optimum z plane for the area being subjected to the uniform field is distant z_1 from the plane of this coil. Taking the effect of the axial length of the coil on the axial spread of its optimum plane, it is readily seen that it is caused to be extended over a distance l.

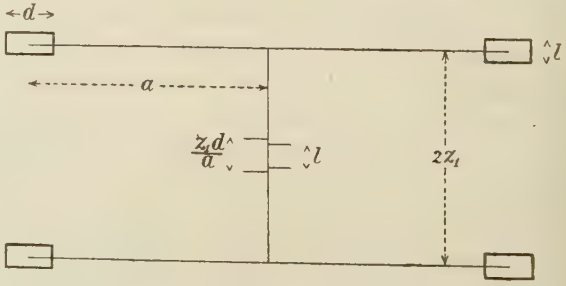

Figure 9. Coil cross-section containing central axis.

(see right-hand half of diagram). Now, taking the effect of radial depth only, the optimum plane for all turns from those of radius $a-d/2$ to those of radius $a+d/2$ must lie within limits separated by a distance $z_1 d/a$ (see left-hand half of diagram). Therefore the effect of radial depth is to the effect of axial length as coil separation is to coil diameter. It follows that for a given cross sectional area of coil (as, in order to attain maximum uniformity these limits should be equal) the axial length should be to the radial depth as the separation to be used is to the mean coil diameter. This, in addition to the comparatively small coils possible, means that the dimensions of the coils need not be such as to give rise to an appreciable effect when the field required is no greater than that of the earth.

(b) *Determination of equivalent separation*

The equivalent coil separation, Z units, can be determined experimentally by a practical method due to Dr. Nettleton and communicated privately to me by him. The fluxes G_1, G_2 produced in a search coil (see below for dimensions) placed axially at the centre of each of the twin coils in turn, by the establishment of the same current i, are determined. For identical coils they will be equal. The average flux for the two positions is $\frac{1}{2}(G_1+G_2)=ki/a$, where k is a constant and a is the coil radius. The twin coils are then arranged in opposition and the centre of the plane of symmetry between them is found by adjusting the position of the search coil, still with its axis along $r=0$, until no flux is produced on establishing a current in the twin coils. This position is critical, so can be located accurately. The coils are then arranged in conjunction and the flux G_T observed when the current i is established in the coils in series.

Then

$$G_T = \frac{2ka^2 i}{(a^2+z_1{}^2)^{3/2}}$$

where $2z_1$ is the coil separation. Hence

$$\frac{G_1+G_2}{G_T} = \frac{(a^2+z_1{}^2)^{3/2}}{a^3},$$

$$\text{i.e.} \quad \frac{z_1}{a} = \left\{\left(\frac{G_1+G_2}{G_T}\right)^{2/3} - 1\right\}^{1/2}.$$

But if $a=10$ units, then $Z=2z_1$ units and

$$Z = 20\left\{\left(\frac{G_1+G_2}{G_T}\right)^{2/3} - 1\right\}^{1/2} \text{ units.}$$

For observations such as these, in which all measurements are made at centres of symmetry of magnetic fields, the search coil should be made of a single-layer solenoid of radius R and half-length L such that $L/R=\sqrt{3}/2$, in order to eliminate the effect of its own finite dimensions. This ratio follows from the well-known fact that the magnetic field just off a centre of symmetry can be given to a first approximation by the relation

$$H(z,r)=H_0(1+bz^2-\tfrac{1}{2}br^2),$$

where H_0 is the field at the centre of symmetry, b is a constant which may be positive

or negative and z and r are the coordinates of the point. The origin is taken at the centre of symmetry. If the flux in the coil is to be proportional only to H_0, then

$$\int_{-L}^{+L}\int_{0}^{R} 2\pi r(bz^2-\tfrac{1}{2}br^2)drdz$$

must be made zero, i.e.

$$\int_{-L}^{+L} 2\pi(\tfrac{1}{2}bz^2R^2-\tfrac{1}{8}bR^4)dz=0,$$

$$L/R=\sqrt{3}/2.$$

ACKNOWLEDGMENTS

I should like to thank Mr. R. E. Siday for his advice, for many valuable discussions and for his supply of the Comrie tables before their publication, and to thank Dr. H. R. Nettleton for his interest and helpful suggestions.

REFERENCES

Comrie, L. J. In course of publication.
Llewellyn, F. H., 1934. *Proc. Phys. Soc.*, **46**, 824.
Nettleton, H. R. and Balls, E. G., 1935. *Proc. Phys. Soc.*, **47**, 54 ; 1942. *Ibid.*, **54**, 27.
Nettleton, H. R. and Llewellyn, F. H., 1932. *Proc. Phys. Soc.*, **44**, 195.
Nettleton, H. R. and Sugden, S., 1939. *Proc. Roy. Soc.*, A, **173**, 313.
Rosa, E. B., 1909. *Bull. Bur. Standards*, **5**, 499.
von Zeipel, E., 1944. *Ark. Mat. Astr. Fys.*, **30**, A32.

DISTRIBUTION COEFFICIENTS FOR THE CALCULATION OF COLOURS ON THE C.I.E. TRICHROMATIC SYSTEM FOR TOTAL RADIATORS AT 1500–250–3500°K., AND 2360°K. (C_2=14 350)

By H. G. W. Harding and R. B. Sisson,
National Physical Laboratory, Teddington, Middlesex

MS. received 28 *January* 1947

ABSTRACT. Tables of the distribution coefficients and the relative energy distributions are given for total radiators at 1500–250–3500° K. and 2360° K., as well as for the equal-energy stimulus and the standard illuminants A, B and C. The energy distributions required for the calculations were obtained from Planck's formula (C_2=14 350) and the distribution coefficients for the equal-energy stimulus are taken from *Condensed Tables for Colour Computation* by T. Smith (1934). By using these tables, with entries at every 0·01 μ, the labour of colour computation is only one-half of that involved by the use of

the C.I.E. standard observer tables, with entries at every 0·005 μ. In nearly every instance the calculated colour will be indistinguishable from that which would be obtained if the C.I.E. tables were used.

§ 1. INTRODUCTION

To facilitate the calculation of colours of materials from their spectral transmission or reflexion factors, it is useful to have tables which give the distribution coefficients of several illuminants. These coefficients are derived from the products of the distribution coefficients for the equal-energy stimulus and the spectral energy distributions of the illuminants. Such tables have been used at the National Physical Laboratory for many years, but failing agreement on the value that should be given to C_2 in Planck's formula they have not been published. However, there have been many requests from colorimetrists for tables, and it is considered that the value 14350 will prove the most satisfactory for this purpose. This conclusion was reached not only because 14350 was used to calculate the spectral energy distributions of the standard illuminants A, B and C in the C.I.E. tables, but also because this value had been adopted for so much work both here and in America.

When the colours of total radiators were published (Harding, 1944 and 1946) with $C_2 = 14384{\cdot}8$ (Birge, 1941), figures were given for the correction which could be applied to compensate for an alteration of C_2, and consequently the usefulness of the tables would not be affected by such an alteration. No such simple procedure is possible with tables of distribution coefficients; nevertheless, if a new value of C_2 is adopted the tables will not be without value, because they will then apply, on the new scale, to a slightly different temperature, obtained by multiplying the stated temperature by the new value of C_2 and dividing the product by 14350. For widely used illuminants, such as 2360 and 2848° K. (illuminant A) it may be preferable, in the event of an alteration of C_2, to assign a new temperature to the present distribution coefficients rather than to retain the numerical value of the temperatures at 2360 and 2848 and re-calculate the distribution coefficients.

The distribution coefficients for the equal-energy stimulus and the standard illuminants A, B and C which have been included with the newly calculated tables, have been taken from *Condensed Tables for Colour Computation* by T. Smith (1934). Offprints of these tables have not been available for some years, and it is felt that the inclusion of these widely used distribution coefficients will make table 2 more comprehensive and, therefore, more useful to colorimetrists.

§ 2. CALCULATION OF COLOURS, AND TRANSMISSION OR REFLEXION FACTORS

A colour, defined on the system recommended for use by the Commission Internationale de l'Eclairage in 1931, is expressed in the form

$$C = xX + yY + zZ,$$

where x, y and z are trichromatic coefficients whose sum is unity and where X, Y and Z denote the standard reference stimuli, X being analogous to red, Y to green and Z to blue. The values of x, y and z are obtained from the distribution

coefficients for an equal-energy stimulus ($\bar{x}_\lambda$, $\bar{y}_\lambda$ and $\bar{z}_\lambda$), the spectral distribution of energy of the illuminant (E_λ) and the spectral transmission or reflexion factor of the specimen (t_λ) by making the following calculations:

$$x = \frac{1}{S}\Sigma(E_\lambda \bar{x}_\lambda t_\lambda), \qquad \ldots\ldots(1)$$

$$y = \frac{1}{S}\Sigma(E_\lambda \bar{y}_\lambda t_\lambda), \qquad \ldots\ldots(2)$$

$$z = \frac{1}{S}\Sigma(E_\lambda \bar{z}_\lambda t_\lambda), \qquad \ldots\ldots(3)$$

where
$$S = \Sigma(E_\lambda \bar{x}_\lambda t_\lambda) + \Sigma(E_\lambda \bar{y}_\lambda t_\lambda) + \Sigma(E_\lambda \bar{z}_\lambda t_\lambda). \qquad \ldots\ldots(4)$$

From equations (1), (2), (3) and (4), it can be seen that, for a given illuminant, the expressions $E_\lambda \bar{x}_\lambda$, $E_\lambda \bar{y}$ and $E_\lambda \bar{z}_\lambda$ are independent of the characteristics of the material, so that if these values for any particular illuminant are tabulated, they form a set of distribution coefficients applicable to any material. As the luminosity factors of the X, Y and Z stimuli are 0, 1, 0 respectively, the transmission or reflexion factor T is given by

$$T = \Sigma(E_\lambda \bar{y}_\lambda t_\lambda)[\Sigma(E_\lambda \bar{y}_\lambda)]^{-1}. \qquad \ldots\ldots(5)$$

Hence, if the sum of the $E_\lambda \bar{y}_\lambda$ coefficients is arranged to be 100, the value $\Sigma(E_\lambda y_\lambda t_\lambda)$ represents the percentage transmission or reflexion factor without any further calculation.

At the laboratory, the computation of x, y, z and T is regularly performed in about thirty minutes with the aid of a suitable electric calculator. Recently the Hollerith section of the Mathematics Division of the Laboratory has been calculating the colours, and by this means the time taken has been approximately halved.

§ 3. PREPARATION OF THE TABLES OF DISTRIBUTION COEFFICIENTS

Tables of the distribution coefficients for total radiators at 1500–250–3500° K. and also for 2360° K. have been prepared in the following way.

The relative energy distributions of the total radiators were calculated from Planck's formula

$$E_{\lambda\theta} = C_1 \lambda^{-5}[\exp.(C_2/\lambda\theta) - 1]^{-1},$$

where $E_{\lambda\theta}$ is the amount of energy radiated at the absolute temperature θ between the wave-lengths $\lambda \pm d\lambda/2$ (microns); C_1 and C_2 are constants. Since only the relative spectral distribution of energy is necessary for these calculations, the value of the constant C_1 is immaterial; for convenience the energies for radiation of wave-length 0·56 μ are made equal to 100·0000. The value given to C_2 is 14350. All the energy values have been checked by forming fifth differences and are estimated to be correct to about one part in a million. These energy distributions, together with those for the standard illuminants A, B and C, are given in table 1.

The distribution coefficients for the equal-energy stimulus are not those of the C.I.E. system (Smith and Guild, 1931–2) which are quoted for the wave-lengths

0·38–0·005–0·78 μ but Smith's condensed values (T. Smith, 1934) which, quoted for wave-lengths 0·38–0·01–0·77 μ, have about half the number of entries of the C.I.E. tables.

The products of the energies given in table 1 and the appropriate distribution coefficients for the equal-energy stimulus given in table 2, columns 1, 2 and 3, were calculated and multiplied by $100[\Sigma(E_{\lambda\theta}\bar{y}_\lambda)]^{-1}$. The distribution coefficients obtained in this way for the various illuminants are tabulated in table 2.

§ 4. ACCURACY OF COLOUR CALCULATIONS USING THESE TABLES

In using these tables, for most practical purposes, the calculated colours are indistinguishable from those that would be obtained if the full C.I.E. standard tables were employed. For example, the colour of a total radiator at 2360° K. calculated by the C.I.E. tables is

$$0{\cdot}489320X + 0{\cdot}414913Y + 0{\cdot}095767Z$$

and when calculated by these tables is

$$0{\cdot}489319X + 0{\cdot}414917Y + 0{\cdot}095764Z.$$

The maximum difference in the trichromatic coefficients is 0·000004, which is much less than the minimum perceptible colour difference. Other examples, quoted by T. Smith (1934), show that for a dichroic filter which has an irregular transmission curve, the difference between the trichromatic coefficients when calculated by the condensed and the C.I.E. tables may be 0·0005; for didymium glasses with very irregular spectral curves the differences may be as much as 0·003.

§ 5. CONCLUSION

Although the use of these condensed tables in place of the full C.I.E. data may introduce significant errors in the calculated colours of some very exceptional materials, in most instances they will give results sufficiently close to the C.I.E. values for the differences to be of no visual significance.

§ 6. ACKNOWLEDGMENTS

The condensed tables of distribution coefficients for the equal-energy stimulus and for the A, B and C illuminants have been included with the approval of Mr. T. Smith, Superintendent of the Light Division of the National Physical Laboratory, and by permission of the Physical Society.

These calculations have been carried out as a part of the research programme of the National Physical Laboratory, and this paper is published by permission of the Director of the Laboratory.

REFERENCES

Birge, R. T., 1941. *Rev. Mod. Phys.*, **13**, 237.
Harding, H. G. W., 1944. *Proc. Phys. Soc.*, **56**, 305.
Harding, H. G. W., 1946. *Proc. Phys. Soc.*, **58**, 1.
Smith, T., 1934. *Proc. Phys. Soc.*, **46**, 372.
Smith, T. and Guild, J., 1931–2. *Trans. Opt. Soc.*, **33**, 73.

Table 1. Relative energy distributions

Wave-length (microns)	Temperature (° K.) (C_2=14350)			
	1500	1750	2000	2250
0·38	0·2126500	0·6756414	1·607880	3·155824
0·39	0·3561294	1·031832	2·291443	4·261929
0·40	0·5793768	1·537854	3·198011	5·651747
0·41	0·9176569	2·241006	4·377885	7·369801
0·42	1·417842	3·198327	5·886990	9·461902
0·43	2·140842	4·477287	7·786404	11·97432
0·44	3·164166	6·156287	10·14175	14·95296
0·45	4·584542	8·324897	13·02238	18·44245
0·46	6·520517	11·08388	16·50054	22·48540
0·47	9·114932	14·54488	20·65031	27·12158
0·48	12·53722	18·82992	25·54662	32·38729
0·49	16·98535	24·07058	31·26401	38·31472
0·50	22·68749	30·40693	37·87575	44·93147
0·51	29·90316	37·98631	45·45264	52·26020
0·52	38·92386	46·96187	54·06199	60·31827
0·53	50·07329	57·49097	63·76674	69·11760
0·54	63·70687	69·73346	74·62463	78·66468
0·55	80·21066	83·84996	86·68733	88·96027
0·56	100·0000	100·0000	100·0000	100·0000
0·57	123·5171	118·3403	114·6007	111·7741
0·58	151·2289	139·0231	130·5199	124·2679
0·59	183·6230	162·1941	147·7804	137·4618
0·60	221·2060	187·9916	166·3969	151·3323
0·61	264·4978	216·5442	186·3766	165·8515
0·62	314·0282	247·9703	207·7184	180·9879
0·63	370·3334	282·3764	230·4133	196·7071
0·64	433·9504	319·8566	254·4455	212·9720
0·65	505·4137	360·4913	279·7914	229·7425
0·66	585·2501	404·3470	306·4208	246·9773
0·67	673·9747	451·4756	334·2972	264·6334
0·68	772·0869	501·9142	363·3778	282·6664
0·69	880·0656	555·6851	393·6151	301·0314
0·70	998·3661	612·7957	424·9558	319·6828
0·71	1127·418	673·2385	457·3430	338·5754
0·72	1267·619	736·9920	490·7156	357·6637
0·73	1419·336	804·0205	525·0090	376·9030
0·74	1582·897	874·2745	560·1564	396·2491
0·75	1758·593	947·6918	596·0885	415·6589
0·76	1946·677	1024·198	632·7336	435·0903
0·77	2147·364	1103·708	670·0196	454·5026

Table 1. Relative energy distributions (*continued*)

Wave-length (microns)	Temperature (° K.) (C_2=14350)				
	2500	2750	3000	3250	3500
0·38	5·412436	8·415148	12·15516	16·59021	21·65663
0·39	7·001587	10·50930	14·74109	19·62634	25·08057
0·40	8·912871	12·93802	17·64894	22·95015	28·74125
0·41	11·17897	15·71932	20·88188	26·55179	32·61856
0·42	13·83054	18·86738	24·43885	30·41774	36·68986
0·43	16·89566	22·39234	28·31475	34·53127	40·93081
0·44	20·39914	26·30018	32·50061	38·87293	45·31581
0·45	24·36209	30·59258	36·98389	43·42103	49·81833
0·46	28·80156	35·26716	41·74888	48·15217	54·41175
0·47	33·73023	40·31740	46·77714	53·04164	59·06961
0·48	39·15632	45·73311	52·04785	58·06399	63·76597
0·49	45·08341	51·50054	57·53830	63·19335	68·47575
0·50	51·51062	57·60280	63·22428	68·40385	73·17510
0·51	58·43271	64·02024	69·08045	73·67004	77·84147
0·52	65·84010	70·73076	75·08079	78·96699	82·45382
0·53	73·71929	77·71032	81·19904	84·27069	86·99271
0·54	82·05318	84·93314	87·40891	89·55830	91·44037
0·55	90·82123	92·37231	93·68438	94·80816	95·78087
0·56	100·0000	100·0000	100·0000	100·0000	100·0000
0·57	109·5634	107·7878	106·3311	105·1150	104·0852
0·58	119·4833	115·7073	112·6540	110·1359	108·0254
0·59	129·7295	123·7300	118·9460	115·0469	111·8117
0·60	140·2706	131·8276	125·1859	119·8340	115·4362
0·61	151·0739	139·9727	131·3537	124·4846	118·8926
0·62	162·1062	148·1385	137·4308	128·9874	122·1763
0·63	173·3337	156·2991	143·4000	133·3332	125·2835
0·64	184·7226	164·4298	149·2457	137·5136	128·2118
0·65	196·2391	172·5071	154·9537	141·5219	130·9599
0·66	207·8501	180·5087	160·5112	145·3524	133·5276
0·67	219·5229	188·4139	165·9069	149·0010	135·9153
0·68	231·2257	196·2031	171·1310	152·4644	138·1244
0·69	242·9278	203·8583	176·1748	155·7405	140·1571
0·70	254·5995	211·3631	181·0310	158·8281	142·0159
0·71	266·2125	218·7024	185·6936	161·7270	143·7045
0·72	277·7400	225·8627	190·1577	164·4376	145·2261
0·73	289·1562	232·8317	194·4197	166·9613	146·5849
0·74	300·4372	239·5986	198·4766	169·2999	147·7856
0·75	311·5607	246·1538	202·3265	171·4559	148·8327
0·76	322·5054	252·4892	205·9684	173·4322	149·7313
0·77	333·2523	258·5979	209·4027	175·2324	150·4867

Table 1. Relative energy distributions (*continued*)

Wave-length (microns)	2360° K.	Standard illuminant		
		A	B	C
0·38	4·058004	9·79	22·40	33·00
0·39	5·371485	12·09	31·30	47·40
0·40	6·988679	14·71	41·30	63·30
0·41	8·949441	17·68	52·10	80·60
0·42	11·29332	21·00	63·20	98·10
0·43	14·05871	24·67	73·10	112·40
0·44	17·28217	28·70	80·80	121·50
0·45	20·99759	33·09	85·40	124·00
0·46	25·23566	37·82	88·30	123·10
0·47	30·02324	42·87	92·00	123·80
0·48	35·38301	48·25	95·20	123·90
0·49	41·33301	53·91	96·50	120·70
0·50	47·88649	59·86	94·20	112·10
0·51	55·05166	66·06	90·70	102·30
0·52	62·83201	72·50	89·50	96·90
0·53	71·22568	79·13	92·20	98·00
0·54	80·22638	85·95	96·90	102·10
0·55	89·82294	92·91	101·00	105·20
0·56	100·0000	100·00	102·80	105·30
0·57	110·7381	107·18	102·60	102·30
0·58	122·0143	114·44	101·00	97·80
0·59	133·8018	121·73	99·20	93·20
0·60	146·0715	129·04	98·00	89·70
0·61	158·7914	136·34	98·50	88·40
0·62	171·9273	143·62	99·70	88·10
0·63	185·4434	150·83	101·00	88·00
0·64	199·3028	157·98	102·20	87·80
0·65	213·4671	165·03	103·90	88·20
0·66	227·8972	171·96	105·00	87·90
0·67	242·5544	178·77	104·90	86·30
0·68	257·3992	185·43	103·90	84·00
0·69	272·3929	191·93	101·60	80·20
0·70	287·4969	198·26	99·10	76·30
0·71	302·6737	204·41	96·20	72·40
0·72	317·8862	210·36	92·90	68·30
0·73	333·0992	216·12	89·40	64·40
0·74	348·2781	221·66	86·90	61·50
0·75	363·3898	227·00	85·20	59·20
0·76	378·4030	232·11	84·70	58·10
0·77	393·2872	237·01	85·40	58·20

Table 2. Distribution coefficients

Equal energy stimulus			Wave-length (microns)	1500° K.		
$\bar{x}$	$\bar{y}$	$\bar{z}$		$E_{1500}\bar{x}$	$E_{1500}\bar{y}$	$E_{1500}\bar{z}$
0·0023	0·0000	0·0106	0·38	0·0000	0·0000	0·0001
0·0082	0·0002	0·0391	0·39	0·0001	0·0000	0·0005
0·0283	0·0007	0·1343	0·40	0·0006	0·0000	0·0027
0·0840	0·0023	0·4005	0·41	0·0027	0·0001	0·0128
0·2740	0·0082	1·3164	0·42	0·0135	0·0004	0·0650
0·5667	0·0232	2·7663	0·43	0·0423	0·0017	0·2063
0·6965	0·0458	3·4939	0·44	0·0768	0·0050	0·3851
0·6730	0·0761	3·5470	0·45	0·1075	0·0122	0·5664
0·5824	0·1197	3·3426	0·46	0·1323	0·0272	0·7592
0·3935	0·1824	2·5895	0·47	0·1249	0·0579	0·8222
0·1897	0·2772	1·6193	0·48	0·0828	0·1211	0·7072
0·0642	0·4162	0·9313	0·49	0·0380	0·2462	0·5510
0·0097	0·6473	0·5455	0·50	0·0077	0·5116	0·4311
0·0187	1·0077	0·3160	0·51	0·0195	1·0496	0·3292
0·1264	1·4172	0·1569	0·52	0·1714	1·9215	0·2127
0·3304	1·7243	0·0841	0·53	0·5763	3·0076	0·1467
0·5810	1·9077	0·0408	0·54	1·2893	4·2334	0·0905
0·8670	1·9906	0·0174	0·55	2·4224	5·5617	0·0486
1·1887	1·9896	0·0077	0·56	4·1406	6·9304	0·0268
1·5243	1·9041	0·0042	0·57	6·5583	8·1924	0·0181
1·8320	1·7396	0·0032	0·58	9·6506	9·1638	0·0169
2·0535	1·5144	0·0023	0·59	13·1345	9·6864	0·0147
2·1255	1·2619	0·0016	0·60	16·3776	9·7233	0·0123
2·0064	1·0066	0·0007	0·61	18·4855	9·2741	0·0064
1·7065	0·7610	0·0003	0·62	18·6667	8·3243	0·0033
1·2876	0·5311	0·0000	0·63	16·6099	6·8511	0·0000
0·8945	0·3495		0·64	13·5211	5·2830	
0·5681	0·2143		0·65	10·0015	3·7728	
0·3292	0·1218		0·66	6·7111	2·4830	
0·1755	0·0643		0·67	4·1201	1·5096	
0·0927	0·0337		0·68	2·4931	0·9063	
0·0457	0·0165		0·69	1·4010	0·5058	
0·0225	0·0081		0·70	0·7825	0·2817	
0·0117	0·0042		0·71	0·4595	0·1649	
0·0057	0·0020		0·72	0·2517	0·0883	
0·0028	0·0010		0·73	0·1384	0·0494	
0·0014	0·0006		0·74	0·0772	0·0331	
0·0006	0·0002		0·75	0·0368	0·0123	
0·0003	0·0001		0·76	0·0203	0·0068	
0·0001	0·0000		0·77	0·0075	0·0000	
21·3713	21·3714	21·3715	TOTALS	148·7536	100·0000	5·4358

$0{\cdot}33333X + 0{\cdot}33333Y + 0{\cdot}33334Z$ COLOUR $0{\cdot}58521X + 0{\cdot}39341Y - 0{\cdot}02138Z$

Table 2. Distribution coefficients (*continued*)

1750° K.			Wave-length (microns)	2000° K.		
$E_{1750}\bar{x}$	$E_{1750}\bar{y}$	$E_{1750}\bar{z}$		$E_{2000}\bar{x}$	$E_{2000}\bar{y}$	$E_{2000}\bar{z}$
0·0001	0·0000	0·0003	0·38	0·0002	0·0000	0·0007
0·0003	0·0000	0·0016	0·39	0·0008	0·0000	0·0038
0·0017	0·0000	0·0081	0·40	0·0038	0·0001	0·0180
0·0074	0·0002	0·0351	0·41	0·0155	0·0004	0·0737
0·0343	0·0010	0·1649	0·42	0·0678	0·0020	0·3257
0·0994	0·0041	0·4850	0·43	0·1855	0·0076	0·9053
0·1679	0·0110	0·8423	0·44	0·2969	0·0195	1·4893
0·2194	0·0248	1·1563	0·45	0·3683	0·0417	1·9414
0·2528	0·0520	1·4507	0·46	0·4039	0·0830	2·3182
0·2241	0·1039	1·4748	0·47	0·3415	0·1583	2·2475
0·1399	0·2044	1·1940	0·48	0·2037	0·2977	1·7387
0·0605	0·3923	0·8778	0·49	0·0844	0·5469	1·2238
0·0115	0·7707	0·6495	0·50	0·0154	1·0305	0·8684
0·0278	1·4989	0·4700	0·51	0·0357	1·9251	0·6037
0·2324	2·6061	0·2885	0·52	0·2872	3·2202	0·3565
0·7438	3·8818	0·1893	0·53	0·8855	4·6214	0·2254
1·5865	5·2092	0·1114	0·54	1·8223	5·9835	0·1280
2·8467	6·5359	0·0571	0·55	3·1589	7·2528	0·0634
4·6547	7·7908	0·0302	0·56	4·9962	8·3624	0·0324
7·0635	8·8234	0·0195	0·57	7·3421	9·1715	0·0202
9·9730	9·4700	0·0174	0·58	10·0500	9·5431	0·0176
13·0420	9·6181	0·0146	0·59	12·7549	9·4064	0·0143
15·6464	9·2892	0·0118	0·60	14·8652	8·8254	0·0112
17·0129	8·5353	0·0059	0·61	15·7171	7·8852	0·0055
16·5699	7·3892	0·0029	0·62	14·8986	6·6439	0·0026
14·2372	5·8725	0·0000	0·63	12·4696	5·1434	0·0000
11·2034	4·3774		0·64	9·5662	3·7377	
8·0193	3·0251		0·65	6·6807	2·5201	
5·2123	1·9285		0·66	4·2398	1·5687	
3·1026	1·1367		0·67	2·4659	0·9034	
1·8219	0·6623		0·68	1·4158	0·5147	
0·9944	0·3590		0·69	0·7560	0·2730	
0·5399	0·1944		0·70	0·4019	0·1447	
0·3084	0·1107		0·71	0·2249	0·0807	
0·1645	0·0577		0·72	0·1176	0·0412	
0·0882	0·0315		0·73	0·0618	0·0221	
0·0479	0·0205		0·74	0·0329	0·0141	
0·0223	0·0074		0·75	0·0150	0·0050	
0·0120	0·0040		0·76	0·0080	0·0026	
0·0043	0·0000		0·77	0·0028	0·0000	
136·3975	100·0000	9·5590	TOTALS	127·2603	100·0000	14·6353

$0{\cdot}55456X+0{\cdot}40658Y+0{\cdot}03886Z$ COLOUR $0{\cdot}52610X+0{\cdot}41340Y+0{\cdot}06050Z$

Table 2. Distribution coefficients (*continued*)

2250° K.			Wave-length (microns)	2500 °K.		
$E_{2250}\bar{x}$	$E_{2250}\bar{y}$	$E_{2250}\bar{z}$		$E_{2500}\bar{x}$	$E_{2500}\bar{y}$	$E_{2500}\bar{z}$
0·0003	0·0000	0·0015	0·38	0·0005	0·0000	0·0026
0·0015	0·0000	0·0073	0·39	0·0026	0·0001	0·0124
0·0070	0·0002	0·0334	0·40	0·0114	0·0003	0·0541
0·0272	0·0008	0·1297	0·41	0·0425	0·0012	0·2025
0·1140	0·0034	0·5474	0·42	0·1714	0·0051	0·8235
0·2982	0·0122	1·4557	0·43	0·4330	0·0177	2·1138
0·4577	0·0301	2·2959	0·44	0·6426	0·0422	3·2235
0·5454	0·0617	2·8747	0·45	0·7417	0·0839	3·9082
0·5755	0·1183	3·3029	0·46	0·7586	0·1559	4·3541
0·4690	0·2174	3·0863	0·47	0·6003	0·2782	3·9503
0·2700	0·3945	2·3047	0·48	0·3359	0·4909	2·8677
0·1081	0·7008	1·5680	0·49	0·1309	0·8486	1·8989
0·0192	1·2781	1·0771	0·50	0·0226	1·5080	1·2708
0·0429	2·3143	0·7257	0·51	0·0494	2·6631	0·8351
0·3350	3·7565	0·4159	0·52	0·3764	4·2201	0·4672
1·0035	5·2373	0·2554	0·53	1·1016	5·7490	0·2804
2·0085	6·5948	0·1411	0·54	2·1561	7·0796	0·1514
3·3894	7·7820	0·0680	0·55	3·5613	8·1766	0·0715
5·2238	8·7433	0·0338	0·56	5·3762	8·9984	0·0348
7·4872	9·3528	0·0206	0·57	7·5533	9·4353	0·0208
10·0045	9·4999	0·0175	0·58	9·8999	9·4006	0·0173
12·4047	9·1481	0·0139	0·59	12·0485	8·8854	0·0135
14·1352	8·3920	0·0106	0·60	13·4843	8·0056	0·0101
14·6233	7·3364	0·0051	0·61	13·7091	6·8778	0·0048
13·5727	6·0526	0·0024	0·62	12·5114	5·5794	0·0022
11·1304	4·5910	0·0000	0·63	10·0940	4·1635	0·0000
8·3717	3·2710		0·64	7·4731	2·9199	
5·7356	2·1636		0·65	5·0421	1·9020	
3·5729	1·3219		0·66	3·0946	1·1450	
2·0409	0·7478		0·67	1·7424	0·6384	
1·1515	0·4186		0·68	0·9694	0·3524	
0·6046	0·2183		0·69	0·5021	0·1813	
0·3161	0·1138		0·70	0·2591	0·0933	
0·1741	0·0625		0·71	0·1409	0·0506	
0·0896	0·0314		0·72	0·0716	0·0251	
0·0464	0·0166		0·73	0·0366	0·0131	
0·0244	0·0105		0·74	0·0190	0·0081	
0·0109	0·0036		0·75	0·0085	0·0028	
0·0058	0·0019		0·76	0·0044	0·0015	
0·0020	0·0000		0·77	0·0015	0·0000	
120·4007	100·0000	20·3946	TOTALS	115·1808	100·0000	26·5915

$0{\cdot}50001X+0{\cdot}41529Y+0{\cdot}08470Z$ COLOUR $0{\cdot}47640X+0{\cdot}41361Y+0{\cdot}10999Z$

Table 2. Distribution coefficients (*continued*)

2750° K.			Wave-length (microns)	3000° K.		
$E_{2750}\bar{x}$	$E_{2750}\bar{y}$	$E_{2750}\bar{z}$		$E_{3000}\bar{x}$	$E_{3000}\bar{y}$	$E_{3000}\bar{z}$
0·0009	0·0000	0·0041	0·38	0·0013	0·0000	0·0060
0·0040	0·0001	0·0189	0·39	0·0056	0·0001	0·0269
0·0169	0·0004	0·0801	0·40	0·0233	0·0006	0·1106
0·0608	0·0017	0·2902	0·41	0·0818	0·0022	0·3902
0·2383	0·0071	1·1447	0·42	0·3125	0·0093	1·5102
0·5849	0·0240	2·8548	0·43	0·7487	0·0307	3·6549
0·8442	0·0555	4·2350	0·44	1·0563	0·0695	5·2987
0·9489	0·1703	5·0011	0·45	1·1614	0·1313	6·1213
0·9466	0·1945	5·4330	0·46	1·1346	0·2332	6·5117
0·7312	0·3389	4·8116	0·47	0·8589	0·3981	5·6522
0·3999	0·5843	3·4131	0·48	0·4607	0·6732	3·9238
0·1524	0·9879	2·2105	0·49	0·1724	1·1174	2·5005
0·0258	1·7184	1·4482	0·50	0·0286	1·9097	1·6093
0·0552	2·9733	0·9323	0·51	0·0603	3·2483	1·0186
0·4120	4·6198	0·5115	0·52	0·4428	4·9651	0·5497
1·1833	6·1756	0·3012	0·53	1·2519	6·5333	0·3187
2·2742	7·4674	0·1597	0·54	2·3698	7·7810	0·1664
3·6910	8·4744	0·0741	0·55	3·7901	8·7020	0·0761
5·4784	9·1696	0·0355	0·56	5·5468	9·2840	0·0359
7·5722	9·4590	0·0209	0·57	7·5631	9·4476	0·0209
9·7695	9·2767	0·0171	0·58	9·6303	9·1446	0·0168
11·7099	8·6358	0·0131	0·59	11·3976	8·4054	0·0128
12·9138	7·6668	0·0097	0·60	12·4161	7·3714	0·0093
12·9433	6·4936	0·0045	0·61	12·2978	6·1698	0·0043
11·6509	5·1956	0·0020	0·62	10·9436	4·8802	0·0019
9·2752	3·8257	0·0000	0·63	8·6159	3·5538	0·0000
6·7787	2·6486		0·64	6·2294	2·4340	
4·5166	1·7038		0·65	4·1076	1·5495	
2·7387	1·0133		0·66	2·4656	0·9122	
1·5240	0·5583		0·67	1·3587	0·4978	
0·8382	0·3047		0·68	0·7402	0·2691	
0·4293	0·1550		0·69	0·3757	0·1356	
0·2192	0·0789		0·70	0·1901	0·0684	
0·1179	0·0424		0·71	0·1014	0·0364	
0·0593	0·0208		0·72	0·0506	0·0177	
0·0300	0·0107		0·73	0·0254	0·0090	
0·0154	0·0066		0·74	0·0130	0·0056	
0·0068	0·0023		0·75	0·0056	0·0019	
0·0035	0·0012		0·76	0·0029	0·0010	
0·0012	0·0000		0·77	0·0010	0·0000	
111·1625	100·0000	33·0269	TOTALS	108·0394	100·0000	39·5477

$0{\cdot}45523X+0{\cdot}40952Y+0{\cdot}13525Z$ COLOUR $0{\cdot}43637X+0{\cdot}40390Y+0{\cdot}15973Z$

Table 2. Distribution coefficients (*continued*)

3250° K.			Wave-length (microns)	3500° K.		
$E_{3250}\bar{x}$	$E_{3250}\bar{y}$	$E_{3250}\bar{z}$		$E_{3500}\bar{x}$	$E_{3500}\bar{y}$	$E_{3500}\bar{z}$
0·0018	0·0000	0·0083	0·38	0·0024	0·0000	0·0109
0·0076	0·0002	0·0361	0·39	0·0097	0·0002	0·0464
0·0306	0·0008	0·1450	0·40	0·0385	0·0010	0·1825
0·1049	0·0029	0·5002	0·41	0·1296	0·0036	0·6177
0·3921	0·0117	1·8836	0·42	0·4754	0·0142	2·2838
0·9205	0·0377	4·4936	0·43	1·0968	0·0449	5·3538
1·2736	0·0838	6·3891	0·44	1·4924	0·0981	7·4865
1·3747	0·1554	7·2451	0·45	1·5853	0·1793	8·3554
1·3192	0·2711	7·5715	0·46	1·4984	0·3080	8·5999
0·9818	0·4551	6·4612	0·47	1·0991	0·5095	7·2326
0·5182	0·7571	4·4230	0·48	0·5720	0·8358	4·8824
0·1909	1·2372	2·7685	0·49	0·2079	1·3476	3·0154
0·0312	2·0829	1·7553	0·50	0·0336	2·2397	1·8874
0·0648	3·4922	1·0951	0·51	0·0688	3·7090	1·1631
0·4695	5·2645	0·5828	0·52	0·4928	5·5253	0·6117
1·3098	6·8355	0·3334	0·53	1·3591	7·0927	0·3459
2·4477	8·0370	0·1719	0·54	2·5121	8·2483	0·1764
3·8668	8·8779	0·0776	0·55	3·9266	9·0153	0·0788
5·5918	9·3594	0·0362	0·56	5·6207	9·4077	0·0364
7·5373	9·4153	0·0208	0·57	7·5020	9·3712	0·0207
9·4915	9·0128	0·0166	0·58	9·3576	8·8857	0·0164
11·1135	8·1959	0·0124	0·59	10·8567	8·0065	0·0122
11·9818	7·1135	0·0090	0·60	11·6016	6·8878	0·0087
11·7494	5·8946	0·0041	0·61	11·2794	5·6588	0·0039
10·3546	4·6175	0·0018	0·62	9·8584	4·3963	0·0017
8·0761	3·3312	0·0000	0·63	7·6276	3·1462	0·0000
5·7864	2·2609		0·64	5·4228	2·1188	
3·7821	1·4267		0·65	3·5179	1·3270	
2·2509	0·8328		0·66	2·0785	0·7690	
1·2301	0·4507		0·67	1·1279	0·4132	
0·6649	0·2417		0·68	0·6054	0·2201	
0·3348	0·1209		0·69	0·3029	0·1094	
0·1681	0·0605		0·70	0·1511	0·0544	
0·0890	0·0320		0·71	0·0795	0·0285	
0·0441	0·0155		0·72	0·0391	0·0137	
0·0220	0·0079		0·73	0·0194	0·0069	
0·0111	0·0048		0·74	0·0098	0·0042	
0·0048	0·0016		0·75	0·0042	0·0014	
0·0024	0·0008		0·76	0·0021	0·0007	
0·0008	0·0000		0·77	0·0007	0·0000	
105·5932	100·0000	46·0422	TOTALS	103·6658	100·0000	52·4306
$0{\cdot}41963X+0{\cdot}39740Y+0{\cdot}18297Z$			COLOUR	$0{\cdot}40479X+0{\cdot}39048Y+0{\cdot}20473Z$		

Table 2. Distribution coefficients (*continued*)

2360° K.			Wave-length (microns)	Standard illuminant A		
$E_{2360}\bar{x}$	$E_{2360}\bar{y}$	$E_{2360}\bar{z}$		$E_A\bar{x}$	$E_A\bar{y}$	$E_A\bar{z}$
0·0004	0·0000	0·0019	0·38	0·0010	0·0000	0·0048
0·0020	0·0000	0·0094	0·39	0·0046	0·0001	0·0219
0·0088	0·0002	0·0419	0·40	0·0193	0·0005	0·0916
0·0335	0·0009	0·1597	0·41	0·0688	0·0019	0·3281
0·1379	0·0041	0·6627	0·42	0·2666	0·0080	1·2811
0·3551	0·0145	1·7335	0·43	0·6479	0·0265	3·1626
0·5365	0·0353	2·6914	0·44	0·9263	0·0609	4·6469
0·6299	0·0712	3·3197	0·45	1·0320	0·1167	5·4391
0·6551	0·1347	3·7598	0·46	1·0207	0·2098	5·8584
0·5266	0·2441	3·4653	0·47	0·7817	0·3624	5·1445
0·2992	0·4372	2·5538	0·48	0·4242	0·6198	3·6207
0·1183	0·7668	1·7157	0·49	0·1604	1·0398	2·3266
0·0207	1·3816	1·1643	0·50	0·0269	1·7956	1·5132
0·0459	2·4727	0·7754	0·51	0·0572	3·0849	0·9674
0·3540	3·9690	0·4394	0·52	0·4247	4·7614	0·5271
1·0489	5·4741	0·2670	0·53	1·2116	6·3230	0·3084
2·0776	6·8218	0·1459	0·54	2·3142	7·5985	0·1625
3·4711	7·9697	0·0697	0·55	3·7329	8·5707	0·0749
5·2983	8·8682	0·0343	0·56	5·5086	9·2201	0·0357
7·5237	9·3984	0·0207	0·57	7·5710	9·4574	0·0209
9·9633	9·4608	0·0174	0·58	9·7157	9·2257	0·0170
12·2468	9·0317	0·0137	0·59	11·5841	8·5430	0·0130
13·8387	8·2160	0·0104	0·60	12·7103	7·5460	0·0096
14·2008	7·1244	0·0049	0·61	12·6768	6·3599	0·0044
13·0773	5·8318	0·0023	0·62	11·3577	5·0649	0·0020
10·6429	4·3899	0·0000	0·63	8·9999	3·7122	0·0000
7·9462	3·1047		0·64	6·5487	2·5587	
5·4054	2·0390		0·65	4·3447	1·6389	
3·3440	1·2372		0·66	2·6234	0·9706	
1·8974	0·6952		0·67	1·4539	0·5327	
1·0635	0·3866		0·68	0·7966	0·2896	
0·5548	0·2003		0·69	0·4065	0·1467	
0·2883	0·1038		0·70	0·2067	0·0744	
0·1578	0·0567		0·71	0·1108	0·0398	
0·0808	0·0283		0·72	0·0556	0·0195	
0·0416	0·0148		0·73	0·0280	0·0100	
0·0218	0·0093		0·74	0·0144	0·0062	
0·0097	0·0033		0·75	0·0063	0·0021	
0·0051	0·0017		0·76	0·0032	0·0011	
0·0017	0·0000		0·77	0·0011	0·0000	
117·9314	100·0000	23·0802	Totals	109·8450	100·0000	35·5824

$0{\cdot}48932X+0{\cdot}41492Y+0{\cdot}09576Z$ Colour $0{\cdot}44757X+0{\cdot}40745Y+0{\cdot}14498Z$

Table 2. Distribution coefficients (*continued*)

Standard illuminant B			Wave-length (microns)	Standard illuminant C		
$E_B\bar{x}$	$E_B\bar{y}$	$E_B\bar{z}$		$E_C\bar{x}$	$E_C\bar{y}$	$E_C\bar{z}$
0·0025	0·0000	0·0113	0·38	0·0036	0·0000	0·0164
0·0123	0·0003	0·0585	0·39	0·0183	0·0004	0·0870
0·0558	0·0014	0·2650	0·40	0·0841	0·0021	0·3992
0·2091	0·0057	0·9970	0·41	0·3180	0·0087	1·5159
0·8274	0·0248	3·9750	0·42	1·2623	0·0378	6·0646
1·9793	0·0810	9·6617	0·43	2·9913	0·1225	14·6019
2·6889	0·1768	13·4883	0·44	3·9741	0·2613	19·9357
2·7460	0·3105	14·4729	0·45	3·9191	0·4432	20·6551
2·4571	0·5050	14·1020	0·46	3·3668	0·6920	19·3235
1·7297	0·8018	11·3825	0·47	2·2878	1·0605	15·0550
0·8629	1·2609	7·3655	0·48	1·1038	1·6129	9·4220
0·2960	1·9190	4·2939	0·49	0·3639	2·3591	5·2789
0·0437	2·9133	2·4552	0·50	0·0511	3·4077	2·8717
0·0810	4·3669	1·3694	0·51	0·0898	4·8412	1·5181
0·5405	6·0602	0·6709	0·52	0·5752	6·4491	0·7140
1·4555	7·5959	0·3705	0·53	1·5206	7·9357	0·3871
2·6899	8·8322	0·1889	0·54	2·7858	9·1470	0·1956
4·1838	9·6060	0·0840	0·55	4·2833	9·8343	0·0860
5·8385	9·7722	0·0378	0·56	5·8782	9·8387	0·0381
7·4723	9·3341	0·0206	0·57	7·3230	9·1476	0·0202
8·8406	8·3947	0·0154	0·58	8·4141	7·9897	0·0147
9·7329	7·1777	0·0109	0·59	8·9878	6·6283	0·0101
9·9523	5·9086	0·0075	0·60	8·9536	5·3157	0·0067
9·4425	4·7373	0·0033	0·61	8·3294	4·1788	0·0029
8·1290	3·6251	0·0014	0·62	7·0604	3·1485	0·0012
6·2135	2·5629	0·0000	0·63	5·3212	2·1948	0·0000
4·3678	1·7066		0·64	3·6882	1·4411	
2·8202	1·0638		0·65	2·3531	0·8876	
1·6515	0·6110		0·66	1·3589	0·5028	
0·8796	0·3223		0·67	0·7113	0·2606	
0·4602	0·1673		0·68	0·3657	0·1329	
0·2218	0·0801		0·69	0·1721	0·0621	
0·1065	0·0384		0·70	0·0806	0·0290	
0·0538	0·0193		0·71	0·0398	0·0143	
0·0253	0·0089		0·72	0·0183	0·0064	
0·0120	0·0043		0·73	0·0085	0·0030	
0·0058	0·0025		0·74	0·0040	0·0017	
0·0024	0·0008		0·75	0·0017	0·0006	
0·0012	0·0004		0·76	0·0008	0·0003	
0·0004	0·0000		0·77	0·0003	0·0000	
99·0915	100·0000	85·3094	TOTALS	98·0699	100·0000	118·2216
$0{\cdot}34842X+0{\cdot}35162Y+0{\cdot}29996Z$			COLOUR	$0{\cdot}31006\,X+0{\cdot}31616\,Y+0{\cdot}37378Z$		

COAXIAL ELECTRON LENSES

By J. W. DUNGEY* and CATHERINE R. HULL,
British Thomson-Houston Co., Rugby
* Now at Magdalene College, Cambridge

MS. received 11 *December* 1946; *read* 30 *May* 1947

ABSTRACT. The resolving power of electron microscopes is limited chiefly by the fact that the spherical aberration of electron lenses of the conventional or " coreless " type can never be eliminated. In this paper a new type of electron lenses is investigated, called *coaxial* lenses. These contain a central cylindrical conductor, surrounded by a number of annular electrodes. The electrostatic fields in such lenses can be produced by superimposing fields of a certain simple type, calculated and tabulated in this paper. This field corresponds to a " one-element " coaxial lens, containing an annular electrode in the form of a perforated disk with rounded edges, preceded and followed by cylindrical guard rings.

At least two such elements are required to correct the aberrations of an ordinary electron microscope objective to the accuracy required, and a fully satisfactory system requires a three-element correcting lens. A two-element and a three-element system are calculated in detail and their theoretical performance is discussed.

§ 1. INTRODUCTION

The resolving power of electron microscopes is at present chiefly limited by the first-order spherical aberration of the objectives, which, by a well-known theorem of Scherzer (1936), can never be eliminated in the absence of space charges. The optimum theoretical resolution has been estimated by several authors (see Zworykin *et al.*, 1945 a; Gabor, 1945) at 5 to 7 A., and recently J. Hillier (1946) has realized about 8·5 A. Further progress can be expected only from a reduction or elimination of the spherical aberration by novel means. Space-charge correction has been suggested by Gabor (1945 b) but has not yet been tried experimentally.

Another possible method is the use of coaxial electron lenses, recently suggested by Gabor (1940). Whereas in the conventional electron lenses the axis is free from electrodes (figure 1 (*a*)), coaxial lenses have one or several central electrodes or cores. Thus only an annular region is accessible to the electron beam. In reality it is not possible to utilize the full annular aperture, as the cores must be supported, but it is easy to see that a full annular aperture produces a diffraction pattern only very little smaller than a sector of this aperture with a tangential extension approximately equal to the radial width. This has the advantage that there is no need for special electron guns for the production of hollow conical beams, any ordinary electron gun with more or less circular cross-section of the beam will do, if the gun is tilted so that the beam passes obliquely through the object and eccentrically through the coaxial lens.

As the fields used in electron lenses must have accurate axial symmetry, and, moreover, as the space in electron-microscope objectives is very restricted, only the simplest arrangements are of any practical interest. The simplest type has a single straight cylindrical wire as central electrode, which must be firmly supported at both ends. The supports themselves must be in the field-free region, where the potential is the same as that of the central wire. In the following, this potential

will always be assumed as zero. There may be one annular electrode with potential different from zero in the lens, or several. In the first case we speak of a one-element coaxial lens. An example of this is shown in figure 1 (*b*). According to the number of annular electrodes with non-zero potentials we speak of two-element, three-element etc. coaxial lenses.

By a zonally corrected electron lens we mean a lens in which the zonal power has a stationary value of at least the second order. If only the first differential quotient of the intercept of the rays starting from an axial object-point with respect to the initial angle of the rays is zero, that is to say, if the zonal power has a simple minimum or maximum, this means merely that an imaging effect exists in an infinitesimally narrow zone. In the case of ordinary, coreless lenses, the first-order imaging condition is always and automatically fulfilled, as the deflection

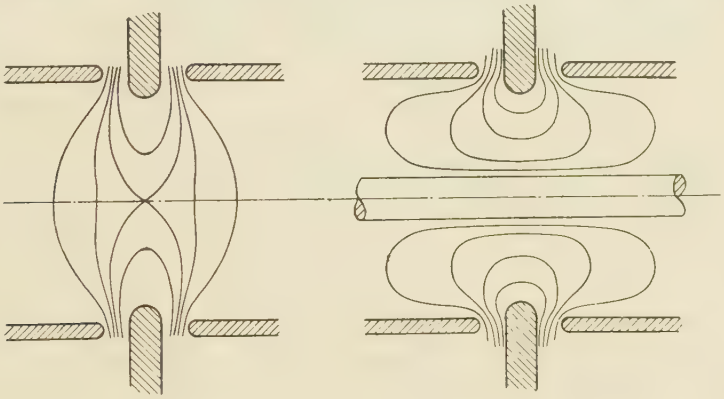

(*a*) Coreless electron lens. (*b*) Coaxial electron lens.

Figure 1.

angle δ is in first approximation always proportional to the off-axis distance r, but in coaxial lenses this condition is by no means automatically fulfilled. It can be satisfied only by two-element lenses or by more complex combinations.

As in the following we shall always have to deal with objectives in which one conjugate is practically at infinity, it is convenient to characterize the zonal position by the final radius r_f at which the ray leaves the lens, practically parallel to the axis. The condition for a lens effect, that is to say, for a stationary intercept, is $d\delta/dr_f = \delta/r_f$ for the centre of the zone, $r_f = \bar{r}_f$. In a corrected combination at least the second differential coefficient must vanish, $d^2\delta/dr_f^2 = 0$, but it has been found in the course of this investigation that in order to obtain objectives better than the existing ones it is necessary to impose a third condition, $d^3\delta/dr_f^3 = 0$. It was found that these three conditions can be satisfied by certain combinations of two-element coaxial lenses with ordinary objectives, but only a three-element coaxial lens combined with a suitable coreless objective, preferably of the magnetic type, gave a convenient position of the corrected zone. This is the lens which was described by Gabor (1945). In the present paper the rather laborious steps will be described which led to this combination.

§ 2. ZONAL CORRECTION BY COAXIAL LENSES

In the following, the deflection angle δ will always be reckoned positive if the ray is deflected towards the axis, as in a condensing lens. By Scherzer's theorem,

$d^2\delta/dr_f^2$ is always positive in ordinary lenses for sufficiently small off-axial distances r_f, but there is good reason to believe that this is also true for any value of r_f, no example to the contrary being known. Thus, as the characteristic $\delta(r_f)$ of an ordinary lens is always positively curved, the first problem in a correcting lens is to produce a negative curvature. This cannot be achieved in a single lens, as shown in figure 1(*b*), but it can be realized by a combination as shown in figure 2. Whether the trajectories are described from the left to the right or in the opposite direction is of no importance, but to simplify references it will always be assumed that the electrons move towards the right. In figure 2 they pass first through a converging lens. A single coaxial lens, whether converging or diverging, will always produce a deflection which is approximately proportional to $1/r$, where r may be the radius of the trajectory in the middle plane of the lens. Let us call the deflection produced by the first lens $\delta_1 = s_1/r_1$, where s_1 is the *strength* of the lens, a quantity of the dimension of a length. Let us now combine this with a

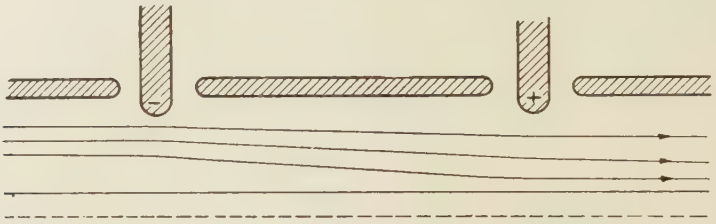

Figure 2. Correction of spherical aberration by a two-element coaxial lens.

diverging lens of strength $s_2 < 0$, so that the combination produces no deflection in a certain zone. The condition for this is

$$s_2/s_1 = -r_2/r_1, \qquad \ldots\ldots(1)$$

but, as the first lens is convergent, $r_2 < r_1$, i.e. the divergent lens must be weaker than the convergent one.

The curvature of the characteristic contributed by each lens, $d^2\delta/dr^2$, is proportional to s/r^3, and has the same sign as the deflection. As s/r is the same for the two lenses in absolute value and r is smaller for the divergent lens, the resulting value of the curvature $d^2\delta/dr^2$ is *negative* for the combination, i.e. of a sign suitable for the correction of ordinary lenses.

This is illustrated in figure 2. It is assumed that the resulting deflection is zero for the two outer rays, hence it will be positive, i.e. towards the axis, in the case of the middle ray. The curvature had to be strongly exaggerated in order to make it visible.

The lens systems considered in the following will be similar to the one shown in figure 2 in that the resulting deflection is nearly zero. The focal power must be supplied by an ordinary lens, preferably a magnetic objective of the conventional type. Coaxial lenses which can be used by themselves as objectives are possible in principle but cannot be realized, as the fields required would cause autoelectronic discharge even under the most favourable conditions.

§ 3. THE ELECTROSTATIC FIELD IN COAXIAL ELECTRODE SYSTEMS

In the theory of ordinary coreless lenses, the potential is entirely determined if it is given along the axis. In the case of coaxial lenses, we are free to prescribe its

values along two surfaces of rotational symmetry. For the above-mentioned practical reasons we need consider only the case in which the inner surface is an equipotential cylinder of radius a with a potential $\phi = 0$. It is convenient to characterize the whole field by prescribing the value of ϕ as a function of the axial co-ordinate z along an outer cylinder of radius b.

In order to represent a general field, it is convenient to expand $\phi(b, z)$ in terms of functions which allow simple analytical representation in the annular space between the radii a and b. The conventional procedure is to expand $\phi(b, z)$ into a Fourier integral,

$$\phi(b, z) = \frac{1}{\pi} \int_0^\infty \psi(x) \cos zx \, dx, \qquad \ldots\ldots(2)$$

where it has been assumed for simplicity that $\phi(b, z)$ has the symmetry plane $z = 0$ and ψ is the Fourier transform of ϕ. To obtain the solution $\phi(r, z)$ in the whole annular space between a and b we have merely to replace each coefficient $\cos zx$ by

$$\frac{I_0(ax)\, H_0(rx) - H_0(ax)\, I_0(rx)}{I_0(ax)\, H_0(bx) - H_0(ax)\, I_0(bx)} \cos zx, \qquad \ldots\ldots(3)$$

where I_0 and H_0 are the modified Bessel functions of the first and second kind of order zero. This expression satisfies Laplace's equation, and it can be seen by

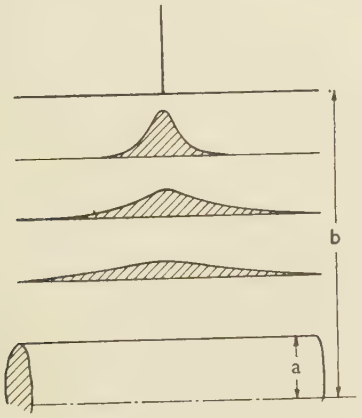

Figure 3. Potential profiles corresponding to a delta-function at the outer diameter δ.

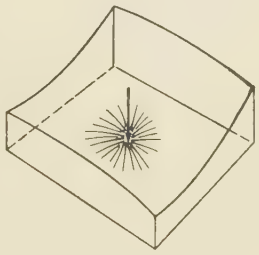

Figure 4. Illustration of relaxation method.

inspection that it satisfies the boundary conditions at $r = a$ and $r = b$. Substituting (3) into the integral (2) instead of $\cos zx$, we obtain the well-known Fourier-Bessel integral.

This procedure is not very satisfactory from a practical point of view. Each of the solutions (3) is infinitely periodic in the direction (3), and to build up functions from them which correspond to practical electrode arrangements is no easy matter. For this reason we have preferred to take as the elementary field one which corresponds to a potential of the form of a delta-function impressed on the outer electrode $r = b$. The general form of this potential distribution is illustrated in figure 3. Once this elementary solution is obtained, any prescribed potential distribution can be obtained from it by a simple integration, but in fact, not even

this is necessary, as the field distribution in figure 3 is one which can be realized with good approximation with electrodes of the shape shown in figure 1 *b*, and coaxial lens systems with almost any desired property can be built up by the combination of a number of these.

Thus our first task is to calculate the potential $\phi(r, z)$ corresponding to a delta function at $r = b$, which we write, with the usual reservations, in the non-convergent form

$$\phi(b, z) = \delta(z) = \frac{1}{\pi}\int_0^\infty \cos zx\, dx. \qquad \ldots\ldots(4)$$

Replacing each $\cos zx$ by the expression (3), we obtain the corresponding $\phi(r, z)$ in the form of a Fourier-Bessel integral. This in turn can be transformed by contour integration into the following infinite series:

$$\phi(r, z) = \frac{\pi}{2}\Sigma k \frac{J_0(ay_k)N_0(ry_k) - N_0(ay_k)J_0(ry_k)}{\left[\frac{J_0(by_k)}{J_0(ay_k)} - \frac{J_0(ay_k)}{J_0(by_k)}\right]} y_k \cosh y_k z, \ldots\ldots(5)$$

where the sum is to be taken over all roots y_k of the equation

$$J_0(ay_k)N_0(by_k) - N_0(ay_k)J_0(by_k) = 0. \qquad \ldots\ldots(6)$$

J_0 and N_0 are the normal Bessel functions of the first and second kinds of order zero.

The series (5), however, converges so extremely slowly that it is almost useless for practical applications. Therefore we have preferred to derive a useful approximation from equation (5), and to correct this by numerical methods.

In the series (5) we replace the cylindrical functions J_0 and N_0 by the asymptotic approximations, valid for large values of the argument

$$J_0(z) \simeq \sqrt{\frac{2}{\pi z}} \sin\left(z + \frac{\pi}{4}\right).$$

$$N_0(z) \simeq \sqrt{\frac{2}{\pi z}} \sin\left(z - \frac{\pi}{4}\right).$$

The series (5) can then be summed.

From now on we put the radius of the central wire $a = 1$, that is to say, all lengths are measured in units of a. We put $b/a = k$ and obtain the approximation

$$\phi(r, z) \simeq \frac{1}{2(k-1)}\sqrt{\frac{k}{r}} \frac{\sin \pi \frac{r-1}{k-1}}{\cosh \frac{nz}{k-1} + \cos \frac{r-1}{k-1}}. \qquad \ldots\ldots(7)$$

This is seen to satisfy the boundary conditions, but not the Laplace equation. It can be, however, used as the starting point of a numerical evaluation of the correct solution, by means of a relaxation method.

§ 4. NUMERICAL CALCULATION OF THE FIELD BY MEANS OF THE RELAXATION METHOD

The relaxation method has been introduced in a systematic way into a great variety of physical and engineering problems by R. V. Southwell (1940), and an application particularly useful for the present problem has been made recently by H. Motz and L. Klanfer (1946), but apart from technicalities, this method is in principle identical with J. Poincaré's *balayage* method, which starts from any

function fulfilling the boundary conditions, and modifies this until Laplace's equation is satisfied, by "sweeping" the space charge gradually into the electrodes (see Picard, 1894).

The principle of the relaxation method can also be illustrated by a physical model, shown in figure 4. It is assumed that the problem is to solve Laplace's equation in two dimensions with prescribed boundary values. It is known that an evenly stretched membrane, fixed at the boundaries, assumes the shape of this function, provided that its height above the base plane varies only within narrow limits. Let us assume that in a first approximation we have arrived at provisional values of this function, and that we have pegged down the membrane to the corresponding heights at the boundaries and at certain mesh points inside the boundaries. We can now improve the solution inside a mesh, by pulling out the central peg, and letting the membrane assume its natural position. We next peg down this point to its new position, and pull out another peg. The process can be repeated any number of times, until the whole membrane is "relaxed" and the pulling out of pegs affects its shape only by a negligible amount.

In the tracing of electron trajectories to be carried out later, the values of the radial field intensity $\partial\phi/\partial r$ must be known with great accuracy. For this reason the relaxation method was applied directly not to ϕ but to $\partial\phi/\partial r$. From the results so obtained, ϕ can be determined with more than sufficient accuracy by an integration.

Differentiating Laplace's equation with respect to r we obtain

$$\frac{\partial^2}{\partial r^2}\left(\frac{\partial\phi}{\partial r}\right)+\frac{1}{r}\frac{\partial}{\partial r}\left(\frac{\partial\phi}{\partial r}\right)-\frac{1}{r^2}\left(\frac{\partial\phi}{\partial r}\right)+\frac{\partial^2}{\partial z^2}\left(\frac{\partial\phi}{\partial r}\right)=0. \qquad \ldots\ldots(8)$$

Assuming a quadratic mesh with a side length σ for each cell, and writing $\rho=r/\sigma$, i.e. measuring the radius in units of σ, we can convert equation (8) into an equation of finite differences, which expresses the value of $\partial\phi/\partial r$ for any mesh point (r, z) in terms of its values at four neighbouring mesh points. In order to make the equation clearer we write $\partial\phi/\partial r=\phi r$,

$$\phi_r(r,z)=\frac{\phi_r(r,z-\sigma)+\phi_r(r,z+\sigma)+\phi_r(r+\sigma,z)(1+1/2\rho)+\phi_r(r-\sigma,z)(1-1/2\rho)}{4+1/\rho^2}. \qquad \ldots\ldots(9)$$

A similar equation, but for ϕ instead of ϕ_r, was used by Motz and Klanfer (1946) (without the third term in equation (8)). Calculating ϕ_r instead of ϕ—which is necessary for reasons of accuracy—another difference also arises. As boundary conditions at the inner electrode we have assumed the values of ϕ_r given by the approximation (7). As these are not the exact values, what we in fact obtain by the relaxation process is a field which satisfies Laplace's equation with high accuracy, but does not correspond exactly to the initially assumed boundary conditions, that is to say, it gives no delta-function at the outer radius, but only a very sharp and narrow potential peak. This, however, is quite sufficient for all practical applications. In all the numerical calculations the outer radius was assumed as five times the inner radius. In practical applications it will be advantageous to approach the outer electrodes nearer to the axis, to save voltage. By choosing as electrode shape any of the equipotentials calculated by the relaxation method one can make sure that the potential values and field intensities calculated in this paper will apply with the indicated high accuracy.

For the start, the field values ϕ_r given by equation (7) were assumed also in the symmetry plane $z=0$, but these were slightly modified later in the relaxation process. As may be seen from figure 5, the potential field obtained finally differs but very little from that produced by a delta function at $r=5$.

Table 1 shows some of the values computed by the relaxation process and allows us to form an estimate of its accuracy. The initial values, obtained from equation (7), are underlined. Intermediate values, calculated by a first application of the relaxation method, are shown in the same row. The row below shows the values obtained finally. The mesh used in this computation was varied according to the strength of the field; in regions where it is strong, twice as fine a mesh was used as the one shown in the table. All values were computed to

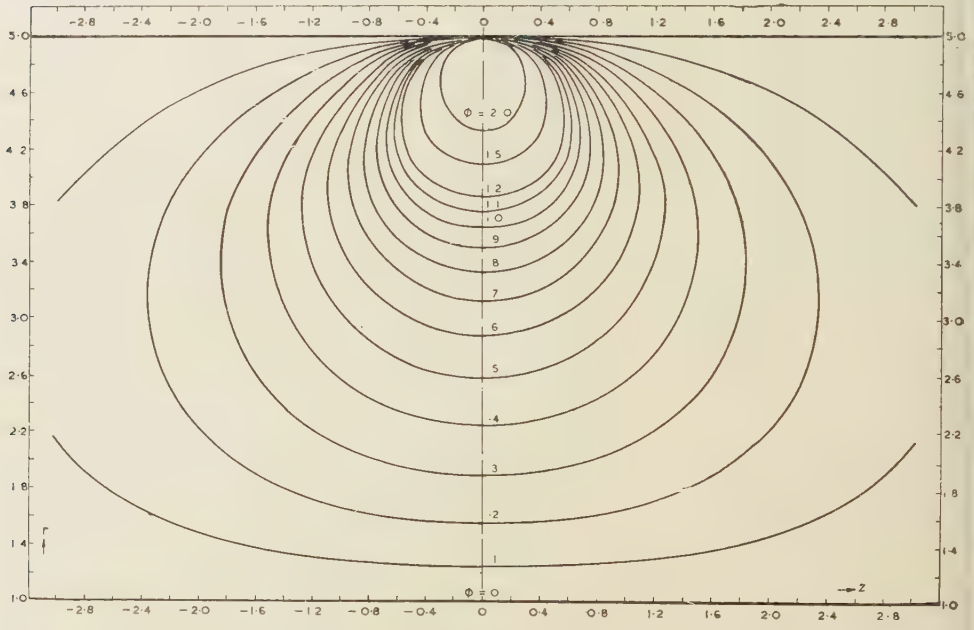

Figure 5. Potential distribution in single coaxial lens.

five figures, and the process was continued until there was no change in the fourth figure.

The accuracy of the table was checked at a number of points by using an interpolation formula more accurate than (9), by considering eight neighbours of a point *Om* numbered as follows:—

$$\begin{array}{ccccccc} & & & 6 & & & \\ & & & 2 & & & \\ 7 & 3 & 0 & 1 & 5 & & \\ & & & 4 & & & \\ & & & 8 & & & \end{array}$$

always with the spacing σ between neighbouring points. The formula is

$$\phi_r(0)=\frac{\sum_1^4 i\,\phi_r(i)-\frac{1}{16}\sum_5^8 i\,\phi_r(i)+\frac{3\sigma}{7r}\left[\phi_r(2)-\phi_r(4)-\frac{1}{16}(\phi_r(7)-\phi_r(8))\right]}{\frac{15}{4}+\frac{3}{4}\left(\frac{\sigma}{r}\right)^2} \qquad \ldots\ldots(9a)$$

Table 1

Computation of radial gradient by relaxation method. Comparison of initial and final values

The numbers underlined have been calculated from equation (7). The values in the top row between the calculated values were computed by the relaxation method in a first approximation. The values underneath have been calculated by the relaxation method in a second approximation, in a mesh four times finer (linear) than the one in this table.

3·0	·39939	·38861	·35758	·31299	·26052	·20841	·16007	·11915	·08462	·05737	·03700	·02396	·01273	·0067	·00090						
	·39827	·38665	·35655	·31187	·25981	·20858	·16124	·11940	·08466	·05763	·03778	·02346	·01299	·00622	·00090						
2·8	·35187	·34309	·32176	·28882	·24976	·20911	·16992	·13514	·10402	·07890	·05832	·04305	·0302	·0223	·01549	·01065	·00705	·00510	·00274	·00170	·00047
	·35136	·34314	·32155	·28880	·25049	·20729	·17008	·13491	·10414	·07876	·05843	·04308	·03085	·02228	·01549	·01065	·00705	·00510	·00274	·00170	·00047
2·6	·31914	·31309	·29732	·27234	·24260	·20970	·17745	·14711	·11982	·09626	·07606	·06176	·04769	·0384	·02938	·02324	·01900	·01464	·00132	·00929	·00732
	·31850	·31311	·29697	·27223	·24235	·20973	·17742	·14717	·11997	·09633	·07664	·06114	·04771	·03769	·02949	·02335	·01833	·01450	·01140	·00906	·00732
2·4	·29770	·29326	·28066	·26116	·23774	·21129	·18419	·15779	·13360	·11198	·09261	·07679	·0627	·0522	·04263	·03533	·02930	·02411	·01987	·01651	·01370
	·29711	·29369	·28083	·26160	·23787	·21112	·18420	·15796	·13369	·11189	0·9267	·07682	·06308	·05211	·04277	·03527	·02925	·02407	·01981	·01648	·01368
2·2	·28557	·28212	·27236	·25668	·23757	·21522	·19215	·16889	·14686	·12629	·10735	·09162	·07267	·0665	·05549	·04715	·03988	·03341	·02830	·02392	·02022
	·28541	·28222	·27243	·25703	·23765	·21505	·19195	·16895	·14691	·12635	·10767	·09171	·07776	·06603	·05566	·04703	·03967	·03348	·02822	·02381	·02012
2·0	·28185	·27896	·27074	·25757	·24142	·22241	·20196	·1812	·16085	·14132	·12272	·10658	·0924	·0799	·06828	·05898	·05060	·04324	·03695	·03127	·02644
	·28175	·27901	·27183	·25782	·24170	·22258	·20203	·18130	·16081	·14114	·12281	·10667	·09239	·07986	·06847	·05871	·05023	·04298	·03663	·03121	·02660
1·8	·28658	·28342	·27711	·26481	·25124	·23405	·21526	·19594	·17612	·15730	·13845	·12254	1·0712	·0941	·08150	·07055	·06089	·05252	·04520	·03882	·03329
	·28646	·28410	·27702	·26512	·25152	·23458	·21565	·19621	·17563	·15598	·13865	·12259	·10755	·09399	·08162	·07070	·06089	·05265	·04528	·03890	·03334
1·6	·30072	·29864	·29183	·28102	·26790	·25186	·23388	·21517	·19531	·17648	·15763	·14100	·1251	·1097	0·9609	·08359	·07255	·06306	·05456	·04709	·04059
	·30075	·29841	·29165	·28090	·26799	·25221	·23450	·21539	·19414	·17458	·15696	·14080	·12473	·10985	·09609	·08366	·07267	·06304	·05456	·04710	·04060
1·4	·32692	·32524	·31835	·30846	·29440	·27844	·25965	·23987	·21876	·20007	·17963	·16185	·14304	·12729	·11140	·09808	·08558	·07477	·06496	·05623	·04860
	·32704	·32536	·31867	·30804	·29525	·27945	·26144	·24113	·22064	·20184	·18109	·16231	·14430	·12785	·11233	·09838	·08585	·07480	·06496	·05626	·04862
1·2	·36981	·36872	·36177	·35076	·33593	·31830	·29827	·27694	·25490	·23311	·21024	·18963	·16878	·14962	·13364	·11638	·10155	·08874	·07724	·06703	·05789
	·37001	·36847	·36244	·35281	·33741	·31949	·29932	·27777	·25539	·23316	·21065	·18991	·16878	·15076	·13221	·11610	·10155	·08870	·07721	·06698	·05789
1·0	·43905	·43635	·42839	·41552	·39842	·37775	·35436	·32914	·30290	·27638	·24925	·22498	·20098	·17855	·15782	·13888	·12157	·10635	·09262	·08046	·06931
	0	0·20	0·40	0·60	0·80	1·00	1·20	1·40	1·60	1·80	2·00	2·20	2·40	2·60	2·80	3·00	3·20	3·40	3·60	3·80	4·00

→ z

Table 2*a*. Radial gradient of the field of a single coaxial lens

Values of r	0	0·05	0·10	0·15	0·20	0·25	0·30	0·35	0·40	0·45	0·50	0·55	0·60	0·65	0·70	0·75	0·80	0·85	0·90	0·95	1·00
2·80	·3514	·3508	·3490	·3465	·3431	·3389	·3339	·3280	·3216	·3142	·3064	·2978	·2888	·2794	·2699	·2602	·2505	·2402	·2299	·2194	·2093
2·75	·3420	·3415	·3399	·3376	·3347	·3307	·3261	·3206	·3146	·3078	·3006	·2926	·2842	·2754	·2668	·2586	·2485	·2388	·2289	·2190	·2094
2·70	·3334	·3328	·3315	·3293	·3267	·3229	·3189	·3137	·3082	·3018	·2952	·2876	·2799	·2717	·2635	·2550	·2462	·2371	·2278	·2186	·2094
2·65	·3255	·3250	·3236	·3220	·3197	·3162	·3124	·3076	·3025	·2965	·2903	·2832	·2759	·2682	·2604	·2523	·2441	·2356	·2269	·2182	·2096
2·60	·3185	·3180	·3168	·3159	·3131	·3099	·3062	·3019	·2970	·2915	·2856	·2791	·2722	·2650	·2576	·2500	·2424	·2344	·2262	·2180	·2097
2·55	·3121	·3117	·3106	·3091	·3072	·3044	·3008	·2967	·2927	·2871	·2815	·2755	·2691	·2623	·2554	·2482	·2409	·2334	·2257	·2179	·2100
2·50	·3065	·3061	·3050	·3037	·3021	·2994	·2960	·2920	·2878	·2831	·2779	·2722	·2662	·2598	·2533	·2465	·2397	·2325	·2253	·2178	·2102
2·45	·3013	·3008	·3000	·2990	·2973	·2949	·2917	·2881	·2840	·2797	·2747	·2695	·2638	·2578	·2517	·2453	·2386	·2318	·2248	·2178	·2107
2·40	·2971	·2968	·2958	·2948	·2937	·2908	·2879	·2846	·2808	·2766	·2720	·2670	·2616	·2559	·2502	·2441	·2379	·2314	·2247	·2180	·2111
2·35	·2935	·2932	·2923	·2911	·2895	·2872	·2846	·2815	·2780	·2741	·2697	·2650	·2600	·2547	·2492	·2434	·2374	·2313	·2250	·2185	·2119
2·30	·2903	·2900	·2893	·2881	·2865	·2842	·2817	·2788	·2756	·2719	·2679	·2633	·2586	·2536	·2483	·2429	·2373	·2314	·2254	·2192	·2127
2·25	·2878	·2874	·2868	·2856	·2841	·2821	·2797	·2769	·2739	·2703	·2665	·2622	·2577	·2529	·2480	·2428	·2373	·2315	·2260	·2200	·2139
2.20	·2854	·2851	·2847	·2836	·2827	·2802	·2780	·2754	·2724	·2690	·2654	·2613	·2570	·2525	·2478	·2428	·2377	·2323	·2268	·2211	·2151
2·15	·2838	·2836	·2831	·2821	·2809	·2790	·2769	·2744	·2715	·2681	·2647	·2609	·2568	·2525	·2480	·2432	·2383	·2331	·2279	·2224	·2166
2·10	·2827	·2824	·2819	·2809	·2797	·2780	·2760	·2735	·2710	·2677	·2646	·2607	·2568	·2526	·2483	·2438	·2391	·2342	·2291	·2238	·2182
2·05	·2822	·2817	·2812	·2803	·2791	2773	·2753	·2731	·2709	·2684	·2644	·2607	·2571	·2530	·2489	·2446	·2402	·2355	·2306	·2256	·2204
2·00	·2819	·2812	·2804	·2797	·2790	·2770	·2749	·2728	·2710	·2686	·2648	·2614	·2576	·2535	·2495	·2455	·2429	·2374	·2327	·2278	·2226
1·95	·2821	·2818	·2813	·2806	·2796	·2780	·2761	·2740	·2717	·2689	·2658	·2624	·2590	·2553	·2513	·2470	·2439	·2397	·2353	·2304	·2254
1·90	·2831	·2829	·2825	·2818	·2809	·2795	·2776	·2756	·2733	·2706	·2674	·2642	·2608	·2573	·2536	·2500	·2462	·2422	·2380	·2333	·2262
1·85	·2845	·2843	·2839	·2833	·2824	·2810	·2791	·2772	·2750	·2724	·2692	·2661	·2628	·2595	·2559	·2524	·2487	·2448	·2406	·2361	·2314
1·80	·2865	·2863	·2857	·2850	·2841	·2828	·2809	·2791	·2770	·2744	·2714	·2683	·2651	·2619	·2585	·2551	·2515	·2477	·2436	·2392	·2346
1·75	·2890	·2888	·2882	·2876	·2866	·2852	·2836	·2817	·2796	·2770	·2741	·2711	·2681	·2649	·2616	·2584	·2549	·2511	·2471	·2429	·2385
1·70	·2923	·2921	·2916	·2909	·2899	·2886	·2870	·2852	·2829	·2804	·2776	·2748	·2718	·2687	·2655	·2623	·2587	·2549	·2510	·2469	·2425
1·65	·2962	·2960	·2956	·2948	·2939	·2926	·2911	·2891	·2870	·2845	·2818	·2789	·2761	·2731	·2699	·2667	·2630	·2593	·2553	·2513	·2473
1·60	·3008	·3006	·3001	·2994	·2984	·2973	·2957	·2938	·2917	·2892	·2864	·2837	·2809	·2781	·2749	·2715	·2680	·2643	·2604	·2564	·2522
1·55	·3060	·3059	·3054	·3046	·3035	·3027	·3011	·2992	·2970	·2970	·2917	·2889	·2862	·2837	·2805	·2772	·2738	·2702	·2663	·2623	·2548
1·50	·3121	·3120	·3115	·3106	·3098	·3090	·3072	·3054	·3030	·3005	·2977	·2950	·2930	·2901	·2870	·2837	·2802	·2769	·2729	·2688	·2645
1·45	·3191	·3190	·3186	·3181	·3174	·3160	·3144	·3125	·3103	·3079	·3053	·3029	·3004	·2975	·2942	·2908	·2874	·2838	·2800	·2759	·2720
1·40	·3270	·3269	·3267	·3262	·3254	·3241	·3226	·3207	·3187	·3164	·3140	·3115	·3088	·3056	·3022	·2984	·2953	·2917	·2878	·2836	·2795
1·35	·3360	·3359	·3357	·3352	·3344	·3333	·3317	·3299	·3280	·3259	·3235	·3210	·3180	·3149	·3115	·3079	·3045	·3007	·2968	·2929	·2885
1·30	·3460	·3459	·3457	·3453	·3445	·3434	·3419	·3403	·3384	·3363	·3340	·3313	·3284	·3252	·3219	·3182	·3146	·3107	·3066	·3023	·2976
1·25	·3573	·3572	·3570	·3566	·3559	·3547	·3534	·3517	·3498	·3477	·3454	·3427	·3398	·3370	·3336	·3294	·3254	·3213	·3170	·3127	·3085
1·20	·3700	·3699	·3697	·3693	·3685	·3674	·3660	·3644	·3624	·3602	·3580	·3553	·3528	·3510	·3458	·3415	·3374	·3332	·3287	·3242	·3195
1·15	·3843	·3842	·3840	·3835	·3827	·3815	·3801	·3784	·3765	·3744	·3719	·3692	·3662	·3653	·3593	·3548	·3509	·3466	·3420	·3374	·3328
1·10	·4004	·4003	·4001	·3996	·3987	·3974	·3959	·3942	·3923	·3900	·3875	·3844	·3810	·3780	·3737	·3699	·3655	·3613	·3566	·3515	·3462
1·05	·4186	·4185	·4181	·4175	·4165	·4151	·4134	·4116	·4095	·4072	·4043	·4011	·3974	·3938	·3899	·3860	·3812	·3767	·3719	·3669	·3620
1·00	·4390	·4389	·4384	·4375	·4364	·4349	·4330	·4309	·4284	·4256	·4226	·4192	·4155	·4117	·4075	·4031	·3984	·3936	·3885	·3832	·3778

Table 2*b*. Radial gradient of the field of a single coaxial lens (*cont.*)

Values of Y	1·0	1·1	1·2	1·3	1·4	1·5	1·6	1·7	1·8	1·9	2·0	2·1	2·2	2·3	2·4	2·5	2·6	2·7	2·8	2·9	3·0	3·1	3·2	3·3	3·4
2·8	·2093																								
2·7	·2094	·1914	·1739	·1573	·1414	·1264	·1124	·0997	·0879	·0773	·0679	·0598	·0523	·0454	·0395	·0345	·0301	·0260	·0225	·0196					
2·6	·2097	·1935	·1774	·1620	·1472	·1331	·1200	·1077	·0963	·0859	·0766	·0686	·0611	·0540	·0477	·0424	·0377	·0333	·0294	·0261	·0234		·0183		·0145
2·5	·2102	·1959	·1809	·1665	·1526	·1395	·1269	·1153	·1043	·0940	·0847	·0767	·0693	·0621	·0557	·0499	·0450	·0403	·0361	·0325					
2·4	·2111	·1976	·1842	·1709	·1580	·1455	·1337	·1225	·1119	·1019	·0927	·0844	·0768	·0697	·0631	·0574	·0521	·0471	·0426	·0387	·0353		·0293		·0241
2·3	·2127	·2002	·1878	·1755	·1633	·1516	·1403	·1295	·1192	·1094	·1003	·0920	·0843	·0771	·0705	·0646	·0591	·0538	·0491	·0449					
2·2	·2151	·2035	·1920	·1804	·1690	·1578	·1469	·1364	·1264	·1167	·1077	·0994	·0917	·0845	·0778	·0717	·0660	·0605	·0555	·0511	·0470		·0397		·0335
2·1	·2182	·2074	·1967	·1858	·1749	·1642	·1537	·1436	·1336	·1241	·1151	·1069	·0991	·0919	·0851	·0789	·0729	·0672	·0619	·0572					
2·0	·2226	·2124	·2020	·1916	·1813	·1710	·1608	·1508	·1411	·1317	·1228	·1145	·1067	·0993	·0924	·0860	·0799	·0739	·0683	·0633	·0587		·0502		·0430
1·9	·2262	·2182	·2083	·1984	·1883	·1782	·1681	·1583	·1486	·1394	·1306	·1224	·1145	·1069	·0999	·0932	·0868	·0806	·0748	·0696					
1·8	·2346	·2252	·2157	·2060	·1962	·1860	·1756	·1656	·1560	·1472	·1387	·1305	·1226	·1148	·1076	·1007	·0940	·0875	·0815	·0760	·0707		·0609		·0526
1·7	·2425	·2336	·2243	·2149	·2049	·1945	·1835	·1737	·1640	·1554	·1473	·1393	·1313	·1235	·1158	·1086	·1017	·0949	·0885	·0827					
1·6	·2522	·2436	·2345	·2250	·2154	·2049	·1941	·1837	·1746	·1649	·1570	·1489	·1408	·1327	·1247	·1171	·1099	·1027	·0961	·0898	·0837		·0727		·0630
1·5	·2645	·2560	·2466	·2371	·2272	·2169	·2066	·1965	·1872	·1770	·1683	·1597	·1510	·1425	·1341	·1261	·1184	·1109	·1037	·0972					
1·4	·2795	·2714	·2614	·2513	·2411	·2308	·2206	·2107	·2018	·1912	·1811	·1716	·1623	·1531	·1443	·1359	·1279	·1199	·1114	·1049	·0984		·0859		·0748
1·3	·2976	·2928	·2794	·2685	·2578	·2471	·2365	·2263	·2157	·2051	·1951·	1850	·1751	·1653	·1558	·1470	·1386	·1386	·1223	·1150					
1·2	·3195	·3095	·2993	·2886	·2778	·2666	·2554	·2443	·2332	·2218	·2107	·2000	·1899	·1792	·1688	·1597	·1508	·1422	·1336	·1259	·1161		·1016		·0887
1·1	·3462	·3356	·3244	·3131	·3013	·2895	·2773	·2654	·2531	·2409	·2288	·2174	·2061	·1950	·1840	·1736	·1640	·1543	·1454	·1366					
1·0	·3778	·3661	·3544	·3418	·3291	·3160	·3029	·2896	·2764	·2628	·2493	·2371	·2250	·2130	·2010	·1898	·1786	·1682	·1582	·1484	·1389		·1216		·1063

Values of Z

Table 3. Values of potential in a single coaxial lens

	0	0·1	0·2	0·3	0·4	0·5	0·6	0·7	0·8	0·9	1·0	1·1	1·2	1·3	1·4	1·5	1·6	1·7	1·8	1·9	2·0	2·1	2·2	2·3	2·4	2·5	2·6	2·7	2·8	2·9	3·0
3·0	·645	·643	·637	·628	·615	·599	·580	·559	·537	·513	·489	·464	·438	·413	·388	·364	·341	·318	·297	·276	·258	·240	·224	·208	·193	·179	·166	·154	·143	·132	·122
2·9	·606	·604	·600	·591	·580	·566	·549	·531	·511	·490	·468	·445	·422	·399	·376	·354	·332	·311	·291	·271	·253	·237	·221	·205	·191	·178	·165	·153	·142	·132	·122
2·8	·570	·569	·564	·557	·547	·535	·520	·504	·486	·467	·447	·427	·405	·384	·363	·342	·322	·302	·283	·265	·248	·232	·217	·202	·188	·176	·164	·152	·141	·131	·122
2·7	·536	·535	·531	·525	·516	·504	·491	·477	·461	·444	·426	·408	·388	·369	·349	·330	·311	·292	·275	·258	·242	·227	·212	·198	·185	·172	·161	·150	·139	·130	·120
2·6	·503	·502	·499	·493	·486	·475	·464	·451	·437	·421	·405	·388	·370	·353	·335	·317	·299	·282	·266	·249	·234	·220	·206	·193	·180	·169	·158	·147	·136	·126	·118
2·5	·472	·471	·468	·463	·456	·447	·437	·425	·413	·399	·384	·369	·352	·336	·320	·303	·287	·271	·256	·241	·226	·213	·200	·187	·175	·164	·153	·143	·133	·124	·116
2·4	·442	·441	·439	·434	·428	·420	·410	·400	·389	·376	·363	·349	·334	·319	·304	·289	·274	·259	·245	·231	·217	·205	·193	·181	·169	·159	·149	·139	·129	·121	·112
2·3	·413	·412	·410	·406	·400	·393	·384	·375	·365	·354	·342	·329	·316	·302	·288	·274	·260	·246	·233	·220	·208	·196	·185	·173	·163	·153	·143	·134	·125	·117	·109
2·2	·384	·383	·381	·378	·373	·366	·359	·350	·341	·331	·320	·309	·297	·284	·272	·259	·246	·233	·221	·209	·197	·186	·176	·165	·155	·146	·137	·128	·119	·112	·104
2·1	·356	·355	·353	·350	·346	·340	·333	·326	·317	·308	·299	·289	·277	·266	·254	·243	·231	·219	·208	·197	·186	·176	·166	·156	·147	·138	·130	·122	·114	·106	·099
2·0	·327	·327	·325	·322	·318	·313	·307	·301	·293	·285	·276	·268	·257	·247	·237	·226	·215	·204	·194	·184	·174	·165	·156	·147	·138	·130	·122	·114	·107	·100	·094
1·9	·299	·299	·297	·295	·291	·287	·281	·276	·269	·262	·254	·246	·237	·227	·218	·208	·199	·189	·180	·170	·162	·153	·145	·137	·129	·121	·141	·107	·100	·094	·087
1·8	·271	·270	·269	·267	·264	·260	·255	·250	·244	·238	·231	·224	·215	·207	·199	·190	·181	·173	·165	·156	·148	·141	·133	·126	·118	·111	·105	·098	·092	·086	·081
1·7	·242	·241	·240	·239	·236	·232	·228	·224	·219	·213	·207	·201	·193	·186	·179	·163	·156	·149	·141	·134	·127	·120	·114	·107	·101	·101	·095	·089	·084	·078	·073
1·6	·212	·212	·211	·209	·207	·204	·201	·197	·192	·187	·182	·177	·171	·164	·158	·151	·144	·138	·132	·125	·119	·113	·107	·101	·095	·090	·084	·079	·074	·070	·065
1·5	·182	·181	·181	·179	·177	·175	·172	·169	·165	·161	·156	·152	·146	·141	·136	·130	·124	·119	·114	·108	·102	·097	·092	·087	·082	·077	·073	·069	·064	·060	·056
1·4	·150	·149	·149	·148	·146	·145	·142	·139	·136	·133	·129	·126	·121	·117	·112	·108	·103	·099	·094	·089	·085	·081	·076	·072	·068	·064	·061	·057	·054	·050	·047
1·3	·116	·116	·116	·115	·114	·112	·110	·108	·106	·103	·100	·097	·094	·091	·087	·084	·080	·077	·073	·070	·066	·063	·060	·056	·053	·050	·047	·045	·042	·039	·037
1·2	·080	·080	·080	·079	·079	·078	·076	·075	·073	·071	·069	·067	·065	·063	·060	·058	·056	·053	·051	·048	·046	·044	·041	·039	·037	·035	·033	·031	·029	·027	·025
1·1	·042	·042	·042	·041	·041	·040	·040	·039	·038	·037	·036	·035	·034	·033	·032	·030	·029	·028	·026	·025	·024	·023	·022	·020	·019	·018	·017	·016	·015	·014	·013

Values of Z

in which the errors arising from the fourth-order derivatives, not considered in equation (9), have been eliminated. At about three-quarters of the points checked equation (9 *a*) gave no change, and in no case did the error exceed three units in the fourth figure. Thus table 2, which contains all values of the radial gradient required for trajectory tracing, can be considered as reliable to at least 0·1%.

The table was extended in order to compute table 3, which contains the potential values. These were obtained by integration from the values of ϕ_r and can be considered as reliable to the fifth figure. In order to draw figure 5 some values of the potential at greater radii were calculated by direct application of the relaxation method to ϕ.

Equation (7), which was used as the starting point, gave a very convenient potential scale, so that there was no need to multiply all values by any constant factor. The equipotential surface $\phi = 1$ gives a very suitable electrode shape. In the corrected objective, to be calculated later, the most convenient cathode potential was found to be -30 units. That is to say, with 60 kev. electrons, as used in many modern electron microscopes, the electrode potentials will be of the order of 1–2 kv., and the accuracy of the calculation corresponds to a few hundredths of a volt.

§ 5. NUMERICAL TRAJECTORY-TRACING

The trajectories were traced in steps of 0·2 length units (one-fifth of the wire radius). Since the angles between the trajectories and the axis never exceeded 0·02, the angles were not distinguished from their sines and the axial velocity was taken as the total velocity calculated from the potential. Errors of this kind, small as they are, cancel out almost entirely, since the main interest is in the deflections at different radii.

Let ϕ_c be the cathode potential, measured, like all other potentials, from the potential of the central wire as zero, ϕ the potential at the point of the trajectory under consideration, and β the angle of the trajectory with the axis. With the above simplifying assumptions we can write

$$\frac{d\beta}{dz} = \frac{1}{2}\frac{\partial\phi/\partial r}{(\phi-\phi_c)}, \qquad \ldots\ldots(10)$$

and if the step length s is sufficiently small, the deflection $\Delta\beta$ suffered along s is

$$\Delta\beta = \frac{s}{2}\frac{\partial\phi/\partial r}{(\phi-\phi_c)}. \qquad \ldots\ldots(11)$$

The trajectories were started parallel to the axis, and equation (11) applied to each step. After every step the new potential value was inserted, belonging to the radius $(r - s\beta)$. The values of ϕ and $\partial\phi/\partial r$ were interpolated from tables 2 and 3. Five decimals of $\partial\phi/\partial r$ were used, and three decimals for ϕ, which, added to $\phi_c = -30$, were sufficiently accurate. Seven decimals were used for the deflections. As the final deflections were of the order 0·001, and since they were the sum of a large number of steps (80 steps in two-element lens), neglecting the seventh decimal might have produced an error in the fifth decimal or third figure of these deflections. The deflections at each step were less than 0·001, so that only four figures were needed, which could be reliably obtained from the tables of $\partial\phi\ \partial r$ and ϕ.

§ 6. TWO-ELEMENT LENSES

Preliminary calculations, carried out by other methods, gave a rough indication of the dimensions of a two-element correcting lens which promised zonal correction. With the cathode at -30 units, the potential impressed on the converging element was -1 unit, on the diverging element 0·86 units, and the distance between the two was 8 wire radii. Apart from the potential of the diverging element, this combination forms part of the three-element system shown in figure 6.

The results of the ray tracing are shown in the following table:—

Table 4

r_0	r_f	$\delta=\delta_1+\delta_2$	δ_1	δ_2
2·6	2·4619	0·002371	0·015972	−0·013601
2·4	2·2556	0·002357	0·016599	−0·014242
2·2	2·0482	0·002338	0·017429	−0·015091
2·0	1·8387	0·002299	0·018520	−0·016221
1·8	1·6262	0·002233	0·019950	−0·017717

The first column gives the initial radii r_0, 4 units before the centre of the converging unit, the second gives the final radii r_f, 4 units beyond the centre of the diverging component. δ is the total deflection produced by the combination, reckoned positive if it is towards the axis. For the purpose of varying the combination, the deflection δ_1, midway between the two components, was also computed. This can be considered roughly as the deflection produced by the first (converging) lens. The last column, $\delta_2=\delta-\delta_1$, can be similarly considered as the deflection produced by the last element, by itself.

In applying the last two columns for the calculation of new combinations, caution is needed, as there is some overlap of fields, and the deflections are not strictly additive or proportional to the lens strength. In combinations with strength ratios appreciably different from the one in the above example, $-1:0{\cdot}86$, new ray tracing may be necessary.

§ 7. FITTING A MAGNETIC LENS

In the above ray tracing, the initial rays were parallel to the axis, corresponding to a corrected image at infinity; thus the magnetic lens should be placed at the other end. The errors produced by this magnetic lens must be such that the rays leaving it tend to one object point.

The deflecting characteristic of the magnetic lens is assumed in the following form:

$$\delta_m=r\,f+C(r/f)^3. \qquad \ldots\ldots(12)$$

Hence r is the radius at which the electrons leave the magnetic lens and enter the correcting lens, that is to say, the radius which has been called r_f in table 4; f is the focal length of the magnetic lens and C is its coefficient spherical aberration. It is possible that in correcting magnetic lenses, higher terms of the series (12) are of importance, but as nothing is known of these it was thought better to leave them out of consideration.

If the magnetic lens and the coaxial lens are to form a corrected combination, the resulting deflection $\delta+\delta_m$ must be proportional to r in a certain zone, as dis-

cussed in § 1. It could not be assumed that the combination described in connection with table 4 hits this off exactly, but there were reasons, justified by the sequel, for believing that a slight variation in the strength of one of the components, say the second, would produce the desired effect. In order to measure this variation directly in potential units, we write the deflection produced by a slightly modified combination $\delta+\epsilon\delta_2/0{\cdot}86$, where ϵ is a small coefficient.

For the purpose of fitting equation (12) to the results of table 4, these results had also to be expressed in the form of a polynomial in r_f. Introducing $x=r_f-2{\cdot}0482$, i.e. measuring the radii from the central ray in table 4, we obtained by Lagrangian interpolation

$$\delta=10^{-4}(23{\cdot}38+1{\cdot}298x-2{\cdot}258x^2+1{\cdot}93x^3+1{\cdot}45x^4) \quad \ldots\ldots(13)$$

and similarly

$$-\delta_2/0{\cdot}86=10^{-4}(175{\cdot}47-54{\cdot}51x+36{\cdot}23x^2-14{\cdot}1x^3+0{\cdot}7x^4) \quad \ldots\ldots(14)$$

We want now to fit the two lenses in a zone centring on a radius $\bar{r}$, which has yet to be found. We write, therefore,

$$\delta+\delta_2/0{\cdot}86=a_0+a_1(r-\bar{r})+a_2(r-\bar{r})^2+a_3(r-\bar{r})^3+a_4(r-\bar{r})^4, \quad \ldots\ldots(15)$$

to which has to be added the deflection δ_m of the magnetic lens, given by equation (12). The resulting deflection, which may be called δ_r, must satisfy the three conditions

$$\frac{d\delta_r}{dr}=\frac{\delta_r}{r}, \qquad \frac{d^2\delta_r}{dr^2}=0, \qquad \frac{d^3\delta_r}{dr^3}=0, \qquad \ldots\ldots(16)$$

which give in turn the three equations

$$2C(\bar{r}/f)^3=a_0-a_1r, \qquad 3C(\bar{r}/f)^3=-a_2\bar{r}^2, \qquad C(\bar{r}/f)^3=-a_3\bar{r}^3. \quad \ldots\ldots(17)$$

The coefficients a, however, themselves depend on $\bar{r}$. In order to give the equations in full, let us write $b_0 \ldots . b_4$ for the numerical coefficients of the polynomial in equation (13) and $c_0 \ldots . c_4$ for the corresponding figures in equation (14). Writing R for the radius of the middle ray from which x was measured, i.e. $x=r-R$ (R was 2·0482 in the above example), we obtain finally two equations:

$$36[b_0-b_1R+\tfrac{2}{3}b_2R^2+\epsilon(c_0-c_1R+\tfrac{2}{3}c_2R^2)](b_4+\epsilon c_4)=[3b_3R-b_2+\epsilon(c_3R-c_2)]^2, \quad \ldots\ldots(18)$$

$$R^2-r^2=\frac{3b_3R-b_2+\epsilon(3c_3R-c_2)}{6(b_5+\epsilon c_4)}. \quad \ldots\ldots(19)$$

These are the two equations for $\bar{r}$ and for ϵ. Once these two are fulfilled, the third of the equations (17) can be fulfilled by a suitable value of Cf^3, that is to say, by a certain series of magnetic lenses.

From the values of equations (13) and (14), ϵ was found to be 0·023. That is to say, the strength of the second lens had to be changed by less than 3% which justifies *a posteriori* the method followed. The value of $\bar{r}$ was found to be 1·50. This is not a convenient value. It falls in a range in which the values of the deflection were found by extrapolation only, but even assuming that the results are reliable, the rays pass uncomfortably close to the inner wire, and the performance

of the lens would be too much dependent on the precision of workmanship. For these reasons the search was continued for a three-element lens of more convenient properties.

§ 8. THREE-ELEMENT CORRECTING LENS

Rough calculations showed that a diverging element of strength 0·4 placed before the converging lens as in figure 6 should make correction possible at a radius of about two units. This element was traced on its own, with the trajectories starting parallel to the axis at 4 units from its centre, at the right. That is to say, the element was traced in opposite direction to the other two, so that it could be added on to the previous combination. A certain error arises of course from the fact that the emerging trajectories are now no longer parallel to the axis.

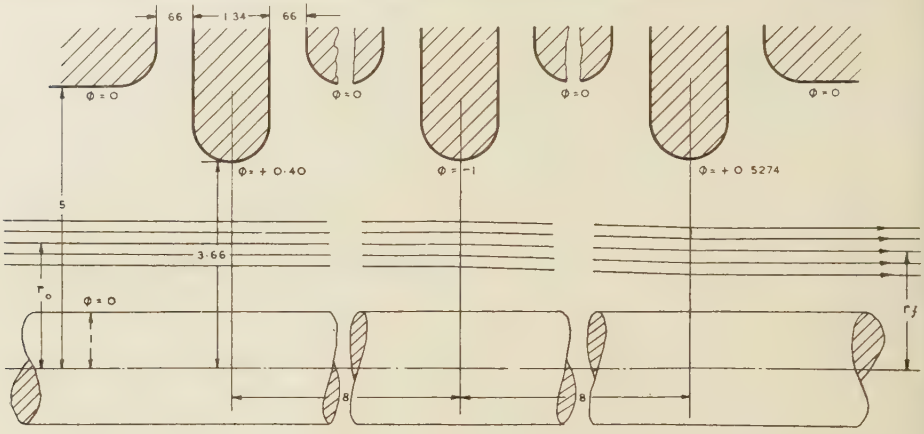

Figure 6. Electrodes and electron trajectories in three-element coaxial correcting lens. Cathode at −30 potential units.

The following values were obtained by direct ray tracing:

r_0	1·8	2·0	2·2	2·4	2·6
δ_3	−0·008068	−0·007459	−0·006972	−0·006585	−0·006274

which can be represented by the following quartic:

$$-\delta_3 = 10^{-4}(69{\cdot}72 - 20{\cdot}800x + 11{\cdot}101x^2 - 3{\cdot}35x^3 - 1{\cdot}41x^4). \quad \ldots\ldots(20)$$

δ_3 was added to δ and the sum was used instead of δ in the calculation of ϵ and $\bar{r}$, which otherwise was carried out by the methods outlined in the last section. The result was $\epsilon = -0{\cdot}333$ and $\bar{r} = 1{\cdot}98$. The original diverging lens was thus reduced to a strength of 0·527. The whole combination with the trajectories is shown in figure 6.

The resulting characteristic of this three-element lens combination is shown in figure 7 (*a*). The magnetic lens which fits it must belong to the series

$$C/f^3 = 0{\cdot}228 \times 10^{-4}$$

or

$$f = 35{\cdot}3C^{1/3} \text{ wire radii.} \quad \ldots\ldots(21)$$

The residual error of the combination is shown in figure 7 (*b*). It has the form of a quartic parabola.

As an example let us assume that the microscope objective lens which is to be corrected is about as good as it can be made. At 60 kev. the best realizable values are about $f = 3$ mm. and $C = 0{\cdot}2$. In this case equation (21) gives a wire diameter of about 0·27 mm., which is a quite convenient value. The bore of the electrode

system is about 1 mm., which means that the construction of the lens requires accuracy of a high order, but not beyond the reach of really good workshop practice.

The residual is less than 10^{-7} radian in a range of $1{\cdot}98 \pm 0{\cdot}135$ wire radii, which, with the focal length chosen, corresponds to an angular range of $0{\cdot}090 \pm 0{\cdot}0062$ radian. For a beam inside these limits the geometrical error is less than 3 A.

In order to estimate the diffraction errors, we must divide the de Broglie wavelength, which for 60 kev. electrons is about 0·05 A., by the angular range, which is about 0·012. This gives about 4 A. for the width of the first maximum in the radial diffraction figure. Two points can perhaps be separated if they are at 0·6 to 0·7 of this distance; thus we can say that the diffraction error is also 3 A. or less. Both the geometrical error and the diffractional error are less than can ever be realized in uncorrected electron microscopes of the current type.

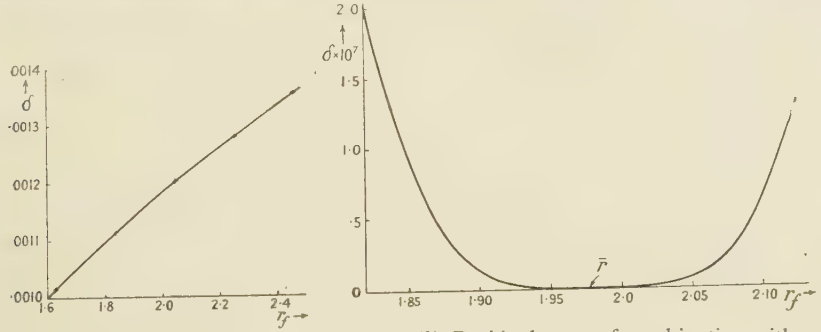

(*a*) Characteristic of electrostatic correcting lens.

(*b*) Residual error of combination with magnetic lens.

Figure 7.

It is impossible to foresee at present how much of the calculated improvement will be realizable in practice. Evidently workmanship of the highest order will be required, and very careful focusing, much more careful than in microscopes of the current type, as the focal depth of the zonally corrected objective will be some 30 to 50 times smaller. On the other hand, this small focal depth might open up the new possibility of exploring objects in depth with an accuracy of the order of 100 A.

ACKNOWLEDGMENTS

These calculations were carried out at the suggestion and under the constant supervision of Dr. D. Gabor.

The authors wish to express their thanks to the Directors of the British Thomson-Houston Co. for permission to publish this paper.

REFERENCES

Gabor, D., 1940. *Nature, Lond.*, **158,** 198; B.T.H. Co. Brit. Patent Appln. No. 22053/45.
Gabor, D., 1945 a. *The Electron Microscope* (London : Hulton Press), Chapter 7.
Gabor, D., 1945 b. *Proc. Roy. Soc.*, A, **183,** 436.
Hillier, J., 1946. *J. Appl. Phys.*, **17,** 307, 411.
Motz, H. and Klanfer, Laura, 1946. *Proc. Phys. Soc.*, **58,** 30.
Picard, E., 1894. *Traité d'Analyse* (Paris : Gauthier Villars), Vol. II.
Scherzer, O., 1936. *Z. Phys.*, **101,** 593.
Southwell, R. V., 1940. *Relaxation Methods in Engineering Science* (Oxford : The University Press).
Zworykin, Morton, Ramberg, Hillier and Vance, 1945. *Electron Optics and the Electron Microscope* (New York : John Wiley), Chapter 19.

NOTE ON APLANATIC LENSES FOR UNIT MAGNIFICATION

By T. SMITH, F.R.S.,
National Physical Laboratory, Teddington

MS. received 30 *December* 1946

ABSTRACT. A formal solution is given for the construction of thin symmetrical cement triple objectives corrected for unit magnification. To any symmetrical objective with a diverging lens between two converging lenses there corresponds another with a converging lens between two diverging lenses, and, with the same kind of glass for the exterior lenses, the curvatures and glass properties for the central lens of one objective can be written down when those of the other objective are known. Both objectives are free from coma and have the same amounts of chromatic and spherical aberrations.

§1. INTRODUCTION

In lenses to be used at unit magnification coma is usually eliminated by using a symmetrical form of construction. A widely-used form consists of an equi-convex lens of a crown glass enclosed by two similar meniscus flint lenses, the three being cemented together. An alternative form, which has been used less extensively, is constructed by cementing an equi-concave flint lens to two similar converging crown lenses. A pair of glasses suitable for securing freedom from chromatic as well as spherical aberration in one type of construction has not the properties required for lenses of the other kind, and the design of one type appears to be distinct from that of the other type. But on looking at the results of some numerical calculations I noticed a connexion which could not be accidental. If a combination of each kind of the same focal length is made with the external lenses of the same glass, the curvatures of the external surfaces of both forms will have the same value if ω_2, ω_1, ω_2' are in arithmetical progression, where ω_1 is the reciprocal of the refractive index of the glass used externally, and ω_2 and ω_2' are the reciprocals of the indices of the glasses used for the central lenses in the two forms. This coincidence implies that a simple relation subsists between the internal curvatures of the two forms, and also a relation between the dispersive properties of the three glasses. But the observation is chiefly of interest as it suggests that lenses of these types can be computed with exceptional facility.

§2. GENERAL THEORY

To investigate this the notation and formulae employed in a recent paper (Smith, 1945) are adopted, so that repetition is unnecessary. Taking unity as the power of the complete lens, and j as the sum of the power and the total curvature, we have

$$\alpha = -j_1 j_2(\omega_1-\omega_2) = (j-j_2)j_2(\omega_2-\omega_1),$$

and

$$\gamma+\gamma_1 = j^2+\alpha(j+j_2)\omega_1 = j^2+(j^2-j_2^2)\omega_1 j_2(\omega_2-\omega_1). \quad \ldots\ldots(1)$$

But since $j=j_1+i_2$, and the power of the lens is $j_1(1-\omega_1)+j_2(1-\omega_2)$,

$$j_1=\frac{j(1-\omega_2)-1}{\omega_1-\omega_2}, \quad j_2=\frac{j(1-\omega_1)-1}{\omega_2-\omega_1}, \qquad \ldots\ldots(2)$$

so that, when j and ω_1 are given, the value of $\gamma+\gamma_1$ is independent of the sign of j_2, i.e. of $\omega_1-\omega_2$. This verifies the numerical result observed, for the condition to be satisfied is $\gamma+\gamma_1=0$. It will be noted that the equality of curvature holds for equal amounts of spherical aberration when the ω's form an arithmetical progression. As the curvatures of the surfaces are

$$\tfrac{1}{2}(j-1), \quad \tfrac{1}{2}j_2\omega_2, \quad -\tfrac{1}{2}j_2\omega_2, \quad -\tfrac{1}{2}(j-1),$$

and j_2 is merely reversed in sign when ω_2 is replaced by ω_2', the connexion between the curvatures of the cemented surfaces is simple. Also since the range of values of ω with the glasses normally employed in optical instruments is small, the differences between the curvatures of these surfaces in the two forms will usually be small. So far as manufacture is concerned, one type of lens has no special advantage over the other. The tendency is for the shallower curves to be obtained when $\omega_1>\omega_2$, i.e. when a flint glass is cemented between two crown lenses. In practice the preference for one type rather than another will depend on the kinds of glass available and the higher-order aberrations which are not considered here.

The dispersive properties of a glass may be represented by the value of $\omega/\delta\omega$, which may be denoted by u. The connexion between this and the quantity ν tabulated in glass lists is $\nu=(1-\omega)u$. Formally there is a change of sign, but this may be neglected as the sign is purely a matter of convention. The condition for freedom from chromatic aberration is

$$\frac{j_1}{u_1}=-\frac{j_2}{u_2}=\frac{j}{u_1-u_2}.$$

Since in the alternative construction the sign of j_2 is altered, the condition that both types of lens are chromatically corrected is that $\frac{\delta\omega_2}{\omega_2}, \frac{\delta\omega_1}{\omega_1}, \frac{\delta\omega_2'}{\omega_2'}$ are in arithmetical progression. More generally, if this condition is satisfied, the amount of chromatic aberration will be the same in both types of lens having the same exterior glass.

To solve the condition $\gamma+\gamma_1=0$ when ω_1 and ω_2 are given, we first make the right side of equation (1) homogeneous in j and j_2, using equation (2) for j_2. The result is

$$\frac{\omega_1}{1-\omega_1}\left(\frac{j_2}{j}\right)^3+\frac{j_2}{j}+\frac{1}{\omega_1-\omega_2}=0.$$

Writing

$$x=2\left(\frac{1-\omega_1}{3\omega_1}\right)^{1/2}, \quad \sinh 3\theta=\frac{3}{(\omega_2-\omega_1)x},$$

the solution is

$$j_2=jx\sinh\theta,$$

and by (2)

$$1/j=1-\omega_1-(\omega_2-\omega_1)x\sinh\theta.$$

Constructional details for lenses of these types, when thicknesses are neglected, can therefore be obtained directly from common tables.

It will be noticed that the problem considered here is essentially the same as the determination of a cemented doublet corrected for parallel light incident initially on a plane surface.

§ 3. EXAMPLES OF APPLICATION

It may be of interest to add two numerical examples, one where the glasses do not differ greatly in their indices, and the other where the difference is large. Let $\omega_1 = 0{\cdot}600$, $\omega_2 = 0{\cdot}610$. Then $x = \frac{2}{3}\sqrt{2}$, $\sinh 3\theta = 225\sqrt{2}$,

giving $$\sinh\theta = 3\sqrt{2}, \quad j = \frac{25}{9}, \quad j_2 = \frac{100}{9},$$

and the curvatures are

$$\frac{8}{9}, \quad \frac{61}{18}, \quad -\frac{61}{18}, \quad -\frac{8}{9}.$$

The corresponding alternative form has

$$\omega_1 = 0{\cdot}600, \quad \omega_2' = 0{\cdot}590,$$

with curvatures

$$\frac{8}{9}, \quad -\frac{59}{18}, \quad \frac{59}{18}, \quad -\frac{8}{9}.$$

For chromatic correction

$$\frac{\delta\omega_2}{\omega_2} : \frac{\delta\omega_1}{\omega_1} : \frac{\delta\omega_2'}{\omega_2'} = 3 : 4 : 5.$$

The 25 per cent differences in these chromatic factors contrast markedly with differences in the indices of under 2 per cent.

For the second example take $\omega_1 = 0{\cdot}500$, $\omega_2 = 0{\cdot}600$. This gives $x = \frac{2}{3}\sqrt{3}$, $\sinh 3\theta = 15\sqrt{3}$, with the solution

$$\sinh\theta = \sqrt{3}, \quad j = \frac{10}{3}, \quad j_2 = \frac{20}{8}.$$

The curvatures are

$$\frac{7}{6}, \quad 2, \quad -2, \quad -\frac{7}{6}.$$

In the associated solution for $\omega_1 = 0{\cdot}500$, $\omega_2' = 0{\cdot}400$ (corresponding to a higher refractive index than has hitherto been obtained in glass) the curvatures are

$$\frac{7}{6}, \quad -\frac{4}{3}, \quad \frac{4}{3}, \quad -\frac{7}{6},$$

and for chromatic correction

$$\frac{\delta\omega_2}{\omega_2} : \frac{\delta\omega_1}{\omega} : \frac{\delta\omega_2'}{\omega_2'} = 1 : 2 : 3.$$

The substantial difference between the curvatures of the inner surfaces of the two lenses is to be expected in view of the very great difference 0·2 in the ω values. The 20 per cent differences in these values are accompanied by 50 per cent differences in the dispersive ratios. The examples suggest that the former difference increases relatively more rapidly than the latter.

§ 4. ACKNOWLEDGMENT

The work described above has been carried out as part of the research programme of the National Physical Laboratory, and this paper is published by permission of the Director of the Laboratory.

REFERENCE

Smith, T., 1945. *Proc. Phys. Soc.*, **57**, 543.

REFLEXION OF CENTIMETRIC ELECTROMAGNETIC WAVES OVER GROUND, AND DIFFRACTION EFFECTS WITH WIRE-NETTING SCREENS

By J. S. HEY, S. J. PARSONS and F. JACKSON,
Ministry of Supply

MS. received 19 *December* 1946

ABSTRACT. Difficulties in the operation of centimetric wave-length radar equipment at low angles of elevation (less than 10°) have led to a detailed consideration of the influence of ground reflexion. A technique is described for the determination of the relation between the signal strength of the echo from an isotropic reflector and the angle of elevation of the reflector. Measurements obtained over natural ground sites are shown to be in accordance with simple theoretical considerations. The effect of wire-netting artificial screening has been examined, the experimental results being in general agreement with those derived by theoretical treatment of diffraction using Sommerfeld's formula.

§ 1. INTRODUCTION

The wartime requirements for Army radar equipments to operate at angles of elevation of a few degrees gave rise to a number of siting problems. In order to avoid the clutter on the cathode-ray tube display of unwanted echoes from ground objects such as buildings or hills, which on high sites may return appreciable signals at many kilometres range, it was found desirable to place the radar set so that a crest within a few kilometres afforded screening from more distant ground objects. Artificial screening by wire netting was also introduced during the flying bomb attacks on London and S.E. England for radar sites where no suitable natural crests were available.

In addition to the requirement for eliminating the clutter of echoes from ground objects, it was essential to know the coverage of the radar set at low elevations, this being profoundly affected by reflexion and diffraction effects of the ground and screen surrounding the set. The present research was carried out between autumn 1944 and spring 1945 at the experimental station of the Army Operational Research Group, Ministry of Supply. The investigation was designed to determine the echo signal strength pattern in the vertical plane for an Army radar equipment operating at a wave-length of 10·7 cm. on typical natural sites both with and without artificial screening. An attempt is here made to relate the results to theoretical considerations of reflexion and diffraction.

§ 2. EXPERIMENTAL TECHNIQUE

The equipment consisted of the British Army set known as G.L. III (see plate 1), with some minor receiver modifications to give a suitable presentation for the measurements required in the present investigation. The transmitter radiated

pulses of 1 microsecond duration with a peak power of about 200 kw. Separate transmitter and receiver paraboloids with apertures of 1·22 m. diameter mounted adjacently with foci at a height of 3·6 m. could be traversed together in bearing or elevation as required. Reflected pulses were displayed on the receiver cathode-ray tube as deflections of a linear range trace. The receiver output circuits were arranged so that the deflection amplitude on the cathode-ray tube was directly proportional to the received signal strength.

The investigation was carried out for vertical polarization (electromagnetic waves with the electric vector in a vertical plane). The transmitting aerial was fixed, but the receiving aerial was displaced alternately to the right and left so as to give a horizontal deflection of the electrical axis of the beam of 1·2° to each side. The received signals for the two positions were presented so as to appear side by side on a second cathode-ray tube, the amplitudes being equal when the paraboloid axis was directed towards the bearing of the reflector. This method was the standard radar technique for determination of bearing by this equipment and was used throughout the investigation to maintain the paraboloid axis on the bearing of the target.

The reflector from which the echoes were obtained consisted of a 0·6 m. diameter papier-mâché sphere, metallized with sprayed zinc, suspended from a tethered balloon at ranges of 2500 to 3000 m. Weather conditions, with frequent gusty winds, often presented a serious handicap to experimental work. The most satisfactory method of supporting the sphere was found to be by means of an "M" type balloon (a spherical fabric balloon of about 4 m. diameter) flying on a nylon cord. The balloon itself gave a signal about $\frac{1}{8}$ of that from the sphere; provided the balloon and sphere were close together, the slight beating of the signal due to this cause could be tolerated. By measurements of the pulse amplitude on the cathode-ray tube, and with the aid of several fixed receiver gain settings in simple ratios, the signal strength could be determined in terms of the "free-space" reflexion signal to an accuracy of roughly 5%. The free-space signal was obtained from observations at an angle of elevation of about 15°, where ground interference effects were negligible.

The transmitter and receiver paraboloid axes were set at a fixed elevation of a few degrees and the height of the spherical reflector was varied at a rate of roughly 15 m. per minute between ground level and about 500 m. The elevation of the reflector was measured by means of a theodolite placed close to the equipment. Readings were taken at intervals of two seconds both of angle of elevation of the reflector and of echo signal amplitude on the cathode-ray tube. The range of the echo was also recorded so that, where necessary, the readings of echo signal amplitude could be normalized to a constant range by the inverse-square law.

§ 3. ELEMENTARY THEORETICAL CONSIDERATION OF GROUND REFLEXION

The manner in which the signal strength echoed from an isotropic reflector varies with the angle of elevation of the reflector for a given bearing, and elevation of the paraboloid axes will here be referred to as the directional sensitivity * of

* In the Services and elsewhere this has often been loosely referred to as the vertical polar diagram of the equipment.

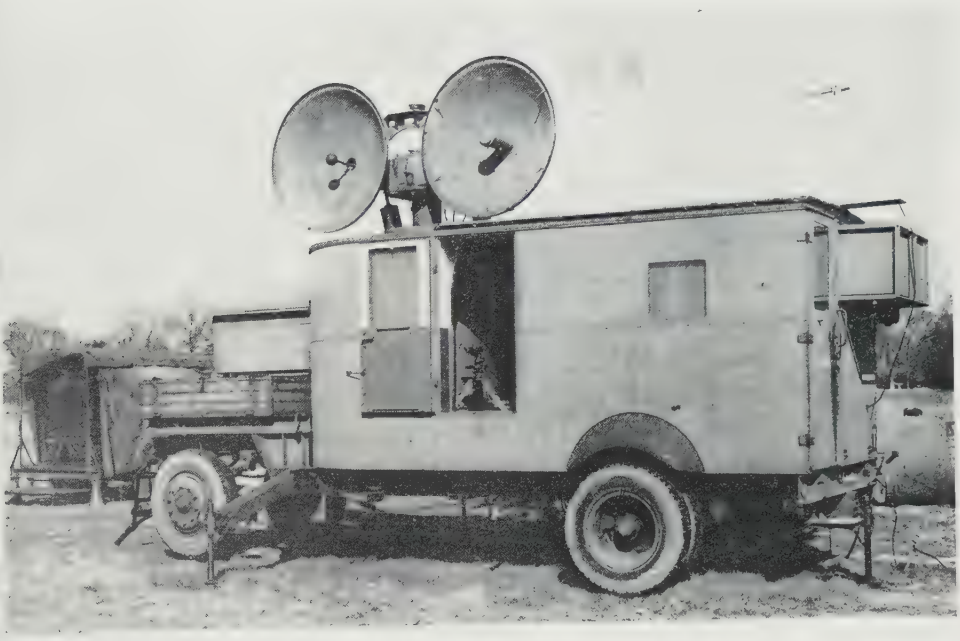

Plate 1.

Plate 2.

the radar equipment for the vertical plane considered. Where ground reflexion is present, the directional sensitivity pattern will depend on the configuration and reflexion coefficient of the ground, the position of the radar aerial, and the free-space directivity factor of the aerial. In the case of the transmitting aerial, we define the free-space directivity factor as the relation between direction and radiated field strength, scaled to a maximum of unity; for the receiving aerial, it is the relation between the direction of an incident plane wave of given amplitude, and the received signal strength, again scaled to a maximum of unity. Suppose the free-space directivity factor of the transmitting aerial in the vertical plane is $F(\theta)$, where θ is the angle between the axis of the paraboloid and the direction of the target, then the field strength at a reflector, elevation α, illuminated by a paraboloid tilted at elevation ϕ, compared with a maximum free-space value of unity, is given by

$$F(\theta)_{\alpha-\phi} + Re^{i\psi}F(\theta)_{-\alpha-\phi},$$

where the expression represents the addition of the direct and reflected waves, R being the reflexion coefficient (which may be a complex quantity), ψ the phase difference due to the path difference between the direct and reflected waves, and $i = \sqrt{-1}$. If the reflector is isotropic, the directional sensitivity of the radar equipment is the product of the above expression and one similarly derived for the receiving aerial.

Figure 1 shows the calculated pattern of directional sensitivity in a vertical plane for the G.L. III aerials, at a height of 3·6 m., directed at grazing incidence to

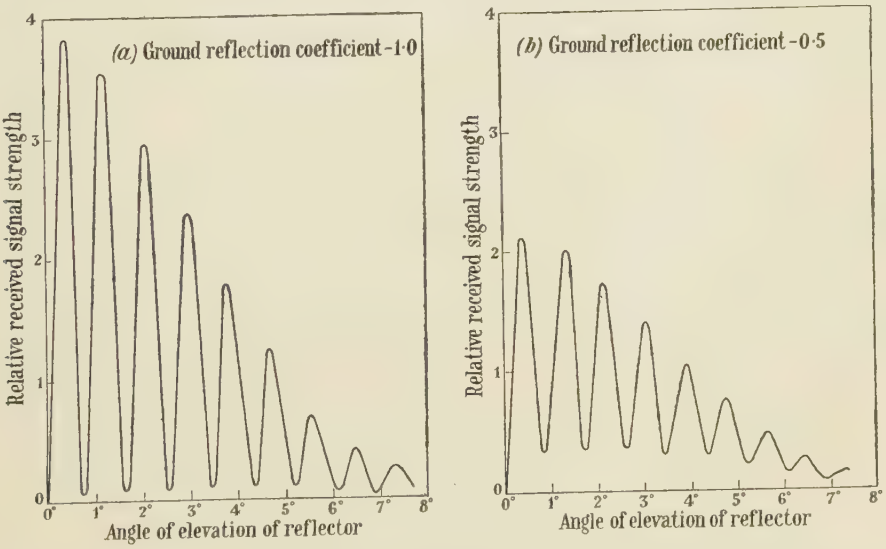

Figure 1. Calculated directional sensitivity patterns for G.L. III.
Aerial height 3·6 m. above horizontal plane ground. Radar axis at 0·8° elevation.

ground having a horizontal plane surface with assumed values of the reflexion coefficient of $R = -1{\cdot}0$ and $R = -0{\cdot}5$ respectively. The diminution in amplitude of the lobes as the elevation increases is due to free-space directivity factor, $F(\theta)$, of the aerials. The multiple lobe structure is due to ground reflexion interference,

The elevations of the maxima are given approximately by

$$\sin\alpha = (n-\tfrac{1}{2})\lambda/2h,$$

and of the minima by

$$\sin\alpha = (n-1)\lambda/2h,$$

where α is the angle of elevation, λ the wave-length, h the aerial height above the plane, and n is an integer. For $\lambda = 10{\cdot}7$ cm. and $R = 3{\cdot}6$ m. the corresponding values of α are as follows:—

Maxima (°)	0·4,	1·2,	2·0,	2·8 ....
Minima (°)	0,	0·8,	1·6,	2·4 ....

If the plane has a slope of angle of elevation β in the direction of the reflector, then the above angles will be increased by β in each case. For the case of a distant slope, differing from that of the near ground, simple image theory leads to substitution of an effective height for h in the above equations for those reflexions that take place on the distant slope (provided at least about half the first Fresnel zone lies on the slope). This effective height is the perpendicular height of the aerials above the plane containing the distant slope. In such cases, however, where the ground surface is discontinuous, multiple reflexions often add further complexity.

Although natural ground is generally far from flat, certain deviations can be tolerated before we may expect serious changes in the shape of the directional sensitivity patterns shown in figure 1. Provided the region around the point of reflexion (as defined by geometrical optics) is flat for an area of the order of half the first Fresnel zone, the reflected wave will be of the same order as that for an infinite reflecting plane. Ground may be said to be flat if the surface irregularities do not cause path differences exceeding a small fraction of a wave-length. This may be expressed in the form

$$H\sin\alpha \ll \lambda/2,$$

where H is the height of the surface irregularity above the mean level. For example, the measurements of Ford and Oliver (1946) indicate that, for $H\sin\alpha$ approximately equal to $0{\cdot}2\lambda$, the value of the reflexion coefficient is about 0·5.

The dimensions of the first Fresnel zone may be calculated as follows. In figure 2, let A represent an aerial at height h above a plane reflecting surface. B is the point of reflexion, such that the angle of incidence is equal to the angle of

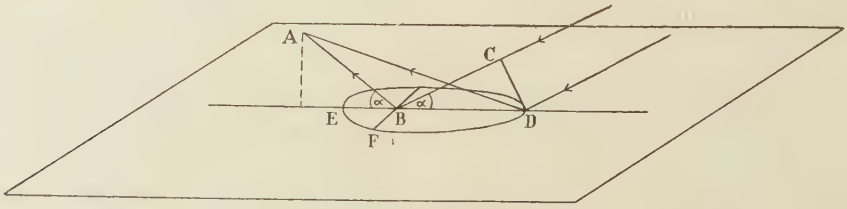

Figure 2. Diagram to illustrate calculation of first Fresnel zone.

reflexion, and CD is the reflected wave front. Then the outer limit D of the first zone is determined by

$$AD - (AB + BC) = \lambda/2.$$

This can be approximately expressed by

$$\mathrm{BD} = \frac{\lambda \cos\alpha + \sqrt{\lambda^2 \cos^2\alpha + 4h\lambda \sin\alpha}}{2 \sin^2\alpha}.$$

Similarly, the inner limit E is approximately given by

$$\mathrm{BE} = \frac{-\lambda \cos\alpha + \sqrt{\lambda^2 \cos^2\alpha + 4h\lambda \sin\alpha}}{2 \sin^2\alpha},$$

and the lateral half-width is approximately given by

$$\mathrm{BF} = (h\lambda/\sin\alpha)^{1/2}.$$

The relations between zone size and angle of elevation are given graphically for $h = 3{\cdot}6$ m. and $\lambda = 10{\cdot}7$ cm. in figure 3. where BD, BE, BF are represented by X_1, X_2, and Z. Two features are of particular note in practical considerations of ground sites. Firstly, the zones are narrow compared with their length, so that the nature of the interference pattern on a given bearing will be determined by the characteristics and slope of the ground in that direction, and will be independent of the ground more than a few degrees away from this bearing. Secondly, as the elevation of the reflector increases, the length of the first zone diminishes and the point of reflexion approaches the equipment. It may be shown that the zones are truly elliptical in shape.

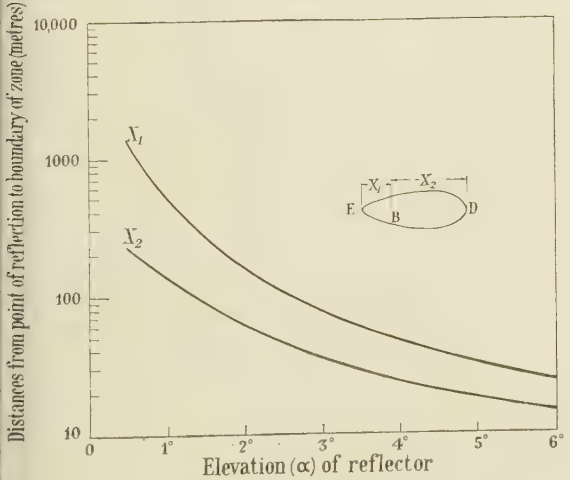

$$X = \pm \frac{\lambda \cos X + \sqrt{\lambda^2 \cos^2\alpha + 4h\lambda \sin\alpha}}{2 \sin\alpha}.$$

$\lambda = 10{\cdot}7$ cm., $h = 3{\cdot}6$ m.

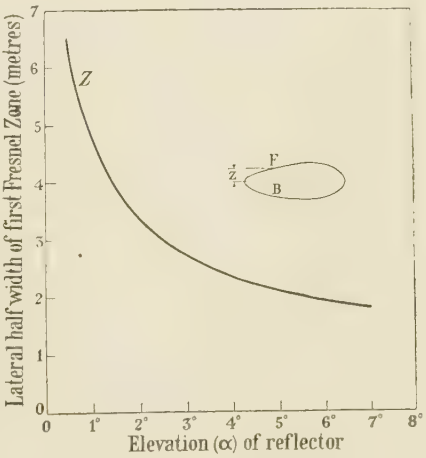

$$Z = \sqrt{\frac{\lambda h}{\sin\alpha}}.$$

$\lambda = 10{\cdot}7$ cm., $h = 3{\cdot}6$ m.

Figure 3. Relations between dimensions of first Fresnel zone and angle of elevation of the reflector.

In order to attempt to apply the above considerations to natural sites, a survey of the ground was made in the directions in which echo signal strength measurements were taken. From the vertical profile, a mean point of reflexion could be estimated for any given value of the reflector elevation α. If the ground around this point was flat (within the specification discussed above) over an extent not less than half the first Fresnel zone, a reflexion could be expected in accordance with simple theory of reflexion from a plane surface.

In the following section a few typical results, obtained at four sites in Richmond Park, are described For two sites (I and II), the above conditions for simple reflexions are largely satisfied; two other sites (III and IV) represent more complex cases. In all cases the results for the echo signal amplitude are expressed in terms of the maximum free-space value.

§4. EXPERIMENTAL RESULTS FOR REFLEXION AT NATURAL SITES

Site I. A photograph of the site is shown in plate 2, and figure 4 gives the measured contour of a vertical section of the ground in the direction in which radar observations were taken. (In the ground contour diagram it should be noted that height variations and angles of elevation appear exaggerated, due to the difference between the height and range scales.)

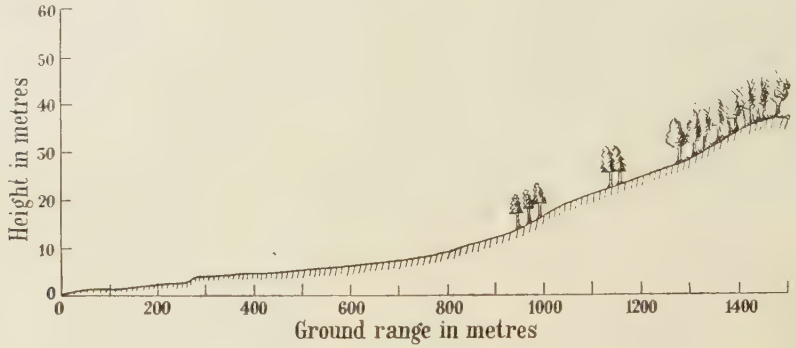

Figure 4. Vertical Section of Site I.
(Note that height and range scales are different.)

Simple theoretical considerations according to the principles outlined above indicate that the ground up to approximately 800 m. from the radar equipment could be considered for the most part flat, with a slope of 0·5°. The angle of elevation of the crest was 2·2°, and for elevations above this value the points of reflexion for a plane surface are within 300 m. Thus we may expect interference maxima at angles of 0·5° greater than those for a horizontal plane reflecting surface. The theoretical lobe maxima will therefore be at 2·5°, 3·3°, 4·1°, etc. The higher lobes are less easily predicted for the following reasons. As the elevation increases, the size of the first Fresnel zone becomes less, and hence departures from the mean slope of 0·5° may occur over the area of the zone; irregularities within the zone also become more important. Further, at the higher angles of elevation, the lobes are more likely to be influenced by secondary reflexions from the crest slope (ranges beyond 800 m. from the equipment), although such reflexions can only have a minor effect owing to the considerable variations in slope and the wooded nature of the ground in this region.

Measurements of the signal reflected from the sphere (at about 3000 m. range) were made with the axes of the radar paraboloids at fixed elevations of 0°, 3° and 5° respectively. Smooth curves drawn through the graphed results are shown in figure 5. In the case of the paraboloid axes at 3° elevation, the points representing the individual measurements have also been marked; this has been chosen as a

typical example to demonstrate the scatter in the observations. It will be seen that there is general agreement between the expected positions of the interference

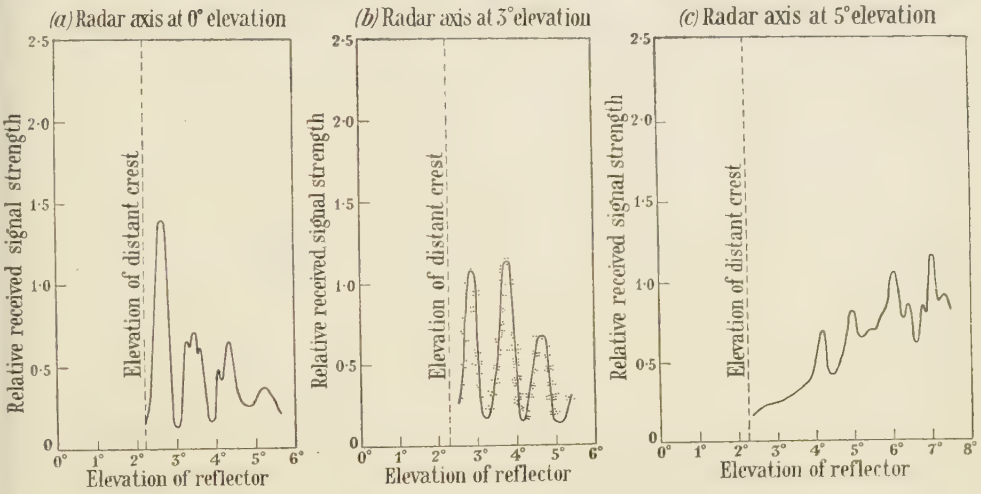
(a) Radar axis at 0° elevation
(b) Radar axis at 5°elevation
(c) Radar axis at 5°elevation
Relative received signal strength
Elevation of distant crest
Elevation of reflector

Figure 5. Directional sensitivity pattern at site I.

lobes and those measured experimentally. The increased magnitude of the first observable lobe, when paraboloids are set with their axes at 0° elevation, is notable and indicates a high value for the reflexion coefficient.

Site II. The vertical ground section for the site is shown in figure 6. The ground from about 100 m. to 300 m. from the radar equipment may be regarded as having an almost uniform mean slope of about 0·9°, the effective height of the aerial with respect to this region being approximately 4 m. The measured vertical directional sensitivity pattern is shown in figure 7. The small lobe at 2·3° could be accounted for by the lobe with predicted maximum at 2·0°, which would be considerably screened by a distant heavily-wooded crest at 2·1° elevation (not shown in figure 6). The observed maxima at 2·8° and 3·6° fit well with

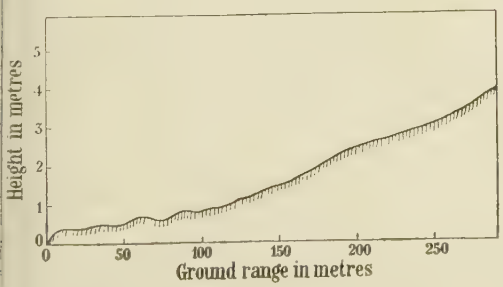

Figure 6. Vertical section of site II. (Note that height and range scales are different.)

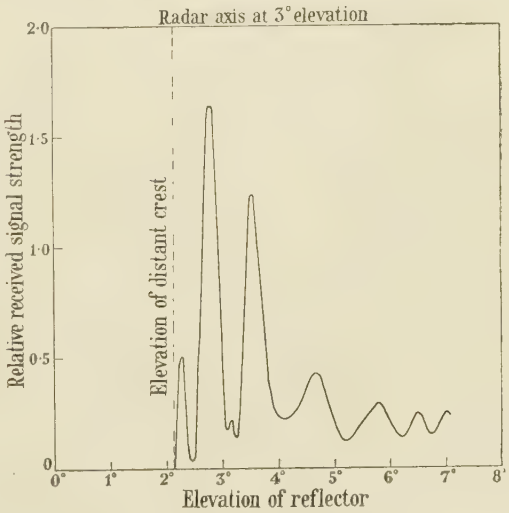

Figure 7. Directional sensitivity at site II.

the values of 2·75° and 3·5°, which would be expected from the above considerations of the site contour. The discontinuities of the ground within about 100 m. make the lobe structure for higher angles of elevation more difficult to estimate.

Site III. The vertical section for this site is illustrated by figure 8, and the measured echo strength pattern in figure 9 shows a strong lobe system extending to high angles. This might be expected from the steepness of the gradients; further, the ground slope changes from concave to convex before attaining a crest only some 500 m. away, and no simple prediction of lobe positions or magnitudes is possible owing to the complexity of the contour.

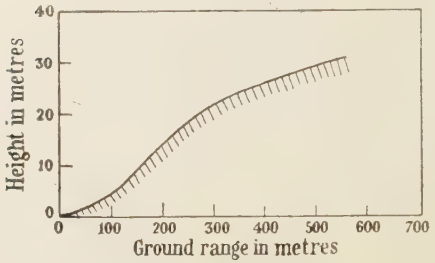

Figure 8. Vertical section of site III. (Note that height and range scales are different.)

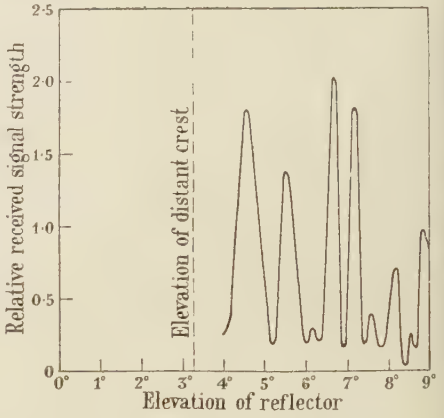

Figure 9. Directional sensitivity pattern at site III. Radar axis at 4° elevation.

Site IV. Consideration of the vertical section at this site, given in figure 10, indicates that double or triple reflexions may occur. A complicated relation between echo strength and reflector elevation might be expected, therefore, and this is shown to be the case in figure 11. As for the previous site, no simple prediction of lobe positions or magnitudes is possible.

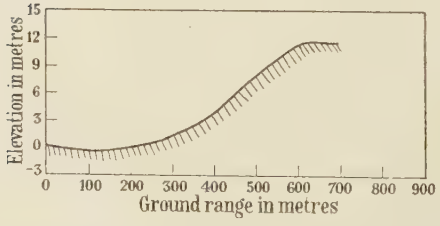

Figure 10. Vertical section at site IV. (Note that height and range scales are different.)

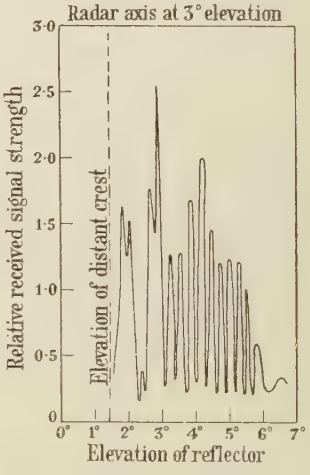

Figure 11. Directional sensitivity pattern at site IV.

§ 5. DIFFRACTION EFFECTS WITH ARTIFICIAL SCREENS

On certain radar sites where there was no natural crest to afford screening from unwanted echoes from ground objects, wire-netting screens of 22 S.W.G. galvanized iron wire and 1·4 cm. mesh were erected after a preliminary trial had indicated their effectiveness for this purpose. These screens were placed at a distance of about 50 m. from the radar equipment, the top edges of the screens being at the lowest elevation compatible with adequate reduction of the ground clutter.

Measurements of the effect of such screens on the directional sensitivity pattern, described below, demonstrated a general agreement with the following theoretical treatment of diffraction using Sommerfeld's solution. The Sommerfeld formula for the diffraction of electromagnetic waves by a semi-infinite perfectly reflecting plane screen was applied to the two parallel edges of a screen of finite width.

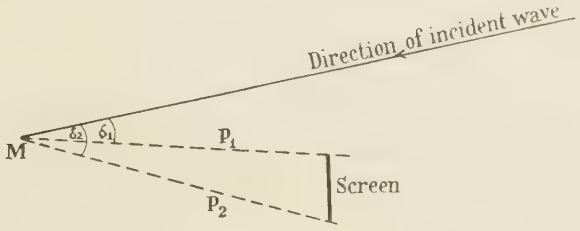

Figure 12. Diagram to illustrate calculation of diffraction effects.

We are here concerned with diffraction through small angles, and in this case, with the notation in figure 12, the received amplitude and phase angle of the wave at a point M, as compared with the value if no screen were present, are given by the complex amplitude

$$A=\frac{1}{\sqrt{2}}e^{\frac{-i\pi}{4}}\left\{\int_{-\infty}^{Z_1}e^{\frac{-i\pi}{2}v^2}\,dv+\int_{Z_2}^{+\infty}e^{\frac{-i\pi}{2}v^2}dv\right\},$$

where

$$Z_1=2\sin\frac{\delta_1}{2}\sqrt{\frac{2p_1}{\lambda}},\qquad Z_2=2\sin\frac{\delta_2}{2}\sqrt{\frac{2p_2}{\lambda}}.$$

The values of these integrals are readily obtainable from Cornu's Spiral.*

Since a paraboloid aerial system is used, and not a point aerial, the following artifice was adopted. Consider first a plane wave received by the paraboloid in free space. The received signal was derived from the wave at the circular aperture of the paraboloid by dividing the aperture into horizontal strips. Let S be the area of a strip expressed as a fraction of the whole aperture. The amplitude and phase of the wave received by the strip, compared with those obtained if the aperture was rotated about its centre so as to be parallel with the wave-front, may be expressed by $Se^{i\phi}$, where ϕ is the phase angle at the centre of the strip with respect to the phase at the centre of the paraboloid aperture. The resultant signal received is given by the complex summation for all the strips.

If now a screen is introduced in front of the aperture, the diffracted signal received by a strip becomes $ASe^{i\phi}$, where A is given by the diffraction formula above. A similar treatment may be carried out for the waves reflected from the ground. In the present case, where the screen is near the radar set, the only important ground reflexion is that which takes place from the ground on the far side of the screen. The resultant received signal, compared with the maximum free-space value, can then be determined by combining the contributions of all the strips for both direct and reflected waves with due regard to their relative phases. By the reciprocity theorem the same result applies for transmission as for reception. This method has been used, assuming flat ground with a reflexion

* For numerical values, see, for example, Jahnke and Emde's *Tables of Functions*.

coefficient of $-1{\cdot}0$ and arbitrarily choosing the number of strips as 5, to derive the theoretical echo strength for various elevations of a spherical reflector in terms of maximum free-space signal.

The experimental measurements with screens were made on Site I (figure 4), which was the flattest available site in the Richmond Park trials ground. It should be noted that a site of this type, with a natural crest at $2{\cdot}2°$ elevation, does not require wire netting to provide screening from the ground clutter. It was possible to demonstrate, however, a satisfactory agreement between experiment and theory by measurements at elevations above that of the natural crest. This is shown, for example, by figure 13, in which measurements and theoretical calculations are compared in the case of a screen of 4 m. vertical depth.

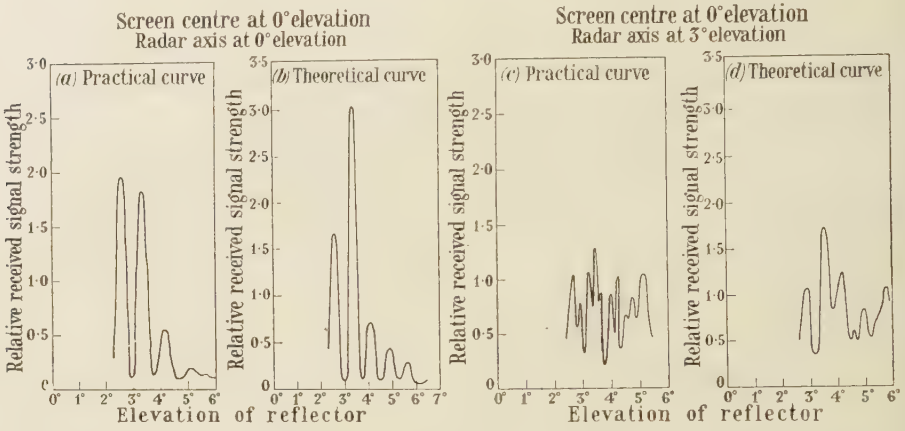

Figure 13. Directional sensitivity patterns showing diffraction effects with a 3-ft. screen.

The possibility of utilizing narrower screens to act as partial zone plates to enhance particular regions of elevation in the directional sensitivity pattern was also considered. In figure 14, theoretical and experimental curves are compared

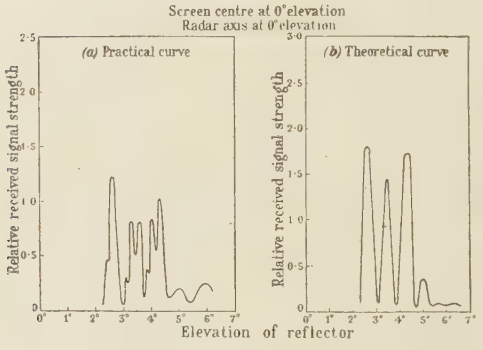

Figure 14. Directional sensitivity pattern showing diffraction effects with a $7\frac{1}{4}$-ft. screen.

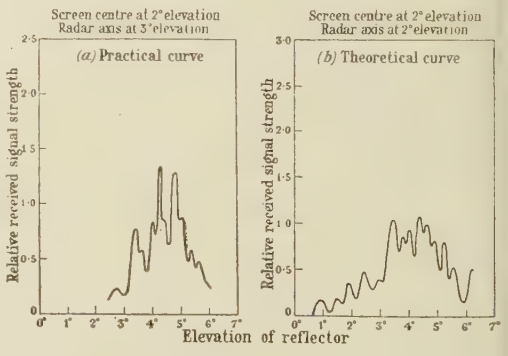

Figure 15. Directional sensitivity pattern showing diffraction effects with a 12-ft. screen.

for screens of vertical depth 1 m. in a position chosen on zone-plate principles so as to enhance the lobes from $2{\cdot}4°$ to $4{\cdot}4°$ elevation. Between these angles, the screen cuts off approximately the second Fresnel zone in the lower half of the direct wave

front and in the upper half of the reflected wave-front. In figure 15, the experimental and theoretical results are shown for a screen of 2·25 m. designed similarly to enhance the lobes between 3·7° and 5·8° elevation by cutting off the second, third and fourth zones. Again a general agreement in form between the measurements and theoretical expectations is apparent.

§ 6. CONCLUSIONS

The investigation described above has demonstrated a method for the determination of the directional sensitivity pattern in a vertical plane for radar equipment of centrimetic wave-length and has shown that the reflexion and diffraction effects can be predicted on many natural sites to a first approximation by simple theoretical considerations. The varying configuration and nature of the ground of natural sites is often such that precise measurements of magnitude and phase of the reflexion coefficients are of little practical value since a solution involving detailed variations would be too complex to solve. It is of practical interest therefore to see how well simple considerations can often give a satisfactory forecast of the directional sensitivity pattern.

The results in figures 5 to 10 suggest, by the depth of the minima and amplitude of the maxima, that the reflexion coefficients for rough pasture land for vertical polarization has a high value for the elevations considered, namely 0° to about 8°. It may be noted that the experiments of Ford and Oliver (1946) showed that, for vertical polarization, grass can give higher values of reflexion coefficient than does bare ground.

The wire-netting screen used in the diffraction experiments was far from opaque, as later experiments revealed. Nevertheless the experimental results show satisfactory general agreement with the simple application of diffraction theory for perfectly reflecting screens. It is also seen that practical realization of zone-plate effects may be obtained by suitable choice of screen dimensions.

§ 7. ACKNOWLEDGMENTS

The above investigation was carried out as part of the programme of the Operational Research Group, Ministry of Supply, J. T. G. Milne and G. S. Stewart taking part in the early experimental investigations with wire-netting screens. The authors are indebted to the Chief Scientist, Ministry of Supply, for permission to publish this communication.

REFERENCE

Ford and Oliver, 1946. *Proc. Phys. Soc.*, **58**, 265.

RADAR OBSERVATIONS OF METEORS

By J. S. HEY and G. S. STEWART,
Ministry of Supply

Read 31 *January* 1947 ; *MS. received* 6 *March* 1947

ABSTRACT. (i) An investigation of short-duration radio echoes observed at 4 to 5 metres wavelength in the neighbourhood of the E region of the ionosphere is described. Observations by vertical beam radio equipments showed that the echoes occurred most frequently at a height of about 95 km. Marked directional characteristics were revealed by the use of equipments with oblique beams, the diurnal variations being different on different bearings.

(ii) Analysis of the results has indicated the close link in characteristics of these echoes and meteors, and has thus confirmed the suggestion of meteoric origin which has been made by some previous workers. A detailed correlation is demonstrated in the present investigation and a method is described for the determination of the radiants of the most active meteor streams. Further, a determination of geocentric velocities was made possible by the introduction of improved photographic techniques for the observation of the Giacobinid meteor shower in October 1946.

§ 1. INTRODUCTION

Since October 1944 we have used Army radar equipment operating on a wavelength of about 5 metres to investigate the transient ionospheric echoes obtained at heights around 100 km. The general occurrence of these short-duration echoes at frequencies exceeding the critical frequencies for either the normal or abnormal E layers was noted by Appleton, Naismith and Ingram (1937) during their Polar Year observations of 1932–33. Schafer and Goodall (1932), who worked in collaboration with Skellett (1932) in an investigation of meteors as a source of abnormal E-region ionization, also recorded them as a specific feature of the 1931 Leonid shower. Skellett (1935) was able to show that in certain cases sudden increases in abnormal E-layer ionization coincided with the passage of visible meteors. Further, Skellett (1938) considered that Eckersley's observations (1937) of the characteristics of the transient echoes indicated the ionization produced by the passage of meteors through the upper atmosphere as the origin of these echoes. Subsequent investigations of the echoes were made by Appleton and Piddington (1938), who determined the range distribution and reflexion coefficients, and Eckersley (1940), who analysed the durations and made some observations of the diurnal variation in rate of occurrence of the echoes. Eckersley and Farmer (1945) have recently made detailed measurements of the polarization and direction of the reflexions received; they thought that their results did not conform with the meteoric hypothesis. Appleton (1945), however, in his Kelvin Lecture, considered that the evidence so far available had strongly suggested the meteoric origin.

The developments in radar techniques which have taken place during the war have made it possible for more exact determinations of some of the characteristics of these transient echoes. We have recently published (1946) a brief description of some of the results of our investigations at wavelengths between

4 m. and 7 m. Ferrell (1946) indicates that measurements are also being made in America on wavelengths of this order. Such wavelengths are considerably shorter than those used in the early work to which reference has been made above. Our investigations, which are here described in detail, provided conclusive proof of the meteoric origin of the echoes by a comparative study of their characteristics and the properties of meteors. The influence of the orientation of the meteor trail * in determining whether or not a reflexion may be obtained from it was first pointed out by Pierce (1938, 1941) and has been found to be a factor of particular importance in the interpretation of our results.

§ 2. INITIAL OBSERVATIONS, OCTOBER–NOVEMBER 1944

Transient ionospheric echoes were observed at wavelengths of 4 to 5 metres on certain long-range Army radar equipments with elevated beams during the latter of part 1944.† A chain of 12 of these radar sets was deployed by A.A. Command, and the authors were directly concerned in an advisory capacity, both in the planning of the system and the investigation of its operational performance. The transmitters each radiated approximately 500 pulses per second with a pulse duration of about 3 microsecs. and a peak power of 150 kw. The aerial systems provided elevated beams with axes around 45° to 55° elevation, some of the equipments having stacks of four dipoles and others single Yagi aerials. The receiver time base was extended to 140 km. and the characteristics of all echoes exceeding 2 seconds in duration were noted by direct visual observation of the cathode-ray tube display.

An analysis of the transient ionospheric echoes recorded between 16 October and 19 November 1944 was made by E. B. Britton, who was working in collaboration with the authors. The analysis showed that of a total of 348 echoes the average duration was about 13 secs. The mean ratio of signal to noise was approximately 4, the peak values in amplitude appearing at the onset of the echo. The average initial range was about 124 km. Assuming the mean elevation of observation to be that of the maximum of the radio beam, the mean heights were calculated to be approximately 93 km. on first appearance and 91 km. on disappearance. The analysis also revealed the interesting feature that although there was a considerable overlap in the coverage of the stations it was rare for an echo to be observed simultaneously by more than one station. Further, a diurnal variation in frequency of occurrence was recorded, the maximum being around sunrise and the minimum after sunset.

§ 3. INVESTIGATIONS FROM JUNE 1945–JUNE 1946

The above series of observations was incidental to an operational watch maintained for other purposes. At the end of the war it became possible through the cooperation of A.A. Command to utilize their Army radar facilities for

* The terms " train ", " streak ", and " trail " have all been used by various writers, sometimes with slight distinctions in meaning (see, for example, Herschel (1911)). In this report we shall refer to the column of glowing gas formed by the passage of a meteor through the upper atmosphere as a " trail ".

† P. E. Pollard informs us that such echoes were observed at these wavelengths in 1937–8 during the development of Army Gun-laying Radar Equipment by the Ministry of Supply. It was not until 1944, however, when this type of equipment was modified to work at very long range, that the echoes were of practical significence in Army Radar operation.

experiments designed to elucidate more specifically the characteristics of these short echoes. To this end a watch was set up involving five radar stations, two with vertical radio beams at Aldeburgh and three with inclined radio beams at Richmond, Aldeburgh, and Walmer respectively. These stations were manned and organized by A.A. Command, while the authors were responsible for the scientific direction of the experiments and the analysis of results.

At the end of July 1945, A.A. Command were unable to continue to provide the personnel to man the five stations. Their participation ceased, therefore, except for some further valuable assistance in the reading of the photographically recorded films, and for a short trial in October with the vertical beam sets at Sheerness. The research was therefore continued on a more limited scale in Richmond Park by the authors, with assistance from other Operational Research Group personnel.

In the following account we begin by describing in chronological order the investigations with the vertical beam stations. During the first few months many important data were collected although no definite conclusion as to the cause of the echoes appeared warranted. The subsequent development of the investigation, however, revealed a significant correlation with meteors.

A. *Observations with two vertical beam equipments, June, July and October* 1945

During June, July, and part of October 1945, a comparison of performance was made for two equipments with beams directed vertically upwards. The polar diagrams showing the variation of radar signal power sensitivity with direction are given in figure 1. The purpose in having two stations was to compare their performance both with similar and varied conditions of operation. In the first

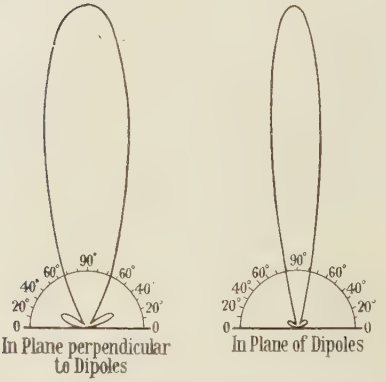

Figure 1. Polar diagram of radar signal power sensitivity. (Vertical-beam equipment A 1, A 2.)

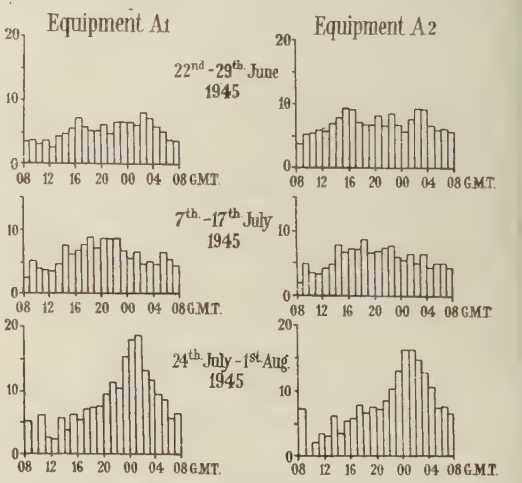

Figure 2. Diurnal variations in hourly rate of occurrence of echoes for vertical-beam equipments. Ordinate = mean hourly rate. Abscissa = time G.M.T.

few weeks they were operated independently at frequencies of 73 Mc./s. ($\lambda = 4{\cdot}1$ m.) and 55 Mc./s. ($\lambda = 5{\cdot}4$ m.); but subsequently both were maintained at 73 Mc./s. and the effects of varying polarization and of using a common transmitter instead of two independent ones were investigated.

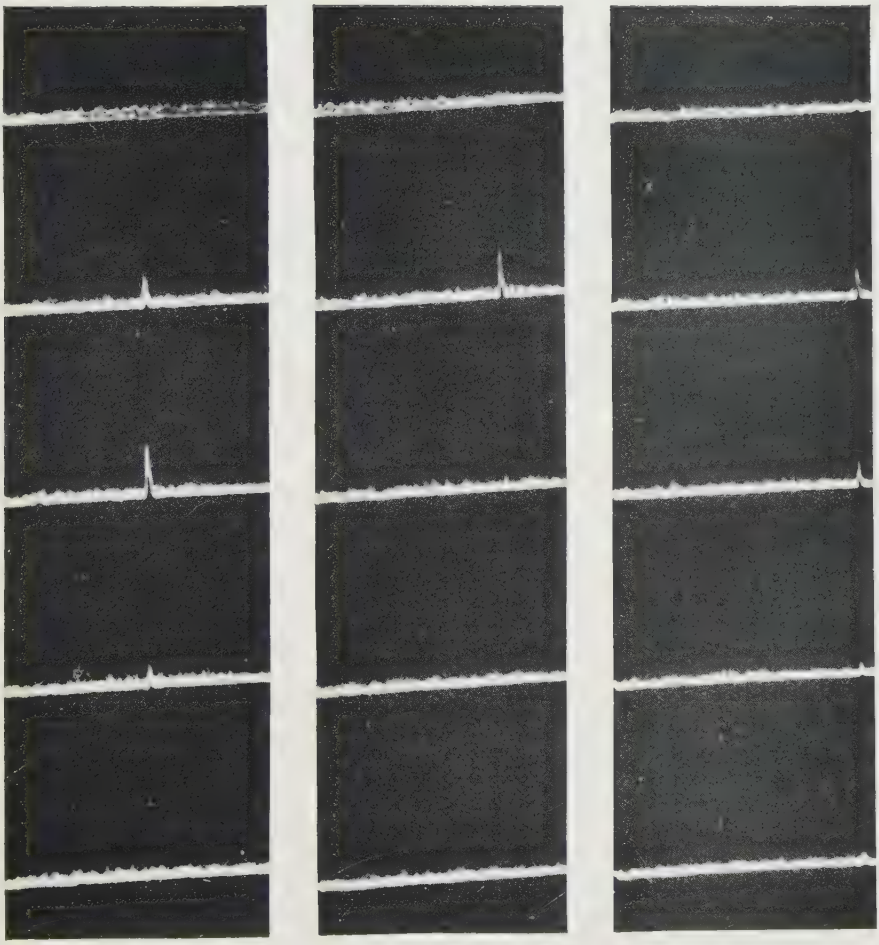

Plate 1.

Ciné photographs of transient ionospheric echoes presented as deflections of a linear range trace (abscissae, 80 to 125 km.); ciné speed—16 frames per second, sequence downwards.

To face page 860

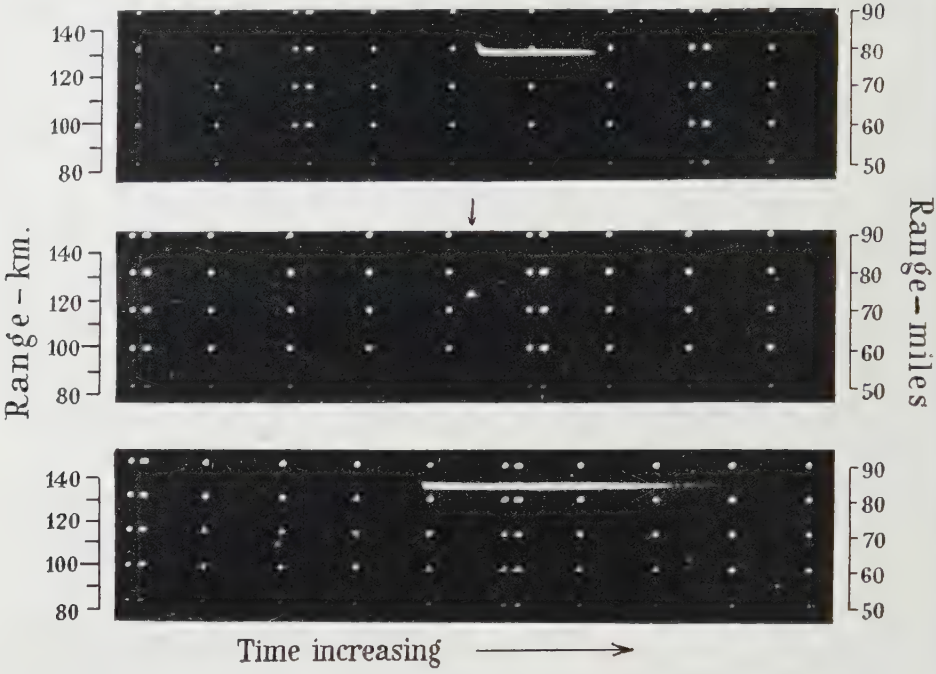

Plate 2.

Photographic records of transient ionospheric records presented as brightness modulation of range trace (ordinates, 80 to 140 km.) on continuously moving film. Range calibration marks appear at six-second intervals.

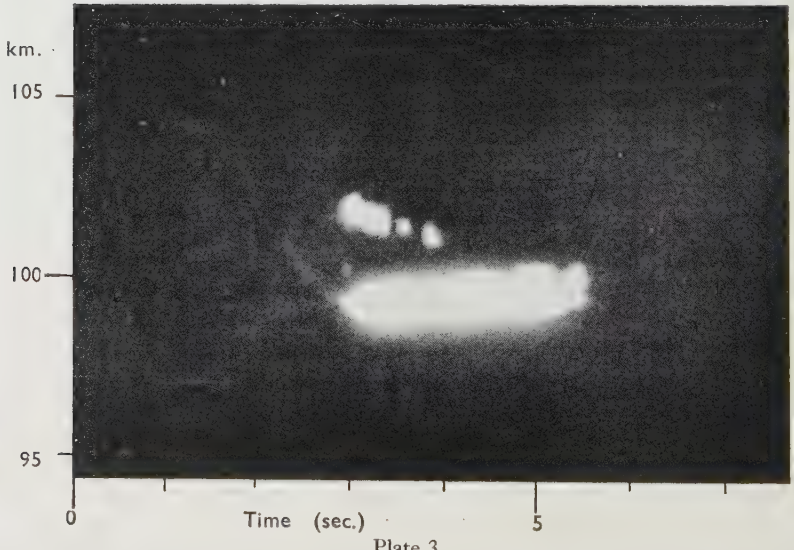

Plate 3.

Photographic record of a transient ionospheric echo during the Giacobinid meteor shower 1946.

A comparison was also made between visual recording of echoes displayed on the cathode-ray tube as deflections of a linear time base, and photographic recording of a brightness-modulated time base on a 16 mm. film moving at a speed of 0·5 mm. per sec. In the latter case, echoes were recorded on the film as spots if the echo duration was short, or as lines if the duration was long enough for the film to have moved appreciably. Ciné photographs of typical echoes presented as deflections on a linear time base, taken at 16 frames per second, are shown in plate 1. These illustrate the appearance of the time base to the operator making visual observations of the cathode-ray tube display. An example of an echo of very short duration is given in plate 1 (*b*) in which the echo can be seen during only one frame, and its duration must hence be about $\frac{1}{16}$ second, or less. Typical echoes obtained by photographic recording of the brightness modulated trace are shown in plate 2, which includes examples of echoes lasting several seconds.

We shall first consider the results for the three periods in table 1, for each of which the total number of echoes observed visually exceeded 1000. We refer to the two equipments as A 1 and A 2 respectively.

Table 1

Period	Details
22–29 June 1945	A 1 on 73 Mc./s., A 2 on 55 Mc./s. Visual recording.
7–17 July 1945	A 1 and A 2 on 73 Mc./s,, with common transmitter. Visual and photographic recording.
24 July–1 Aug. 1945	A 1 and A 2 on 73 Mc./s., with separate transmitters. Visual and photographic recording.

Graphs showing how the number of echoes per hour recorded visually varied with the time of day are given in figure 2 and the range distribution is shown in figure 3. These graphs demonstrate substantial agreement between the two stations, although the hourly rate for the 55 Mc./s. station, A 2, in the first period, is higher than that of the 73 Mc./s. station, A 1. Certain differences between the three periods are apparent in the mean diurnal variations of rate of occurrence, most particularly the pronounced peak in hourly rate which occurs around midnight in the third period; the interpretation of this peak is discussed later in this report (§ 4*c*). The range distributions show no marked changes for the three periods. Since the radio beam is fairly narrow with its axis vertical, these represent approximate height distributions; thus the height of the region in which the maximum number of echoes occur is around 97 km. for each period.

Despite the fact that the two sets were on the same site with almost identical radar coverage, and that the form of the results reveals general similarity, the number of simultaneous observations recorded visually at the two stations amounted to slightly under 50% of the echoes seen by either station. This is explicable by the fact that the greater number of echoes were of momentary duration and small signal strength. As an example, the ratio of numbers of

echoes of duration less than 1 second to those of greater duration was 3·4 : 1, while the ratio of the number of signals exceeding twice noise power to those exceeding four times noise power was 2·2 : 1. It is understandable therefore that observers might be especially liable to miss a proportion of echoes owing to the preponderance of echoes of short duration and small signal amplitude.

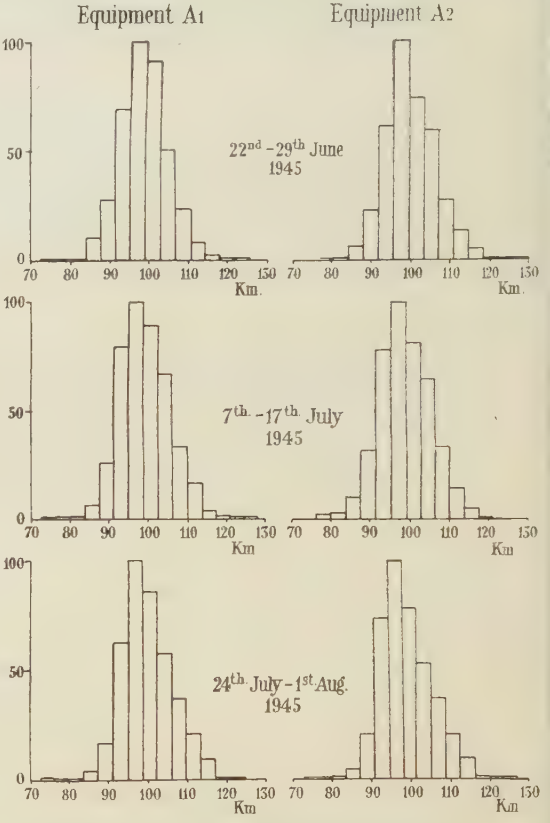

Figure 3. Range distribution of echoes for vertical-beam equipments.
Ordinate = relative number.
Abscissa = range.

Operation of the photographic recording of the brightness-modulated time-base was intermittent owing to technical faults, but the results indicated an increase of about 20% in the total number of echoes and a slight increase in the proportion of coincidences. The efficiency of this system depended on careful adjustment and stability in the setting of trace brightness and of receiver gain, these factors determining the noise level, which appears as a speckled background on the film. Imperfections in the recording apparatus prevented the coincidence rate from being greater, but it must be noted that the difficulties of recognizing small, short-duration echoes on a noise background are such that 100% coincidences can never be expected. With the knowledge of the earlier experiences, special precautions were taken during a few days of photographic recordings obtained at Sheerness in early October 1945, and the coincidence rate then rose to 85%.

In addition to the three periods of observation tabulated above, several experiments on polarization effects were undertaken for periods of one or two days. Although these tests covered such limited periods, the results indicated that there was no significant change when the plane of polarization was turned through 90°, from East–West to North–South. Further, when the polarization of a transmitter was at 90° to that of the receiver the number of echoes fell considerably, showing that the polarization of the echoed field tended to be the same as that transmitted.

B. *Observations with vertical beam equipment, December* 1945–*June* 1946

It was not practicable, owing to staffing problems, to continue the watch further until early December 1945. It was resumed at that date with a single

vertical beam station in Richmond Park, the plan being to investigate over a long period any correlation between frequency of occurrence of echoes and meteor showers. Owing to the limitations in available staff the watch was kept only between 0915–1200 hrs. and 1400–1630 hrs., G.M.T. daily; these daily observations were made over a period December 1945 to June 1946 inclusive. All recording was made by visual observation of the echoes on the cathode-ray tube. During the period April 20–22 inclusive, the time of the Lyrid shower, the watch was carried out at night together with a visual watch for meteors in the sky. Daily measurements of transmitter field strength and receiver sensitivity were made so as to exclude equipment performance as a possible variable affecting the observed rate of occurrence of echoes.

(i) *Record of mean hourly rate, December* 1945–*June* 1946. The correlations in hourly rate of occurrence of echoes with the main meteor showers during this period has been discussed in a previous publication by the authors (1946). It will suffice here to illustrate the results by figure 4, and to draw attention to the marked peaks in hourly echo rate corresponding to the Quadrantid meteor shower on 2—3 January, and the Lyrids, on 20–22 April. The correlation is

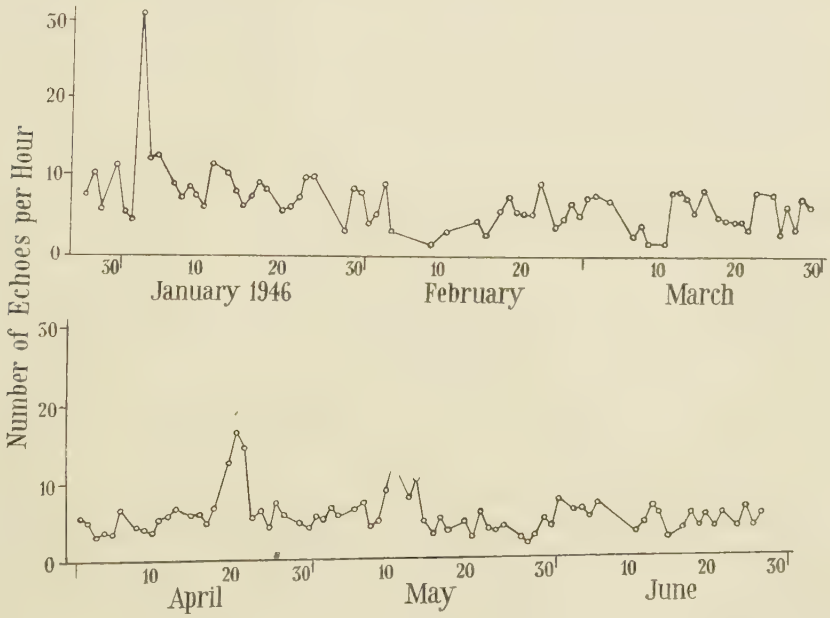

Figure 4. Mean hourly rate of occurrence of echoes. Vertical-beam station, Richmond Park.

shown in an even more striking manner by figure 5, in which the hourly rate of broad and multiple echoes is plotted. A prominent peak for a single day occurs at the time of the Quadrantid shower, while a marked broader peak with a maximum on 21 April occurs at the time of the Lyrids. This faithful reproduction of the meteor characteristics in the hourly rate of the transient echoes provided us with unmistakable evidence of the meteoric origin of at least a major proportion of these echoes.

(ii) *Simultaneous echo observation and visual meteor watch*, 20–22 *April* 1946. A direct visual watch for meteors in the sky during the time of the Lyrid shower

afforded further verification that the echoes are associated with meteors. These observations were made during 2030–2400 hrs. G.M.T. on each of the nights of 20–22 April. The sky was observed through a horizontal rectangular frame fixed vertically above the observer. The angular subtension of the frame roughly corresponded with the radar-beam coverage so that the field of view within the frame included most of the region in which a good radar response might be expected. It was possible to see a considerable region of the sky outside the rectangular frame although not to give it detailed attention. A celluloid sheet mounted in the frame and divided into zones enabled the apparent track of a meteor to be described approximately.

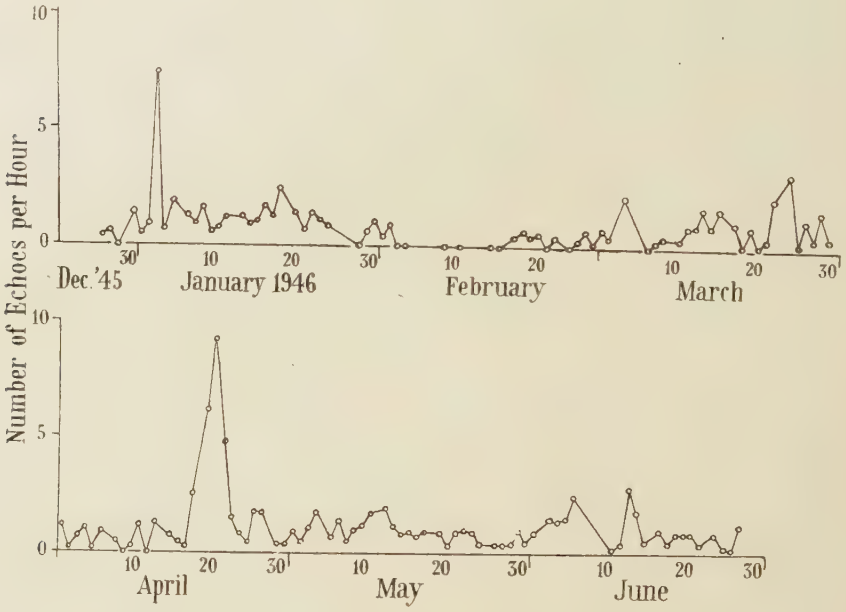

Figure 5. Mean hourly rate of occurrence of broad and multiple echoes. Vertical beam station, Richmond Park.

The sky was clear throughout the whole period of observation, with the exception of about twenty minutes on the second night when a filmy and broken patch of cirro-stratus entered the field of view, but this was not sufficiently dense to impair observation very seriously. The list of meteors, 13 in all, and particulars of the radar echoes, are given in table 2.

In table 2 there were 8 meteors whose tracks, produced if necessary, passed through the region of the viewing frame, and of these, 7 were associated with radar echoes. As to the remaining one, the observer stated that the track was extremely faint and he doubted whether he had genuinely seen a meteor. The visible tracks of three of the meteors which gave radar echoes were completely outside the frame, but in two cases the produced tracks passed through it.

We may conclude that certain meteors entering the radar coverage can definitely be associated with transient echoes. In addition to the radar echoes listed in the above table there were about seven times as many echoes with no meteors apparent in the sky. The existence of faint meteors which are observable

telescopically although not visible to the unaided eye is well-known to astronomers. It is further possible that ionization trails undetected even by telescopes may originate radar echoes. The large number of echoes with no apparent visible meteor is therefore a result to be expected.

Table 2

METEORS				RADAR ECHOES				
No.	Date in April 1946	Time (G.M.T.)	Tracks passing through frame	Time (G.M.T.)	Dur. (sec.)	Range (km.)	Signal Noise	Details of wide echoes
1	21	20.50.01	Yes	20.50.01	M	98	1½	—
2	21	20.59.20	Yes	20.59.20	3	121	Saturation	Beating 3 km. broad
3	21	21.57.00	No	No echo seen				
4	21	21.59.28	Yes	No echo seen				
5	21	22.27.51	Yes	22.27.53	M	112	1½	—
6	21	22.31.21	No	No echo seen				
7	21	22.32.39	Yes	22.32.40	1	113–116	1½	3 peaks moving outwards
8	21	23.39.43	Yes	23.39.51	M	98	1½	—
9	21	23.45.00	No	No echo seen				
10	22	22.08.03	Yes	22.08.05	¼	107	2	2 km. broad
11	22	22.23.34	No	No echo seen				
12	22	22.40.27	No	22.40.27	M	102	5	2 km. broad
13	22	23.31.48	Yes	23.31.51	M	106	2	—

(M = echoes of duration less than 1 second.)

C. *The meteoric hypothesis*

The most important outcome of the investigations described above was the conclusion that at least a large proportion of the ionospheric echoes are caused by meteors. Skellett (1932, 1938) first suggested that the ionization caused by meteoric impact with the molecules in the upper atmosphere was the probable source of both the abnormal E ionization and the short duration echoes. Trowbridge (1907) had pointed out earlier the similarity between the visible radiation from meteor trails, which may persist many minutes, and the afterglow produced by electrical discharge in gases, which thus suggested that ionization had occurred. In their theoretical work, Lindemann and Dobson (1923), Sparrow (1926), and Maris (1929) all agreed that ionization would result from the impact between meteors and the molecules of the upper atmosphere. We shall now proceed to review our experimental data, formulating the ionospheric scatter echo characteristics more precisely and discussing in further detail the extent to which their properties conform to the meteoric explanation.

D. *Signal strength distribution*

We will first consider the distribution of signal strengths of the echoes. This is needed in taking the finite beam width into account to calculate the true heights from the apparent heights. Further, the distribution of equivalent echoing areas * is of interest for any determination of the density of ionization produced, although this subject is not pursued in the present paper.

The operator estimates the maximum amplitude reached by the echo pulse seen on the cathode-ray tube face. This maximum appears to be attained

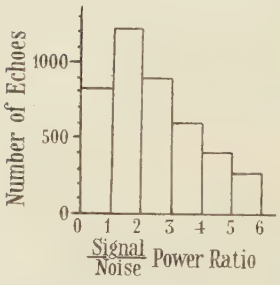

Figure 6. Observed echo power distribution, vertical-beam station A 2, June and July 1945. Note:—No experimental measurements above S/N=6.

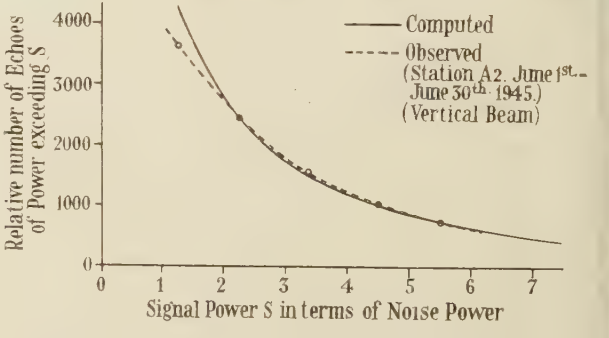

Figure 7. Comparison of computed and observed forms of distribution of echo powers; assumed mean equivalent echoing area :—430 square metres.

rapidly on first appearance. The receiver display is known to give approximate proportionality between echo height and the peak echo power. Figure 6 shows the observed distribution of echo powers in relation to the noise level. Owing to the liability of error in the operator's estimation of very low signal amplitudes,

* The equivalent echoing area A of an echo source may be defined by the relation:

Echoed power flux at distance $r = \frac{A}{4\pi r^2} \times$ incident power flux.

we have considered only the cases where the ratio of signal power to mean noise power exceeds $1\frac{1}{4}$, and have therefore taken this as our lower limit of observation. The true distribution of echoing areas is modified, as regards the received power distribution, by the form of the radar beam, in which the sensitivity decreases progressively in regions further and further from the axis.

It was found that a reasonable agreement with the observed signal strength distribution could be obtained by assuming that the elementary probability δp that an echo will have a (maximum) equivalent echoing area between the limits A and $A+\delta A$ is of the form

$$\delta p = Ce^{-A/K} . \delta A,$$

where C and K are constants.

Since $\int_{A=0}^{A=\infty} dp = 1$, we derive at once that $C = 1/K$.

Further, the mean echoing area $\bar{A}$ is given by

$$\bar{A} = \int_{A=0}^{A=\infty} A . dp = \int_0 \frac{A}{K} . e^{-A/K} . dA = K,$$

whence we may write

$$\delta p = \frac{1}{\bar{A}} e^{-A/\bar{A}} . \delta A.$$

From the foregoing it may readily be shown that of a large number N of echoing sources, the number with echoing areas exceeding a chosen value A' would be

$$N . e^{-A'/\bar{A}} \quad \text{as} \quad N \to \infty.$$

The peak echo power received from a scattering source of equivalent echoing area A at a range R from the equipment is given by

$$S = \frac{P\lambda^2 G_T G_R}{64\pi^3 R^4} . A,$$

where P = peak power radiated, λ = wavelength, and G_T and G_R are respectively the power gains of the transmitting and receiving aerials in the direction of the scattering source.

Consider an elementary region of space of volume δv, such that the value of $G_T G_R / R^4$ remains sensibly constant throughout the region. Within this region, S is proportional to A, and the rate of appearance of echoes of power exceeding the lower limit S' will be proportional to

$$\delta v . e^{-A'/\bar{A}}$$
$$= \delta v . e^{-S'/\bar{S}},$$

where $\bar{S}$ is the mean signal power received from this region. For any given value of $\bar{A}$, and with a knowledge of the polar diagrams of the equipment and the transmitter power, we can derive the form of the variation of $S'/\bar{S}$ throughout space. By integration we may then determine the relative numbers of echoes exceeding given values of signal power.

We have performed the integration for the case of a station with a vertical beam, with the simplifying assumption that all the scattering sources occurred in a single thin layer at a height of 97 km. Comparing the theoretical results

with the distribution observed at the appropriate station (during June 1945), we find that the value of $\bar{A}$ which gives closest agreement is in the neighbourhood of 430 m². The agreement between the observed distribution of echo powers and that computed by the above method is shown in figure 7.

It is to be emphasized that the choice of an exponential form of distribution is based purely on empirical grounds; also that the estimate of 430 m² as a mean equivalent echoing area only applies to a frequency of 73 Mc./s. ($\lambda = 4{\cdot}1$ m.). On account of the meteoric origin of the scattering sources, it is probable that the value of $\bar{A}$ will vary with the incidence of meteor streams of differing densities and velocities.

E. *Height distribution*

We have already seen in figure 3 that the range distribution of the echoes, as measured by the vertical stations, remained substantially the same for three separate periods during June and July 1945. Figure 8 shows the range distribution, analysed in 4 km. range bands, of all echoes observed in June and July 1945 by the vertical beam stations A 1 and A 2. In order to convert the smoothed distribution into a true height distribution, we must allow for the spread in range which results from the finite width of the radar beam. Suppose, for example, all echoes occurred at a fixed height of 100 km. Owing to the width of the radar beam, the distribution would have an abrupt near edge and then trail as shown in figure 9. The following method, illustrated in figure 10, was adopted to correct this effect. The observed range distribution was taken as a first assumed true height distribution, which we will call distribution "B". When the effect of the finite beam is applied we obtain a new distribution, "C". A distribution "A", determined by $AC = B^2$, was then deduced and used as the new assumed distribution for continuing the method by successive approximations. The solution obtained is shown in figure 11, the maximum being about 95 km., and 90% of all echoes being contained in a layer extending from 87·5 to 107·5 km. This corresponds well with the normal observed heights of meteors and their trains. Denning (1898) concluded that, in general, meteors appear at about 76 miles (approx. 122 km.) and disappear at about 51 miles (approx. 82 km.).

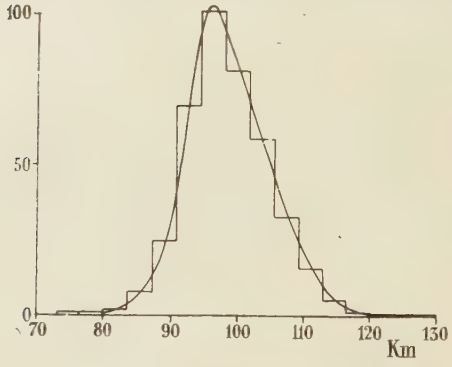

Figure 8. Mean range distribution of echoes for vertical-beam stations. June and July 1945.
Ordinate = relative number.
Abscissa = range.

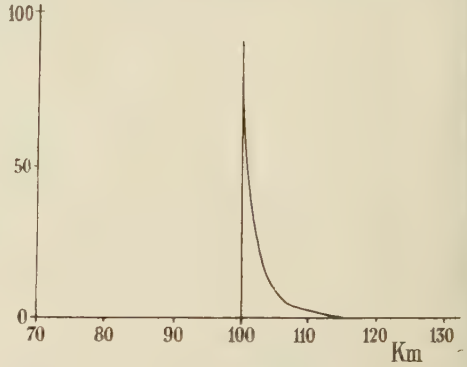

Figure 9. Range distribution of echoes from a thin layer at 100 km. height showing effect of radar beam width.
Ordinate = relative number.
Abscissa = range.

Trowbridge (1907) computed that the mean height of trains was 87 km., the limits for appearance and disappearance being 103 km. and 70 km. respectively. In more recent analyses of available data, Olivier (1942) deduced an average first height for night meteor trains as 102 km. and the end height as 74 km.; while Porter (1944) has given the mean heights for the beginning and end of the observed paths for sporadic meteors as approximately 103 km. and 86 km. respectively, although he also shows that there is a clear dependence of height on the elongation (the angular distance between the meteoric radiant and the apex of the earth's way) which determines the geocentric velocity.

It has been known from the earliest observations of the transient ionospheric echoes that they are roughly situated in the E region of the ionosphere. It is therefore of interest to consider to what extent the region of most frequent

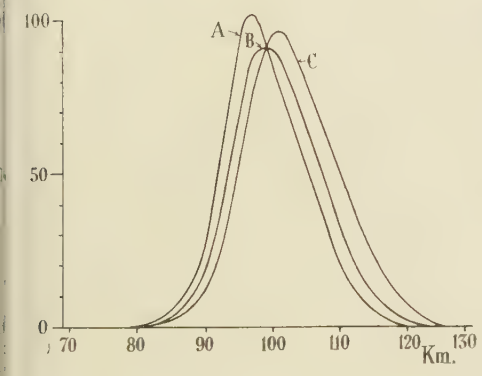

Figure 10. Illustrating method of deriving height distribution.
Ordinate = relative number.
Abscissa = range.

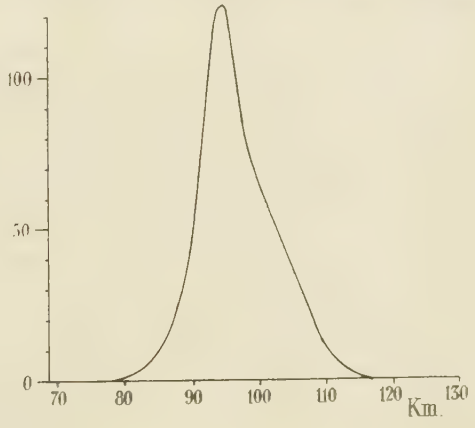

Figure 11. Mean height distribution of echoes for June and July 1945.
Ordinate = relative number.
Abscissa = range.

occurrence of echoes is related to the normal or abnormal E layers. Now, Appleton and Naismith (1940) found that the mean heights of the maximum ionization level for the normal E were 120 and 134 km. for summer and winter, while for the abnormal E they were 113 and 130 km. Since the region of maximum frequency of occurrence of the transient echoes is around 95 km. we conclude at once that it does not coincide in height with the maximum of either E layer. We may thus consider the region as a separate one and we refer to it as the *meteoric layer*. It will be seen that the shape of the height curve (figure 11) is similar to that of a Chapman region, which might be expected even for ionization produced by an external agency of this nature although the ionization is only of transient duration.

It is of interest to determine whether the range distributions are the same for transient ionospheric echoes of different characteristics in duration or complexity. In figure 12 the range distribution for momentary echoes (duration less than $\frac{1}{2}$ sec.), is compared with that of echoes of longer duration, and that for echoes of complex appearance with that for single echoes. In both cases we see that longer duration echoes and complex ones show a range coverage extending to slightly greater heights. Variations in meteors, such as size, velocity and fragmentation,

are assumed to be the controlling factors. Meteors of greater speed might be expected to produce ionization at greater heights where the rate of ionic recombination is slower due to reduced pressure and the echo consequently of longer duration. It does not appear justifiable to postulate origins of a different

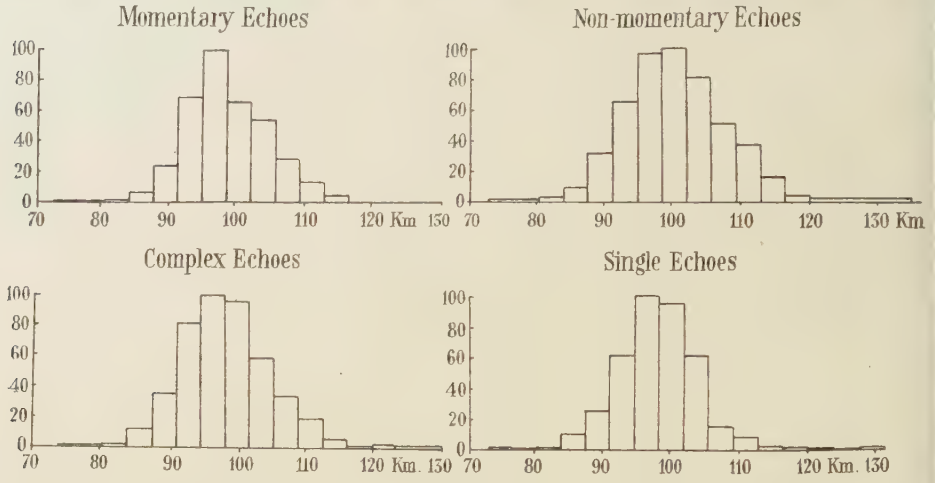

Figure 12. Range distributions of numbers of echoes of different characteristics. Vertical-beam station, June and July 1945. Ordinate = relative number. Abscissa = range.

nature according to the echo characteristics, particularly as the differences in range distribution are small. Further support for this view is afforded by the determination of correlation coefficients for the entities in table 3 :—

Table 3

Entities		Period for analysis	Correlation coefficient
a Momentary echoes	*b* Longer duration echoes	30 days, by days	0·67
Single echoes	Complex echoes (multiple or broad)	30 days, by days	0·56
(No correlation was found between complex echoes and long duration echoes)			

Although the height distribution was essentially constant for three separate periods during June and July 1945, a small diurnal variation is discernible. The average range corresponding to the maximum frequency of occurrence of echoes has been plotted for each hour of the day in figure 13. This shows a diurnal variation of approximately 3 km., the maximum height being reached shortly after noon. The average rate of decrease of height which occurs from this time until after midnight is of the same order as that observed by Öpik (1937) from visual observation of night meteor trails, namely 0·3 km. per hour.

In order to investigate any seasonal variations of height we have plotted in figure 14 the mean range distribution for the vertical beam stations showing

four successive periods between December 1945 and June 1946. There are some changes both in the width of the distribution and the height of maximum frequency of occurrence, in particular the period 1 February–30 March being characterized by a reduction in the tail of the distribution corresponding to echoes

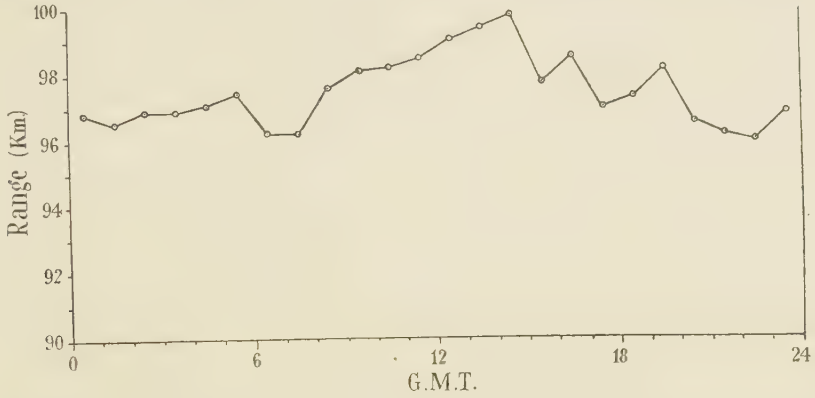

Figure 13. Diurnal variation in range of region of maximum density of echoes. Average of results for vertical-beam stations during June and July 1945.

at the greater heights. This shows an agreement with visual meteor observations by Öpik (1937), who stated that there is a seasonal variation in height with a minimum near 1 March. It should be noted that Porter (1944) has shown

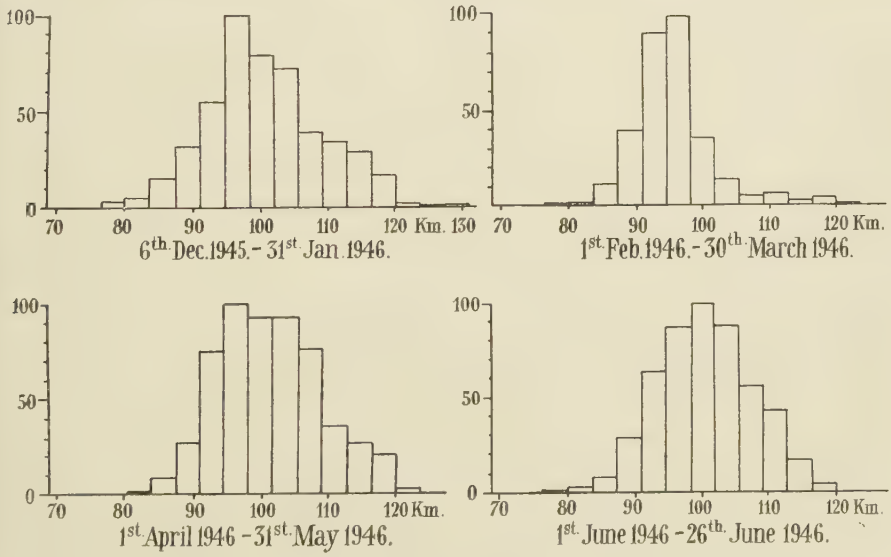

Figure 14. Seasonal variations in range distribution of echoes for vertical-beam stations.

Ordinate = relative number. Abscissa = range.

that variations in meteor heights are not seasonal in the sense of being dependent on geophysical seasonal variations but are explicable in terms of the changes in average elongation which occur as the Earth moves along its annual orbit.

F. *Motion of scatter echoes*

The majority of the echoes appear stationary in range; approximately 2% of all echoes show a movement. Any change is most clearly detected in the case of the long duration echoes; 15% of echoes of duration exceeding 1 sec. show a movement, and the mean can be deduced with reasonable accuracy. These results are illustrated in figure 15, and the biggest group lies in the velocity interval between 0 and −5 km. per sec. The velocities are not, in general, sufficient for the movement to be explained by the velocity of the meteor itself. If the ionized column produced by the meteor is the source of the echo we should expect the maximum echo from the broadside-on view, and if the trail size remained constant and its position did not drift, the range would remain constant. One cause of the average reduction of range may well be the lateral expansion of the ionized column. Trowbridge (1907) noted that the average rate of diffusion appeared to be about 0·002 km. per sec. for periods of observation of the order of 10 minutes, but the rates were considered to be much greater immediately after formation of the trail. If the rates in the first few seconds are of the order of 1000 times greater this effect might account for the trend towards reduced range.

Drifts and distortion of the trail present another factor which can cause range movements. Visual observations by Olivier (1933, 1942) and others, have demonstrated that the winds in different strata show both different velocities and different directions. These velocities are generally of the order of 0·05 km. per sec., but the apparent rate of movement resulting from the shifting of the point of reflexion on the distorted train might be much greater. In this connexion we may refer to Eckersley and Farmer (1945) who considered the meteoric explanation unlikely from their observations that when a transient ionspheric echo is produced, a "mirror" type reflexion occurs, while after a few seconds there appears to be a number of widely spaced centres. This result, however, might well be expected from meteor trails, which are at first comparatively straight and then become distorted. The detailed description by Porter and Prentice (1939) of a long enduring trail may be taken as an example. The trail first appeared as a straight line of light but in a few seconds it was deformed and subsequently rotated through nearly 100°.

The observation of "whistles" in receivers tuned to carriers of short wave transmitters was made by Chamanlal and Venkataraman (1941), who reported some coincidence with visually observed meteors. These "whistles" were assumed to be due to the Doppler effect arising from the relative movement of the meteor itself. This apparent discrepancy with our pulse reflexion observations indicating that the majority of echoes seen show little or no range movement, and our consequent assumption that the echoes are broadside reflexions from the trails, requires explanation. We can suggest tentatively the following possibilities: (*a*) the echo from the head of the ionized column may be more readily detectable around 7 Mc./s., the radio frequency of the Indian observations, than at our radio frequency of about 70 Mc./s., and a continuous note presented aurally in any case provides a more sensitive means of detection than the visual presentation of a pulse on a cathode-ray tube; (*b*) the meteoric "whistles" may be, in fact, caused by the lateral expansion of the meteor trail; (*c*) that some of our observations of echoes moving in range

(see figure 15) represent actual movement of the head of the ionized column, but that in general such echoes are missed in comparison with the stronger and more enduring reflexions from the column viewed from the side.

Chamanlal and Venkataraman found that E-layer returns were obtained by pulse reflexion methods on 7 Mc./s. immediately after the passage of a meteor as indicated by a whistle in a receiver tuned to a C.W. transmitter on a slightly different frequency. They considered this to be explained by the settling into a stratified layer of the ionization produced by the passage of the meteor. On a few occasions only they noticed a weak pulse-return with rapidly decreasing range occurring simultaneously with a strong Doppler whistle. In our view the most likely explanation is that the ionized air at the head of the meteor is

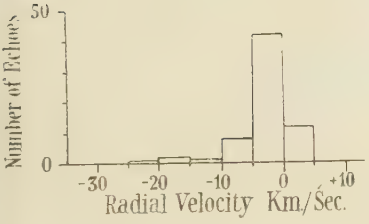

Figure 15. Distribution of radial velocity of moving echoes of duration exceeding $\frac{1}{2}$ sec.
(Vertical beam station, July 1945.)

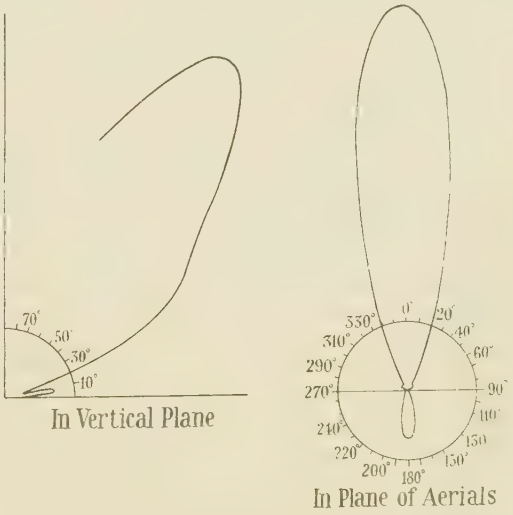

Figure 16. Polar diagram of radar signal power sensitivity.
(Inclined beam equipments, B_1, B_2, B_3.)

generally missed by pulse reflexion methods because of the weak amplitude of the echo, the C.W. method with aural presentation of the Doppler note being more sensitive; further, the subsequent stationary pulse reflexion echo is from the meteor trail which cannot appear until the train has reached approximately the point of intersection of the normal from the observing station to the line of travel of the meteor.*

§ 4. INVESTIGATIONS WITH INCLINED RADIO BEAMS, JUNE–AUGUST 1945

In addition to the observations with vertical looking equipments, a number of experiments using equipments with inclined beams are described below. The equipments had single Yagis for the transmitting aerials and twin Yagis for reception. The combined polar diagram of radar signal power sensitivity is shown in figure 16, the maximum occurring at approximately 55° elevation.

* The above suggestion has since received confirmation in recordings with improved photographic techniques during the Giacobinid meteor shower of October 1946. These results are in course of publication in the *Monthly Notices of the Royal Astronomical Society*, and are outlined briefly in § 5.

A. *Observations during the Perseid shower*, 1945

An attempt to determine specific changes in rate of echo occurrence at an inclined beam station during one of the more notable meteor showers was made during the Perseid shower of August 1945. The equipment was sited in Richmond Park, and the watch was carried out daily from August 10–14 incl. between 0930 and 1230 hrs. G.M.T., the expected peak of the shower being 11–12 August. The set was maintained on a 90° bearing throughout. The Perseid radiant is R.A. 48°, Decl. +58°, and as observed from Richmond Park, should move in bearing from 300° to 320° and in elevation from 60° to 40° during the time of the watch. From the polar diagram of the aerial sensitivity shown in figure 16, and the range limits of observation, in this case from 80 km. to 200 km., it was deduced that the beam of the set covered directions at right angles to the radiant during the period of the watch. The authors are indebted to B. Rimmington for his assistance in carrying out the photographic recording and subsequent reading of the film.

One of the most striking results which emerged was the increased duration of the echoes, as compared with those of the previous months. The number of echoes of long duration rose to a pronounced peak on 12 August, when 24% of the echoes persisted more than 5 sec. This may be compared with the last week of July when less than 2% of the echoes were of more than 5 sec. duration. The frequency of occurrence of the echoes reached its maximum on 11 August. These two results are represented graphically in figure 17, and for comparison

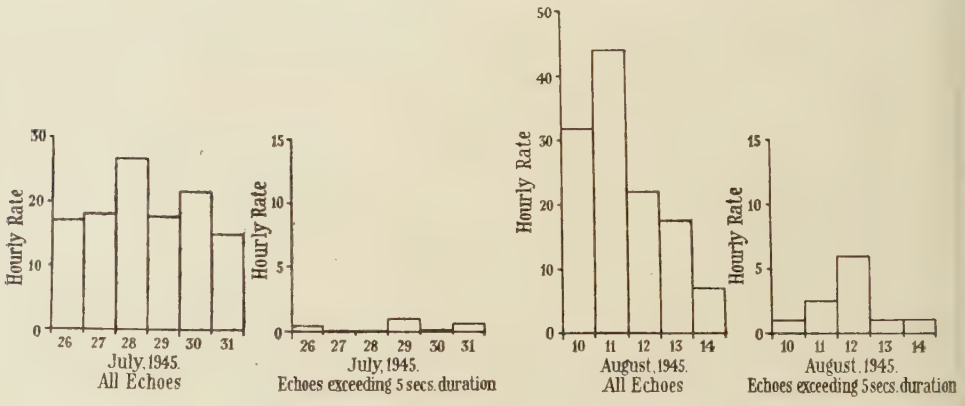

Figure 17. Hourly rate of occurrence of echoes.

we have included those obtained during 26–31 July for the same daily period, set bearing, and recording method. The peak in the frequency of occurrence of echoes of more than 5 sec. duration is particularly marked. Although no direct visual observation of the meteor shower was attempted, it is known that the Perseids appear with no remarkable variations in numbers practically every August. The stream begins to cut the earth about the middle of July, and the maximum may be expected on 11 August. Meteors are still very frequent for the following two nights, after which there is a sharp decline (see, for example, Olivier, 1925). The observations therefore correspond well with the known astronomical characteristics.

B. *Observations with three inclined beam stations, June–July* 1945

Three similar beam equipments, which we shall refer to as B 1, B 2, and B 3, sited at Aldeburgh, Walmer, and Richmond respectively, were maintained on continuous watch throughout June and July 1945. As previously mentioned, this investigation was made possible through A.A. Command, who supplied the operators and administrative organization. The bearings of the three stations were initially chosen so that the axes of the radio beams intersected at a point about 100 km. in height and approximately equidistant from each station. The system is illustrated in figure 18. The purpose of this experiment was firstly, to fix the location in space of echoes seen simultaneously by the three stations by the range measurements, and secondly, to investigate any aspect effects, that is, variation of reflected signal according to the direction of incidence of the radio waves. It was realized that both of these aims might not be fulfilled, since if aspect proved a critical factor the chances of simultaneous observation of echoes by the three stations would be diminished. In the latter part of July the three stations were set on other bearings in order to compare the results for several directions, the axes of the three beams in these cases no longer having a common point of intersection. Visual recording was used throughout, with some additional checking of results by photographic recording. All the equipments were operated on 73 Mc./s. The experiments and the results obtained, for three periods in table 4, will now be discussed.

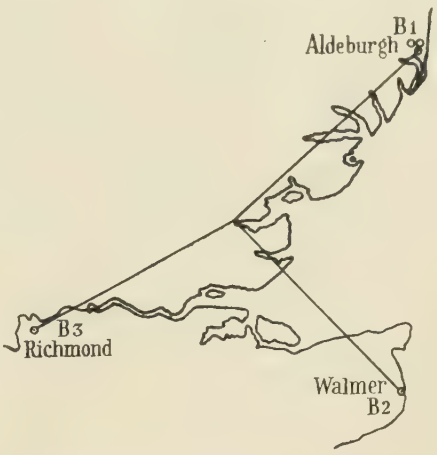

Figure 18. Equipments in operation, June and July 1945.

Table 4

Period	O.S. grid bearing of stations
1 June–17 July 1945	B 1, 230° ; B 2, 315° ; B 3, 62° (Beam axes intersecting)
17 July–26 July 1945	B 1, 180° ; B 2, 270° ; B 3, 90°
26 July–1 Aug. 1945	B 1, 180° ; B 2, 0° ; B 3, 90°

In comparison with the vertical beam stations it was found that the number of echoes had increased and the range distribution extended to greater ranges. These facts may be interpreted in terms of the greater area of the meteoric layer intercepted by the beams of the inclined beam equipments.

(i) *Aspect sensitivity of the echoes.* One of the most interesting features of the inclined-beam station results was presented by the marked diurnal variations in the frequency of occurrence of the echoes, the maxima and minima occurring

at different times for the three stations respectively (see figures 19 and 21). This indicates at once that the sources of reflexion show marked aspect effects which are more apparent with inclined beams than with vertical. Confirmatory evidence of the aspect sensitivity of the sources of reflexion was provided by the rarity of simultaneous echo observations by the three stations. In order to allow for lags in operator's recording, a time difference of up to 5 sec. was permitted in regarding echoes entered in the logs of the respective stations as simultaneous.

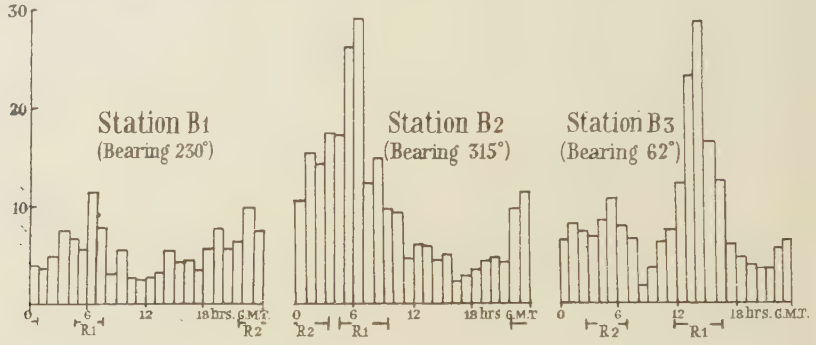

Figure 19. Diurnal variation of mean hourly rate of occurrence of echoes, 6 – 13 June 1945.
Time at which radiants R_1 and R_2 are favourable are indicated by heavy lines.
Ordinate = mean hourly rate.
Abscissa = time G.M.T.

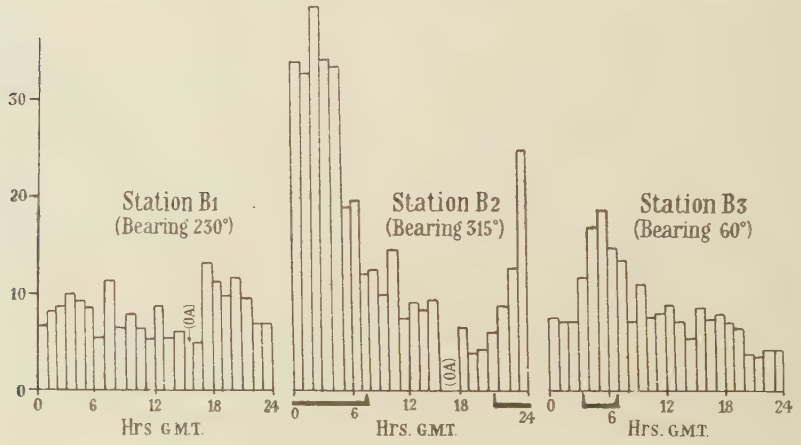

Figure 21. Diurnal variations of mean hourly rate of echoes, 26 July – 1 August 1945.
Times at which the variant R is favourable are indicated by heavy lines.
Ordinates = relative number.
Abscissa = time G.M.T.
O.A. = out of action.

Now, in the period 1 June to 17 July 1945, on only four occasions was this criterion satisfied out of an average of over two thousand echoes observed by each station when they were all in operation at the same time. If the stations are considered in pairs, the average percentage of incidents observed by two stations, with not more than 5 sec. interval between recorded times, was approximately 3% of the total number of echoes seen by one station. In order to appreciate the theoretical chances of such coincidences, we must consider the extent of

overlapping coverage. The probability of coincidence in different cases has been calculated assuming isotropic scattering sources in a single thin layer at 97 km. height, and an echo strength distribution as observed by the vertical beam stations (see § 3 D). The percentage coincidences calculated on this basis are compared below with the observed results for visual recordings.

Triple coincidences for B 1, B 2, B 3:—

Calculated probability = 3·1% of total number of echoes seen by all stations.

Observed coincidences = 0·003%.

Double coincidences for B 1 and B 3:—

Calculated probability = 10·5% of total number of echoes seen by both stations.

Observed coincidences = 1·6%.

Thus we see that even if we multiply the observed coincidences by a factor of 4 in the case of double coincidences and of 12 in the case of triple coincidences in order to allow for a 50% chance of an echo being missed by any one station, the calculated probability, based on the assumption of isotropic scattering sources, is greater than the observed probability. We may therefore conclude that the echoes show differential effects according to the direction of observation. This is further borne out by the coincidence percentage observed between B 1, the oblique beam station at Aldeburgh, and the vertical beam station A 1 (or A 2), situated on the same site. If the echoing sources are sensitive to the direction of incidence, then the probability of coincidence between B 1 and A 1 (or A 2) might be increased over that calculated on the basis of isotropic sources. This is actually the case as shown by the following figures.

Double coincidences for B 1, and A 1 (or A 2):—

Calculated probability = 1·2% of all the echoes seen by both stations.

(This figure is more liable to error than those quoted above owing to incomplete knowledge of the beam of the inclined station in the vertical direction.)

Observed coincidence = 3%.

This difference is accentuated by allowing for visual echoes missed. We conclude therefore that both the reduction of coincidences for stations on separated sites but with intersecting beams, and the increase for stations on the same site with partial overlap of coverage, as compared with the calculated values, accord with the assumption that the echo sources are sensitive to aspect.

(ii) *Meteoric explanation of aspect effects.* In terms of the meteoric explanation of the origin of the transient ionospheric echoes, the aspect effects are readily explicable. In discussing the range movements of the echoes we have already associated the main echoes with reflexions obtained by viewing the meteor trails along their normals. Pierce (1938, 1941) emphasized that meteor trails should, for radio waves, give specular reflexions appropriate to a reflecting cylinder. The maximum echoing area would therefore occur for a direction of incidence at right angles to the axis of the trail. We thus have at once the reason why the ranges of echoes generally remain nearly constant, namely that the ionized column is usually only sufficiently reflecting to be observable when viewed along the normal. The inability to obtain simultaneous

observations of an echo by viewing the same region from different directions is at once explained. Further, the diurnal variations would be expected from the daily cycle of changes in bearing and elevation of the meteor radiants active at the time.

C. *Determination of meteor radiants*

As we pointed out above, the diurnal variations in frequency of occurrence of the echoes for the oblique stations according to their direction of look may be explained in terms of aspect sensitivity of the echoing source, the main echoes occurring when the trails are viewed along their normals. In this case it should be possible from the time of occurrence of the peaks in the diurnal variation to make some inference about the main directions of travel of the meteor streams and hence their radiants. Olivier (1925) has demonstrated that minor radiants exist in very great numbers scattered all over the visible heavens, and that any radiant is not worthy of consideration if it rests on observations of more than a few days. With these facts in mind we have chosen for analysis several periods of not more than one week, and have attempted to deduce only those radiants which might account for the main peaks in the diurnal variations.

We shall consider first the week 6–13 June 1945. The mean of the hourly rate for the three stations, B 1, B 2, and B 3, on bearings 230°, 315° and 62° respectively, are shown in figure 19. We note that the main peaks occur, for B 1 and B 2 at about 0630 hrs., and for B 3 at about 1430 hrs. In figure 20 we

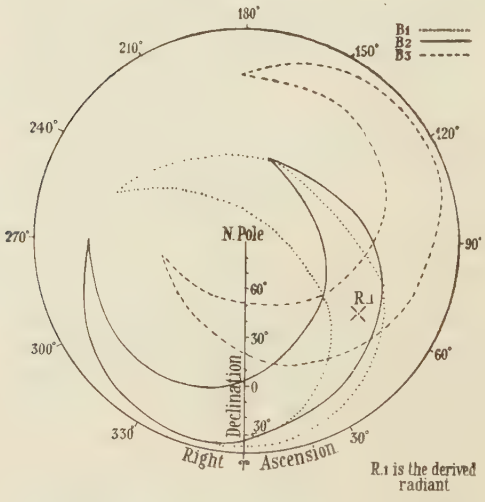

Figure 20. Coverage of possible radiant positions for main peaks in hourly rate of B 1, B 2, B 3.

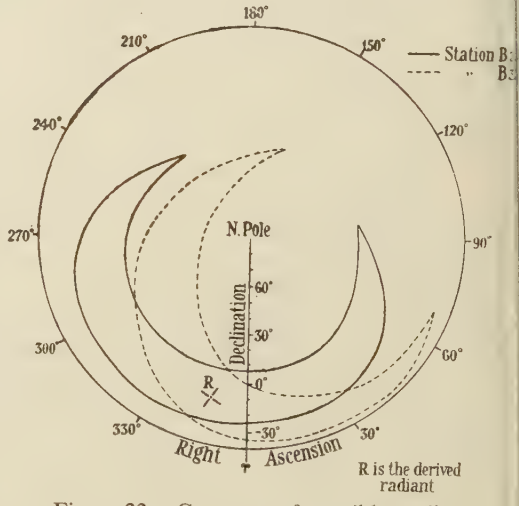

Figure 22. Coverage of possible radiant positions for main peaks in hourly rate of stations B 2 and B 3.

have drawn the coverage of possible radiant positions in the sky for each of these stations, at the time of their respective peak rates. It has been assumed that any possible radiants are at right angles to the radio beam. From a consideration of the beam characteristics and echo strength distribution the angular dimensions of the beam likely to contain 90% of the observed echoes were computed. The coverages shown in figure 20 represent possible directions at right angles to any part of this beam. We notice that the coverages for the peak hourly rate of

B 1, B 2, and B 3 all intersect in a common area, and we may assume this to contain the mean radiant, R 1. The position of this radiant appears to be within 10° of R.A. 58°, Decl. +5°. If we plot the secondary peaks in the hourly rate, namely at 2030 hrs. for B 1, and at 0530 hrs. for B 3, we can deduce by the same method a secondary radiant, R 2, within about 10° of R.A. 300°, Decl. −5°.

We must now verify that radiants in these positions give a satisfactory explanation of the observed hourly rate for both stations, and do not introduce any additional maxima to those which are observed. The times for which these radiants are within the station coverages may readily be determined graphically, the results being shown in table 5.

Table 5

Radiant	Site	Times for which radiant position is favourable (G.M.T.)
R 1 (R.A. 58° Decl. +5°)	B 1	0440–0730
	B 2	0430–0930
	B 3	1140–1640
R 2 (R.A. 300° Decl. −5°)	B 1	2130–0100
	B 2	2210–0310
	B 3	0240–0700

These periods have been marked below the time scale (abscissa) in figure 19 and they demonstrate that the radiants R 1 and R 2 give a satisfactory explanation of the times of the occurrence of the major and minor peaks for all three stations.

We shall next consider the diurnal variation of hourly rate for the period 26 July – 1 August, as shown in figure 21, and we shall here amplify the brief discussion of this case previously given by the authors (1946). The coverages of possible radiant positions corresponding to the marked peaks for B 2 at 0230 hrs., and B 3 at 0430 hrs., are shown in figure 22 and give a derived radiant in the neighbourhood of R.A. 345°, Decl. −10°. In figure 23 we have plotted the track of the radiant across the coverages, and marked the corresponding periods below the time scale for B 2 and B 3. The striking agreement is made even more remarkable by consideration of B 1 which exhibits a notably lower level of activity. As the coverage of this site never includes the radiant R in a favourable position, the absence of a marked peak in hourly rate is readily explained. The radiant R is plainly that of the δ Aquarids, a prominent stream of this epoch. The Perseid radiant may also be expected to have commenced activity towards the end of July. It can readily be shown that this radiant can only be viewed favourably by station B 1, between 1210–2320 hrs. G.M.T., and a small peak between these times is seen to occur.

In the above analysis we have not included a description of the effect of the radiants on the vertical beam station results. These stations give a ring type of

coverage for possible radiant positions (see figure 24), and in many cases radiants may cross the coverage twice. This corresponds to the rising and setting of the radiant in the sky. This double intersection tends to even out the diurnal variation of hourly rate, which is in accordance with observation, the diurnal variations being of much less prominence than for inclined beam stations. In the case of only one of the radiants derived above is the radiant position so placed.

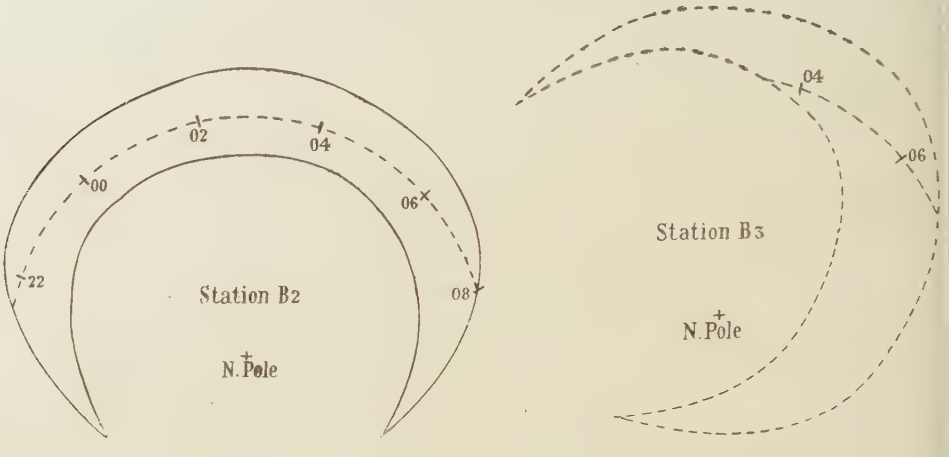

Figure 23. Tracks (dotted line) of meteor radiant R within coverages of stations B 2 and B 3. Time in hours G.M.T. marked on track.

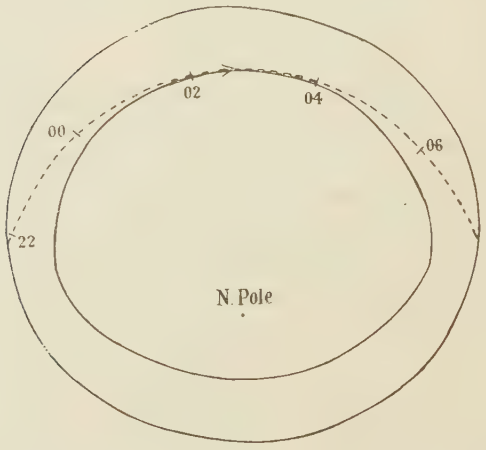

Figure 24. Track (dotted line) of meteor radiant within coverage of vertical beam stations A 1, A 1. Time in hours F.M.T. marked on track.

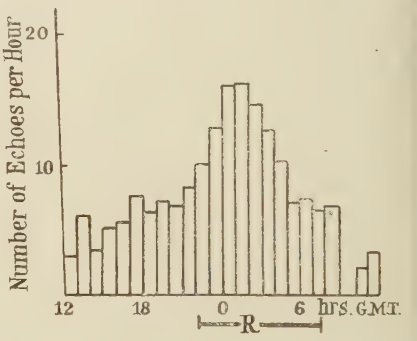

Figure 25. Diurnal variation of mean hourly rate of echoes for vertical beam station A 1. 26 July – 1 August 1945. Times for which radiant R is favourable are indicated by heavy lines.

that it remains within the coverage for the whole of the time between the rising and setting of the radiant. This is the δ Aquarid radiant, and its track with respect to the coverage of a vertical beam station (A 1 or A 2) is shown in figure 24. We should therefore expect, in this case, the vertical beam station to give a clear peak between 2100 and 0630 hrs.; comparison with figure 25 demonstrates

that this is the case, a more prominent peak being apparent for the vertical stations than at any other time in the June–July watch (see figure 2).

An accuracy in position of better than 10° cannot be claimed for the radiants determined above. Many other minor radiants must of course be active, but the width of the radio beams has not warranted any more detailed analysis at this stage. Further, there may be other factors which we are not in a position to assess as yet, such as the optimum angle of incidence of the meteor in the ionization layer for giving an effective radio response. Refinement of the method of observation by using narrower radio beams will undoubtedly lead to elucidation of these factors and to more accurate determination of radiants. An examination of the diurnal variations in rate of occurrence to determine whether there was any influence arising from the existing E-layer ionization yielded negative results. If such a variation exists, it is of a minor character at wavelengths of 5 metres in comparison with the major controlling factor, namely the direction of the radiant relative to that of the radio beam. This is not surprising since the wavelengths we have used are of the order of one-tenth the critical values for total reflexion from the E layers. As the critical wavelength is inversely proportional to the square of the electron density, we may infer that the electron densities giving rise to the transient echoes at 5 metres wavelength very greatly exceed those of the ionospheric E layer, and that existing ionization in this layer has little influence. A different result may well apply in transient echo observations at much longer wavelengths.

§ 5. THE GIACOBINID SHOWER OCTOBER 1946

An account of observations during this shower appears in a separate report by Hey, Parsons and Stewart,* and a brief outline of additional data and of certain points of importance to a general survey of the meteoric radar echoes will be given here. The rate of occurrence of the transient ionospheric echoes attained a remarkable peak between 0330 and 0400 hrs. G.M.T. on 10 October 1946, coinciding, as expected, with the maximum for visual observation of the shower as reported to us by J. P. M. Prentice. We found (§ 3, A) from observations during June 1945 that more echoes were observed at 55 Mc. s. ($\lambda = 5{\cdot}4$ m.) than on a similar equipment at 73 Mc. s. ($\lambda = 4{\cdot}1$ m.). The decrease in number of echoes observed as the radio frequency is increased had been noted by Appleton (1946). During the Giacobinid shower some observations were made at 212 Mc. s. ($\lambda = 1{\cdot}4$ m.) which is believed to be the highest frequency at which the meteoric echoes have been obtained. Between 0500 hrs. and 0545 hrs. G.M.T. on 10 October 1946, the number of echoes observed on the cathode-ray tube display of a 212 Mc. s. ($\lambda = 1{\cdot}4$ m.) equipment with vertically directed beam was seven as compared with about ten times that number on 64 Mc. s. ($\lambda = 4{\cdot}7$ m.) with a similar aerial system and power. A reduction in echoing area with increase of frequency is readily explicable in terms of gaseous ionization as the source of reflexion.

An important consequence of the introduction of improvements in resolution the of photographic recording method for the Giacobinid shower was the derivation of geocentric meteor velocities. On a 55 Mc. s. ($\lambda = 5{\cdot}4$ m.) equipment

* *Monthly Notices of the Royal Astronomical Society* (in publication).

wtih vertically directed beam, higher resolution was obtained by displaying a limited range band of 80 to 115 km. over the full width of the cathode-ray tube, and by using a 35-mm. film moving at 2·4 mm. per sec. instead of a 16-mm. film moving at 0·5 mm. per sec. Some of the recordings revealed a faint fast-moving echo prior to the main echo; an example is shown in plate 3, time 2·0–3·0 sec. This fits well with the views we expressed above (§ 3 F) in connexion with the Doppler whistles observed by Chamanlal and Venkataraman (1941), for we may associate the first faint trace with the ionization in the immediate vicinity of the approaching meteor. If we consider the meteor trail as a cylindrical column of ionized gas it is evident that the approaching head of the column, around the meteor itself, may originate a reflexion, although of smaller magnitude than the broadside echo from the column which occurs after the meteor has passed the point of minimum range. Similar weak echoes as the head of the meteor column recedes do not appear, presumably because whereas specular reflexion can occur from the rounded head of a cylindrical column as it approaches, only a diffracted echo of far smaller amplitude is possible as the head recedes. The secondary large echo shown in plate 3 may be due to distortion of the early part of the train resulting from drifts.

The faint tracks associated with the approaching meteor were mostly found to have range-time characteristics appropriate to uniform motion in a straight line, and the geocentric velocities could be determined from the formula

$$V=(R^2-R_0^2)^{1/2}/(T_0-T),$$

where V is the geocentric velocity, R the range at time T, and R_0 the minimum range at time T_0. The mean geocentric velocity derived from an analysis of 22 tracks was found to be 22·9 km./sec. which is in good agreement with the theoretically expected value of 23·7 km./sec. supplied to us by Dr. J. G. Porter. These results thus provided a further instance of the successful application of the radar methods to meteor observation.

§ 6. ACKNOWLEDGMENTS

We wish to acknowledge the valuable assistance placed at our disposal by the G.O.C. in C., A.A. Command, and we are indebted to Messrs. E. B. Britton, B. Rimmington and A. Sommi of the Operational Research Group, Ministry of Supply, for their help, and to all our assistants who took part in the subsequent analysis of results.

We wish to thank Sir Edward Appleton, F.R.S., and Mr. R. Naismith for supplying E-layer critical-frequency data and for helpful discussions, and to Mr. J. P. M. Prentice and Dr. J. G. Porter for their advice on meteor data.

Finally, we are indebted to the Chief Scientist, Ministry of Supply, and to the Superintendent of the Operational Research Group for their encouragement and interest in the investigations and for permission to publish this report.

REFERENCES

Appleton, E. V., 1945. *J. Instn. Elect. Engrs.*, **92**, I, 340.
Appleton, E. V., 1946. *J. Instn. Elect. Engrs.*, **93**, IIIA, 110.
Appleton E. V. and Naismith, R., 1940. *Proc. Phys. Soc.*, **52**, 402.
Appleton, E. V., Naismith, R. and Ingram, L. J., 1937. *Phil. Trans.*, A, **236**, 191.

Appleton, E. V. and Piddington, J. H., 1938. *Proc. Roy. Soc.*, A, **164**, 467.
Chamanlal and Venkataraman, 1941. *Electrotechnics*, **14**, 28.
Denning, W. F., 1898. *Nature, Lond.*, **57**, 540.
Eckersley, T. L., 1937. *Nature, Lond.*, **140**, 846.
Eckersley, T. L., 1940. *J. Instn. Elect. Engrs.*, **86**, 548.
Eckersley T. L. and Farmer, F. T., 1945. *Proc. Roy. Soc.*, A, **184**, 195.
Ferrell, O. P., 1946. *Phys. Rev.*, **69**, 32.
Herschel, A. S., 1911. *Observatory*, **438**, 291.
Hey, J. S. and Stewart, G. S., 1946. *Nature, Lond.*, **158**, 481.
Lindemann, F. A. and Dobson, G. M. B., 1923. *Proc. Roy. Soc.*, A, **102**, 411.
Maris, H. B., 1929. *Terr. Mag.*, **34**, 309.
Olivier, C. P., 1925. *Meteors.*
Olivier, C. P., 1933. *Proc. Amer. Phil. Soc.*, **72**, 215.
Olivier, C. P., 1942. *Proc. Amer. Phil. Soc.*, **85**, 93.
Öpik, E., 1937. *Harvard Annals*, **105**, 549.
Pierce, J. A., 1938. *Proc. Inst. Radio Engrs.*, **26**, 892.
Pierce, J. A., 1941. *Phys. Rev.*, **59**, 625.
Porter, J. G., 1944. *Mon. Not. R. Astr. Soc.*, **104**, 20.
Porter, J. G. and Prentice, J. P. M., 1939. *Brit. Astr. Assn. J.*, **49**, 337.
Schafer, J. P. and Goodall, W. M., 1932. *Proc. Inst. Radio Engrs.*, **20**, 1131 and 1941.
Skellett, A. M., 1932 *Proc. Inst. Radio Engrs.*, **20**, 1933.
Skellett, A. M., 1935. *Proc. Inst. Radio Engrs.*, **23**, 132.
Skellett, A. M., 1938. *Nature, Lond.*, **141**, 472.
Sparrow, C. M., 1926. *Astrophys. J.*, **63**, 90.
Trowbridge, C. C., 1907. *Astrophys. J.*, **26**, 114.

A STUDY OF THE NUCLEAR TRANSMUTATIONS OF LIGHT ELEMENTS BY THE PHOTOGRAPHIC METHOD

By C. M. G. LATTES, P. H. FOWLER and P. CUER,
H. H. Wills Physical Laboratory, University of Bristol

MS. received 2 *January* 1947

ABSTRACT. The photographic method has been employed in a study of the transmutation of lithium, beryllium, boron and oxygen by 900 kev. deuterons using the new Ilford Nuclear Research emulsion, type B1, for recording the tracks of the disintegration particles. The relation between the energy of a homogeneous group of particles and the mean range of the corresponding tracks in the emulsion has been determined both for α-particles and for protons. With protons, the mean stopping power of the emulsion, relative to standard air, varies from about 1800 at 2 Mev. to 2000 at 13 Mev. Curves showing the stopping power of the emulsion as a function of range are given for both protons and α-particles.

The experiments show that the uncertainty in the energy of an individual proton, as deduced from the length of the track which it produces in the emulsion, is only slightly greater than that due to straggling. In view of the very refined geometry which can be employed when using the photographic method, it follows that it can be applied in experiments of the highest precision.

The observations with a beryllium target give evidence for the existence of a group of particles, not previously observed, which we attribute to protons from the reaction ${}^{9}_{4}\mathrm{Be}+{}^{2}_{1}\mathrm{H}\rightarrow{}^{*10}_{4}\mathrm{Be}+{}^{1}_{1}\mathrm{H}$, in which the ${}^{10}_{4}\mathrm{Be}$ nucleus is formed in an excited state of energy $3{\cdot}40\pm0{\cdot}08$ Mev.

The difference in the appearance of the tracks of protons and α-particles in the B1 emulsion is sufficiently great to enable the two types to be distinguished by inspection. It is thus possible to make measurements on groups of protons in the presence of α-particles of the same range.

§ 1. INTRODUCTION

In a recent publication (Powell, Occhialini, Livesey and Chilton, 1946), which we shall refer to as (I), an account has been given of the prototype of new photographic emulsions for recording the tracks of fast charged particles from nuclear transformations. These emulsions are now being produced in the research laboratories of Ilford Ltd. and are described as *Nuclear Research Emulsions* (N.R.). The visibility of the tracks in the N.R. emulsions is greatly superior to that obtained with ordinary half-tone plates, and the previous work shows that the field of application of the photographic method is thus extended and its precision improved.

In this paper we describe experiments in which we have investigated the characteristics of the emulsion in more detail, giving particular attention to the following technical aspects of the method:—

(*a*) The range-energy relation for protons and α-particles in the emulsion.

(*b*) The energy "resolving power" of the method.

(*c*) The "discriminating power" of the emulsion.

In the case of the ordinary half-tone emulsion it has been shown (Powell, 1943; Guggenheimer, Heitler and Powell, 1946), that the length of the track of a proton ot an α-particle is proportional to its range in standard air for particles of all energies in the interval from 1 to 13 Mev. Owing to the much higher concentration of silver halide relative to gelatine, this simple relationship is not valid for the N.R. emulsions. It is therefore important to make experiments to determine the range-energy relation for the different particles so that the distribution in length of the tracks measured in any experiment may be transformed to a distribution in energy.

For this purpose we have made measurements with various homogeneous groups of particles of known energy. In addition to the α-particles from the naturally occurring radio-active nuclei, we have employed the groups of protons and α-particles emitted from the light elements under bombardment with 900 kev. deuterons. Values of the energy release, Q, in these reactions are in many cases now established with high precision. It follows that the energy of the corresponding particles can be calculated from the known energy of the primary deuterons and from the direction of emission relative to the primary beam at which the observations are made. By comparing the mean lengths of the tracks, produced by homogeneous groups of protons and α-particles, with the corresponding values of the energy, we can deduce the relation between the energy and the range in the emulsion for particles of the different types.

Having established the range-energy relations, we can proceed to examine the energy "resolving power" which the method allows. For this purpose we transform the observed range distributions to an energy scale. The width of the resulting peaks at half maximum can, by analogy with the corresponding optical problem, be taken as a measure of the capacity of the method to distinguish between homogeneous groups of similar particles of different energy, and in conformity with previous workers we define this as the *energy resolving power*.

The third aspect of the method, the discriminating power, refers to the possi-

bility of distinguishing different types of particles of the same range by the differences in the numbers of grains per unit length in the corresponding tracks. The performance of an emulsion in this respect depends, amongst other factors, on the mean grain size of the silver halide particles and varies from one type of emulsion to another. Our present experiments are confined to observations with the B1 emulsion, in which the mean grain size is $0{\cdot}4\,\mu$, and we show that it is possible to distinguish protons and α-particles with high efficiency. Thus, if we examine a plate containing a group made up of α-particles and protons of the same range, we can decide in 90% of the cases, by simple inspection, whether a track is due to a proton or an α-particle. In the remaining 10% of the cases the correct allocation is uncertain. For many purposes this degree of discrimination is sufficient, but further improvement is desirable since, with the present emulsions, there may be an ambiguity in the interpretation of individual events such as occur in the nuclear explosions produced by exposures to cosmic radiation or high energy γ-rays.

This is achieved in the C1 and E1 types of emulsion, where the difference between the tracks of protons and α-particles of the same range is greatly accentuated. These emulsions have the disadvantage, however, that for work where exposures of saveral months are employed there is a marked fading of the latent image. The tracks produced by lightly ionizing particles tend to disappear first, and in certain experiments this fact can be employed to increase the discrimination between, for example, tritons and α-particles. With E1 emulsions the tracks of protons disappear almost completely after one week and, with C1, after two weeks.

§ 2. EXPERIMENTAL METHOD

The apparatus employed is similar to that described in (I), with small modifications shown in figure 1. The primary beam of fast deuterons from the Cambridge high-tension generator, after magnetic analysis to remove molecular ions,

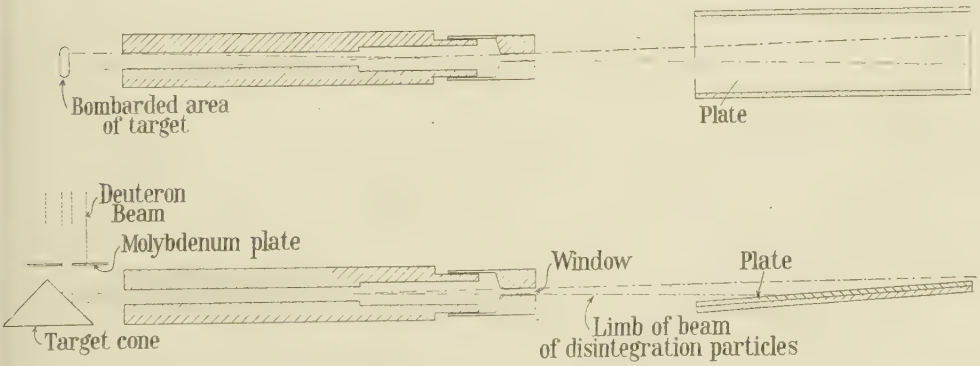

Figure 1.

falls on a molybdenum plate in which there is a central aperture 3 mm. in diameter. The defined beam strikes the layer of target material carried on a shaped metal block which can be rotated on a cone. The different surfaces, carrying thin layers of various target materials, can thus be rotated into the beam in succession.

In making exposures, targets of the following light elements were employed :—

(a) *Beryllium.** A thin layer of metallic beryllium was deposited on one face of the brass block by evaporating the metal from a tantalum boat *in vacuo*. This target had a brilliant metallic lustre and its stopping power was of the order of 0·5 mm. of air. The plates obtained therefore record disintegration particles produced by a beam of deuterons nearly homogeneous in velocity, the loss of energy of the particles in passing through the beryllium layer being less than 20 kev. for protons and 80 kev. for α-particles.

(b) *Lithium oxide.* This target was produced by burning lithium in air and allowing the white smoke of lithium oxide to condense on the target surface. Thick targets of this material were employed since it was found to be rapidly removed by the impact of the beam. In order to avoid contamination of the target chamber by lithium, this material was employed last in the series of exposures and was mounted on a separate supporting cone.

(c) *Boron.* A layer of amorphous boron was applied to the copper surface by grinding the material in a mortar with xylol and painting the resulting material on to the copper with a brush.

The disintegration particles were observed in a direction making an angle of $90 \pm 1°$ with the primary stream of deuterons. Simple calculations show that in all cases the conditions of observation are well within the limits of "good geometry" as defined by Livingston and Bethe (1937). The particles emerge from the vacuum chamber through a window of formvar having a stopping power of 3·1 mm. of air for polonium α-particles. The pressure in the camera containing the plate is reduced, during the exposures, to such a value that the loss of energy suffered by the particles in passing between the window and the plate is negligible.

The formvar window, in spite of its low stopping power, was sufficiently strong to withstand a pressure difference of more than 1 atmosphere. This result was achieved by covering the film with a thin protective layer of silver deposited by evaporation *in vacuo*. Ordinary windows of the formvar type are subject to deterioration through oxidation processes promoted by ionization. In addition to giving a marked increase in strength, the silver therefore serves also to protect the window from this type of chemical attack. The presence of the window allows the removal of exposed plates from the "camera" and the reloading of new ones without admitting air to the vacuum system containing the targets. The speed at which exposures can be made is thus greatly increased.

The angle of approach at which the disintegration particles, emerging through the window, meet the photographic emulsion can be varied at will, and we have found a suitable value to be 4°. Such a disposition ensures, firstly, that the proportion of particles entering the plate which are deflected from their original direction, through small-angle Coulomb scattering, to such an extent that they return to the surface of the emulsion is very small. If a particle leaves the emulsion its range cannot be determined, and such particles are not measured. Secondly, a small angle of approach ensures that relatively few of the fast particles traverse the whole thickness of the emulsion to enter the glass.

The thickness of the emulsions employed in the present experiment was 40 μ. There are no particular difficulties in processing such plates, but the following

* We are indebted to Dr. J. W. Mitchell for the preparation of the beryllium target.

procedure, for which we are indebted to Dr. G. P. S. Occhialini, is adopted as standard practice and is of importance in dealing with thicker emulsions of the order of 100 μ. The plates are developed in Ilford I.D.19 (x-ray developer), at a dilution of 1 of developer to 3 of water, for 35 minutes at 18° c., with constant rocking. For this purpose a mechanical device is employed which gives regular sudden changes of tilt to the dish and provides laminar flow of the developer over the plate. After development, the plate is washed for 1 min., bathed for 1 min. in 2% acetic acid, and fixed. A novel feature of the fixing, which presents the most serious technical difficulties with these emulsions, is that it is important to rock the fixing bath. The emulsions contain roughly a hundred times as much silver per unit area as an ordinary plate, and it becomes important to ensure that sufficient fixing salt is provided. We find it an advantage to employ freshly prepared fixing solution of the following composition: two parts of saturated sodium thiosulphate solution and one part of Kodak acid fixing bath at standard concentration added to six parts of water.

The bath is renewed several times during fixation, the plate being washed for a minute whilst the solution is being changed. It is of some advantage to maintain the surface of the emulsion face downwards in the bath to facilitate the removal of the heavy silver salts from the emulsion, and for this purpose the plate is supported by attaching a suction pad, carried by a metal stem, to the glass.

Considerable variation of development time can be tolerated without appreciable changes in the visual quality of the image seen under the microscope. As the development time increases, the background grains become numerous, but the tracks are denser. In our experience it is better for the development time to be too long than too short, especially for work with protons, when a sharply defined beginning to the tracks is important. A certain concentration of background grains is useful in allowing the surfaces of the emulsion to be easily distinguished, since this allows a quick decision as to whether or not a particular track has passed out of the emulsion. If good discrimination between different particles is important, it is of some advantage to under-develop.

§ 3. EXPOSURES AND METHOD OF MEASUREMENT

The following are the particulars of the exposures given to the plates on which the present measurements were made:—

No.	Target	Stopping power in air equivalent (mm.)	Beam current (μa.)	Time of exposure (min.)
1	Beryllium	0·5	50	60
2	Lithium oxide	Variable	70	10
3	Boron	Thick	70	16

The plates were examined using a variety of objectives and eye-pieces, different observers making observations on the same plate with different magnifications. We draw attention to the fact that, when using binocular microscopes, the overall magnification depends on the interocular distance employed and, therefore, varies

with different observers. Individual calibration of the micrometer scale for each observer is therefore essential. We take as our standard of length a 1-mm. graticule by Cooke divided into one hundred parts.

In determining the length of the tracks we chose to measure the length of the projection of the trajectory of the particle on the plane of the surface of the emulsion. The value so obtained is then multiplied by $\sec\theta$, where θ is the average angle of approach of the particles to the emulsion. The errors introduced by ignoring the effect of changes in the angle of "dip" of the tracks are very small. It would be possible to make appropriate corrections but, owing to the frequent small changes in the direction of the particles, due to Coulomb scattering, the work of measurement would be very greatly complicated. We therefore preferred to sacrifice a small degree of precision in favour of the very important advantage of speed of measurement. In making the measurements we define as the *length* of a track the distance between the extremities of the first and last grains recognized as belonging to it, and we reorientate the scale to lie parallel to the projection of the track whenever changes in direction occur. We thus take account of the changes in direction of the projection of the track, although the changes in "dip" are ignored. The average error in the range measurements due to this approximation is much less than the fluctuations due to straggling.

§ 4. EXPERIMENTS WITH LITHIUM OXIDE

A typical photo-micrograph of a small area of the surface taken with the target of lithium oxide is shown in plate 1. The prominent dense tracks are due to α-particles and the thinner tracks produced by protons can be clearly distinguished from them. The finite depth of focus of the objective prevents the tracks from being sharply in focus throughout their length, but the ends can in many cases be distinguished. We can therefore identify the reactions leading to the emission of particular particles.

In figure 2*a*, we show the distribution in length of 2000 tracks taken from measurements on this plate. Three different magnifications were employed. The short tracks in the range from 10 μ to 50 μ were measured with a Cooke $\times 95$ O.I. achromatic objective with $\times 15$ eye-piece, in which one small division in the eye-piece corresponds to 0·442 μ.* The tracks from 50 μ to 100 μ were measured with the same objective and a $\times 10$ eye-piece (1 div. = 0·555 μ), and the longest tracks with a Leitz $\times 65$ apochromat with $\times 6$ eye-piece (1 div. = 0·984 μ). The resulting measurements are transformed to length in microns and plotted in the same diagram, but the relative numbers of particles in the three ranges have not been adjusted to correspond to the true values. The main features in the observed distribution are the succession of groups, marked (i) to (viii) inclusive, which we attribute to the following well established reactions:—

(i) corresponds to the continuous distribution of α-particles from the reaction ${}^{7}_{3}\mathrm{Li} + {}^{2}_{1}\mathrm{H} \rightarrow 2\,{}^{4}_{2}\mathrm{He} + {}^{1}_{0}\mathrm{n}$. Near the long-range end of this continuous distribution there is a clearly defined peak (ii) which we attribute to the alternative reaction ${}^{7}_{3}\mathrm{Li} + {}^{2}_{1}\mathrm{H} \rightarrow {}^{5}_{4}\mathrm{He} + {}^{4}_{2}\mathrm{He}$ corresponding to the formation of unstable ${}^{5}_{2}\mathrm{He}$ nuclei and their subsequent disintegration into α-particles and neutrons (Williams, Haxby and

* For a particular interocular distance. The difference between the observed and the nominal magnification is due to the use of the binocular eye-piece attachment.

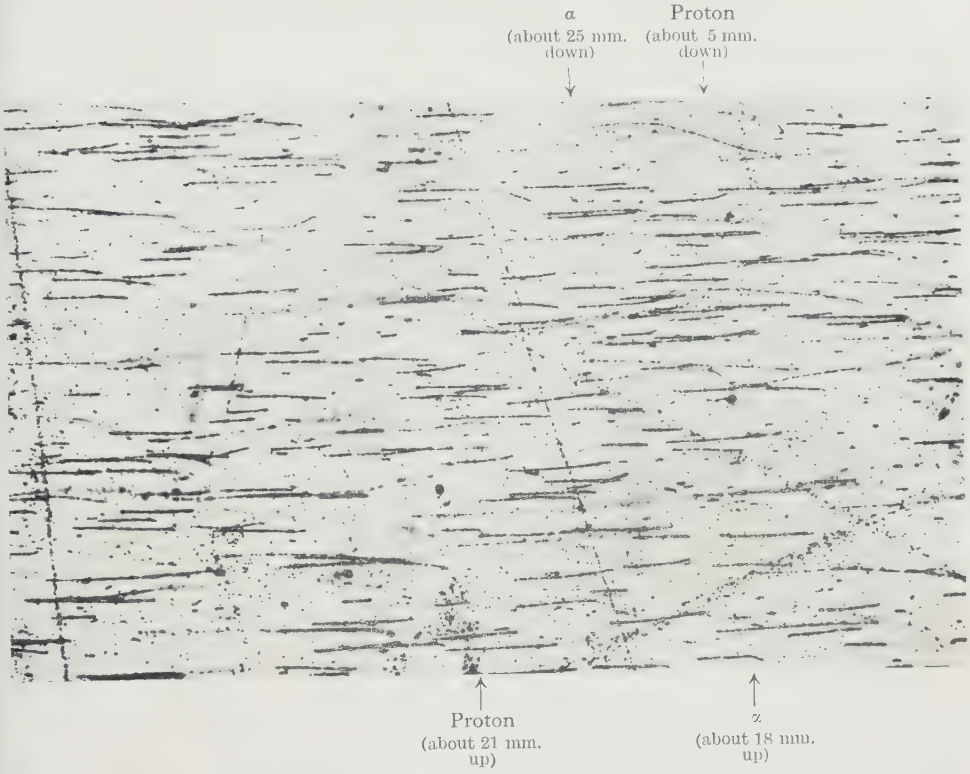

Plate 1.

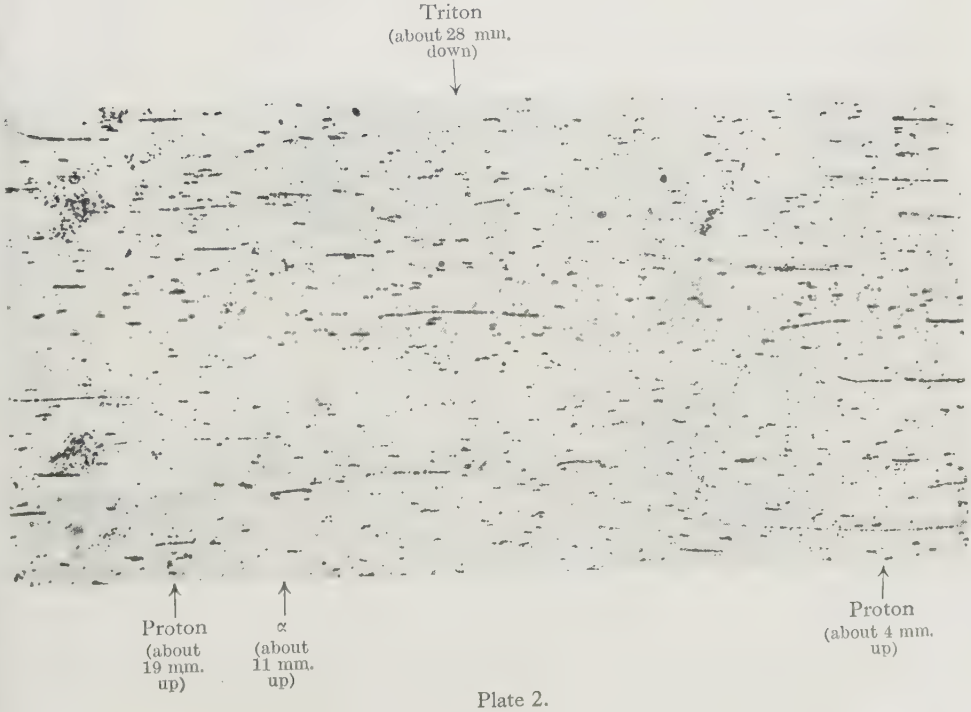

Plate 2.

To face page 888

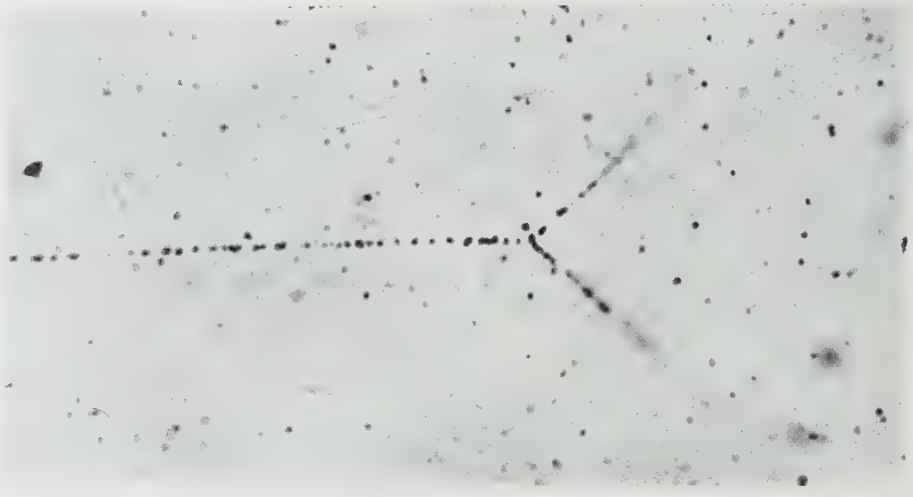

(*a*)

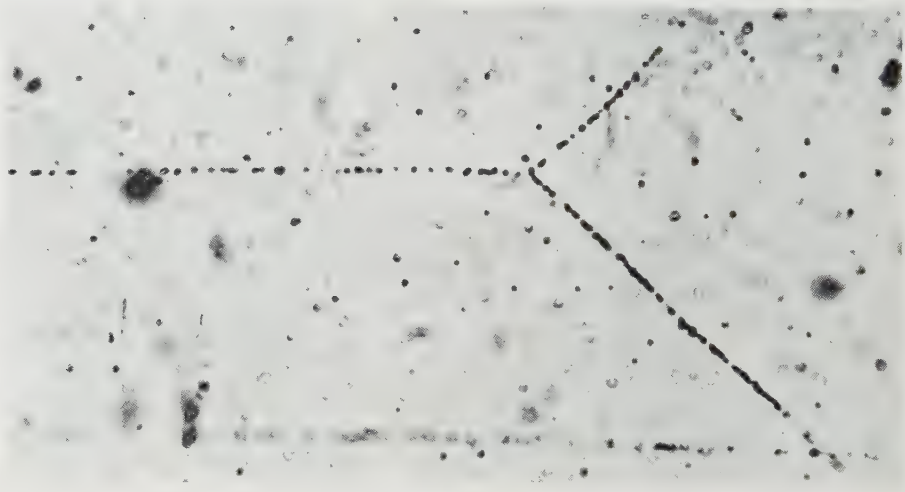

(*b*)

(*c*)

Plate 3.

Shepherd, 1937 a). From the range-energy relation for α-particles, established in the present experiments, we can deduce the energy of the α-particles produced in the reaction and hence the corresponding energy release, Q. We thus obtain the value $Q = 13{\cdot}43$ Mev., which corresponds to a mass of 5·0146 m.u. for $^5_2$He. The corresponding values deduced from the experiments of Williams *et al.* (1937 b) are $Q = 12{\cdot}66$ Mev., $^5_2$He = 5·01543 m.u. According to the present determination of its mass, a $^5_2$He nucleus should dissociate into an α-particle and a neutron with a release of energy of 1·3 Mev. In order to confirm the existence of a group of

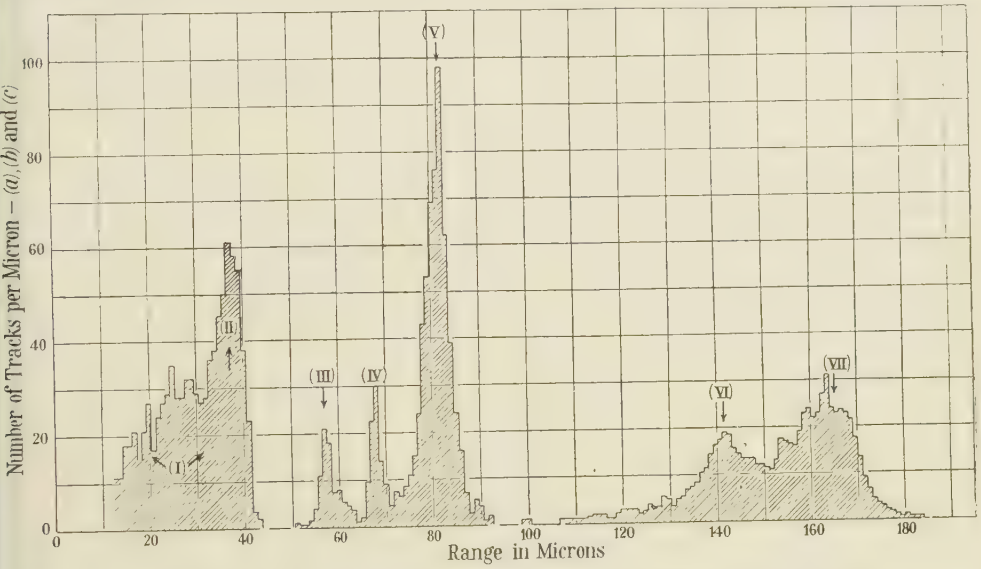

Figure 2 (*a*). Distribution in range of particles from bombardment of LiO by 900 kw. deuterons. Distributions (*a*), (*b*), (*c*) are obtained from plates exposed to the particles from a thick target; distributions (*b*) results from accepting only α-particles for measurement ; distribution (*c*) protons only; distributions (*a*) and (*d*) from measurements on all tracks without discrimination.

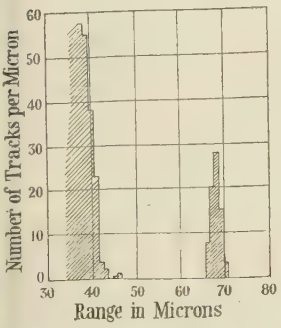

Figure 2 (*b*).

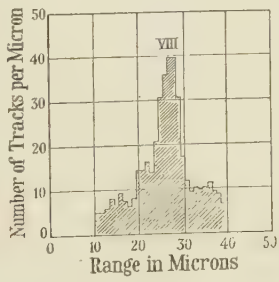

Figure 2 (*c*).

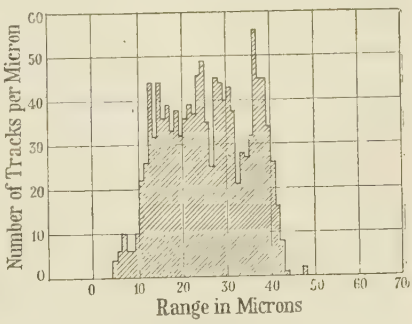

Figure 2 (*d*).

α-particles corresponding to the formation of ^{5}He, we made a separate exposure with a thin target of lithium oxide, and the results of measurements on the plates so obtained are shown in figure 2(*d*). It will be seen that there is an improved resolution of the α-particle group. The difference between the distribution at the lower ranges is due to the fact that in the second series of measurements the tracks of protons and α-particles were accepted without distinction, whereas the first observations were confined to α-particles.

We attribute peak (iii), figure 2(*a*), to protons from the reaction $^{16}_{8}O + ^{2}_{1}H \rightarrow ^{17}_{8}O + ^{1}_{1}H$, the $^{17}_{8}O$ nuclei being left in the ground state. Peak (iv) is due to α-particles from the reaction $^{6}_{3}Li + ^{2}_{1}H \rightarrow ^{4}_{2}He + ^{4}_{2}He$. The peak (v) may be due to protons either from the reaction $^{2}_{1}H + ^{2}_{1}H \rightarrow ^{3}_{1}H + ^{1}_{1}H$, or from $^{12}_{6}C + ^{2}_{1}H \rightarrow ^{13}_{6}C + ^{1}_{1}H$, the expected difference in energy of the protons in the two cases being only 30 kev. in the conditions of our experiments. We think it probable that it is due mainly to the presence of carbon because of the method of preparing the target and the relatively great intensity of the group as compared with that of nearly the same range obtained in the experiments with beryllium. Finally, peaks (vi) and (vii) are due to protons from the reaction $^{6}_{3}Li + ^{2}_{1}H \rightarrow ^{7}_{3}Li + ^{1}_{1}H$, the $^{7}_{3}Li$ nuclei being produced in the ground state or in the well known excited state at 440 kev.

Table 1

Reaction	*Q* (Mev.)	*E* (Mev.)	*R* (microns)	*d* (microns)	Ref.
(i) $^{7}_{3}Li + ^{2}_{1}H \rightarrow 2\,^{4}_{2}He + ^{1}_{0}n$					(1)
(ii) $^{7}_{3}Li + ^{2}_{1}H \rightarrow ^{4}_{2}He + ^{5}_{2}He$	12·7 (13·43)	7·3 (7·76)	39·5	0·10	(5)
(iii) $^{16}_{8}O + ^{2}_{1}H \rightarrow ^{17}_{8}O + ^{1}_{1}H$	1·95 ± 0·06	2·59 ± 0·06	59·6	0·3	(2)
(iv) $^{6}_{3}Li + ^{2}_{1}H \rightarrow ^{4}_{2}He + _{2}He$	22·20 ± 0·04	11·32 ± 0·02	70·8	0·2	(3)
(v) $^{2}_{1}H + ^{2}_{1}H \rightarrow ^{3}_{1}H + ^{1}_{1}H$ $^{12}_{6}C + ^{2}_{1}H \rightarrow ^{13}_{6}C + ^{1}_{1}H$	3·98 ± 0·02 2·71 ± 0·05	3·20 ± 0·02 3·23 ± 0·05	83·9	0·1	(4) (2)
(vi) $^{6}_{3}Li + ^{2}_{1}H \rightarrow *^{7}_{3}Li + ^{1}_{1}H$	4·58 ± 0·12	4·51 ± 0·12	147·0	0·2	(1)
(vii) $^{6}_{3}Li + ^{2}_{1}H \rightarrow ^{7}_{3}Li + ^{1}_{1}H$	5·35 ± 0·12	4·96 ± 0·12	170·0	0·2	(1)
(viii) $^{16}_{8}O + ^{2}_{1}H \rightarrow \dagger^{17}_{8}O + ^{1}_{1}H$	(1·12)	(1·81)	27·9		(2)

(1) Rumbaugh, Roberts and Hafstad (1938).
(2) Cockcroft and Lewis (1936 b).
(3) Smith (1939).
(4) Oliphant, Kempton and Rutherford (1935 a).
(5) Williams, Haxby and Shepherd (1937 a).

The bracketed values are those deduced from the present experiments.

A correction for the "thick target effect" has been applied to the results for every group of particles except in the case of the protons from the reaction.

* $^{7}_{3}Li$: residual nucleus left in the excited level at 440 kev.

† $^{17}_{8}O$: residual nucleus left in the excited level at 850 kev.

Confirmation for the correctness of the above interpretation of the results is provided by similar observations in which we accept for measurement either only α-particles or only protons. The difference in the characteristics of the tracks of the two types of particles is well displayed in plate 1, where typical α-particles and protons are indicated. In figure 2(*b*) we show the results of observations in which we accept only α-particles for measurement. It will be seen that group (iii), which we have attributed to protons, has completely disappeared.

The results of independent observations in which protons only are accepted for measurement are represented in figure 2(*c*). The peak, (viii), in this figure occurs

at a range in the middle of the continuous distribution of α-particles. It corresponds well with protons from the reaction $^{16}_{8}O + ^{2}_{1}H \rightarrow ^{17}_{8}O + ^{1}_{1}H$, the $^{17}_{8}O$ nuclei being formed in the excited state at 0·85 Mev. (Cockcroft and Lewis, 1936 b).

The results of the measurements of the mean range of the particles constituting the different groups, the reactions to which we attribute them, the corresponding Q values and the calculated mean energy of the particles, are tabulated in table 1. We use the values of Q obtained in the most accurate measurements, references being given to the sources from which they are taken. d is the probable error in the determination of the mean range of a group due to statistical fluctuations only. The calculated values of the energy take into account the thick-target corrections as treated by Bethe and Livingston (1937).

§ 5. EXPERIMENTS WITH BERYLLIUM

Because of the thinness of the beryllium film and its resistance to corrosion under the impact of the beam, the plate obtained with this target provided the most satisfactory conditions for measurement. A typical photo-micrograph of 0·1 mm^2 of the surface of the exposed plate is shown in plate 2. Owing to the relatively low exposure, the number of disintegration particles per unit area is small compared with that obtained with the lithium target, and the most prominent feature in the photograph is the large number of short tracks. These are due to the elastically scattered primary deuterons and the nuclear recoil particles formed in the various disintegration processes.

The range distribution obtained from the measurement of 2000 tracks is shown in figure 3, the reactions giving rise to the particles which produce the different peaks being tabulated with other details in table 2.

The α-particles from the bombardment of beryllium by deuterons have been studied in detail by Graves (1940). These authors found that the distribution in energy of the particles is complex, corresponding to the formation of the product nuclei, $^{7}_{3}Li$, either in the ground state or in an excited state of energy between 400 and 500 kev. The number of particles measured in our experiments is not sufficiently great to enable us to separate the two groups. The mean range of the observed distribution, peak (ii), figure 3, agrees well with the assumption that the most probable mode of disintegration is that giving rise to the $^{7}_{3}Li$ nuclei in the well known excited state at 440 kev.

The particles giving rise to peak (iii) produce tracks with a grain-spacing characteristic of protons and the mean range of the groups corresponds to an energy of 1·69 ± 0·8 Mev. Of the light elements which might be present as contaminants in the beryllium target, the only one which could give rise to a group of protons of about this energy is $^{16}_{8}O$. Protons of energy 1·81 Mev. could then be produced in the reaction $^{16}_{8}O + ^{2}_{1}H \rightarrow ^{17}_{8}O + ^{1}_{1}H$, the $^{17}_{8}O$ nuclei being left in the excited state at 0·85 Mev. If the observed proton group were produced by this reaction we should expect, however, to find a second group, of about the same intensity, corresponding to the formation of $^{17}_{8}O$ in the ground state. There is no trace of such a group, and we can conclude that there is no appreciable oxygen contamination of the target. We therefore assume that the observed protons are produced in the reaction $^{9}_{4}Be + ^{2}_{1}H \rightarrow ^{10}_{4}Be + ^{1}_{1}H$, the $^{10}_{4}Be$ nucleus being formed in an excited state. On this assumption, the energy released in the reaction is 1·11 Mev., a value which

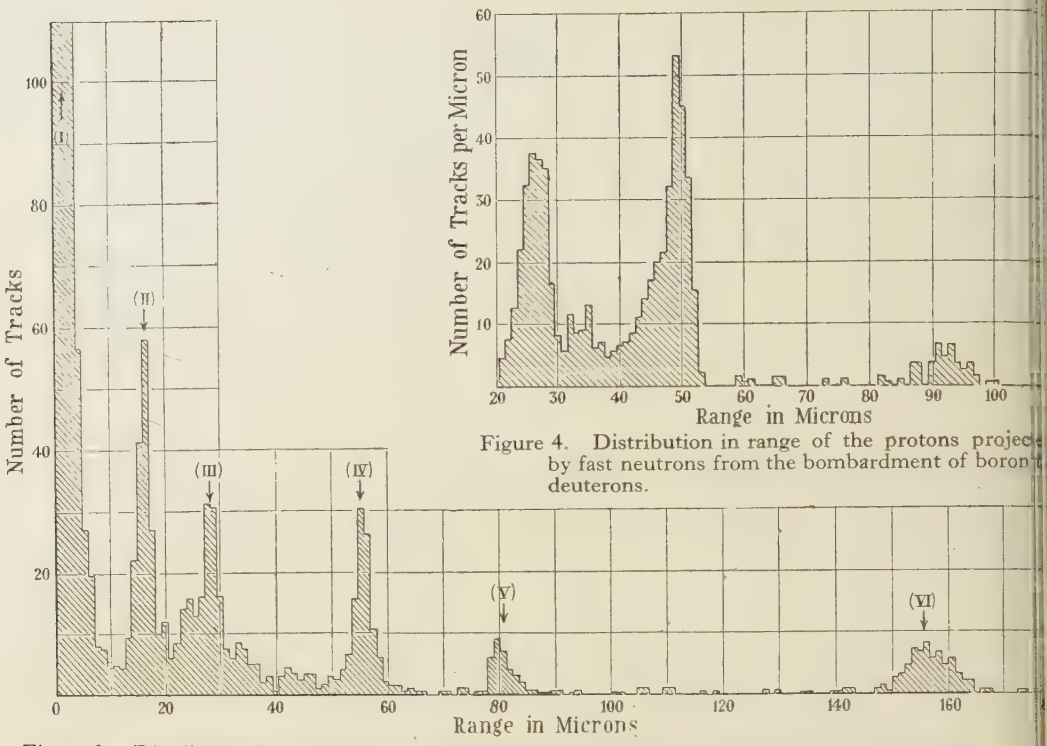

Figure 4. Distribution in range of the protons projected by fast neutrons from the bombardment of boron by deuterons.

Figure 3. Distribution in range of particles from the bombardment of beryllium by 900 kev. deuterons.

Table 2

Reaction	Q (Mev.)	E (Mev.)	R (microns)	d (microns)	Ref.
(i) Elastically scattered deuterons and recoil nuclei from (ii) and (iii)					
(ii) $^{9}_{4}Be+^{2}_{1}H\rightarrow *^{7}_{3}Li+^{4}_{2}He$	6·65±0·02	4·64±0·02	18·2	0·10	(1)
(iii) $_{4}Be+^{2}_{1}H\rightarrow ^{7}_{3}Li+^{4}_{2}He$	7·09±0·02	4·92±0·02	—	—	(1)
(iv) $^{9}_{4}Be+^{2}_{1}H\rightarrow \dagger^{10}_{4}Be+^{1}_{1}H$	(1·11±0·08)	(1·66±0·08)	29·8	0·1	
(v) $^{9}_{4}Be+^{2}_{1}H\rightarrow ^{8}_{4}Be+^{3}_{1}H$	4·32±0·05	3·63±0·04	57·8	0·10	(2), (3)
(vi) $^{2}_{1}H+^{2}_{1}H\rightarrow ^{3}_{1}H+^{1}_{1}H$ or $^{12}_{6}C+^{2}_{1}H\rightarrow ^{13}_{6}C+^{1}_{1}H$	3·08±0·02 2·71±0·05	3·20±0·02 3·25±0·02	82·7	1·2	(2)
(vii) $^{9}_{4}Be+^{2}_{1}H\rightarrow ^{10}_{4}Be+^{1}_{1}H$	4·51±0·10	4·75±0·10	159·5	0·2	(2), (3)

(1) Graves (1940).
(2) Oliphant, Kempton and Rutherford (1935 b).
(3) Williams, Haxby and Shepherd (1937 b).

For the reaction (vi) we adopted the mean value of Q given in references (2) and (3).

* $^{7}_{3}Li$ left in the well known excited level of energy 440 kev.

† Values of Q and E, for reaction (iii), are calculated assuming that the proton group corresponds to a $^{9}_{4}Be+^{2}_{1}H\rightarrow ^{10}_{4}Be+^{1}_{1}H$ reaction in which $^{10}_{4}Be$ is left in an excited level.

corresponds to an excited state of energy 3·40 Mev. in $^{10}_{4}$Be. This value is deduced from the mass of Be in the ground state corresponding to the mean of the values for the energy released in the reaction $^{9}_{4}\mathrm{Be}+{}^{2}_{1}\mathrm{H}\rightarrow{}^{10}_{4}\mathrm{Be}+{}^{1}_{1}\mathrm{H}$, determined by Oliphant, Kempton and Rutherford (1935 b) and by Williams, Shepherd and Haxby (1937 a), viz. 4·50 Mev. Alternatively, we can assume the particles to be tritons corresponding to the formation of $^{8}_{3}$Be in an excited state. The corresponding value of the energy of this state is then found to be 2·2 Mev. Since no such state has been observed and since, in addition, we should expect the group to be inhomogeneous owing to the rapid disintegration of the $^{8}_{3}$Be nuclei, we can reject this interpretation of the results.*

We have mentioned that most of the short-range particles are due to elastically scattered deuterons with a continuous distribution in range. In addition, however, we may expect to observe $^{7}_{3}$Li recoil nuclei of energy 2·95 Mev. produced in the reaction $^{9}_{4}\mathrm{Be}+{}^{2}_{1}\mathrm{H}\rightarrow{}^{7}_{3}\mathrm{Li}+{}^{4}_{2}\mathrm{He}$, and we believe that the discriminating power of the emulsion allows us to distinguish such tracks, in some cases, from the deuterons of approximately the same range. Characteristic tracks of tritons constituting group (iv) and protons from groups (v) and (vi) are indicated in plate 2. It is not possible, in our experience, to distinguish by inspection the tracks of tritons from those of α-particles of the same range in the B_1 emulsion.

§ 6. EXPERIMENTS WITH BORON

The exposures obtained with a boron target were not so satisfactory as those with beryllium and lithium because emulsions covered with a gelatine supercoat, 2 μ thick, were employed. Such a supercoat is designed to prevent surface marks from pressure or light friction, and the plates were produced for work on neutron spectra where the protons recoil start in the body of the emulsion. For experiments with fast-charged particles, the use of such plates leads to the difficulty that the beginnings of the tracks are not clearly defined, with a consequent loss of precision in the range measurements.

We may point out that the application of such a supercoat is also not entirely satisfactory for work with neutrons. Our preliminary observations indicate that there is a diffusion of silver halide grains into the supercoat so that the surface of the emulsion proper tends to be ill defined. As a result it becomes difficult to decide, in some cases, whether a track has left the emulsion, and such an ambiguity is serious in experiments where the "escape" of tracks has to be taken into account.

In spite of this difficulty we have made measurements of the lengths of the long protons produced in the reaction $^{10}_{5}\mathrm{B}+{}^{2}_{1}\mathrm{H}\rightarrow{}^{11}_{5}\mathrm{B}+{}^{1}_{1}\mathrm{H}$, which are grouped in three peaks, corresponding to the formation of $^{11}_{5}$B nuclei in the ground state or in excited states at 1·5 and 3·4 Mev. (Cockcroft and Lewis, 1936 a). The results of the measurements of 400 tracks are tabulated in table 3.

Plate 3 shows photo-micrographs of two interesting rare events observed in the course of the measurements of the plates obtained with the boron target. (*a*) is a proton-proton collision; (*b*), a photograph of the same event, was obtained by inclining the plate on the microscope stage so that the two branches could be observed in focus at the same time, and it established the fact that the three component tracks are co-planar. The poor optical conditions, due to the inclined

* In a letter to *Nature* (Lattes, Fowler and Cuer, 1947) the excited state of $^{10}_{4}$Be was incorrectly stated to be 2·2 Mev. instead of 3·4.

plate, result in a photograph of inferior quality, but it may be noticed that, even with such a large tilt in the subject, the essential details of the collision can be well displayed.

The angle between the two arms of the tracks as measured in the photograph is 86°. This apparent degree of departure from a right angle, 4°, is greater than that which must have existed when the particles were produced in the emulsion, before development, but when the correction for shrinkage is applied a discrepancy

Table 3

Reaction	Q (Mev.)	E (Mev.)	R (microns)	d (microns)	Ref.
(i) $^{10}_{5}B+^{2}_{1}H\rightarrow *^{11}_{5}B+^{1}_{1}H$	4·71	4·99	171	2·5	(1), (2)
(ii) $^{10}_{5}B+^{2}_{1}H\rightarrow \dagger^{11}_{5}B+^{1}_{1}H$	7·00	7·09	320	3·0	(1), (2)
(iii) $^{10}_{5}B+^{2}_{1}H\rightarrow ^{11}_{5}B+^{1}_{1}H$	9·14±0·06	9·05±0·06	474	3·0	(1), (2)

(1) Cockcroft and Lewis (1936).
(2) Livingston and Bethe (1937).
Ranges corrected for " thick target " effect.
*† : $^{11}_{5}B$, residual nuclei left in 2·14 and 4·13 Mev. excited levels respectively.

of about 3° remains. This may be attributed to a small-angle scattering of one of the protons within one or two microns of the point of collision. Such small-angle Coulomb scattering is very frequent at low energies in the N.R. emulsions because of the high concentration of silver and bromine.

The second event, shown in (*c*), is a large-angle deflection of a proton by collision with a nucleus of silver or bromine. If we assume that it was produced by an elastic collision, the energy of the proton at the point of scattering was 4 Mev. Such large-angle deflections are rare with protons of this energy.

§ 7. EXPERIMENTS WITH NEUTRONS *

In order to determine the range of protons with energies greater than the values available in the previous reactions, measurements have been made on plates exposed to fast neutrons from the reaction $^{11}_{5}B+^{2}_{1}H\rightarrow^{12}_{6}C+^{1}_{0}n$, the exposure being made in the manner described by Powell (1943). In examining the plates, only protons projected at angles less than 8° with the direction of the incident neutrons were accepted for measurement.

From the approximate value of the range-energy relation we can determine the energy E of the proton projected at an angle θ. The energy E_0 of the primary neutron producing the recoil track can then be found together with ΔR, the amount by which the observed range of the recoil track is less than the value to be expected for head-on collision, $\theta=0$. The corrected values so obtained are used to obtain the distribution in range shown in figure 4, which displays the three well known groups for which the values of the mean neutron energy are approximately 6, 9 and 13 Mev. respectively in the conditions of our exposure. The values of the mean ranges of these groups and other particulars are shown in table 4.

* We are indebted to Mrs. Andrews for the measurements in § 7.

§ 8. THE RANGE-ENERGY RELATION FOR PROTONS

From the values of the energy and mean range of the different groups of particles given in tables 1 to 4 we can determine a range-energy curve for protons in the

Table 4

Reaction	Q (Mev.)	E (Mev.)	R (microns)	d (microns)	Ref.
(i) $^{10}B+^{2}H\rightarrow ^{11}C+^{1}n$	6·08	6·24	256	1·00	(1), (2)
(ii) $^{11}B+^{2}H\rightarrow *^{12}C+^{1}n$	9·10	9·09	482	0·83	(1), (2)
(iii) $^{11}B+^{2}H\rightarrow ^{12}C+^{1}n$	13·40 ± 0·30	13·06 ± 0·30	896	3·6	(1), (2)

(1) Bonner and Brubaker (1936).
(2) Livingston and Bethe (1937).
Ranges corrected for " thick target " effect.
* ^{12}C : residual nuclei left in 4·4 Mev. excited level.

Table 5

Reaction	E (Mev.)	R (cm. air)	r (μ in emulsion)	d	R/r
$^{11}B+^{2}H\rightarrow ^{12}C+^{1}n$	13·06 ± 0·30	185·0	896·1	4·0	2064 ± 9
$^{11}B+^{2}H\rightarrow *^{12}C+^{1}n$	9·09	97·0	482·0	1·0	2012 ± 5
$^{10}B+^{2}H\rightarrow ^{12}B+^{1}H$	9·05	96·2	474·0	3·0	2029 ± 15
$^{10}B+^{2}H\rightarrow *^{11}C+^{1}n$	6·24	50·0	256·0	1·0	1953 ± 8
$^{10}B+^{2}H\rightarrow ^{11}B+^{1}H$	7·09	62·6	321·0	3·0	1950 ± 20
$^{10}B+^{2}H\rightarrow *^{11}B+^{1}H$	4·99	33·8	171·0	2·5	1977 ± 28
$^{6}Li+^{2}H\rightarrow ^{7}Li+^{1}H$	4·96 ± 0·12	33·5	170·0	0·2	1970 ± 2
$^{9}Be+^{2}H\rightarrow ^{10}Be+^{1}H$	4·75 ± 0·10	31·0	159·5	0·2	1943 ± 3
$^{6}Li+^{2}H\rightarrow *^{7}Li+^{1}H$	4·51 ± 0·12	28·4	147·0	0·2	1931 ± 2
$^{2}H+^{2}H\rightarrow ^{3}H+^{1}H$	3·20 ± 0·02	15·7	82·7	0·2	1898 ± 5
$^{12}C+^{2}H\rightarrow ^{13}C+^{1}H$	3·25 ± 0·05	16·0	83·9	0·1	1907 ± 3
$^{16}O+^{2}H\rightarrow ^{17}O+^{1}H$	2·59 ± 0·06	11·0	59·6	0·3	1845 ± 9
$^{9}Be+^{2}H\rightarrow ^{8}Be+^{3}H$	3·63 ± 0·04	9·3	57·8	0·1	1606
Proton of same velocity	1·20 ± 0·02	3·1	19·3	0·04	1606 ± 15

R denotes range in air in cm. ; r denotes range in the emulsion in microns.

Assuming that peak (v), figure 2, obtained in the lithium exposure is due to carbon contamination of the target.

d refers only to the " probable error " in measuring the baricentre of a group and gives only the statistical weight of the point. Other sources of error may arise from the calibration and from uncertainties in the value of Q.

emulsion. The results are summarized in table 5 and shown diagrammatically in figure 5 (*a*) and 5 (*b*). From the range-energy curve in air given by Bethe we can determine the variation of the stopping power of the emulsion relative to air, and the results are represented in figure 6. It will be seen that there is a considerable

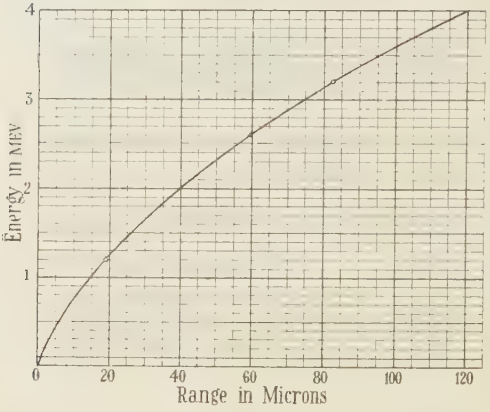

Figure 5 (*a*). Range-energy curve for protons. Nuclear research emulsion, type B1.

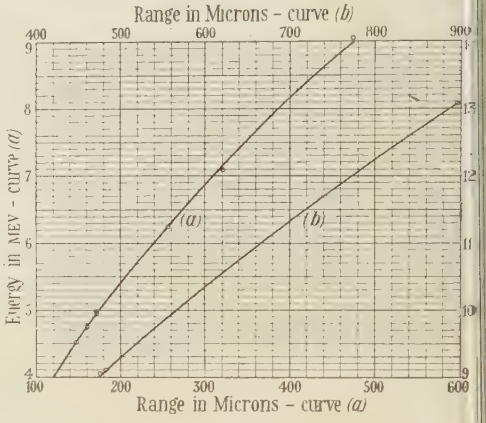

Figure 5 (*b*).

variation of the mean stopping power as the range of the protons increases. The point at 1·2 Mev. is deduced from the observed mean range of the tritons produced in the reaction ${}^{9}_{4}\mathrm{Be}+{}^{2}_{1}\mathrm{H}\rightarrow{}^{8}_{3}\mathrm{Be}+{}^{3}_{1}\mathrm{H}$, for which the release of energy, Q, has been determined by Williams, Haxby and Shepherd (1937 b), $Q=4{\cdot}32\pm0{\cdot}05$ Mev. The calculated energy of the tritons emitted at 80° with the direction of the primary deuterons, of energy 900 kev., is $3{\cdot}63\pm0{\cdot}05$ Mev. If we assume that the range of a triton is three times that of a proton of the same velocity, we obtain the value given in table 5 for the range of protons of energy 1·21 Mev.

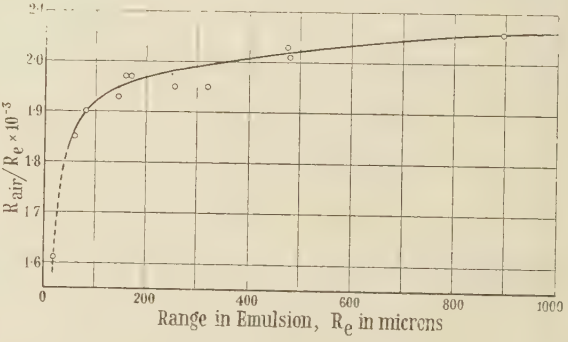

Figure 6. Mean stopping power of emulsion for protons of different ranges.

Although out present measurements are confined to the emulsion of type B1, we may assume that they will apply to the other types, after small corrections, since the manufacturers aim at producing emulsions of constant atomic composition. There may, however, be small changes in stopping power in plates in different batches, although we have not yet detected such an effect.

§ 9. RANGE-ENERGY RELATION FOR α-PARTICLES

The range-energy relation for α-particles has been determined, up to an energy of 9 Mev., by measurements of the lengths of the tracks produced by the homogeneous groups of particles emitted by the natural radioactive substances. The value at 13 Mev. has been deduced by employing the α-particles from the reaction ${}^{6}_{3}\mathrm{Li}+{}^{2}_{1}\mathrm{H}\rightarrow{}^{4}_{2}\mathrm{He}+{}^{4}_{2}\mathrm{He}$.

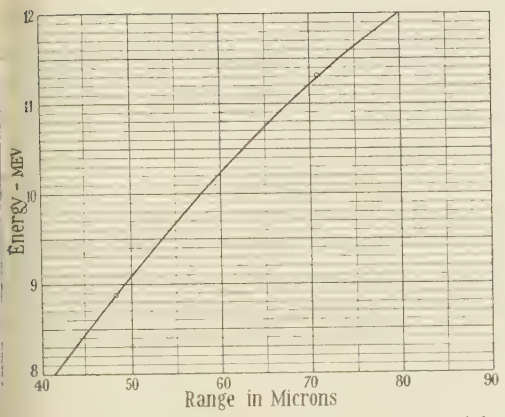

Figure 7 (*a*). Range-energy curve for α-particles. Nuclear research emulsion, type B1.

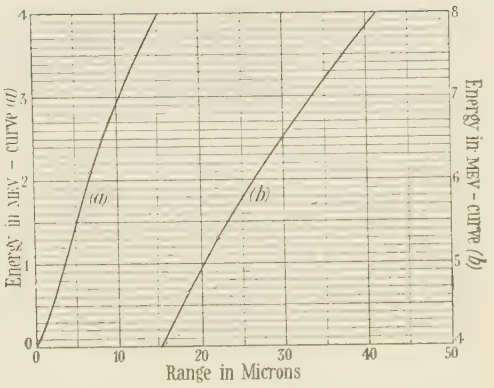

Figure 7 (*b*).

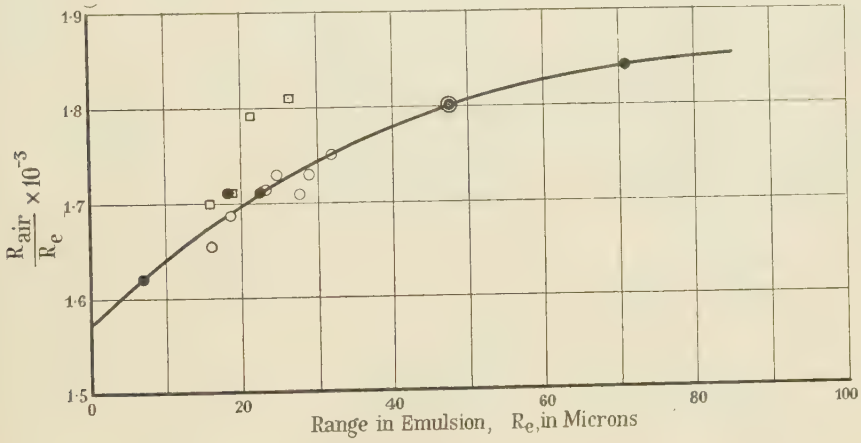

Figure 8. Stopping power for α-particles.
● Present experiments (B1).
□ Tsien, Chastel, Faraggi and Vigneron, 1946 (A1).
○ D. L. Livesey and Green—private communication (C2).

Table 6

Reaction	E (Mev.)	Ranges in air R (cm.)	Ranges in emulsion R (2)	$\frac{R_a}{R_e} \times 10^{-3}$
${}^{6}_{3}\mathrm{Li} + {}^{2}_{1}\mathrm{H} \rightarrow {}^{4}_{2}\mathrm{He} + {}^{4}_{2}\mathrm{He}$	11·32±0·02	13·04	70·8 ±0·2	1·842±0·005
ThC′ α-particles	8·78	8·57	47·5 ±0·05	1·804±0·002
Po α-particles	5·30	3·84	22·5 ±0·06	1·707±0·003
${}^{9}_{4}\mathrm{Be} + {}^{2}_{1}\mathrm{H} \rightarrow {}^{*7}_{3}\mathrm{Li} + {}^{4}_{2}\mathrm{He}$	6·64	3·12	18·2 ±0·1	1·715±0·010
Sm α-particles	2·1	1·13	6·95±0·05	1·628±0·012

Table 6 gives a summary of the results used in drawing the curves shown i figures 7 (*a*) and 7 (*b*). We are indebted to L. L. Green, W. M. Gibson and D. I Livesey for permission to include the results of their measurements on the α-part cles from U I, U II, ThC and ThC′. Figure 8 gives the variation of the stoppin power of the emulsion with the range of the particles.

§ 10. RESOLVING POWER

In order to display the resolving-power of the method, we show in figures and 10 the apparent distribution in energy of the tracks produced by typica homogeneous distribution in energy tritons and α-particles. The curves ar

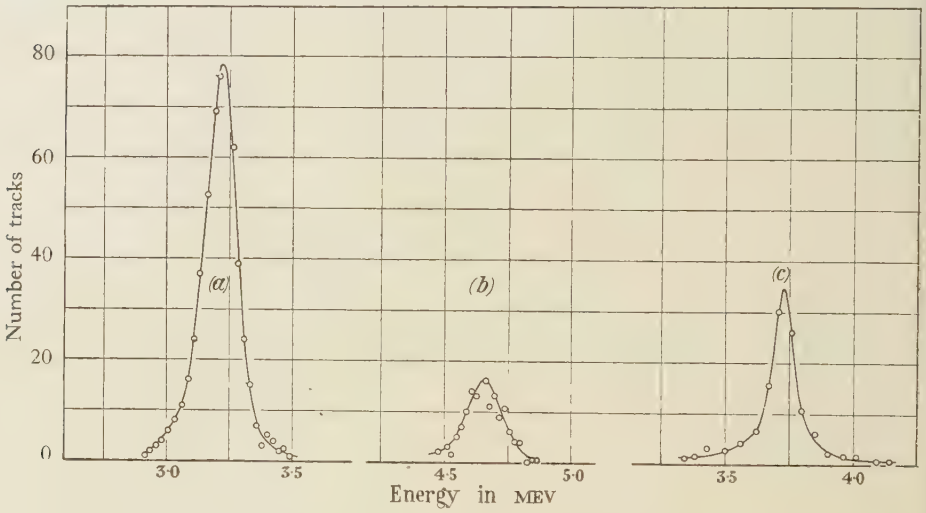

Figure 9. Distribution in energy of protons from (*a*) ${}^{2}_{1}\mathrm{H}+{}^{2}_{1}\mathrm{H}\rightarrow{}^{3}_{1}\mathrm{H}+{}^{1}_{1}\mathrm{H}$; (*b*) ${}^{9}_{4}\mathrm{Be}+{}^{3}_{1}\mathrm{H}\rightarrow{}^{10}_{4}\mathrm{Be}+{}^{1}_{1}\mathrm{H}$; and of tritons from (*c*) ${}^{9}_{4}\mathrm{Be}+{}^{2}_{1}\mathrm{H}\rightarrow{}^{8}_{4}\mathrm{Be}+{}^{3}_{1}\mathrm{H}$.

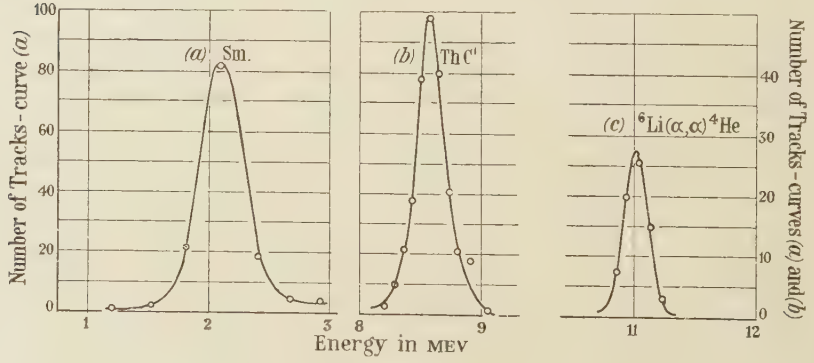

Figure 10.

deduced from the observed distribution in range of the tracks corresponding to the different groups, using the appropriate range-energy curve, and a summary is given in table 7. The most significant results are those obtained with a beryllium target which was exceptionally thin. In this case the observed width of the proton group is only 25% greater than that expected from straggling. In the other cases, the observed width can be accounted for in terms of the thickness of the targets

employed. We may conclude that for protons in the interval from 2 to 13 Mev. the uncertainty in the energy of a particle, as deduced from its range in an emulsion, is not appreciably greater than that due to straggling.

Table 7

Reaction	E (Mev.)	$R_e(\mu)$	S (%)	S' (%)	Remarks
		Protons			
${}^{9}_{4}\mathrm{Be}+{}^{2}_{1}\mathrm{H}\rightarrow{}^{10}_{4}\mathrm{Be}+{}^{1}\mathrm{H}$	4·75	159·5	1·96	2·4	
${}^{2}_{1}\mathrm{H}+{}^{2}_{1}\mathrm{H}\rightarrow{}^{3}_{1}\mathrm{H}+{}^{1}_{1}\mathrm{H}$	3·20	82·7	2·05	2·5	Beryllium target
${}^{2}_{1}\mathrm{H}+{}^{2}_{1}\mathrm{H}\rightarrow{}^{3}_{1}\mathrm{H}+{}^{1}_{1}\mathrm{H}$ ${}^{12}_{6}\mathrm{C}+{}^{2}_{1}\mathrm{H}\rightarrow{}^{13}_{6}\mathrm{C}+{}^{1}_{1}\mathrm{H}$	3·20	83·9	2·05	5·75	Probably due to ${}^{12}_{6}\mathrm{C}+{}^{2}_{1}\mathrm{H}\rightarrow{}^{13}_{6}\mathrm{C}+{}^{1}_{1}\mathrm{H}$ Lithium target
${}^{9}_{4}\mathrm{Be}+{}^{2}_{1}\mathrm{H}\rightarrow{}^{8}_{4}\mathrm{Be}+{}^{3}_{1}\mathrm{H}$	3·63	57·8		4·8	
${}^{11}_{5}\mathrm{B}+{}^{2}_{1}\mathrm{H}\rightarrow{}^{12}_{6}\mathrm{C}+{}^{1}_{0}\mathrm{n}$	13·06	896·0	1·8	3·3	Thick target
${}^{11}_{5}\mathrm{B}+{}^{2}_{1}\mathrm{H}\rightarrow{}^{*12}_{6}\mathrm{C}+{}^{1}_{0}\mathrm{n}$	0·99	482·0	1·7	3·3	Thick target
		α-particles			
${}^{6}_{3}\mathrm{Li}+{}^{2}_{1}\mathrm{He}\rightarrow{}^{4}_{2}\mathrm{He}+{}^{4}_{2}\mathrm{He}$	11·32	70·8	1·05	3·5	Thick target
ThC′ α-particles	8·78	47·5	1·07	2·7	
Po α-particles	5·30	22·0	1·17	4·0	
Sm α-particles	2·1	6·95		14·0	

S = theoretical straggling in air (Bethe and Livingston, 1937).

S' = "experimental straggling" $= \sqrt{\frac{\pi}{2}} \times \sqrt{\Sigma_n \frac{(x-x_i)^2}{n}}$, where x_2 is the range corresponding to the "baricentre" of the group, x the range of a particular track and n the number of tracks composing the "group".

The corresponding results for α-particles are shown in figure 10. They indicate that, because of the much less favourable range-energy relation, the uncertainty in the true range, due to the finite size of the silver halide grains, leads to errors in the estimated energy of the particles, which are much greater than those due to straggling. This effect is especially marked at low energies, so that the peak of greatest "width" is that obtained in experiments with the α-particles from samarium. As the energy of the α-particles increases, the "half-width" becomes smaller. We must anticipate that with particles of progressively greater energies than those of which we have experience, the half-width will reach a minimum and then increase again as the errors due to the finite grain size become small compared with those due to straggling. For work at moderate energies it is therefore desirable to reduce the errors due to "apparent straggling" by working with emulsions of smaller grain size such as are provided by the C, E and D series of emulsions. Such an improvement in precision would seem to be particularly important in measurements of the multiple disintegration phenomena which we

meet in the disintegration of nuclei produced by the high-energy γ-rays from t betatron or the cosmic rays (Heitler, Powell and Fertel, 1939; Heitler, Pow and Heitler, 1940; Baldwin and Klauber, 1946).

ACKNOWLEDGMENTS

The present work was carried out in the H. H. Wills Physical Laborator University of Bristol, and we wish to express our appreciation to the Director the laboratory, Prof. A. M. Tyndall, for much kindness and hospitality. Th experiments were made at the suggestion of Dr. C. F. Powell and under his dire tion. We had the advantage of being able to make full use of the technique developed by him and Dr. G. P. S. Occhialini, and of the special facilities of th laboratory for the application of the photographic method to nuclear physic The authors wish to express their gratitude to them for their continuous interes and active help.

We are indebted to Sir Lawrence Bragg, Dr. Burcham and Mr. Livesey of th Cavendish Laboratory, who kindly made it possible for us to obtain the exposure on the Cambridge High Tension set, and to several of our colleagues in th laboratory for assistance on many occasions, especially to Mr. R. M. Payn and Mr. E. Samuel. We are also indebted to W. M. Gibson, L. L. Gree and D. L. Livesey for permission to include in table 6 the results o their measurements on the α-particles from UI and UII and from the T radioactive series.

One of us (C. M. G. L.) was enabled to undertake the work by a grant from th University of Bristol and from the Getulio Vargas Foundation.

REFERENCES

BALDWIN and KLAIBER, 1946. *Phys. Rev.*, **70,** 259.
BONNER and BRUBAKER, 1936. *Phys. Rev.*, **50,** 781.
COCKCROFT and LEWIS, 1936 a. *Proc. Roy. Soc.*, A, **154,** 246 ; 1936 b. *Ibid.*, **154,** 261.
GRAVES, 1940. *Phys. Rev.*, **57,** 855.
GUGGENHEIMER, HEITLER and POWELL. In the press.
HEITLER, POWELL and FERTEL, 1939. *Nature, Lond.*, **144,** 283.
HEITLER, POWELL and HEITLER, 1940. *Nature, Lond.*, **146,** 65.
LATTES, FOWLER and CUER, 1947. *Nature, Lond.*, **159,** 301.
LIVINGSTON and BETHE, 1937. *Rev. Mod. Phys.*, **9,** 326.
OLIPHANT, KEMPTON and RUTHERFORD, 1935 a. *Proc. Roy. Soc.*, A, **149,** 406; 1935 b. *Ibid.*, **150,** 241.
POWELL, 1943. *Proc. Roy. Soc.*, A, **181,** 344.
POWELL, OCCHIALINI, LIVESEY and CHILTON, 1946. *J. Sci. Instrum.*, **23,** 102.
RUMBAUGH, ROBERTS and HAFSTAD, 1938. *Phys. Rev.*, **54,** 657.
SMITH, 1939. *Phys. Rev.*, **56,** 548.
WILLIAMS, HAXBY and SHEPHERD, 1937 a. *Phys. Rev.*, **52,** 390 ; 1937 b. *Ibid.*, **52,** 1031.

DISCUSSION

on paper by E. F. DALY and G. B. B. M. SUTHERLAND entitled "An Infra-red Spectroscope with Cathode-ray Presentation" (*Proc. Phys. Soc.*, **59**, 77 (1947)).

Dr. F. AUGHTIE. Plate 1 of this paper shows two displays: (*a*) without and (*b*) with smoothing by a resistance capacity filter stated to be of about 2 cycles/sec. width. No reference is made in the paper to the time delay of the filter; this will be of the order of the reciprocal of the band width and will cause the appropriate vertical deflection of the trace to occur at a position displaced horizontally by a distance corresponding to this time interval. It is quite noticeable that several distinctive features of the trace of plate 1(*b*) are displaced to the left by 2–3 mm. from the corresponding features of 1(*a*). This displacement is of the order to be expected from the band and sweep frequency employed.

Thus if the smoothed curves are to be employed, the wave length scale should be displaced by a distance corresponding to the time delay. Preferably the cam should be arranged to operate an auxiliary shutter which would momentarily interrupt the light at known settings, so that the wave length scale appropriate to the sweep-speed in use can be determined from a blank observation.

The effect of filter delay would, of course, be more serious if a faster rate of scan were used.

AUTHORS' reply. We are grateful to Dr. Aughtie for drawing attention to this point, which, perhaps, ought to have been more fully explained in our paper. We are, of course, well aware of the distortion both in amplitude and in phase introduced by the narrow band-resistance capacity filter, and we did remark that its use is accompanied by a sacrifice in the precision with which spectra are displayed. We do not feel, however, that this small displacement in the trace in going from one type of presentation to the other is important because in practice calibration is always done by reference to the spectra of compounds having sharp absorption bands of which the wave length has been determined accurately by grating measurements. Consideration of the filter delay is thus unnecessary provided the calibration spectra are displayed in the same way as the spectra under consideration.

CORRIGENDA

"The lines of force through neutral points in a magnetic field", by DAVID OWEN (*Proc. Phys. Soc.*, **59**, 14 (1947)).

Page 17. The words "this case is illustrated in figure 3" should be deleted.

"Theory of the proton synchrotron", by J. S. GOODEN, H. H. JENSEN and J. L. SYMONDS (*Proc. Phys. Soc.*, **59**, 677 (1947)).

Page 680, eleventh line from foot of page. The equation should read

$$(\phi_2+\phi_1-\pi)\sin\phi_1+\cos\phi_2+\cos\phi_1=0.$$

Page 686, equation (5). The numerical constant (3·3) on the right-hand side should be replaced by (0·53).

Page 686, equation (7). R_0 should be R_0^2.

Page 686, equation (8). In the right-hand side the factor 2 in the numerator should be 6.

Page 690, equation (11). In the right-hand side the factor 2 in the numerator should be 8.

Page 691, equation (17) should read

$$B=\frac{ps\cot\phi_1\tan\theta}{2(s+1)(1-n)}.$$

REVIEWS OF BOOKS

The Physical Principles of Wave Guide Transmission and Antenna Systems, by W. H. WATSON. Pp. xiii + 208 with 95 figures. (Oxford: Clarendon Press, 1947.) 20*s*. net.

It may be said immediately that this is a good book. It does not always follow that one who is an expert original worker in a given field is also good at giving an account of the work in that field, but Professor Watson has succeeded in this case.

It is stated: "The aim of this book, which is addressed to physicists and engineers with theoretical interests, is to describe the way in which the technique of handling radio frequency transmission-lines has been extended to deal with propagation through hollow metal pipes known as wave guides." It is shown that simple circuit ideas, such as are applicable to ordinary transmission-line theory, may, to a large extent, be developed to treat many features of the propagation of the "dominant" wave in wave guides, as well as the loading of such guides by coupling and matching devices. Here the "dominant" wave is the one and only characteristic mode of propagation possible in a given wave guide when the dimensions of the latter are suitably chosen in relation to the frequency of the radiation concerned. Whilst in the main this is a theoretical treatise, the author has in mind the emphasis of the underlying physical principles, and he has succeeded admirably in his aim, namely, to bring out these principles in a clear and understandable manner.

Chapter I contains a treatment of the elements of wave propagation using the impedance concept. With the aid of the simple strip transmission-line it is shown how to transfer the circuit ideas of impedance and admittance to waves in space. As a result it is possible to discard the elaborate differential equations employed even with such simple waves, and to use instead algebra of no great complexity. The algebraic equations representing waves either on a transmission-line, or in space, can be easily connected with a geometrical representation in terms of the circle diagram. From this algebraic representation it follows that the propagation and loading of waves may be regarded as transformations which are found to be simple in type, and may be conveniently represented by matrices. This matrix algebra is developed in some detail, and the algebraic transformations necessary for dealing with various characteristics of plane wave propagation are considered.

Chapter II is devoted to a consideration of the dominant wave (H_{10} or TE_{10}) in a rectangular wave guide. This problem is attacked from the physical point of view, and the solution is obtained from the investigation of a system of two interfering trains of plane waves rather than by the more common procedure of simply applying Maxwell's equations and the boundary conditions—a procedure which does not lend itself so readily to a formation of a clear picture of the processes involved. Various aspects of the propagation of the dominant wave are dealt with: the energy flux, the current distribution on the walls of the wave guide, impedance, and the attenuation of the wave due to the finite conductivity of the walls.

A description is given in Chapter III of various measurement techniques which are necessary for an experimental investigation of the phenomena in wave-guide systems. This includes wave-meters, standing-wave detectors and power measurement: a short section deals with wave-guide stubs for impedance matching purposes. The treatment in this chapter is rather cursory and does no more than describe the underlying principles of the various instruments and techniques; it would not meet the needs of one who wished to design such equipment, but it should be stated that the author quite clearly does not aim at satisfying this requirement.

In Chapter IV there is a brief discussion of the general problem of multiple mode propagation of both E- and H-waves in rectangular and circular wave guides. The question of multiple propagation on the outside of a guide, which arises when an aperture is cut in the wall of the guide, is also mentioned, but is not developed to any great extent. The author then returns in Chapter V to a more detailed consideration of phenomena related to the propagation of the dominant wave in a rectangular wave guide, particularly in so

far as the problem is affected by irises across the guide, and by coupling to the guide by slots cut in the walls. Babinet's principle is here extended to be of use in the microwave field. A restatement of the principle is necessary to deal with vector waves and reflecting screens. The iris is then considered as a grating problem. Bends in wave guides are discussed, and also the coupling of a wire antenna to the H_{10} wave in a rectangular guide: the impedance of such an antenna under these conditions is determined.

Chapters VI, VII and VIII cover the behaviour of slots cut in both the broad and narrow faces of a rectangular wave guide. Such characteristics as the coupling of these slots to the guide and their susceptance and conductance are determined. The various ways in which one guide may be coupled to another by suitably disposed slots in each are elaborated, and in general in these three chapters the theory is developed in some detail. A section is devoted to the consideration of antenna arrays using wave guides : this includes both arrays of linear dipoles energized by probes coupling through the broad face of the guide, and also arrays of slot radiators. The design of arrays to give various types of radiation pattern is discussed : this involves the determination of the distribution of conductances, amplitudes of excitation, and spacing of slots. Although in the main only linear arrays are considered, it is indicated also how two-dimensional wave-guide arrays may be constructed.

These three chapters are very well done : this is perhaps not surprising in view of the important contributions to the subject made by Professor Watson and his colleagues at McGill University during the late War.

In Chapter IX the author describes some further microwave devices, including the design of an array to produce a cosecant pattern, a Yagi array of slots, wave-guide switching systems and phase changers. Resonant cavities and the " Magic Tee " junction are dealt with in brief.

In the final chapter (X) Professor Watson considers field representations in connection with radiation and reception by antenna systems in wave guides. The basis of the analysis is the determination of expressions for the Hertz vectors of the field in a wave guide due (*a*) to an electric dipole, and hence to a current element, and (*b*) to a magnetic radiator which is realized by a distribution of tangential electric force on a surface where an aperture replaces part of a wave-guide wall. The thesis is developed in considerable detail, and such problems as those presented by an axis in a rectangular wave guide, radiation by an electric dipole and the impedance of such a linear antenna in a guide, and the characteristics of a resonant slot are analysed.

In general it may be said that the treatment is concise yet lucid throughout, and that Professor Watson has succeeded in bringing out clearly the physical principles involved in the transmission of waves through wave guides. He is to be congratulated on having filled so well a definite gap in the literature of this still quite new field. There is a minor criticism in relation to the title : at first glance one might imagine that the book was intended to deal with antenna systems in general, whereas, in fact, only some of those systems in which the wave guide plays an important part are discussed.

The book is well illustrated and produced, but it is a pity that so many references must still be to unpublished work. It is to be hoped that, in so far as it becomes possible, the author will endeavour to remedy this defect in any future editions. J. A. Saxton.

The Metre-Kilogram-Second System of Electrical Units, by R. K. Sas and F. B. Pidduck. Pp. v+60. (London: Methuen and Co. Ltd., 1947). 4*s*. net.

A booklet to bring the metre-kilogram-second system of units to the notice of the scientific and technical public has been wanted in this country for several years, especially as the admirable publication of G. A. Campbell (*Bulletin* of the National Research Council, Washington, 1933, No. 93, p. 48) is not available here to a large circle of readers. For that reason the present publication is welcome and is bound to serve a useful purpose, if only to stimulate interest and discussion.

Put briefly, it happens that the orders of magnitude of the ampere and volt were so chosen that when the metre and kilogram are used as units of length and mass, the unit of power is the watt. This purely accidental coincidence is the main argument in favour

of the MKS system. The authors are a trifle apologetic about the fact that in this syst the density of water is 1000 kg. per m³, but there should be no difficulty whatever th if the distinction between density and specific gravity is maintained. In the MKS syste as in other systems, the magnetic units can be chosen in two ways, which give rise to t normal and the so-called " rationalized " system respectively. The book under revie rightly we think, considers the latter system only. The main argument for a rationaliz system is that it confines the factor 4π to formulae dealing with problems whose geome is spherical, e.g., the potential due to a point charge, whereas the factor does not appe in problems of rectangular geometry, e.g., the capacitance of a parallel plate condenser.

The booklet is commendably short and can be read in an hour, but adequate ca does not appear to have been given to its preparation, and the text does not see to have been discussed with physicists intimately conversant with the subject. As result a number of blemishes occur which may well produce the opposite of what t authors set out to achieve—the reader may be discouraged by finding too much complicati in an inherently very simple system.

The proposal to use the word " pulse " for ω has no connection with the MKS syste In the past much thought has been given to this matter, but no entirely satisfactory soluti appears to have been found. The proposal to call " aperture " what is generally call " solid angle " is also irrevelant.

These proposals are harmless, but that of the name " oersted " for the ampere-tu per metre is definitely in a different category: apart from the confusion its adoption wou cause, it violates the excellent principle that special names should not henceforth assigned to derived units when expression in terms of primary units is at the same tir simple and indicative of the derivation. This rule applies to the ampere-turn per metr whereas in the case of the volt-second per turn the first condition hardly applies, a accordingly the name "weber" has been proposed. The reviewer is not now connecte with the national and international bodies dealing with nomenclature, but he ventures express the hope that those responsible will resist any attempts to multiply christenin in the MKS family.

It is not clear how confusion would be avoided between permeability, i.e., ratio B/H and relative permeability if the nomenclature proposed in the book were adopted. the MKS system the symbol μ must be reserved for permeability, i.e., ratio B/H in a medium; μ_0 is then used to denote the corresponding quantity for a vacuum, and th ratio μ/μ_0, denoted, say, by μ_r, must be given a name other than just " permeability ": th name *relative permeability* possesses the advantage of indicating the meaning of the symb without further definition. The parallel case of permittivity should be similarly treate This point is stressed here because lack of a well-thought-out nomenclature can caus pitfalls, instances of which are found on p. 45, line 2, where the ratio B/H for the conducto μ, not μ_0, should have been used, and on p. 46, where $\boldsymbol{B}$, and not $\boldsymbol{H}$, should be equate to curl $\mathbf{A}$, in which $\mathbf{A}$ is the vector potential expressed in webers per metre.

The first sentence of p. 52, which contains the amazing statement that " Neumann formula has a factor 10^{-7} " can only add to the " tribulations of the student " describe in pp. 16–17, for the poor student had previously been induced to think that he woul never again meet powers of 10 in his algebraic formulae. Neumann's formula contai nothing of the sort, and should be written

$$M = \frac{\mu}{4\pi} \int \frac{d\boldsymbol{l} \,.\, d\boldsymbol{l}'}{r},$$

where μ for a vacuum is 1·257 microhenry per metre.

The root of the trouble is that the authors, after giving on p. 23 the value of μ as $4\pi/10^7$ preserve this value explicitly in their formulae. Let them by all means explain that th ohm is chosen so that μ_0 has that value, but ever afterwards write this value as 1·257 micro henry per metre, in the same way as ϵ_0 on p. 41 is given as 8·854 micromicrofarads per metre These are the values that " the reader must learn ", and not 10^{-7}. Incidentally, th opening sentences of pp. 38 and 51 are examples of the lack of care devoted to th preparation of the book. It may not be out of place here to recall to those wishing t employ or teach the MKS system the advisability of stating the units after formulae e.g., $\boldsymbol{h} = 6{\cdot}62 \times 10^{-34}$ joule-seconds, $\boldsymbol{J} = 4185$ joules per kg.-calorie.

P. VIGOUREUX